



<https://theses.gla.ac.uk/>

Theses Digitisation:

<https://www.gla.ac.uk/myglasgow/research/enlighten/theses/digitisation/>

This is a digitised version of the original print thesis.

Copyright and moral rights for this work are retained by the author

A copy can be downloaded for personal non-commercial research or study,
without prior permission or charge

This work cannot be reproduced or quoted extensively from without first
obtaining permission in writing from the author

The content must not be changed in any way or sold commercially in any
format or medium without the formal permission of the author

When referring to this work, full bibliographic details including the author,
title, awarding institution and date of the thesis must be given

Enlighten: Theses

<https://theses.gla.ac.uk/>
research-enlighten@glasgow.ac.uk

HETEROGENEOUS AND HYBRID CONTROL WITH
APPLICATION IN AUTOMOTIVE SYSTEMS

A DISSERTATION
SUBMITTED TO THE DEPARTMENT OF MECHANICAL ENGINEERING
OF GLASGOW UNIVERSITY
IN COMPLETE FULFILLMENT OF THE REQUIREMENTS
FOR THE DEGREE OF
DOCTOR OF PHILOSOPHY

By
Jens Lüdemann
March 2002

© Copyright 2002 by Jens Lüdemann
All Rights Reserved

ProQuest Number: 10662769

All rights reserved

INFORMATION TO ALL USERS

The quality of this reproduction is dependent upon the quality of the copy submitted.

In the unlikely event that the author did not send a complete manuscript and there are missing pages, these will be noted. Also, if material had to be removed, a note will indicate the deletion.



ProQuest 10662769

Published by ProQuest LLC (2017). Copyright of the Dissertation is held by the Author.

All rights reserved.

This work is protected against unauthorized copying under Title 17, United States Code
Microform Edition © ProQuest LLC.

ProQuest LLC.
789 East Eisenhower Parkway
P.O. Box 1346
Ann Arbor, MI 48106 – 1346

GLASGOW
UNIVERSITY
LIBRARY:

12632

COPY 2

Abstract

Control systems for automotive systems have acquired a new level of complexity. To fulfill the requirements of the controller specifications new technologies are needed. In many cases high performance and robust control cannot be provided by a simple conventional controller anymore. In this case hybrid combinations of local controllers, gain scheduled controllers and global stabilisation concepts are necessary. A considerable number of state-of-the-art automotive controllers (anti-lock brake system (ABS), electronic stabilising program (ESP)) already incorporate heterogeneous and hybrid control concepts as ad-hoc solutions.

In this work a heterogeneous/hybrid control system is developed for a test vehicle in order to solve a clearly specified and relevant automotive control problem. The control system will be evaluated against a state-of-the-art conventional controller to clearly show the benefits and advantages arising from the novel approach.

A multiple model-based observer/estimator for the estimation of parameters is developed to reset the parameter estimate in a conventional Lyapunov based nonlinear adaptive controller. The advantage of combining both approaches is that the performance of the controller with respect to disturbances can be improved considerably because a reduced controller gain will increase the robustness of the approach with respect to noise and unmodelled dynamics. Several alternative resetting criteria are developed based on a control Lyapunov function, such that resetting guarantees a decrease in the Lyapunov function.

Since ABS systems have to operate on different possibly fast changing road surfaces the application of hybrid methodologies is apparent. Four different model based wheel slip controllers will be presented: two nonlinear approaches combined with parameter resetting, a simple linear controller that has been designed using the technique of simultaneously stabilising a set of linear plants as well as a sub-optimal linear quadratic (LQ)-controller. All wheel slip controllers operate as low level controllers in a modular structure that has been developed for the ABS problem.

The controllers will be applied to a real Mercedes E-class passenger car. The vehicle is equipped with a brake-by-wire system and electromechanical brake actuators. Extensive real life tests show the benefits of the hybrid approaches in a fast changing environment.

Acknowledgements

This exposition has been carried out in the Department Research and Technology of the DaimlerChrysler AG, section Cognition and Robotics (FT3/AI), Berlin.

First of all I would like to express my gratitude to Dr. Jens Kalkkuhl for his friendly and excellent advice and for his continuing encouragement and support. Furthermore, grateful acknowledgement is made to Prof. Kenneth J. Hunt, Department of Mechanical Engineering at Glasgow University for supervising this work.

For a good working atmosphere and the permanent willingness for professional discussions I thank all my colleagues. Particularly I would like to thank Mr. Andreas Queda who extended the results within the framework of his diploma thesis.

Grateful thanks also to the DaimlerChrysler AG for giving me the possibility to realize this project and for providing the opportunity to make test drives.

Finally I wish to thank my dear family, my wife Angelika and our two children Konstantin and Gustav for their patience and for rendering every possible assistance, enabling me to carry on and complete my work.

Grateful acknowledgement is also made to all which were not involved officially in this project but nevertheless made a contribution for its success.

Contents

Abstract	i
Acknowledgements	iii
1 Introduction	1
I Theory	7
2 An Introduction to Hybrid Control Systems	8
2.1 Hybrid Systems	9
2.2 Stability of Hybrid Systems	15
2.3 Introduction to Hybrid Control	20
3 Multiple Model based Nonlinear Adaptive Control	26
3.1 Constructive Nonlinear Control	27
3.1.1 Control Lyapunov function	27
3.1.2 Inverse Optimal Control	28
3.1.3 Nonlinear Adaptive Backstepping	30
3.2 Stability analysis of parameter resetting	35
3.3 Hybrid Observer and Estimation	43
3.4 Multiple model parameter estimation	45
3.5 Multiple model observer	47
3.5.1 A set of parallel observer	49
3.5.2 Decision logic	50
3.5.3 Multiple model observer (MMO)	52
3.5.4 Parameter estimation in the first order case	52
3.6 Parameter resetting	59

3.6.1	Multiple model parameter estimate used for resetting	59
3.6.2	Using the properties of the MMO for a first order system	64

II Application 71

4 The ABS Control Problem 72

4.1	Anti-lock Brake System	74
4.1.1	Problem description	75
4.1.2	Conventional Approach	76
4.1.3	Modular ABS system	77
4.1.4	Equations of motion of a quarter car	79
4.1.5	Tyre friction characteristics	80
4.1.6	Dynamics of the uncontrolled system	85
4.1.7	Mathematical Structure of the tyre slip dynamics	87
4.1.8	Specification of an ABS	88
4.2	A nonlinear PI tyre slip controller	89
4.2.1	Design of a globally stabilising control law	89
4.2.2	Linear Analysis	92
4.3	Sontags’s universal formula used for ABS	93
4.4	SSP wheel slip controller	96
4.5	LQRC wheel slip controller	97
4.6	Activation and Bumpless Transfer	102
4.7	Tyre friction estimate resetting	104
4.7.1	Friction coefficient estimation using MMO	104
4.7.2	Estimation of the friction coefficient using MME	109
4.8	Simulation	110
4.8.1	PI wheel slip controller simulation	111
4.8.2	Simulation results of the “Sontag” controller	113
4.8.3	Simulation of the SSP wheel slip controller	115
4.8.4	Simulation of the LQRC wheel slip controller	115
4.8.5	Four controllers compared	121
4.8.6	Conclusions	121

5 Experimental results 123

5.1	ABS test vehicle	123
5.2	Applicational viewpoint	130

5.3	Experimental Methods	131
5.3.1	Presentation of the results	132
5.3.2	Evaluation criteria	133
5.4	Car tests	134
5.4.1	Test 1: Straight ahead braking on dry road	134
5.4.2	Conventional ABS on dry road	144
5.4.3	Test 3: Straight ahead braking on ice	147
5.4.4	Conventional ABS on ice	156
5.4.5	Test 10: Braking in a turn	159
5.4.6	MMO verification tests	166
5.4.7	Discussion of results	181
5.4.8	Conclusions	186
6	Conclusions	188
	Bibliography	192
	Appendix	203
A	Four wheel car model	205
A.1	Geometry of the Vehicle	205
A.2	Forces at the Wheel	207
A.3	Torque Caused by the Forces at the Wheel	208
A.4	Dynamic Equations for the Forces	210
A.4.1	Expression in Body Fixed Coordinates	210
A.4.2	Expression in Velocity and Side Slip Angle	212
A.5	Balance of Torques	213
A.6	Determination of the Tyre Slip Angle	214
A.7	Wheel Dynamics	215
A.8	Vertical forces	215
A.9	Linear four-wheel cornering car model	216
A.10	The "bicycle" model	219
B	Definitions	221

List of Figures

2.1	Variable structure system I	10
2.2	Saddle point	10
2.3	Unstable focus	10
2.4	Variable structure system II	11
2.5	Systems classification	14
2.6	Flower system and non-smooth Lyapunov function	19
2.7	Multiple models, switching and tuning	21
2.8	Reconfigurable control	24
3.1	Trajectory initialisation with reference model	33
3.2	Trajectory initialisation with given reference signal y_r	34
3.3	Parameter jump in the Lyapunov function	38
3.4	Parameter resetting law	39
3.5	System and multiple models	45
3.6	Multiple Model Observer parameter estimation	48
3.7	Parameter resetting law	55
3.8	Estimated region of the true parameter θ	56
3.9	Simulation results.	62
3.10	Absolute value of prediction errors after parameter step change ($ e_2(t) $ (dotted), $ e_3(t) $ (dash dot), $ e_4(t) $ (dashed), $ e_5(t) $ (solid)).	64
3.11	Performance signals $\Delta V_1, \Delta V_2, \Delta V_3, \Delta V_4$ and ΔV_5 of the five models.	65
3.12	Worst case stability analysis	67
3.13	Switching Areas	68
3.14	Simulation results.	70
4.1	Vehicle dynamics	73
4.2	Modular structure of the ABS system	78
4.3	Quarter car slip model	80

4.4	Tyre friction curves	81
4.5	Definition of wheel slip angle	82
4.6	Definition of friction lateral force μ_y in dependence of wheel slip angle α	83
4.7	Slip equilibrium points	87
4.8	Friction as a function of μ_H with slip as parameter	94
4.9	Tyre friction curves with 12 linearisation points	96
4.10	Bode plots (I) and closed-loop step responses (SSP controller)	98
4.11	Bode plots (II) and closed-loop step responses (SSP controller)	99
4.12	On/Off automaton	102
4.13	Mode changes automaton	103
4.14	Normalised derivative of the tyre friction force $\frac{\partial F_x(x_1, v, \mu_H)}{\partial \mu_H}$	105
4.15	Region of “nice” stability in the z -plane	108
4.16	Wheel slip, clamping force, tyre friction and vehicle speed of the PI-wheel slip controller (without resetting: black, using MME: grey, using MMO: light grey).	112
4.17	Wheel slip, clamping force, tyre friction and vehicle speed of the “Sontag”-wheel slip controller (without resetting: black, using MME: grey, using MMO: light grey).	114
4.18	Wheel slip, clamping force, tyre friction and vehicle speed of the “Sontag”-wheel slip controller with low gain (black) and high gain (grey).	116
4.19	Wheel slip, clamping force, tyre friction and vehicle speed of the “Sontag”-wheel slip controller with low gain (with resetting: black, using MMO: grey).	117
4.20	Wheel slip, clamping force, tyre friction and vehicle speed of the “Sontag”-wheel slip controller with high gain (with resetting: black, using MMO: grey).	118
4.21	Wheel slip, clamping force and vehicle speed of the SSP-wheel slip controller.	119
4.22	Wheel slip, clamping force, tyre friction and vehicle speed of the LQRC-wheel slip controller.	120
4.23	Wheel slip, clamping force, tyre friction and vehicle speed of three different Slip controller simulations (PI-controller with MMO (black), “Sontag’s” controller with MMO (grey) and the SSP controller (light grey)).	122
5.1	Photo of the ABS test vehicle	124
5.2	ABS test vehicle hardware architecture	124

5.3	Slip controller interface	125
5.4	Photo of the electro-mechanical brake	126
5.5	Electro-mechanical brake	126
5.6	Physical EMB model	127
5.7	Clamping force hysteresis	128
5.8	scheme of the cascade structure of the EMB servo controller	129
5.9	Validation of the brake models	130
5.10	Test 1 results with “Sontag” tyre slip controller braking on dry road with reference slip $\lambda_0 = 0.14$	136
5.11	Accelerations a_x and a_y	137
5.12	Lateral speed v_y	137
5.13	Test 1 results with nonlinear PI tyre slip controller braking on dry road with setpoint slip $\lambda_0 = 0.14$	138
5.14	Accelerations a_x and a_y	139
5.15	Lateral speed v_y	139
5.16	Test 1 results with LQRC tyre slip controller braking on dry road with setpoint slip $\lambda_0 = 0.14$	140
5.17	Accelerations a_x and a_y	141
5.18	Lateral speed v_y	141
5.19	Test 1 results with SSP tyre slip controller braking on dry road with setpoint slip $\lambda_0 = 0.14$	142
5.20	Accelerations a_x and a_y	143
5.21	Lateral speed v_y	143
5.22	Conventional production car ABS on dry road (front wheels)	145
5.23	Conventional production car ABS on dry road (rear wheels)	146
5.24	Test 3 results with “Sontag” tyre slip controller braking on ice with setpoint slip $\lambda_0 = 0.05$	148
5.25	Accelerations a_x and a_y	149
5.26	Lateral speed v_y	149
5.27	Test 3 results with nonlinear PI tyre slip controller braking on ice with setpoint slip $\lambda_0 = 0.05$	150
5.28	Accelerations a_x and a_y	151
5.29	Lateral speed v_y	151
5.30	Test 3 results with LQRC tyre slip controller braking on ice with setpoint slip $\lambda_0 = 0.05$	152
5.31	Accelerations a_x and a_y	153

5.32	Lateral speed v_y	153
5.33	Test 3 results with SSP tyre slip controller braking on ice with setpoint slip $\lambda_0 = 0.05$	154
5.34	Accelerations a_x and a_y	155
5.35	Lateral speed v_y	155
5.36	Conventional production car ABS on icy road	155
5.37	Conventional production car ABS on wet road (front wheels)	157
5.38	Conventional production car ABS on wet road (rear wheels)	158
5.39	Test 10 results with “Sontag” tyre slip controller braking in a turn with setpoint slip $\lambda_0 = 0.1$	160
5.40	Accelerations a_x and a_y	161
5.41	Lateral speed v_y	161
5.42	Test 10 results with nonlinear PI tyre slip controller braking in a turn with setpoint slip $\lambda_0 = 0.1$	162
5.43	Accelerations a_x and a_y	163
5.44	Lateral speed v_y	163
5.45	Test 10 results with LQRC tyre slip controller braking in a turn with setpoint slip $\lambda_0 = 0.1$	164
5.46	Accelerations a_x and a_y	165
5.47	Lateral speed v_y	165
5.48	“Sontag” tyre slip controller with MMO braking on a dry road.	169
5.49	Accelerations a_x and a_y	170
5.50	Lateral speed v_y	170
5.51	Nonlinear PI tyre slip controller without MMO braking on snow.	171
5.52	Accelerations a_x and a_y	172
5.53	Lateral speed v_y	172
5.54	Nonlinear PI tyre slip controller with MMO braking on snow.	173
5.55	Accelerations a_x and a_y	174
5.56	Lateral speed v_y	174
5.57	LQRC tyre slip controller without MMO braking on snow.	175
5.58	Accelerations a_x and a_y	176
5.59	Lateral speed v_y	176
5.60	“Sontag” tyre slip controller without MMO braking on ice.	177
5.61	Accelerations a_x and a_y	178
5.62	Lateral speed v_y	178
5.63	“Sontag” tyre slip controller with MMO braking on ice.	179

5.64	Accelerations a_x and a_y	180
5.65	Lateral speed v_y	180
5.66	Nonlinearity and control	182
5.67	Filtered vertical force of one wheel	184
5.68	Tyre friction spline approximation (summer)	185
5.69	Tyre friction spline approximation (winter)	185
5.70	Tyre friction spline approximation (summer(grey)/winter(black) compared)	186
A.1	Vehicle axis system and geometric definitions	206
A.2	Generalized quarter-car	206
A.3	Definition of the steer angle	206
A.4	Definition of the tyre forces	207
A.5	Torque generated by the tyre forces	208
A.6	Tyre forces in body fixed coordinates	209
A.7	The body fixed coordinate system in the inertial system	210
A.8	Definition of the side slip angle	212
A.9	Definition of the tyre slip angle	214
A.10	Compound of the total tyre velocity	214
A.11	Tyre side slip angle in local coordinates	214
B.1	Nonlinear feedback loop with the control law $k(x)$ and input uncertainty Δ [110]	223

1 Introduction

The focus of this thesis will be the analysis and design of heterogeneous and hybrid control systems with application in automotive control.

In automotive engineering currently a new development can be observed which is very similar to the development in aerospace engineering a couple of years ago. Automotive vehicles are increasingly equipped with modern control systems to reduce weight, hardware costs, fuel consumption and to improve safety. Control systems like anti-lock brake systems (ABS), cruise controls and engine management systems have been developed in the last two decades. This development will be followed up by new concepts like anti-skid systems, drive-by-wire systems and autonomous driving. Consequently, control systems for automotive systems have acquired a new level of complexity. To fulfill the requirements of the controller specifications new technologies will be needed. The subject of hybrid and heterogeneous control systems within the automotive industry is of increasing relevance. Basically there are three main reasons for the interest in automotive control systems:

1. Automotive vehicles are highly nonlinear dynamic systems where the main nonlinear effects arise from
 - characteristics of combustion engine and drive train,
 - tyre friction generating longitudinal and lateral forces necessary for accelerating, braking and steering,
 - coupling of longitudinal and lateral motion via Coriolis forces.

Thus, in many cases high performance and robust control cannot be provided by a simple conventional controller or even a single nonlinear controller anymore. In this case hybrid combinations of local controllers, gain scheduled controllers and global stabilisation concepts are necessary.

2. In many respects automotive systems are genuinely hybrid systems due to discrete gear changes in the drive train, actuator saturation, abruptly changing road conditions, loads and faults in the system. In such cases hybrid control approaches can contribute to a systematic design methodology.
3. Since automotive control systems are often safety critical devices they have to be fault-tolerant and they should not affect the normal way of driving. In situations where faults occur, the controller should switch into a safe mode of operation with graceful degradation of the performance.

A considerable number of state-of-the-art automotive controllers (ABS, ESP) already incorporate heterogeneous and hybrid control concepts as ad-hoc solutions. An improvement of the drive dynamic quality can be obtained by a combination of wheel individual slip control and steer-by-wire [19]. It is desirable to provide automotive engineers with a sound theoretical basis for designing model based controllers.

Model based and modular or decentralised control architectures offer several advantages [102]:

- the complexity of these systems is kept on a manageable level,
- control modules can be reused across different products,
- new features can be seamlessly integrated,
- obsolete features can be easily removed,
- the control parameters can be easily changed,
- less system complexity.

Most adaptive controllers are designed to adapt to a set of fixed unknown parameters. In practical applications, however, the environmental conditions change. The new paradigm should be adaptation in a time varying environment. In adaptive control, disturbance rejection requires high gain. Increasing the controller gain has the trade off that unmodelled dynamics can be excited. Furthermore, the control system becomes less robust to computational delays, sampling and noise. The multiple model/observer approach together with a resetting strategy of a conventional adaptive controller could be a solution.

Hybrid parameter estimation offers a possibility of fast parameter estimation. A multiple model observer consists of a set of parallel observers. A model or observer is

assigned to each possible system dynamics or environmental condition. In the simplest case all models have the same structure. Only the parameterisation is different. Each individual observer observes only a small region of the parameter space. A cost index based selection is used to find the best model and consequently the best parameter.

Additional information on the parameter can be used to reset the estimation of an adaptive controller in a fast changing environment. This resetting can cause instability of the adaptive controller. Hence, a stability preserving resetting strategy is needed. Furthermore, the parameter should only be reset if the transient performance can be increased.

The robust overall system with improved transient response consists of

- a nonlinear adaptive Lyapunov function based controller,
- a finite set of parallel observers or estimators,
- a cost index based selection procedure to find the best observer/estimator and thus, the best parameter estimation
- a resetting of the continuous slow adaptation, whereby a stability examination is made. Before and after the resetting the continuous adaptation is left alone. Only at discrete time steps in order to reduce transients in the controller, is the continuous controller adaptation reset.

The approach is applied to a wheel slip control system where the slip controller operates in a new drive-by-wire ABS system as low level controller. A fast adaptation to respective road conditions (modelled by using the tyre friction coefficient μ_H) is very important to maintain the steerability of the car when driving on a heterogeneous road surface which is for example, partly covered with ice or water .

Main Contribution

A heterogeneous/hybrid control system will be developed for a test vehicle to solve a clearly specified and practically relevant automotive control problem. The control system will be evaluated against a state-of-the-art conventional controller to clearly show the benefits and advantages arising from the novel approach.

A real full size experimental vehicle will be used for implementation and testing of the approaches. Thus, not only simulations will be performed. Furthermore the controllers will be tested under real life conditions on a test track.

The main contribution is in the use of multiple models or multiple observers to reset the parameter estimate of a nonlinear adaptive backstepping control law in order to speed up the convergence rate. Such a resetting is of particular importance in such applications where the environment or system parameters change rapidly or even instantaneously. The multiple model adaptive control design ideas will be extended to nonlinear systems where an adaptive control system is designed first using control Lyapunov functions and adaptive backstepping [70, 110]. The resetting algorithm is different from the ones suggested in literature for linear systems because adaptive backstepping does not rely on the certainty equivalence principle.

It is not only shown that stability is preserved when resetting occurs. Moreover, the local convergence-rate is increased. This fact has not been investigated so far [87, 88, 89, 84, 85, 90] although it was the main motivation of the multiple model approaches. Uncertainty (modelling and noise) limits the attainable performance. Therefore, uncertainty is considered in the reset algorithm. The main contributions are

- an extension of multiple model based adaptive control to the class of parametric strict feedback nonlinear systems (see Chap. 3),
- the formulation of a set of sufficient closed loop stability conditions for resetting tuning function based nonlinear adaptive controllers (see Sec.3.2),
- a fast multiple model based estimation algorithm(see Sec. 3.4),
- the use of a fast multiple model observer, from which even under transient conditions an accurate parameter estimate can be obtained(see Sec. 3.5),
- the application and implementation of different control approaches such as
 - a Lyapunov based nonlinear PI-type controller (see Sec. 4.2),
 - an inverse optimal controller (see Sec. 4.3),
 - a very simple simultaneously stabilising (SSP) controller (see Sec. 4.4) and
 - a sub-optimal constrained LQ-controller (see Sec. 4.5)

to automotive wheel slip control.

- the application and implementation of the resetting technique to friction estimation in wheel slip control (cf. Sec. 4.7). The transient performance is improved in the case of fast changing road conditions by resetting the estimate of the adaptive tyre slip controller.

Within the evaluation, it is recognised that it is important to compare the performance of the presented methods with existing solutions. The controllers developed within the thesis will be benchmarked against a production car ABS which has been implemented in the same test vehicle. The evaluation process was carried out in accordance with existing SAE and ISO guidelines and the results will be presented.

Organisation

Beginning with an introduction of the theory of hybrid systems, Chap. 2 gives an overview of the relevant control theory that will partly be applied to a real application. The theory of constructive Lyapunov based design methods [70, 110] with their problems of fast adaptation in Chap. 3 leads directly to a stability-preserving resetting strategy for adaptive Lyapunov based controllers. It will be shown that the transient performance of the control system with respect to fast parameter changes can be improved without increasing the gain. Fast multiple model observer estimation algorithms are developed.

Chap. 4 shows recent trends in automotive and wheel slip control (which is the core of automotive ABS). A modular model based wheel slip controller structure is proposed. Four different wheel slip controllers will be designed.

1. One design is a nonlinear PI-type tyre slip controller.
2. The second controller is based on the inverse optimality of “Sontag’s” formula [115, 117].
3. A very simple linear PI controller will be designed using the algorithms for simultaneously stabilising a family of linear plants.
4. A constrained sub-optimal LQ-controller.

Both nonlinear approaches estimate a tyre friction value. A multiple model/observer estimate of the road condition is used to reset the continuous tyre road friction estimate of the adaptive controllers. This increases the (local) convergence-rate without loss of stability.

Preliminary tests in a nonlinear simulation environment show the advantages of the hybrid approaches.

All wheel slip controllers and the multiple model/observer tyre road friction estimation will be applied to a real Mercedes E-class brake-by-wire car in Chapter 5.

Extensive tests under real life conditions have been carried out in order to evaluate the controller, and are reported here.

Chap. 6 gives a short overview of the achievements and discusses related problems.

Publications

The following number of publications are closely related to this work: One conference paper [64], one book chapter [63] and one journal article [62] on the multiple model/observer based adaptive control (cf. chapter 3). One technical report [61] on nonlinear adaptive wheel slip control (cf. Sec. 4.2), one conference paper [55] on hybrid wheel slip approaches (cf. Sec. 4.2–4.5), one journal article on the benchmarking of different wheel slip approaches [75], one journal article on nonlinear adaptive wheel slip control [74] and Chapter 5) as well as a conference paper [98] on sub-optimal constrained LQ wheel slip control (cf. Sec. 4.5).

Part I

Theory

2 An Introduction to Hybrid Control Systems

This chapter includes an introduction to hybrid systems and control with their special descriptions and phenomena. The introduction to hybrid systems (given in Sec. 2.1) is important to understand the theoretical background of hybrid systems and to emphasise its special properties. Since stability results of non-hybrid systems cannot be transferred stability recent investigations for hybrid systems are presented in Sec. 2.2. Concepts of existing hybrid control approaches will be discussed in Sec. 2.3. Some of the presented approaches will later be applied to the automotive control example.

Systems with mode switches appear in numerous contexts and in many application areas. Combinations of continuous time systems and switching elements appear under many different names. The term hybrid system has been generally accepted as a collective term [78, 7, 9, 126, 79]. A characteristic feature of such systems is that they can be represented as a mixture of ordinary differential equations and logic where the continuous and discrete dynamics not only coexist but interact [126]. The system state can change due to discrete external events as well as in response to continuous dynamics. A hybrid system can be seen as a composition of continuous time dynamical systems and a discrete time system that switches between the continuous systems. Examples for hybrid systems can be found in the literature such as hysteresis, relay, saturation, bouncing ball, temperature control, ideal diode and switching gear box [100, 126].

There is no unified approach for modelling and control of hybrid systems. When systems become more complex and when switching takes place a classification of systems as linear or nonlinear proves not to be sufficient anymore. Therefore, such systems should be described as hybrid systems. Because of the variety of hybrid phenomena there is no unified approach that deals with hybrid controllers. Some examples are shown for hybrid controllers as well as for hybrid system behaviour.

2.1 Hybrid Systems

A dynamical system can be considered as a structure that receives an input $u(t)$ at each time and emits an output $y(t)$. The output does not only depend on the input but also on the past history of the inputs and the initial state. The concept of state was introduced to predict the future behaviour of the system.

Hybrid systems as they will be discussed in the following are combinations of continuous systems and logical or discrete systems.

Continuous Systems Continuous dynamic systems are described by models consisting of differential equations [128, 66, 129]

$$\begin{aligned}\frac{dx(t)}{dt} &= f(x(t), u(t)) \\ y(t) &= h(x(t), u(t))\end{aligned}\tag{2.1}$$

derived from physical laws with the state $x(t) \in \mathbb{R}^n$, the input $u(t) \in \mathbb{R}^r$, and output $y(t) \in \mathbb{R}^p$. The functions f and h are in general smooth functions of time, system states and inputs.

Consider the special case where the function f is discontinuous [39, 40]. In this case the differential equation has a discontinuous right hand side. The main feature of variable structure systems (VSS) is that new system properties are obtained by composing a desired trajectory from the parts of trajectories of different structures [36](cf. Example 2.1.1). A fundamental aspect of VSS is the possibility to obtain trajectories not inherent of any structures. These trajectories describe sliding modes [125].

Example 2.1.1 (VSS) Consider a second order system

$$\ddot{x} = -\Psi x$$

having two structures defined by $\Psi = \alpha_1^2$ and $\Psi = \alpha_2^2$. The phase portrait consists of families of ellipses (see Fig. 2.1) and hence, neither of the structures are asymptotically stable. Asymptotic stability is obtained when the structure of the system is changed on the coordinate axes.

$$\ddot{x} = -\Psi x$$

$$\Psi = \begin{cases} \alpha_1^2 & \text{if } x\dot{x} > 0 \\ \alpha_2^2 & \text{if } x\dot{x} < 0 \end{cases}, \quad \alpha_1^2 > \alpha_2^2$$

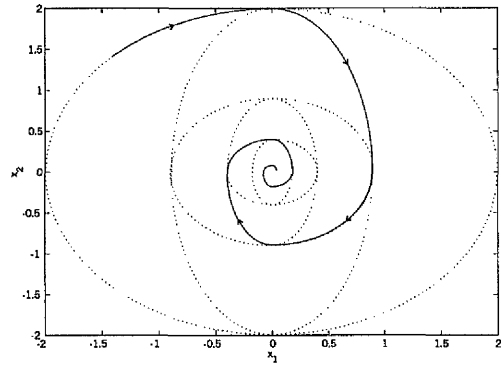


Figure 2.1: Variable structure system I

Example 2.1.2 (VSS and sliding mode) Consider the second order system [125]

$$\ddot{x} - \xi \dot{x} + \Psi x = 0, \quad \xi > 0 \quad (2.2)$$

where the linear feedback is negative or positive corresponding to either $\Psi = \alpha > 0$ or $-\alpha$. Both structures are unstable (cf. Fig. 2.3 and Fig. 2.2). Only motion along

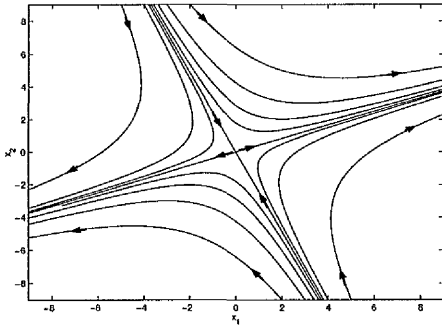


Figure 2.2: Saddle point

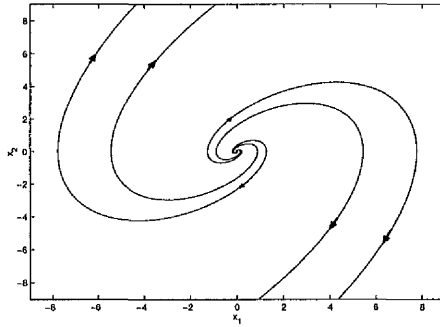


Figure 2.3: Unstable focus

the stable eigenvector of the structure with $\Psi = -\alpha$ (cf. Fig. 2.2) converges to the origin. If switching between the two structures occurs at this line and on $x = 0$ with the switching law

$$\Psi = \begin{cases} \alpha & \text{if } xs > 0 \\ -\alpha & \text{if } xs < 0 \end{cases}$$

where

$$s = cx + \dot{x}, \quad c = -\frac{\xi}{2} \pm \sqrt{\frac{\xi^2}{4} + \alpha}$$

the resulting VSS will be asymptotically stable (cf. Fig. 2.4).

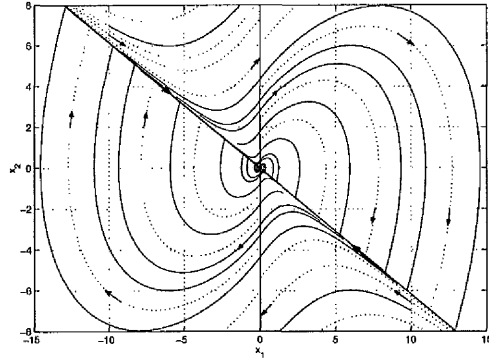


Figure 2.4: Variable structure system II

Irrespective of the system parameters and disturbances the solution of the second order equation in sliding mode always tends to the solution of the first order linear differential equation which depends only on the slope c of the switching line.

Discrete Systems In continuous systems the state space X is a continuum consisting of a n -dimensional vector of real numbers. This normally leads to differential equation as in (2.1).

In discrete state systems the state space is a discrete set. The values of the state change discontinuously with time and can be described as follows:

$$\begin{aligned} z^+ &= \phi(z, \sigma) \\ \sigma^+ &= \zeta(z, \sigma) \end{aligned} \tag{2.3}$$

where $z \in \{z_1, z_2, \dots, z_o\}$ the state, $\sigma \in \{\sigma_1, \sigma_2, \dots, \sigma_p\}$ the system input and $o \in \{o_1, o_2, \dots, o_q\}$ the system output are taken from finite sets \mathcal{Z} , Σ and \mathcal{O} respectively, and $z^- = z(t^-) = \lim_{t \downarrow t^*} z(t)$ and $z^+ = z(t^+) = \lim_{t \uparrow t^*} z(t)$ denote the one-sided limits.

Hybrid Systems There are many situations where a hybrid model is appropriate. A hybrid system model has discrete as well as continuous state variables, inputs and outputs.

In the literature [99, 52, 47, 123, 44, 119, 23, 11, 23, 13, 71, 77, 26, 82, 100, 126, 18] numerous descriptions of hybrid systems have been developed. The main problem is to describe the interaction (the interface) between the continuous and discrete dynamics. Computer engineers look at this primarily from a discrete point as this is the way a computer interacts with a continuous environment [126]. Control scientists put the

emphasis more on the continuous behaviour. Thus different models were developed for different purposes with assumptions made accordingly. There are more or less three types of models.

- Finite state machines where each discrete state represents a local continuous dynamic behaviour [11, 47].
- Differential equations in combination with some discrete state equations [123, 23].
- Higher level models with an interface between the continuous and discrete time parts [119, 71].

A quite general model consists of two different state variables, namely continuous and discrete ones [100].

Definition 2.1.1 *A hybrid system $\mathcal{H} = (\mathbb{R}^n \times \mathcal{Z}, \mathbb{R}^p \times \Sigma, \mathbb{R}^q \times \mathcal{O}, f, \phi)$ consists of:*

- a nonempty set $H = \mathbb{R}^n \times \mathcal{Z}$ as the hybrid state space of \mathcal{H} ;
- a set $\mathbb{R}^p \times \Sigma$ as the external input sequence of \mathcal{H} ;
- transition functions $f : D_f \longrightarrow \mathbb{R}^n$ and $\phi : D_\phi \longrightarrow \mathcal{Z}$, where

$$\begin{aligned} \dot{x}(t) &= f(x(t), z, u(t)), \\ z^+ &= \phi(x(t), z, u(t), \sigma) \end{aligned} \tag{2.4}$$

and

$$\begin{aligned} D_f &\subseteq \mathbb{R}^n \times \mathcal{Z} \times \mathbb{R}^p \\ D_\phi &\subseteq \mathbb{R}^n \times \mathcal{Z} \times \mathbb{R}^p \times \Sigma, \end{aligned}$$

- a set $\mathbb{R}^q \times \mathcal{O}$ called the output space
- an output relation $h : D_h \longrightarrow \mathbb{R}^q$ and $\zeta : D_\zeta \longrightarrow \mathcal{O}$, where

$$\begin{aligned} y(t) &= h(x(t), z, u(t)), \\ o^+ &= \zeta(x(t), z, u(t), \sigma) \end{aligned} \tag{2.5}$$

and

$$\begin{aligned} D_h &\subseteq \mathbb{R}^n \times \mathcal{Z} \times \mathbb{R}^p \\ D_\zeta &\subseteq \mathbb{R}^n \times \mathcal{Z} \times \mathbb{R}^p \times \Sigma. \end{aligned}$$

The continuous state vector is denoted by x , z is the discrete state vector, u the continuous input, σ the discrete input, y the continuous output and o the discrete output. The discrete state may change due to internal or external events. The internal events cause a state change when x and z take certain values.

In the following some other system descriptions will be discussed. The problem of describing systems with combined discrete and continuous processes can be formulated by a sequence of differential equation sets [18]. This formulation cannot describe the discrete dynamic behaviour. Alternatively the continuous and discrete time dynamics can be modelled by a finite state automaton (FSA) [52]. This requires a discretisation of the continuous state space. A FSA is not sufficient to describe a discretised continuous system. Thus, the concept has to be extended. To introduce the time into automaton leads to stochastic timed automata and the Generalized Semi-Markov Process (GSMP). The GSMP [44] is an extension on FSA and is a stochastic discrete event model for a process generating a piecewise constant output signal. A discrete event system is a system where state transitions are only observed at discrete points of time. These transitions are associated with events [26]. Lunze [77] deals with continuous variable systems with quantised state measurements. The discrete event behaviour of the quantised system is represented by a stochastic automaton as an approximation for the continuous system. The main problem of a quantised system results from the nondeterminism of the approximation of a continuous system. This means that the quantised system may generate for a given qualitative initial state and a qualitative input sequence a set of possible output sequences. A Hybrid Automaton (HA) [11, 47] represents a system with discrete events as well as continuous time elements. The HA is described by graphs whose edges represent discrete transitions and whose vertices represent continuous activities. This model represents continuous as well as discrete behaviour. Contrary to Finite State Machines, Petri [99] nets can represent concurrent activities. Grafset [13] is a graphical language for modelling and specification of sequential processes and can be viewed as a special kind of Petri net. Nerode and Kohn [94] dealt with systems as a composition of interacting ordinary differential equations and finite state automaton FSA. Taverini introduced the differential automaton $\dot{x}(t) = f(x(t), q(t))$, $q^+ = \nu(x(t), q(t))$ in [123], where $x \in \mathbb{R}^n$ models the continuous and $q \in \mathcal{Z}$ the discrete dynamics. The differential automaton is quite similar to the model of [100] having neither inputs or outputs. Brockett [23] developed several models to describe motion systems. For his D-class hybrid system he mixed continuous and “symbolic” controls. Morari [82] introduced the mixed logic dynamical system as a model of systems described by interacting physical laws, logic rules and operating

constraints. Antsaklis et al. [119] models hybrid control systems for a special subclass of hybrid systems in three parts: The plant as LTI system, the controller as deterministic automaton and an interface that converts continuous time signals to sequences of events and vice versa. The connection between the continuous and the discrete part is an explicit interface. Lennartson et al. [71] also model the system in three parts.

System classification A possible systems classification of special subclasses of hybrid systems is shown in Figure 2.5. The hybrid system representation is the most general

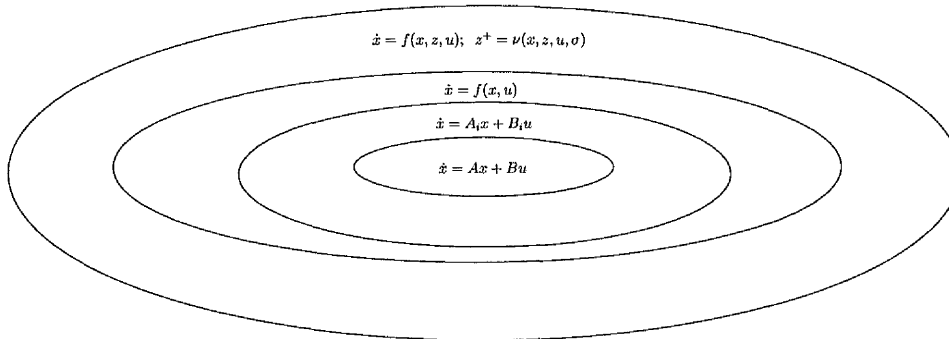


Figure 2.5: Systems classification

description including continuous as well as discrete states. It captures all other effects. The nonlinear system description captures all linear and piecewise affine linear effects. A piecewise linear system is a system of the form

$$\frac{dx(t)}{dt} = A_i x(t) + b_i u(x) \quad (2.6)$$

with $x \in X_i^n$. $\{X_i^n\}$ is a partition of the state space into operating regimes [58]. The dynamics in each region is described by linear dynamics. In each partition only one linear is system valid. The discrete state space for piecewise linear systems is void. An index i points to the valid region. The simplest piecewise linear system is the linear system itself with only one partition. The simplest subclass of hybrid systems are linear systems. The linear system is a dynamic system which is linear in the states and in- and output characteristics. That means a linear system fulfills the property of superposition. Linear systems are well explored.

A nonlinear system is quite general, but has a void discrete state space. Piecewise linear effects are captured if the function f is piecewise continuous. To use the powerful tools of the linear systems the nonlinear system can be linearised, if possible, around some operating point.

A different classification of hybrid systems is into heterogeneous and homogeneous hybrid systems.

Definition 2.1.2 (Homogeneous hybrid system) *A hybrid system that switches between a collection of continuous dynamical systems of uniform structure is called homogeneous hybrid system.*

Definition 2.1.3 (Heterogeneous hybrid system) *A hybrid system that switches between a collection of continuous dynamical systems that might have different structure is called heterogeneous hybrid system.*

For example the switching between a number of different PI controllers results in a homogeneous hybrid system and the switching between PI and PID controllers result in a heterogeneous system. The homogeneous hybrid system is a subclass of heterogeneous systems.

2.2 Stability of Hybrid Systems

The stability of hybrid systems depends on the interaction of continuous dynamics and switching. Even if every individual continuous time system is stable, the hybrid system will not necessarily be stable and switching between individually unstable systems does not imply that the resulting hybrid system is unstable (see Examples 2.1.1 and 2.1.2). Starting with the stability of equilibrium points and the stability in the sense of Lyapunov, a sufficient stability condition for hybrid systems will be given.

Continuous stability[66, 129, 70] A point $x = x_G$ in the state space is said to be an equilibrium point of (2.1) if it has the property that whenever the states of the system starts at x_G it will remain at x_G for all future time. Physically, a system is in equilibrium when it remains in one state in the absence of any external (exogenous) input. This means the time derivative \dot{x} is zero. Without loss of generality it is assumed that $f(0) = 0$, and stability of the origin $x = 0$ is investigated. The equilibrium $x_G = 0$ of the system (2.1) is said to be stable in the sense of Lyapunov if:

$$\forall \epsilon > 0, \quad \exists \delta > 0 : \quad |x(t_0)| < \delta \Rightarrow |x(t)| < \epsilon \quad \forall t \in [t_0, \infty). \quad (2.7)$$

Furthermore, if $\lim_{t \rightarrow \infty} x(t) = 0$ the equilibrium point is called asymptotically stable. That means an equilibrium point is stable when all solutions starting nearby stay nearby, otherwise it is unstable. It is called asymptotically stable when it tends to

the equilibrium point as time approaches infinity. The equilibrium point is uniformly stable when δ in (2.7) can be chosen independently of t_0 .

Stability of automaton The automaton (2.3) is called stable if the input σ together with the current automaton state z causes no new state z^+ different of $z = \phi(z, \sigma)$ [139]

$$z^+ = z^- = \phi(z, \sigma) = \phi(\phi(z, \sigma), \sigma). \quad (2.8)$$

Stability in the sense of Lyapunov

Among the many definitions that have been proposed for the concept of stability the one formulated by Lyapunov [66, 129, 70, 110] is particularly suited to our discussions and is presented below.

Definition 2.2.1 (Lyapunov function) Let $x(t) \in \mathbb{R}^n$ and $V(x(t))$ a scalar radially unbounded function. $V(x(t))$ is said to be a Lyapunov function if $\forall t \in \mathbb{R}$:

$$\forall x(t) \in \mathbb{R}^n \quad V(x(t)) \begin{cases} > 0 & \text{if } x(t) \neq 0 \\ = 0 & \text{if } x(t) = 0 \end{cases} \quad (2.9)$$

$$\forall x(t) \in \mathbb{R}^n \quad \dot{V}(x(t)) \begin{cases} \leq 0 & \text{if } x(t) \neq 0 \\ = 0 & \text{if } x(t) = 0 \end{cases} \quad (2.10)$$

A function that satisfies condition (2.9) is said to be positive definite. If $\forall x(t) \in \mathbb{R}^n \setminus \{0\} \quad V(x(t)) \geq 0$ the function is said to be positive semi-definite.

A function that satisfies condition (2.10) is said to be negative definite. If $\dot{V}(x(t)) \leq 0 \quad \forall x(t) \in \mathbb{R}^n \setminus \{0\}$ the function is said to be negative semi-definite.

Theorem 2.2.1 (Lyapunov Stability) The equilibrium point $x_G = 0$ of the autonomous system $\frac{dx(t)}{dt} = f(x(t))$ is asymptotically stable in the sense of Lyapunov if there exists a Lyapunov function $V(x(t))$ for the system. Furthermore the system is said to be globally asymptotically stable if

$$V(x(t)) \longrightarrow \infty \quad (2.11)$$

as

$$\|x\| = \sqrt{x_1^2 + x_2^2 + \dots + x_n^2} \longrightarrow \infty. \quad (2.12)$$

The proof and more general stability results for time varying systems can be found in [114, 66].

Theorem 2.2.2 (Lyapunov Stability for non-autonomous systems) *The equilibrium point $x_G = 0$ of the non-autonomous system $\frac{dx(t)}{dt} = f(x(t), t)$ is Lyapunov stable if there exists a scalar function $V(x(t), t)$ with continuous first order derivatives and a class- \mathcal{K} function α (cf App. B) so that $\forall x \neq 0$:*

1. $V(x(t), t) \geq \alpha(|x(t)|) > 0$
2. $\dot{V}(x(t), t) \leq 0$

Furthermore, if there is a class- \mathcal{KL} function (cf App. B) β so that $V(x(t), t) \leq \beta(\|x(t)\|)$ the equilibrium point is uniformly stable.

Another stability concept is that of input-to-state stability (ISS) by Sontag [116]. The system (2.1) is said to be input-to-state stable (ISS) if for any $x(t_0)$ and any input u continuous and bounded on $[t_0, \infty)$ the solution exists for all $t \geq t_0$ and satisfies

$$|x(t)| \leq \beta(|x(t_0)|, t) + \gamma \left(\sup_{0 \leq \tau \leq t} |u(\tau)| \right) \quad (2.13)$$

where β and γ are class- \mathcal{KL} and class- \mathcal{K} functions respectively.

To transfer the stability results to hybrid systems, the key constraint is the Lipschitz condition, whereby $f(x(t), t)$ satisfies the inequality

$$\|f(x, t) - f(y, t)\| \leq L\|x - y\|. \quad (2.14)$$

In the context of hybrid systems the Lipschitz condition does not hold since the differential equation has a discontinuous right hand side. For this reason the use of Lyapunov's stability criterion for continuous systems is not straightforward. However, some remarks on stability for hybrid systems can be found in [78, 111, 112, 101, 59, 72, 126]. Easily it can be shown that switching between stable systems can result in an unstable system and contrary Example 2.1.1 shows that switching between two unstable vector fields can result in a stable hybrid system. Some extensions to Lyapunov's theory can be found:

1. The differentiable Lyapunov function can be replaced by a non-smooth Lyapunov function [78] for systems with discontinuous right hand side. Stability of the continuous parts of hybrid systems can be analysed using Lyapunov's stability theory

for nonlinear systems. Only at the switching points the non-smooth technology must be used because \dot{V} is undefined. The time derivative at the switching points is avoided by requiring $V(x^+) \leq V(x^-)$ i.e. the Lyapunov function makes a non-positive step. Example 2.2.1 shows a non-smooth Lyapunov function for a piecewise linear system.

2. The Lyapunov function is a continuous function depending on the system states that are discontinuous in time. For stability it is sufficient that [126]
 - a) $V(x)$ is continuous with respect to its arguments
 - b) $V(x)$ is non-increasing along trajectories in between switching events,
 - c) $V(x^+) \leq V(x^-)$ whenever there is a jump from x^- to x^+ at some time instant t^* .

3. If a family of systems has a common Lyapunov function, then the resulting system is stable for any switching between subsystems [33, 92, 136, 112, 72]. Such a common Lyapunov function is in general not easy to find. In [92] conditions for the existence of a common Lyapunov function are given. Often it is impossible to find such a function even though it is known that the system is stable.

Example 2.2.1 (Flower system) *Consider the piecewise linear system*

$$\dot{x}(t) = A_i x(t) \tag{2.15}$$

$$i(t) = \begin{cases} 1, & x_1^2(t) - x_2^2(t) < 0 \\ 2, & x_1^2(t) - x_2^2(t) \geq 0 \end{cases} \tag{2.16}$$

In Fig. 2.6 the trajectory and a non-smooth Lyapunov function is displayed. The search for a piecewise quadratic Lyapunov function can be formulated as a convex optimisation problem [59]. Note that for such systems no common Lyapunov function exists.

In [54] a procedure for computing a Lyapunov function (if one exists) for the equilibrium point $x = 0$ for a class of nonlinear systems is described.

In the literature some other, less general Lyapunov techniques for hybrid systems have been proposed [21, 97, 136, 137, 22, 72]. All approaches show a non-increasing sequence of energy at consecutive switching times for stability. A continuous behaviour between switches, bounded only by a continuous function which is zero at the origin is described in [137].

If the objective is to design controllers, the Lyapunov stability methods need to be extended in order to design stable controllers more than to analyse given systems.

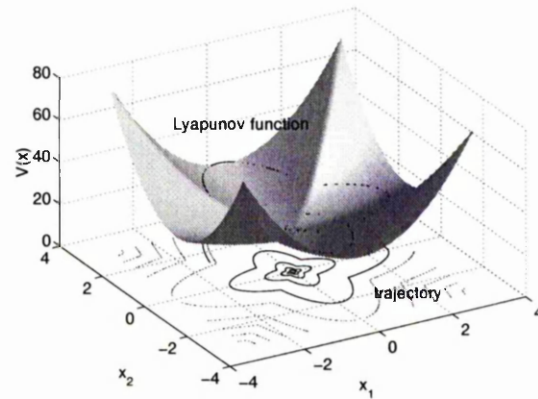


Figure 2.6: Flower system and non-smooth Lyapunov function

Another aspect is the stability analysis of the discrete part of a hybrid system. The discrete part is stable if (cf. (2.8))

$$\phi(x(t), z, u(t), \sigma) = \phi(x(t), \phi(x(t), z, u(t), \sigma), u(t), \sigma). \quad (2.17)$$

2.3 Introduction to Hybrid Control

Hybrid control is control with either [21]

1. Structural changes in the controller caused by discontinuities in the control strategy or logical elements in the controller.
2. Structural changes in the system caused e.g. by external disturbances or system failures.

That means control of hybrid systems or hybrid control of continuous systems or a mixture of both. There are several reasons why switching of the controller may become necessary:

- The system has different dynamics in different operating regimes.
- The system is time-varying.
- The system is not stabilisable using continuous feedback. Even some continuous systems cannot be controlled using continuous feedback [118].
- The performance of the system can be increased by switching between different controllers [89].

In the following classes of hybrid control systems that have received major interest in the literature will be presented. So far there does not seem to be a systematic approach for hybrid control but different methods have been reported in the literature. Some of the relevant concepts of the hybrid regulation are presented.

Multiple models, Switching and Tuning and Supervisory control A hybrid or switching controller selects between a number of controllers based on some performance index derived by a supervisor. The supervisor selects an output or a weighted sum of control outputs from several controllers. The use of multiple models to switch or reset parameter estimators has been proposed in order to speed up the convergence rate of certainty equivalence adaptive control of linear systems [81, 87, 88, 89, 84, 85, 90, 7, 93, 140, 9].

External disturbances, changes in the system dynamics, parameter variations etc., can be seen as unknown different environments in which the system has to operate. Multiple linear models to describe different environments are used by [87, 88, 89, 90]. The models can be either fixed or adaptive. Each model I_j represents one environment.

In the simplest case all models can have the same structure but different environments are expressed by different values of a constant parameter vector. All models operate in parallel. Corresponding to each of the models there exists a parameterised controller C_j . At every instant one of the models is chosen on the basis of some measure of the identification errors $e_j = \hat{y}_j - y_j$. A suitable switching criterion is determined as [88]

$$\operatorname{argmin}_j [J_j(t)] = \operatorname{argmin}_j \left[\alpha e_j^2(t) + \beta \int_0^t \exp(-\lambda(t - \tau)) e_j^2(\tau) d\tau \right],$$

and the corresponding controller C_j is used to control the plant. The structure of such a configuration is shown in Fig. (2.7). It can be applied to linear as well as to non-

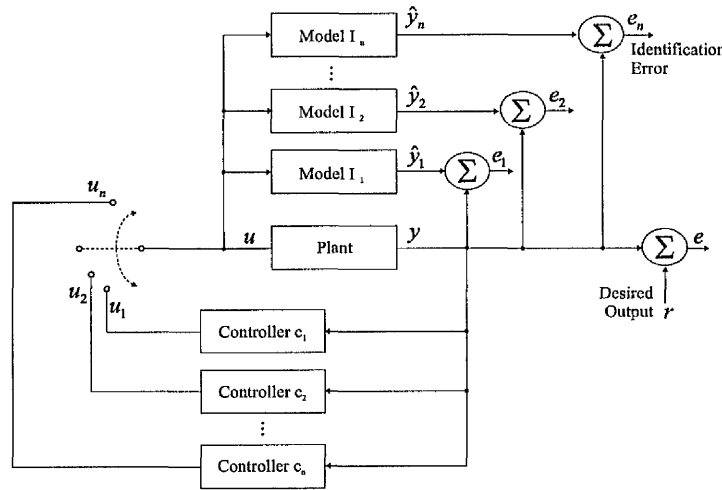


Figure 2.7: Multiple models, switching and tuning

linear systems [89]. In the case the choice of models, the controllers and the adaptive algorithms are different.

Similarly, the supervisory control approach in [84, 85, 51, 27] compares in real-time the norm-squared output prediction errors of a number of available estimators instead of models and uses the estimator with the least prediction error. Both approaches base decision making on the principle of certainty equivalence [83, 17, 70] that is, an adaptive feedback controller is designed on the basis of current values of plant parameter estimates with the understanding that these estimates are to be viewed at as correct, even though they may not be.

Various strategies have been proposed to prevent the system from arbitrarily fast switching [81, 84]. To prevent the system from chattering a dwell time switching logic [84] is applied. The system is prevented from switching until the dwell time has

been reached. After the switch the dwell time is set to zero again. Another suggested method for this is the so called hysteresis switching [50].

The approach in [140] differs from the approaches above. The methodology is to design stable linear controllers for LTI and LTV systems. The state space is decomposed into subsets and a common quadratic Lyapunov function is derived for each subset giving the admissible controller.

The concept of constructive nonlinear control in Sec. 3.1 can be extended to hybrid systems. Sontag [117] presents a formula for a stabilising feedback law under the assumption that a piecewise smooth control Lyapunov function (CLF) exists.

In this thesis a reset strategy using an estimate from a multiple model/observer based approach is used to reset the parameter estimate of a nonlinear adaptive backstepping controller.

Simultaneous stabilisation Consider a system with switches. An important question is whether a single linear controller exists that stabilises the system or not. A theory to find a controller that stabilises all possible system configurations or parameterisations is presented in [130, 131, 132]. The simultaneously stabilising problem (SSP) can be formally stated as follows: Given an r -tuple $G_1(s), \dots, G_r(s)$, of proper distinct transfer functions for plants, find a compensator $C(s)$ (if it exists) such that all closed-loop systems

$$\frac{C(s)G_i(s)}{1 + C(s)G_i(s)}, \quad (i = 1, 2, \dots, r)$$

are internally stable. If the compensator $C(s)$ is further restricted to be stable, i.e. it has no unstable poles, then the SSP is referred to as a strong SSP (SSSP). SSP is a computationally tractable approach which aims to ensure that the characteristic roots of the closed-loop systems for the r -tuple plants all lie in a desired region where certain stability properties are assured (a subset of the Hurwitz stability region) rather than simply the Hurwitz stability region. The so called D stability specification [131] allows for the consideration of both stability and transient performance.

Using this method it is possible to find a minimum number of stabilizing controllers. If it is not possible to find one stabilizing controller, perhaps it is possible to split the problem into sub-problems and to find stabilising controllers for these sub-problems.

Please note that stabilising each individual system does not imply that a system that switches between the individual systems is stable.

Sub-optimal Constrained LQR The sub-optimal constrained linear quadratic regulation with state and input constraints (LQRC) [57] is based on a decomposition

of the Hamilton Jacobi Bellmann equation in two parts. One part is a suboptimal strategy for explicit off-line design of LQ-controllers with subject to state and input constraints. The second part is an on-line finite discrete optimisation. The optimal controller according to the present constraints is computed on-line. A key feature of the approach is that it facilitates constrained sub-optimal control in real-time. Essentially, the resulting controller is switching between various linear control laws and therefore constitutes a hybrid controller. The so-called explicit method does not rely on real-time optimisation but rather on explicit evaluation of the resulting piecewise linear state feedback.

Optimal control of hybrid systems Optimal control of hybrid systems described in [49] is based on discretisation of Bellmann's inequality, dynamic programming and convex optimisation. The discretisation of Bellmann's inequality gives a lower bound on the optimal cost in terms of linear programming. The lower bound and a control law leads to an upper bound on the optimal cost. The disadvantage is that the method needs discretisation of the state space that is only an approximation. It suffers from the curse of dimensionality, i.e. the cost of discretisation grows exponentially with the dimension of the state space.

Hierarchical control Hierarchical Control uses hierarchical models for modelling dynamical processes with different levels of abstraction. Large, complex systems often possess a hierarchical structure and recognizing such a structure has several practical benefits [107]. System design is easier since the design process can proceed independently on simpler subsystems with well defined interfaces. The integration of all subsystems results in a complete system. There are several approaches for decomposing a large system into a hierarchical structure. One approach is the physical decomposition where the hierarchy is chosen to match the physical components. Another approach is to perform a functional, or semantic, decomposition in which the hierarchy is chosen based on functions or goals achieved. This is a common approach to complex control problems. At the lowest level there are continuous stabilising controllers for a subsystem or for a special task. At the upper level the strategic planning, supervisory functions and fault tolerant methods are implemented.

Weakly coupled control systems can be regulated decentralised, if a superordinated structure monitors the subordinates or if individual subsystems have different time scales. An example is the relatively slowly superordinated electronic stabilisation program (ESP) and a fast low level wheel slip controller.

Reconfigurable Control Complex systems must have the capability for exception handling to operate successfully over a long period of time. The same holds for safety critical applications. Control reconfiguration is normally based on stored control laws tailored to each anticipated fault condition [106, 124] (see Fig. 2.8). Three examples

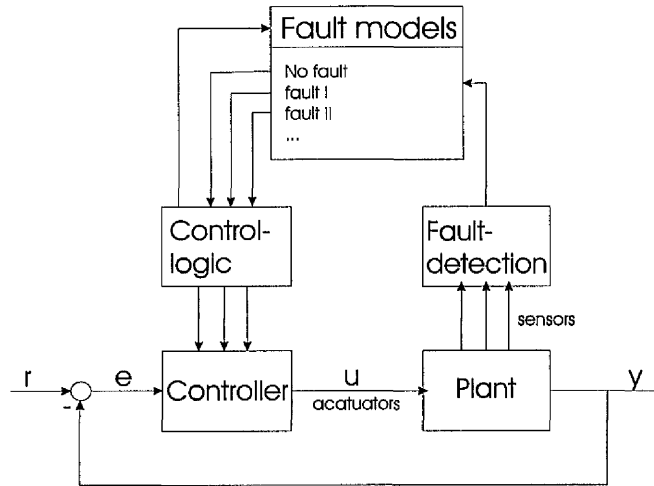


Figure 2.8: Reconfigurable control

of the useful methods are given.

- Fault detection uses qualitative models to express system dynamics by the qualitative values of signals. Therefore the continuous behaviour of the system is discretised (value not time). Then, the qualitative continuous system dynamics can be represented by a discrete event model. The discrete event behaviour of a system can be modelled by a stochastic automaton [77]. A qualitative observer is built from this automaton. Diagnosis is done by comparing the observed event sequence with the discrete event dynamics of the system.
- In the case of failures the control system should switch to a mode of graceful degradation. Large performance degradation should be avoided. This requires redundancy in actuators and sensors. In the case of failures, the remaining actuators or sensors not only need to take the functionality of the defective actuator or sensor respectively. Furthermore they need to compensate the side effects of actuator failures (disturbances). Conditions to compensate actuator failures of LTI-systems are described in [122].
- Switching between controllers results in reconfiguration transients and serious

performance degradation. Three methods for active transient control are discussed in [113]:

- After a switch between controllers the state zeroing method sets the state variables of the new controller to zero. This always causes transients.
- The state preserving method takes the state of the old controller and uses this for the initialisation of the new controller. This can only be applied if both controllers have the same structure. The transient behaviour depends on the last state of the old controller.
- If the control error is zero just before a switch the output fitting method initialises the new controller in a way that it has the same output as the old controller. If the control error is not zero the output of the new controller should be close to the output of the old controller. A transient management algorithm keeps the control signal smooth around the reconfiguration with the trade off that transients can not be completely removed.

3 Multiple Model based Nonlinear Adaptive Control

In this chapter a new method combining the nonlinear adaptive control theory [70] with the multiple model approaches (cf. Sec. 2.3) is proposed, whereby the stability of the adaptive controller is preserved. Later, this method will be applied to wheel slip control and results from real vehicle tests shall be presented.

Adaptive control is control of unknown plants or adapting to an unknown environment. Traditional adaptive controllers rely on the principle of certainty equivalence [83, 17]. Unfortunately, certainty equivalence controllers do not necessarily achieve stabilisation and tracking [70]. Even a stable controller may be destabilised by a bad parameter estimate.

In Lyapunov based design the estimation procedure is included within the stability proof of the control design. Together with recursive design procedures this is not limited to first or second order systems.

The concept of control Lyapunov functions (clf) offers the possibility of a constructive control design including the parameter estimation.

The question is of how to combine a fast hybrid estimation with the Lyapunov function based adaptive controller design without destroying stability in order to increase the control performance.

Contrary to the approaches in the literature the proposed resetting is based on investigations of a switched Lyapunov function. The new result is the combination of the continuous adaptation with a parameter resetting taking stability into account.

The advantage of combining both approaches is that transients due to adaptation can be damped out while the robustness and performance of the controller with respect to disturbances can be improved. As a consequence the gain of the continuous adaptive controller can be considerably lowered. The parameter resetting is based on a Control Lyapunov function and can guarantee asymptotic stability. Note that the combination

of the continuous controller and the resetting results in a hybrid system.

Transient improvement is important for example in adaptation to possible fast changing road condition in wheel slip control because large transients results in either wheel locking or in a longer braking distance with both undesirable.

The main contributions are the extension of multiple model based adaptive control to the class of parametric strict feedback nonlinear systems and the formulation of a set of sufficient closed loop stability conditions for resetting tuning functions based nonlinear adaptive controllers. Later, the use of multiple models resetting the parameter estimation in a nonlinear adaptive controller is proposed.

The chapter is organised as follows: In Sec. 3.1 some results of constructive nonlinear adaptive control are briefly reviewed and a motivation for discontinuous parameter resetting is given. This is followed by an analysis of the closed loop stability implications of resetting parameter estimates (Sec. 3.2) where a first order and a second order example are used to illustrate the results.

In Sec. 3.3 the use of estimators and observers for parameter estimation will be discussed and extended in Sec. 3.4 to the use of multiple estimators and in Sec. 3.5 to multiple model observers. In Sec. 3.6 the estimates of multiple models and multiple model observers are used for the parameter resetting of nonlinear adaptive controllers.

3.1 Constructive Nonlinear Control

3.1.1 Control Lyapunov function

Suppose that our problem for the time invariant system

$$\dot{x} = f(x(t), u(t)), \quad x \in \mathbb{R}^n, \quad u \in \mathbb{R}, \quad f(0, 0) = 0, \quad (3.1)$$

is to design a feedback control law $\alpha(x)$ for the control variable u such that the equilibrium $x = 0$ is globally asymptotically stable.

An extension of the Lyapunov concept is the so called control Lyapunov function (CLF) [70, 110]. The idea is to find a Lyapunov function $V(x)$ in a way that

$$\begin{aligned} \dot{V}(x(t)) &= \frac{\partial V(x(t))}{\partial x(t)} \cdot \frac{dx(t)}{dt} \\ &= \frac{\partial V(x(t))}{\partial x(t)} \cdot f(x(t), \alpha(t)) \leq -W(x) \end{aligned} \quad (3.2)$$

for all $x \in \mathbb{R}^n$, where $W(x)$ is a positive function. The objective is to create a closed

loop system with desirable stability properties rather than to analyse the properties of a given system.

A smooth positive definite radially unbounded function $V : \mathbb{R}^n \rightarrow \mathbb{R}_+$ is called a control Lyapunov function (CLF) [70, 110] for (3.1) if

$$\inf_{u \in \mathbb{R}} \left\{ \frac{\partial V(x(t))}{\partial x(t)} \cdot f(x(t), u(t)) \right\} < 0, \quad \forall x \neq 0. \quad (3.3)$$

The existence of a CLF is equivalent to global asymptotic stabilisability.

For systems affine in control

$$\frac{dx(t)}{dt} = f(x(t)) + g(x(t))u(x(t)), \quad (3.4)$$

the CLF inequality becomes

$$L_f V + L_g V u < 0, \quad (3.5)$$

where $L_f V = \frac{\partial V(x(t))}{\partial x(t)} f(x(t))$ and $L_g V = \frac{\partial V(x(t))}{\partial x(t)} g(x(t))$ are the Lie derivatives. The inequality is only satisfied iff

$$L_g V = 0 \implies L_f V < 0, \quad \forall x \neq 0. \quad (3.6)$$

There are two main questions which will be addressed in the following sections:

1. How to construct the control law?
2. How to construct the CLF?

3.1.2 Inverse Optimal Control

Here it is explained how to get a control law for a given CLF.

A particular optimal stabilising control law u_S is given by Sontag's formula [115, 117, 70, 110],

$$u_S = \begin{cases} - \left(c_0 + \frac{a(x) + \sqrt{a^2 + (b^T(x)b(x))^2}}{b^T(x)b(x)} \right) b(x) & , \quad b(x) \neq 0 \\ 0 & , \quad b(x) = 0; \end{cases} \quad (3.7)$$

where $a(x) = L_f V(x)$, $b(x) = (L_g V(x))^T$, and $c_0 \in \mathbf{R}_+$.

u_S is optimal, because it minimizes the cost function

$$J = \int_0^\infty \left(\frac{1}{2} p(x) b^T(x) b(x) + u_s^T \frac{1}{2p(x)} u_s \right) dt \quad (3.8)$$

if $p(x)$ is defined by the following equation:

$$p(x) = \begin{cases} \left(c_0 + \frac{a(x) + \sqrt{a^2 + (b^T(x)b(x))^2}}{b^T(x)b(x)} \right) & , \quad b(x) \neq 0 \\ c_0 & , \quad b(x) = 0; \end{cases} \quad (3.9)$$

The control law (3.7) is continuous at $x = 0$ iff the CLF satisfies the small control property: for each $\epsilon > 0$, we can find a $\delta(\epsilon) > 0$ such that, if $x \neq 0$ satisfies $\|x\| < \delta$, there is some u_s with $\|u_s\| \leq \epsilon$ such that $L_f V(x) + (L_g V)^T(x)u_s < 0$.

The approach is called inverse optimal approach because a stabilising feedback is designed first and then shown to be optimal for a cost functional of the form $J = \int_0^\infty (l(x) + u_s^T R(x)u_s) dt$. The problem is inverse because the functions $l(x) \geq 0$ and $R(x) > 0$ are determined after finding the controller u_s , rather than a priori chosen by the designer. The controller u_s is the inverse optimal control of the system (3.4) if:

- it guarantees asymptotic stability of the system (3.4)
- it fulfills the condition

$$u_s(x) = -\frac{1}{2}R(x)^{-1}(L_g V(x))^T$$

where $V(x)$ is a positive semidefinite function with the property

$$\dot{V} |_{u=\frac{1}{2}u_s} = L_f V + \frac{1}{2}L_g V u \leq 0$$

without explicitly solving the Hamilton Jacobi Bellmann equation (HJB) [66, 110]

$$l(x) + L_f V(x) - \frac{1}{4}V(x)R(x)^{-1}(L_g V(x))^T = 0, \quad V(0) = 0. \quad (3.10)$$

Note that in general Eq. (3.10) cannot be solved explicitly.

For the general case, Sontag's control law guarantees a sector margin $(\frac{1}{2}, \infty)$ (cf. Definition B.0.10). This means that the loop gain can be reduced by 0.5 or increased to infinity without losing Global Asymptotic Stability (GAS). Achieving a disc margin (cf. Definition B.0.11) in general is not guaranteed. However, for the scalar case (first order system) it can be shown that Sontag's control law does achieve a disc margin $D(\frac{1}{2})$. Possessing a disc margin $D(\frac{1}{2})$ implies that a sector margin $(\frac{1}{2}, \infty)$ exists. In addition the control system can tolerate unmodelled input or output dynamics which do not change the relative degree. For fast unmodelled dynamics of relative degree one stability will be preserved in a certain region of attraction. For higher order cases a disc margin can be achieved by domination re-design as described in [110].

The main task of the inverse optimal design is the construction of positive (semi)definite functions whose time-derivatives can be rendered negative semidefinite by feedback control. This function becomes the optimal value function.

3.1.3 Nonlinear Adaptive Backstepping

In the following it will be explained how to construct a CLF for a parametric strict feedback system.

Finding a Lyapunov function has a simple solution for first order systems that are affine in control. It is very difficult for the general higher order case. Integrator backstepping, presented in [70] provides a systematic method to stabilisation of nonlinear systems in strict feedback form. The idea of (adaptive) backstepping is to design a controller recursively by considering some of the state variables as "virtual controls" and designing for them intermediate control laws. Since parameters are unknown, this task is solved by an adaptive controller consisting of the control law and the parameter update law. This design has also some disadvantages

- There is no freedom for designing parameter update laws.
- When many parameters are unknown the dynamic order of the controller is high.
- For higher-order systems its nonlinear expressions become increasingly complex due to a interaction between the estimator and the control law.

These drawbacks could be removed by a modular design where any stabilising controller can be combined with any estimator. The major obstacle is that it relies on certainty equivalence. The weakness of certainty equivalence can be overcome by input-to-state-stability (ISS) controllers or small gain controllers [70].

The constructive adaptive backstepping design method [70] starts with the stabilisation of a first order subsystem and step by step increases the order of considered subsystems. Consider the adaptive tracking problem for a parametric strict-feedback system

$$\begin{aligned}
 \dot{x}_1 &= x_2 + \varphi_1(x_1)^T \theta \\
 \dot{x}_2 &= x_3 + \varphi_2(x_1, x_2)^T \theta \\
 &\vdots \\
 \dot{x}_{n-1} &= x_n + \varphi_{n-1}(x_1, x_2, \dots, x_{n-1})^T \theta \\
 \dot{x}_n &= \beta(x)u + \varphi_n(x)^T \theta \\
 y &= x_1
 \end{aligned} \tag{3.11}$$

where $\theta \in \mathbb{R}^p$ is a vector of unknown constant parameters and the input nonlinearity $\beta(x)$ and the state dependent function

$$F = [\varphi_1(x), \dots, \varphi_n(x_1 \dots x_n)]$$

are smooth nonlinear functions taking arguments in \mathbb{R}^n . It has been shown that in a tuning function adaptive controller for such a system the adaptive control law and parameter update law takes the following form

$$u = \frac{1}{\beta(x)} \left[\alpha_n(x, \hat{\theta}, \bar{y}_r^{(n-1)}) + y_r^{(n)} \right] \quad (3.12)$$

$$\dot{\hat{\theta}} = \Gamma \tau_n(x, \hat{\theta}, \bar{y}_r^{(n-1)}) \quad (3.13)$$

where y_r is the reference signal to be tracked by the output y and

$$\bar{y}_r^{(i)} = (y_r, \dot{y}_r, \dots, y_r^{(i)}).$$

The control law and the tuning functions are given recursively by

$$z_i = x_i - y_r^{(i-1)} - \alpha_{i-1} \quad (3.14)$$

$$\begin{aligned} \alpha_i(\bar{x}_i, \hat{\theta}, \bar{y}_r^{(i-1)}) &= -z_{i-1} - c_i z_i - w_i^T \hat{\theta} + \sum_{k=1}^{i-1} \left(\frac{\partial \alpha_{i-1}}{\partial x_k} x_{k+1} + \frac{\partial \alpha_{i-1}}{\partial y_r^{(k-1)}} y_r^{(k)} \right) \\ &\quad - \kappa_i |w_i|^2 z_i + \frac{\partial \alpha_{i-1}}{\partial \hat{\theta}} \Gamma \tau_i + \sum_{k=2}^{i-1} \frac{\partial \alpha_{k-1}}{\partial \hat{\theta}} \Gamma w_i z_k \end{aligned} \quad (3.15)$$

$$\tau_i(\bar{x}_i, \hat{\theta}, \bar{y}_r^{(i-1)}) = \tau_{i-1} + w_i z_i \quad (3.16)$$

$$w_i(\bar{x}_i, \hat{\theta}, \bar{y}_r^{(i-1)}) = \varphi_i - \sum_{k=1}^{i-1} \frac{\partial \alpha_{i-1}}{\partial x_k} \varphi_k \quad (3.17)$$

$$i = 1 \dots n \quad (3.18)$$

$$\bar{x}_i = (x_1, \dots, x_i), \quad (3.19)$$

$$\alpha_0 = 0 \quad (3.20)$$

$$\tau_0 = 0 \quad (3.21)$$

$$c_i > 0 \quad (3.22)$$

The control law together with the parameter update law render the time derivative of the Lyapunov function

$$\dot{V}_n = \frac{1}{2} z^T z + \frac{1}{2} \tilde{\theta}^T \Gamma^{-1} \tilde{\theta} \quad \text{with} \quad \tilde{\theta} = \theta - \hat{\theta} \quad (3.23)$$

negative semidefinite:

$$\dot{V}_n = - \sum_{k=1}^n c_k z_k^2 - \sum_{k=i}^n \kappa_i |w_i|^2 z_i^2 \leq -c_0 |z|^2 \quad \text{where} \quad c_0 = \min_{1 \leq i \leq n} c_i \quad (3.24)$$

The resulting closed loop system is of the form

$$\dot{z} = Az + W\tilde{\theta} \quad (3.25)$$

$$A = \begin{bmatrix} -c_1 - \kappa_1|w_1|^2 & 1 & 0 & \cdots & 0 \\ -1 & -c_2 - \kappa_2|w_2|^2 & 1 + \sigma_{23} & \cdots & \sigma_{2n} \\ 0 & -1 - \sigma_{23} & \ddots & \ddots & \vdots \\ \vdots & \vdots & \ddots & \ddots & 1 + \sigma_{n-1,n} \\ 0 & -\sigma_{2n} & \cdots & -1 - \sigma_{n-1,n} & -c_n - \kappa_n|w_n|^2 \end{bmatrix}$$

$$W = \begin{bmatrix} w_1^T \\ \vdots \\ w_n^T \end{bmatrix} \quad (3.26)$$

$$\sigma_{ik} = -\frac{\partial \alpha_{i-1}}{\partial \hat{\theta}} \Gamma w_k \quad (3.27)$$

where

$$\tilde{\theta} = \theta - \hat{\theta} \quad (3.28)$$

denotes the parameter estimation error and the matrices A and W depend on the state x , the tracking signal y_r and the parameter estimate $\hat{\theta}$.

It is a well known fact that for this adaptive control scheme the transient performance can be improved by increasing any of the design parameters c_i , κ_i and Γ .

The control law α_i is augmented by so called nonlinear damping terms $-\kappa_i|w_i|^2 z_i$ [70]. This way a strengthening of the negativeness of the new time derivative of the Lyapunov function is obtained. The controller gain gets selectively high to overcome disturbances. In absence of adaptation nonlinear damping can be still used to render the system ISS provided that a bound on the parameter error is known. In this case the system states are driven to a residual set. Since the described nonlinear damping strategy is based on domination by taking the square of the nonlinear functions w_i the resulting controller gain may become very large. It has therefore been suggested to use damping functions that contain the norms rather than the squares of norms:

$$s_i = \kappa_i|w_i| + g_i \left| \frac{\partial \alpha_i}{\partial \hat{\theta}^2} \right| \quad (3.29)$$

This type of nonlinear damping is employed in weak ISS-controllers [70].

In practical applications however, high gain should be avoided as there are always unmodelled dynamics, noise or even time delays (related to computer implementation) in the system which may lead to instability if the loop gain is too high. One method avoiding high gain in the backstepping procedure is to avoid cancellations of stabilising terms [70, 110].

Other strategies of counteracting uncertainties are highly desirable. In the following, two methods for a transient improvement of the controller will be given. The reference trajectory initialisation reduces transients by initialisation of the initial controller states while the multiple model and switching approach uses external information to reduce the uncertainty of the parameter in a discontinuous way.

Reference trajectory initialisation Reference trajectory initialisation is a tool for improving the transients in adaptive tuning function control systems [70]. The goal of adaptation is to reduce uncertainty, that is, to make $\tilde{\theta}(t)$ smaller. It has been shown that $\tilde{\theta}^T(t)\Gamma\tilde{\theta}(t) \leq 2V_n(t) \leq 2V_n(0)$, that is,

$$\tilde{\theta}^T(t)\Gamma\tilde{\theta}(t) \leq z(0)^T z(0) + \tilde{\theta}^T(0)\Gamma\tilde{\theta}(0).$$

This shows that a possibility for reducing $\tilde{\theta}(t)$ lies in $z(0)$. If $z(0)$ is set to zero by an appropriate initialisation of the reference trajectory, transients due to $\tilde{\theta}(t)$ will be damped.

Reference trajectory resetting can be applied most easily in the case where y_r and its derivative are generated by a linear reference model

$$y_r = G_m(s)r(s) = \frac{k_m}{s^n + m_{n-1}s^{n-1} + \dots + m_0}r(s) \quad (3.30)$$

realised in phase-canonic form where the derivatives of y_r are available as the states of the reference model $y_r^{(i)} = x_{m,i+1}$, $i = 0, \dots, n - 1$. The reference model is driven by some external reference input signal $r(t)$ (see Fig. (3.1)). For the following calculations, the existence of a reference model is assumed since the states of such a model can be reset directly. In the other case where y_r and its derivatives are gener-

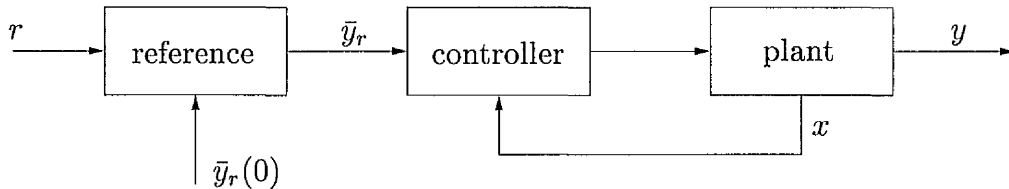
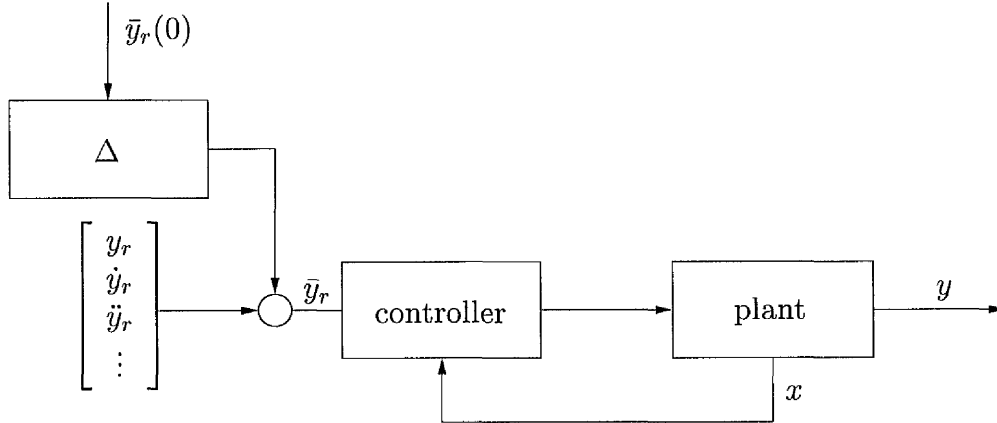


Figure 3.1: Trajectory initialisation with reference model

ated externally the reset is accomplished by modification of the reference signal using the output $\delta, \delta^{(1)}, \dots, \delta^{(n-1)}$ of an additional linear asymptotically stable autonomous system (see Fig. (3.2)).

$$y_{rmod}^{(i)} = y_r^{(i)} + \delta^{(i)} \quad (3.31)$$


 Figure 3.2: Trajectory initialisation with given reference signal y_r

In fact, by resetting the n values

$$y_r(0), \dot{y}_r(0), \dots, y_r^{(n-1)}(0)$$

an additional degree of freedom is obtained which enables us to set $z(0) = 0$. From Eq. (3.14) it can be seen that $z(0) = 0$ requires the solution of set of equations

$$\begin{aligned} y_r(0) &= x_1(0) \\ \dot{y}_r(0) &= x_2(0) - \alpha_1(x_1(0), \hat{\theta}(0), y_r(0)) \\ \ddot{y}_r(0) &= x_3(0) - \alpha_1(x_1(0), x_2(0), \hat{\theta}(0), y_r(0), \dot{y}_r(0)) \\ &\vdots \\ y_r^{(i-1)}(0) &= x_i(0) - \alpha_{i-1}(x_1(0), \dots, x_{i-1}(0), \hat{\theta}(0), y_r(0), \dots, y_r^{(i-2)}(0)) \end{aligned} \quad (3.32)$$

It can be shown [70] that the solution to these equations does not depend on the controller parameters.

Multiple model and switching A hybrid strategy is provided by the multiple model and switching approach, where additional information on parameter uncertainties is used to instantaneously reset the parameter estimate $\hat{\theta}$ of the adaptive controller. In the following section the properties of parameter resetting of adaptive controllers will be investigated. This is necessary in order to avoid erroneous resetting that destroys stability.

3.2 Stability analysis of parameter resetting

Suppose the best estimate of a fast hybrid estimation algorithm is

$$\hat{\theta}^+ = \hat{\theta}_j. \quad (3.33)$$

Then a decision has to be made whether or not to use this additional information. In the case when the new estimate is used the current continuous estimate $\hat{\theta}^-$ will be discarded and the continuous adaptation law (3.13) reset to the new value. This resetting decision should not be based on the modelling performance alone. It should also be guaranteed that the control performance and in particular the transient behaviour is improved via resetting.

In between the resetting events the parameter estimate will still be governed by the continuous adaptation law and it will thus be piecewise continuous. This will result in discontinuous control and adaptation laws, which means discontinuous switching of the actually continuous parameter adaptation $\hat{\theta}^-$ to the new value, thus resetting the integrator of Eq. (3.13). Between the switching events the continuous adaptation remains isolated. Since the state transformation in Eq. (3.14) is parameterised by $\hat{\theta}$ the states z_2, \dots, z_n will be discontinuous in time.

In the following the implications of such a resetting strategy will be studied.

In Lyapunov control, stability must not be destroyed by resetting the adaptation. Sufficient stability conditions will be derived from the results for discontinuous Lyapunov functions described in Sec. 2.2. These conditions have the disadvantage that they are not evaluable, because the system parameter θ is unknown. Nevertheless, possibilities are pointed out how these criteria can be analysed.

First and second order nonlinear adaptive controller examples will be given.

Consider the Lyapunov function (3.23) of the tuning function approach (cf. Sec. 3.1.3)

$$V_n(z, \theta, \hat{\theta}) = \frac{1}{2} z^T z + \frac{1}{2} \tilde{\theta}^T \Gamma^{-1} \tilde{\theta} \quad \text{with} \quad \tilde{\theta} = \theta - \hat{\theta} \quad (3.34)$$

For the tuning function approach it can easily be shown that Lyapunov's stability properties hold when no resetting is applied. When the parameter estimate $\hat{\theta}$ is reset, the state variable z changes discontinuously with time because it depends on $\hat{\theta}$. In order to obtain a sufficient condition for stability it remains to be analysed whether

$$\Delta V_n = V_n(z(\hat{\theta}^+), \theta, \hat{\theta}^+) - V_n(z(\hat{\theta}^-), \theta, \hat{\theta}^-) \leq 0 \quad (3.35)$$

holds. The states z^- and z^+ are computable. Thus, (3.35) could be checked provided θ was known. If (3.35) holds then a resetting of $\hat{\theta}$ from $\hat{\theta}^-$ to $\hat{\theta}^+$ is admissible. In

general, the state vector z will depend on $\hat{\theta}$ in a nonlinear way. In order to develop some stability criteria the following assumption may be made. It will be shown in later sections how this can be dropped:

Assumption 3.2.1 *Set the step change in parameter*

$$\Delta\hat{\theta} = \hat{\theta}^+ - \hat{\theta}^-. \quad (3.36)$$

There exist a matrix-valued function $M(z^-, \hat{\theta}^-, \bar{y}_r^{(i-1)})$ such that

$$(z^+)^T (z^+) \leq (z^- + M\Delta\hat{\theta})^T (z^- + M\Delta\hat{\theta}) \quad (3.37)$$

for some bounded $\Delta\hat{\theta} \in D \subseteq \mathbb{R}^p$

Under assumption 3.2.1 the following bound on the step change of the Lyapunov function (3.23) can be given:

$$\begin{aligned} \Delta V_n &= (z^+)^T (z^+) + (\theta - \hat{\theta}^+)^T \Gamma^{-1} (\theta - \hat{\theta}^+) \\ &\quad - (z^-)^T (z^-) - (\theta - \hat{\theta}^-)^T \Gamma^{-1} (\theta - \hat{\theta}^-) \\ \Delta V_n &\leq 2 \left[M^T z^- - \Gamma^{-1} \tilde{\theta}^- \right]^T \Delta\hat{\theta} + \Delta\hat{\theta}^T [M^T M + \Gamma^{-1}] \Delta\hat{\theta} \end{aligned} \quad (3.38)$$

For positive definite $M^T M + \Gamma^{-1} > 0$ the sufficient condition for stability $\Delta V_n \leq 0$ is satisfied inside the hyper-ellipse

$$2 \left[M^T z^- - \Gamma^{-1} \tilde{\theta}^- \right]^T \Delta\hat{\theta} + \Delta\hat{\theta}^T [M^T M + \Gamma^{-1}] \Delta\hat{\theta} = 0 \quad (3.39)$$

The set of admissible parameter changes $\Delta\hat{\theta}$ depends on the state z and on the parameter error $\tilde{\theta}$. Thus, in general, additional information on the estimation error is necessary to check the admissibility of $\Delta\hat{\theta}$. It can be easily verified that even in the case when $\hat{\theta}$ steps from $\hat{\theta}^-$ to the *correct parameter value* $\hat{\theta}^+ = \theta$ the condition for stability is not necessarily satisfied because in this case the requirement would be:

$$2(z)^T M\tilde{\theta} + \tilde{\theta}^T (M^T M - \Gamma^{-1})\tilde{\theta} \leq 0. \quad (3.40)$$

Assumption 3.2.1 can be dropped by utilising the properties of the reference trajectory initialisation.

Reference trajectory resetting

The condition (3.35) on $\Delta\hat{\theta}$ can be considerably simplified when resetting of the reference trajectory y_r is used in combination with parameter resetting. Reference trajectory initialisation is originally a tool for improving the transients in adaptive tuning function control systems (cf. Sec. 3.1.3).

The corresponding step change in the Lyapunov function with reference trajectory resetting is

$$\begin{aligned}\Delta V_n &= (\theta - \hat{\theta}^+)^T \Gamma^{-1} (\theta - \hat{\theta}^+) \\ &\quad - (z^-)^T (z^-) - (\theta - \hat{\theta}^-)^T \Gamma^{-1} (\theta - \hat{\theta}^-) \\ &= \Delta \hat{\theta}^T \Gamma^{-1} \Delta \hat{\theta} - 2 (\tilde{\theta}^-)^T \Gamma^{-1} \Delta \hat{\theta} - (z^-)^T (z^-)\end{aligned}\quad (3.41)$$

for which we can obtain a controller independent upper bound

$$\Delta V_n \leq \Delta \hat{\theta}^T \Gamma^{-1} \Delta \hat{\theta} - 2 (\tilde{\theta}^-)^T \Gamma^{-1} \Delta \hat{\theta}.\quad (3.42)$$

For low order systems (3.42) can be shown to have a geometric interpretation.

Application to a first order system

Consider the tracking control of the first order system

$$\dot{x}_1 = \varphi_1(x_1)\theta + u.\quad (3.43)$$

An adaptive tuning function controller is simply

$$u = -\varphi_1(x_1)\hat{\theta} - c_1 z_1 - \dot{y}_r\quad (3.44)$$

$$\dot{\hat{\theta}} = \gamma z_1 \varphi_1(x_1) = \gamma \tau_1\quad (3.45)$$

$$z_1 = x_1 - y_r.\quad (3.46)$$

This controller is based on the control Lyapunov function

$$V = \frac{1}{2} z_1^2 + \frac{1}{2\gamma} (\theta - \hat{\theta})^2\quad (3.47)$$

and renders the derivative of the Lyapunov function

$$\dot{V} = -c_1 z_1^2 \leq 0$$

negative semi-definite. The closed loop system is given by

$$\dot{z}_1 = -c_1 z_1 + \varphi_1(x_1)\tilde{\theta}.\quad (3.48)$$

The time derivative of the squared error along the solution of (3.48) is

$$\begin{aligned}\frac{d}{dt} \left(\frac{1}{2} z_1^2 \right) &= z_1 \dot{z}_1 \\ &= -c_1 z_1^2 + z_1 \varphi_1(x_1)\tilde{\theta}.\end{aligned}\quad (3.49)$$

For the rest of the discussion of the first order case we assume that $\varphi_1(x_1) > 0$. This assumption is not necessary for the approach in general but it simplifies the switching law considerably.

For the first order system (3.43) and the Lyapunov function (3.47) we obtain by the use of Eq. (3.38) the following sufficient stability condition:

$$\begin{aligned} \Delta V &= V^+ - V^- \\ &= \frac{1}{2\gamma} (\hat{\theta}^+ - \hat{\theta}^-)^2 - \frac{1}{\gamma} \left((\theta - \hat{\theta}^-) (\hat{\theta}^+ - \hat{\theta}^-) \right) \leq 0. \end{aligned} \quad (3.50)$$

This gives the following bounds on the step change in the parameter estimate:

$$\text{sgn}(\Delta \hat{\theta}) = \text{sgn}(\tilde{\theta}^-) \quad (3.51)$$

$$|\Delta \hat{\theta}| \leq 2 |\tilde{\theta}^-|. \quad (3.52)$$

Fig. 3.3 shows the meaning of the conditions. The Lyapunov function (3.47) is displayed but only the dependence of the adaptation error $\tilde{\theta}$. It has a minimum at $\tilde{\theta} = \theta - \hat{\theta} = 0$. A resetting of the adaptation $\hat{\theta}^-$ to $\hat{\theta}^+$, is equal to $\tilde{\theta}^-$ to $\tilde{\theta}^+$. It applies

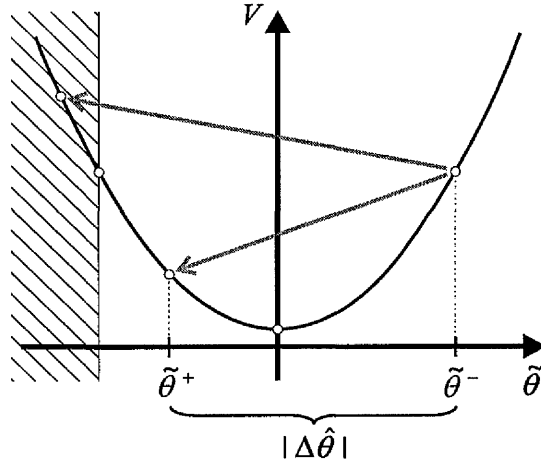


Figure 3.3: Parameter jump in the Lyapunov function

$$\tilde{\theta}^+ - \tilde{\theta}^- = -\Delta \hat{\theta}. \quad (3.53)$$

The sign condition (3.51) ensures a jump towards the minimum of the parabola while the absolute value condition (3.52) ensures that the jump is not too large.

In general, condition (3.52) cannot be verified without additional information on the parameter estimate. However a switching law $S(z_1, \Delta \hat{\theta})$ can be designed such that condition (3.51) holds.

Using this switching law the parameter resetting law is constructed in the following way

$$\begin{aligned}\hat{\theta} &= \hat{\theta}^- + (\hat{\theta}^+ - \hat{\theta}^-) S(z_1, \Delta\hat{\theta}) \\ &= \hat{\theta}^- + \Delta\hat{\theta} S(z_1, \Delta\hat{\theta})\end{aligned}\quad (3.54)$$

where S takes the values 1 or 0 according to the following set of inequalities

$$\begin{aligned}S &= 1 \quad \text{whenever} && \begin{cases} z_1 > \varepsilon_1 & \wedge & \Delta\hat{\theta} > \varepsilon_2 \\ & & \vee \\ z_1 < -\varepsilon_1 & \wedge & \Delta\hat{\theta} < -\varepsilon_2 \end{cases} \\ S &= 0 \quad \text{elsewhere}\end{aligned}\quad (3.55)$$

The switching law is depicted in Fig. 3.4.

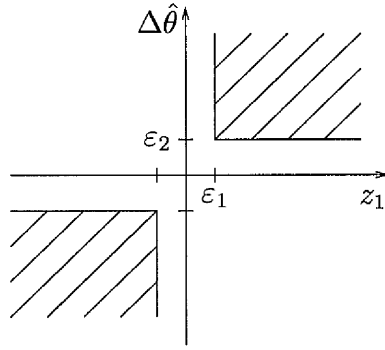


Figure 3.4: Parameter resetting law

Condition (3.54) states that resetting occurs whenever the magnitude of the control error z_1 exceeds some threshold ε_1 and at the same time there is a significant discrepancy between continuous parameter estimate and multiple model parameter estimate having the same sign as the control error.

Note that due to the assumption that φ is always positive we obtain from the closed loop error Eq. (3.48):

$$\dot{z}_1 z_1 > 0 \quad \text{implies} \quad \text{sgn}(\dot{z}_1) = \text{sgn}(\tilde{\theta}) \quad (3.56)$$

Thus, provided that $|z_1|$ is increasing while it crosses the threshold ε_1 the sign of \dot{z}_1 is a direct indicator of the sign of the parameter error $\tilde{\theta}$. In the general case, the sign of φ will be known and the resetting law can be modified accordingly.

This leads us to the following new theorem:

Theorem 3.2.1 1. Consider the first order system (3.43) together with the continuous control law (3.44) and the update law (3.45). Assuming $\varphi > 0$, $\gamma > 0$ and $c_1 > 0$. If the parameter $\hat{\theta}$ is reset under the condition

$$z_1 \text{sgn}(\dot{z}_1) > \varepsilon_1 \bigwedge z_1 \Delta \hat{\theta} > \varepsilon_1 \varepsilon_2, \quad \varepsilon_1 > 0, \varepsilon_2 > 0 \quad (3.57)$$

then, the sign condition (3.51) is satisfied.

2. Provided the sign condition is satisfied, then a decrease of V in Eq. (3.47) at the switching instant is obtained provided that

$$|\Delta \hat{\theta}| < 2 |\tilde{\theta}^-| \quad (3.58)$$

holds. Thus a sufficient condition for stability is satisfied.

3. If to the contrary

$$|\Delta \hat{\theta}| \geq 2 |\tilde{\theta}^-| \quad (3.59)$$

holds then the control error z_1 is driven towards zero as long as $|z_1| > \varepsilon_1$ despite of the increase in value of V .

Proof The first and second part of the theorem has been proven above. The sign condition (3.56) ensures a jump towards the minimum of the Lyapunov function parabola while the absolute value condition (3.52) ensures that the jump is not to large.

If the assumptions of the third part of the theorem hold then, outside $|z_1| > \varepsilon_1$ we have along the solutions of the closed loop equation:

$$\begin{aligned} \frac{d}{dt} \left(\frac{1}{2} z_1^2 \right) &= z_1 \dot{z}_1 \\ &= z_1 \left(-c_1 x_1 + \varphi_1 \tilde{\theta} \right) \\ &= -c_1 z_1^2 + x_1 \varphi_1(x_1) \tilde{\theta} \\ &= -c_1 z_1^2 + z_1 \varphi_1(x_1) \left[\tilde{\theta}^- - \Delta \hat{\theta} S(y, \Delta \hat{\theta}) \right] \\ &\leq -c_1 z_1 + |z_1 \varphi_1(x_1)| \left[|\tilde{\theta}^-| - |\Delta \hat{\theta}| \right] < 0 \end{aligned} \quad (3.60)$$

due to (3.59) which implies that z_1 is driven towards the origin. ■

As a remark, one might note, that case 3 of Theorem 3.2.1 implies stability but possibly with reduced transient performance and chattering.

The negative jump in the Lyapunov function could be interpreted as improved transient performance. This follows from the dependency of transient performance of the tuning function approach on the initial conditions which has been analysed in [70]. First a bound on the \mathcal{L}_2 norm of the state of the system is derived.

Theorem 3.2.2 *The \mathcal{L}_2 transient performance of the adaptive system (3.11), (3.12), (3.13) the following inequality holds [70]*

$$\|z\|_2^2 \leq \frac{|\tilde{\theta}(0)|}{\sqrt{2c_0\gamma}} + \frac{1}{\sqrt{2c_0}} |z(0)|. \quad (3.61)$$

Proof From (3.24), we have

$$\dot{V}_n \leq -c_0 |z|^2. \quad (3.62)$$

Since $V_n = \frac{1}{2}|z|^2 + \frac{1}{2\gamma}|\tilde{\theta}|^2$ is nonincreasing and bounded from below by zero, it has a limit as $t \rightarrow \infty$, so

$$\begin{aligned} \|z\|_2^2 &= \int_0^\infty |z(\tau)|^2 d\tau \leq \int_0^\infty \dot{V}_n(\tau) d\tau \\ &= \frac{1}{c_0} V_n(0) - \frac{1}{c_0} V_n(\infty) \leq \frac{1}{c_0} V_n(0) \\ &\leq \frac{1}{c_0} \left(\frac{1}{2} |z(0)|^2 + \frac{1}{2\gamma} |\tilde{\theta}(0)|^2 \right), \end{aligned} \quad (3.63)$$

which implies (3.62).

By applying trajectory resetting (3.32) we set $z(0) = 0$ and obtain

$$\|z\|_2 \leq \frac{|\tilde{\theta}^+|}{\sqrt{2c_0\gamma}}. \quad (3.64)$$

Please note that the transient performance depends on $\tilde{\theta}^+$ but not on z .

Application to a second order system

Consider the second order system with one parameter

$$\begin{aligned} \dot{x}_1 &= x_2 + \varphi(x_1)\theta \\ \dot{x}_2 &= u. \end{aligned} \quad (3.65)$$

Designing the tuning function controller [70] for such a system requires one backstep. Setting

$$\begin{aligned} z_1 &= x_1 - x_r \\ z_2 &= x_2 - \alpha_1(x_1, \hat{\theta}, x_r, \dot{x}_r) - \dot{x}_r \end{aligned} \quad (3.66)$$

and assuming that the parameter estimate $\hat{\theta}$ can vary discontinuously with time we will have also discontinuous changes with time in α_1 and z_2 and in the corresponding Lyapunov function

$$V = \frac{1}{2}z_1^2 + \frac{1}{2}z_2^2 + \frac{1}{2\gamma}\tilde{\theta}^2 \quad (3.67)$$

The step change in the Lyapunov function can be expressed as

$$\begin{aligned}\Delta V = V^+ - V^- &= z_2^- \varphi_1(x_1) \Delta \hat{\theta} + \frac{1}{2} \varphi_1^2(x_1) \Delta \hat{\theta}^2 - \frac{1}{\gamma} \tilde{\theta}^- \Delta \hat{\theta} + \frac{1}{2\gamma} \Delta \hat{\theta}^2 \\ &= \frac{1}{2} \left(\frac{1}{\gamma} + \varphi_1^2(x_1) \right) \Delta \hat{\theta}^2 - \left(\frac{1}{\gamma} \tilde{\theta}^- - z_2^- \varphi_1(x_1) \right) \Delta \hat{\theta}.\end{aligned}\quad (3.68)$$

This corresponds with Assumption 3.2.1 where

$$\begin{aligned}z^+ &= z^- + M \Delta \hat{\theta} \\ M &= \begin{pmatrix} 0 \\ \varphi_1(x_1) \end{pmatrix}, \quad M^T M = \varphi_1^2(x_1).\end{aligned}$$

Assuming $\varphi(x_1) \geq 0$ we obtain the sufficient stability condition

$$\Delta \hat{\theta}^2 - 2 \frac{\tilde{\theta}^- - \gamma z_2^- \varphi_1(x_1)}{1 + \gamma \varphi_1^2(x_1)} \Delta \hat{\theta} \leq 0. \quad (3.69)$$

Similar to the first order case a switching law can be derived from the closed loop error equations

$$\begin{aligned}\dot{z}_1 &= -c_1 z_1 + z_2 + w_1 \tilde{\theta} \\ \dot{z}_2 &= -z_1 - c_2 z_2 + w_2 \tilde{\theta}\end{aligned}$$

Under the condition $w_i > 0$ it is obtained

$$[\dot{z}_1 > 0 \wedge -c_1 z_1 + z_2^- < 0] \vee [\dot{z}_2 > 0 \wedge -c_2 z_2^- + z_1^- < 0] \quad \text{implies} \quad \tilde{\theta} > 0 \quad (3.70)$$

$$[\dot{z}_1 < 0 \wedge -c_1 z_1 + z_2^- > 0] \vee [\dot{z}_2 < 0 \wedge -c_2 z_2^- + z_1^- > 0] \quad \text{implies} \quad \tilde{\theta} < 0$$

The reset conditions require the information whether the states of z_1 and z_2 cross some threshold from above or below. No explicit knowledge of the derivatives of the states is required. In case of noisy state measurement multiple crossing of the threshold may occur, however, by imposing an additional threshold on $\Delta \hat{\theta}$ a hysteresis is introduced and chattering cannot occur.

3.3 Hybrid Observer and Estimation

Since system states and parameters often cannot be measured, observation and estimation algorithms are required. Also, parameter estimation can be formulated as nonlinear observation problem if the time behaviour of the parameter can be modelled. In the simplest case of a constant parameter θ such a model is $\dot{\theta} = 0$. For parameter estimation an observer can be used, if the uncertain parameter is considered as an augmented state.

Throughout the thesis full state measurement is assumed. Only the parameters need to be observed.

Several contributions to nonlinear observer design are reported in the literature. Isidori [69, 53] deals with nonlinear systems for which a change of variables can be found such that they have their nonlinearities only as functions of the measured output. A Lyapunov based approach for systems where the nonlinearity does not depend on the measured states can be found in [104, 105, 32]. The quadratic Lyapunov function guarantees the design of a stable error dynamics. For systems with monotonic nonlinearities¹ in the unmeasured states an observer design is given in [15].

A single observer will adapt to the environment represented by the unknown parameter value [42]. However, the slowness of adaptation can result in large transients [70]. Hybrid algorithms can be used to speed up the estimation transients [87, 88, 89, 84, 85, 90].

Using discontinuous output injection functions is common in sliding mode observers [35]. A hybrid observer using convergence information to switch between several discontinuous output injection functions for nonlinear systems has been reported in [73]. Lunze [76] gives sufficient conditions for stable error dynamics of linear observer for systems where the number of measured states varies. Parallel Kalman filters are used to detect failures [46] by using the residuals of the Kalman filter bank. Here the use of a set of observers with fixed output injection functions which can have considerably faster transients is proposed.

In this section non-stochastic methods for hybrid estimation will be considered.

For linear systems observability is characterised by the Kalman rank condition [30]. Observability conditions for nonlinear systems can be found in [95, 100]. The nonlinear system $\dot{x} = f(x) + g(x)u$, $x \in \mathbb{R}^n$ with the output $y = h(x)$ is locally observable in a

¹Monotonic means that the function is either nondecreasing or nonincreasing with respect to its arguments.

neighborhood of x_0 if

$$\text{rank} \begin{bmatrix} h(x) \\ L_f h(x) \\ \vdots \\ L_f^{n-1} h(x) \end{bmatrix} = n. \quad (3.71)$$

An observer can be described as a dynamic system that is driven by the output of another dynamic system with the property that the observer states converges to the states of the plant.

An observer for the nonlinear system $\frac{dx(t)}{dt} = f(x(t), u(t))$ with the output $y(t) = h(x(t), u(t))$ is a dynamic system with the observer state $\hat{x}(t)$, excited by the systems output $y(t)$, having the property that the error

$$e = x(t) - \hat{x}(t) \quad (3.72)$$

converges to zero [42]. One possible way to obtain that is to excite the observer with the so called residual:

$$r = y - \hat{y} = y - h(\hat{x}, u) \quad (3.73)$$

The observer equation becomes

$$\dot{\hat{x}} = f(\hat{x}, u) + k(y - h(\hat{x}, u), \hat{x}, u, y) \quad (3.74)$$

where k is a suitably chosen may be non-linear function called injection function.

Starting from an augmented observer for parameter estimation and multiple model parameter estimation a multiple model observer will be designed. In general the multiple model observer is a fast estimator for system structures. In the particular case the observer is used to determine an estimate for an uncertain parameter vector.

Disturbance Observer

Consider the parametric nonlinear system $\frac{dx(t)}{dt} = f(x(t), \theta, u(t))$ with the output $y(t) = h(x(t), \theta, u(t))$ where $\theta \in \mathbb{R}^r$ is a vector of unknown parameters or inputs.

It is assumed that the k_{th} derivative of $\theta(t)$, denoted by $\frac{\partial \theta^k(t)}{\partial t^k} \equiv 0 \quad \forall t$. The above observer can be modified to estimate both the states and the parameter. Define an augmented state vector x_{aug} as follows:

$$x_{aug} = \begin{bmatrix} x \\ \theta \\ \dot{\theta} \\ \vdots \\ \frac{\partial \theta^k}{\partial t^k} \end{bmatrix} \quad (3.75)$$

Then

$$\dot{x}_{aug} = \begin{bmatrix} \dot{x} \\ \dot{\theta} \\ \vdots \\ \frac{\partial \theta^{k-1}}{\partial t^{k-1}} \\ 0 \end{bmatrix} \quad (3.76)$$

and the observer can be designed for the augmented system (3.76) just as done for the original system. The augmented observer estimates both the states and the parameter or system inputs.

3.4 Multiple model parameter estimation

The presented method is based on the results described in [87, 88, 89, 90]. When multiple models are used to describe different environments the system can be identified by the analysis of the quality of each model.

Consider the nonlinear system $\dot{x} = f(x(t), u(t), \theta_i)$. Different environments can be described by different sets of parameters θ_i . If the environment changes can not be described only by parameter changes each model can have a different structure.

The structure of the system together with the multiple models is shown in Fig. 3.5. There are N models with their corresponding outputs \hat{y}_i . Each of the models represents one environment or at least one region where the parameter θ_i is valid. At any instant, some measure of the output error $e_i = \hat{y}_i - y$ of each model is determined ($i = 1, 2, \dots, N$). The minimum output error $\min\{e_i\}$ determines the valid corresponding model for the system and thus the valid parameter.

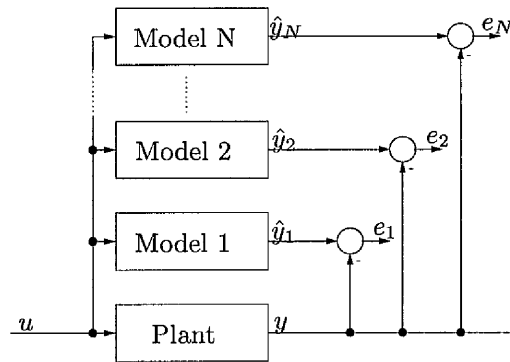


Figure 3.5: System and multiple models

The open loop estimation is not robust according to noise in the system. To achieve more robustness the error signal e_i needs to be filtered.

The following multiple model estimator and observer estimates parameters in a fast way. The estimate will later be used in a reset algorithm of the adaptive controller.

Multiple model estimation

The approach in [62] further referred as multiple model estimation (MME) uses a finite number of identical models each parameterised with fixed parameter hypotheses $\theta_1, \dots, \theta_k$. At each time instant the prediction error is used to find the best model. Contrary to the approach in [88] no adaptive models are used. To illustrate consider a linear parametric model of the form

$$y(t) = \zeta^T(t)\theta + \epsilon(t) \quad (3.77)$$

where θ is an unknown parameter vector, $y(t) \in \mathbb{R}^m$ is an output vector and $\zeta(t) \in \mathbb{R}^{p \times m}$ is a regressor matrix. Such a model can be constructed in many ways.

For example, consider a first order system $\dot{x} = \varphi^T(x)\theta + u + \nu$, define $y(t) = sH(s)x(t) - H(s)u(t)$, $\zeta(t) = H(s)\varphi(x(t))$ and $\epsilon(t) = H(s)\nu(t)$, where $H(s)$ is typically a lowpass or bandpass filter. The main purpose of this filter is to make transfer functions such as $sH(s)$ proper and, additionally to reduce the effect of high-frequency noise and low-frequency disturbances in the estimation model. The finite number of fixed parameter hypotheses θ_i are now assessed using the predictors

$$\hat{y}_i(t) = \zeta^T(t)\theta_i \quad (3.78)$$

for all $i = 1, 2, \dots, k$. Prediction errors are defined as

$$e_i(t) = y(t) - \hat{y}_i(t) = \zeta^T(t)(\theta - \theta_i) + \epsilon(t). \quad (3.79)$$

In order to achieve invertability, this equation is premultiplied by the matrix $\zeta(t)$ and integrated on the time interval from $t - T$ to t , where $T > 0$ is a finite time window:

$$\int_{t-T}^t \zeta(\tau)e_i(\tau)d\tau = \int_{t-T}^t \zeta(\tau)\zeta^T(\tau)d\tau(\theta - \theta_i) + \int_{t-T}^t \zeta(\tau)\epsilon(\tau)d\tau \quad (3.80)$$

Notice that all signals are defined to be zero for $t < 0$. Eq. (3.80) can be written as

$$d_i(t) = R(t)(\theta - \theta_i) + \delta(t) \quad (3.81)$$

with the following definitions:

$$d_i(t) = \int_{t-T}^t \zeta(\tau) e_i(\tau) d\tau \quad (3.82)$$

$$R(t) = \int_{t-T}^t \zeta(\tau) \zeta^T(\tau) d\tau \quad (3.83)$$

$$\delta(t) = \int_{t-T}^t \zeta(\tau) \epsilon(\tau) d\tau. \quad (3.84)$$

Assuming persistence of excitation, i.e. $R(t) > 0$, the following expression follows from (3.81) by inversion:

$$\theta - \theta_i = R^{-1}(t) (d_i(t) - \delta(t)). \quad (3.85)$$

Note that (3.85) relies on the invertability of (3.81), that is not valid for systems non-linear in the parameter. By finding the minimum of Eq. 3.85 the parameter estimate θ_i that fits best can be determined. The time window T should be selected to address the tradeoff between noise sensitivity, persistence of excitation and estimator transients. In general, a large T will reduce the effect of uncertainty, but at the cost of a delay in the convergence time.

In order to avoid the time delay of filtering a set of observers can be used instead as presented in the following section.

3.5 Multiple model observer

As explained in Sec. 3.1 a fast converging estimate of an unknown parameter provided by a multiple model observer approach can be used to avoid large transient errors in continuous adaptive control [64]. Quite similar to the multiple model estimation described in Sec. 3.4, the idea is to construct a finite set of parallel individual observers each designed for a fixed parameter value or a fixed plant structure respectively. Fig. (3.6) shows the structure of a multiple model observer parameter estimation. Each of the observer estimates the states of the system and is driven by the residual $e_{1i} = x_1 - \hat{x}_{1i}$. Since any mismatch between a single observer and the physical system will in general lead to an estimation error, this error can be used to determine the best observer for the actual system. In contrast to the use of observers for state reconstruction we are only interested in the error but not in the estimated state.

A performance index $Q_i(\hat{x}_i, y)$ is defined for each observer o_i . The performance index weighs the output error of the observer e_i , thus quantifying the mismatch between the

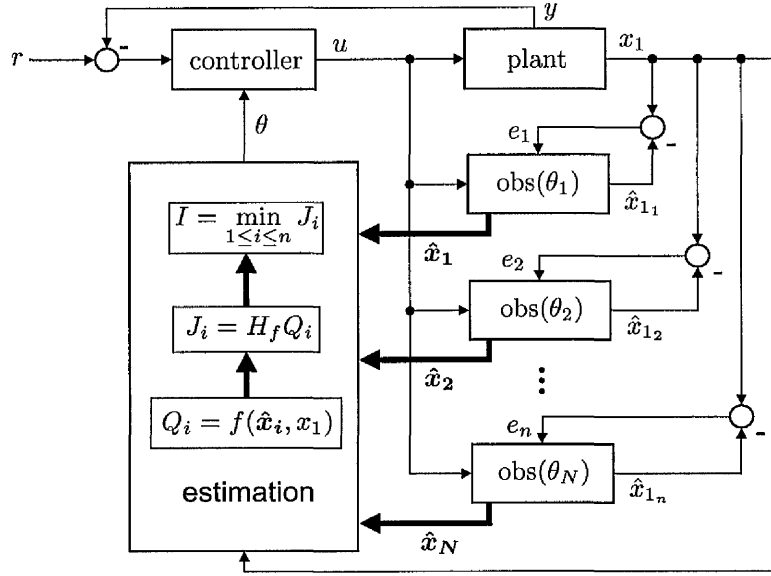


Figure 3.6: Multiple Model Observer parameter estimation

plant and the individual observer. A decision logic \mathfrak{E} is used to determine the best observer of the multiple observer \mathfrak{D} . \mathfrak{E} satisfies two purposes:

1. selecting the coefficient θ_i corresponding to the observer o_i with the best performance.
2. providing a mechanism that ensures a convergence of the estimator after a finite number of switches to the θ_j that is closest to the fixed real parameter θ .

The concept of multiple model observer (MMO) can be extended beyond parameter estimation. In its simplest form each individual observer stands for a discrete value θ_i , $i = 1, \dots, N$ covering the range of admissible parameter values.

Generally, the starting point is any observable system,

$$\begin{aligned} \dot{\mathbf{x}} &= \mathbf{f}(\mathbf{x}, \mathbf{u}, t) \\ \mathbf{f} : D_{\mathbf{f}} &\longrightarrow \mathbb{R}^n \\ D_{\mathbf{f}} &\subseteq \mathbb{R}^n \times \mathbb{R}^m \times \mathbb{R} \end{aligned} \quad (3.86)$$

where $\mathbf{x} \in \mathbb{R}^n$ are the states and $\mathbf{u} \in \mathbb{R}^m$ are the inputs of the system. The outputs of the system are

$$\begin{aligned} \mathbf{y} &= \mathbf{h}(\mathbf{x}, u) \\ \mathbf{h} : D_{\mathbf{h}} &\longrightarrow \mathbb{R}^p \\ D_{\mathbf{h}} &\subseteq \mathbb{R}^n \times \mathbb{R}^m. \end{aligned} \quad (3.87)$$

The multiple model observer consists of two parts:

1. The multiple observer \mathfrak{D} consists of a set of individual observers with different structure. Each particular individual observer observes the system (3.86).
2. The decision logic \mathfrak{E} analyses the information supplied by the multiple observer. The observer that is most appropriate to the present original system structure is selected due to a quality measure by the decision logic.

The set of observers together with the cost index based decision will be called multiple model observer (MMO).

3.5.1 A set of parallel observer

The multiple observer consists of a finite set \mathbf{O}_x of N individual state observers o_i observing the state vector $\mathbf{x} = (x_1, \dots, x_n)^T \in \mathbb{R}^n$ of the system 3.86:²

$$\mathbf{O}_x = \{o_i(\hat{\mathbf{x}}_i, \mathbf{y}, \mathbf{x}_{\text{mea}}, \mathbf{u}_i^*) \mid i \in \mathcal{I} = \{1, \dots, N\}\} \quad (3.88)$$

The index of the individual observer is denoted by i . Generally, these observers are nonlinear systems with different structure. The state vector $\hat{\mathbf{x}}_i$ of the observer i is calculated by the nonlinear mapping

$$\begin{aligned} \dot{\hat{\mathbf{x}}}_i &= \mathbf{o}_i(\hat{\mathbf{x}}_i, \mathbf{y}, \mathbf{x}_{\text{mea}}, \mathbf{u}_i^*) \\ \mathbf{o}_i : D_{\mathbf{o}_i} &\longrightarrow \mathbb{R}^{n'} \\ D_{\mathbf{b}_i} &\subseteq \mathbb{R}^n \times \mathbb{R}^p \times \mathbb{R}^{n_{\text{mea}}} \times \mathbb{R}^{m'} \end{aligned} \quad (3.89)$$

with the observer states $\hat{\mathbf{x}}_i$, the system outputs \mathbf{y} and optionally further measured states \mathbf{x}_{mea} or inputs \mathbf{u}_i^* of the original system. The output is

$$\hat{\mathbf{y}}_i = \mathbf{h}_i(\hat{\mathbf{x}}_i, u). \quad (3.90)$$

By the construction of N individual observers o_1, \dots, o_N the multiple observer gives N estimates $\hat{\mathbf{x}}_i \in \mathbb{R}^n$ of the original states vector \mathbf{x} .

Definition 3.5.1 (Multiple observer) *The multiple observer is a nonlinear mapping \mathfrak{D}*

$$\begin{aligned} \dot{\hat{\mathbf{X}}} &= \mathfrak{D}(\hat{\mathbf{X}}, \mathbf{y}, \mathbf{x}_{\text{mea}}, \mathbf{U}^*) \\ \mathfrak{D} : D_{\mathfrak{D}} &\longrightarrow \mathbb{R}^{(n,N)} \\ D_{\mathfrak{D}} &\subseteq \mathbb{R}^{(n,N)} \times \mathbb{R}^p \times \mathbb{R}^{n_{\text{mea}}} \times \mathbb{R}^{(m',N)}. \end{aligned} \quad (3.91)$$

²Observer refers in the context of the MMO to different variables: The MMO observes the model structure, the multiple observer the state vector.

where

$$\hat{\mathbf{X}} = (\hat{\mathbf{x}}_1, \dots, \hat{\mathbf{x}}_N) \in \mathbb{R}^{(n,N)} \quad (3.92)$$

denotes the states in matrix notation, $\mathbf{U}^* = (\mathbf{u}_1^*, \dots, \mathbf{u}_N^*) \in \mathbb{R}^{(p',N)}$ are the optional inputs in matrix notation and

$$\hat{\mathbf{Y}} = (\hat{\mathbf{y}}_1, \dots, \hat{\mathbf{y}}_N) \in \mathbb{R}^{(p,N)}. \quad (3.93)$$

is the output. The elements $\hat{\mathbf{x}}_i$ of the state matrix are calculated from Eq. (3.89), the output matrix \mathbf{y}_i from Eq. (3.90). The system output \mathbf{y} and the measurable states \mathbf{x}_{mea} are of the original system (3.86).

The rows of the state matrix $\hat{\mathbf{X}} = (x_{ij})$ cover the n system states and the columns the N observer.

3.5.2 Decision logic

In the decision logic \mathfrak{E} a cost index Q_i gives an estimated index of the best model structure. This is done on basis of the observation errors

$$\mathbf{e}_{i,y} = \mathbf{y} - \hat{\mathbf{y}}_i \quad (3.94)$$

$$\mathbf{e}_{i,\text{mea}} = \mathbf{x}_{\text{mea}} - \hat{\mathbf{x}}_{i,\text{mea}}, \quad (3.95)$$

where $\hat{\mathbf{x}}_{i,\text{mea}}$ consists of the measurable elements of the estimate $\hat{\mathbf{x}}_i$. With the cost function

$$\begin{aligned} \mathbf{q} : D_{\mathbf{q}} &\longrightarrow \mathbb{R}^N \\ D_{\mathbf{q}} &\subseteq \mathbb{R}^{(n,N)} \times \mathbb{R}^{(p,N)} \times \mathbb{R}^p \times \mathbb{R}^{n_{\text{mea}}} \end{aligned} \quad (3.96)$$

a cost vector for the N observer is obtained

$$\mathbf{q} = \mathbf{q}(\hat{\mathbf{X}}, \hat{\mathbf{Y}}, \mathbf{y}, \mathbf{x}_{\text{mea}}) = \begin{pmatrix} Q_1(\hat{\mathbf{x}}_1, \hat{\mathbf{y}}_1, \mathbf{y}, \mathbf{x}_{\text{mea}}) \\ \vdots \\ Q_N(\hat{\mathbf{x}}_N, \hat{\mathbf{y}}_N, \mathbf{y}, \mathbf{x}_{\text{mea}}) \end{pmatrix}. \quad (3.97)$$

The structure having the smallest cost index is selected as estimation of the physical system:

$$k = \underset{i \in \mathcal{I}}{\text{argmin}}(\mathbf{q}). \quad (3.98)$$

The argmin-operator (cf. Appendix B.0.6)

$$\text{argmin} : \mathbb{R}^N \longrightarrow \mathcal{I} \quad (3.99)$$

chooses the index $k \in \mathcal{I} = \{1, \dots, N\}$ of the smallest component of the cost vector \mathbf{q} . If this minimum is not unique, one of the minimum candidates is selected according to additional considerations. However, the selection must be prevented from changing too fast. If one switches too fast to the new suggestion, then it can come to infinitely fast switching between the models. Instability of the multiple model observer may result. This can be prevented by the introduction of a hysteresis H [50]:

$$\begin{aligned} j^+ &= H(\mathbf{q}, k, j) \\ H : \quad \mathbb{R}^N \times \mathcal{I} \times \mathcal{I} &\longrightarrow \mathcal{I} \end{aligned} \quad (3.100)$$

The index selected up to time t^- is the discrete state j^- of the hysteresis. By means of the function H on the basis of the current quality vector \mathbf{q} it is decided, whether this state changes to the new value ($j^+ = k$), or not ($j^+ = j^-$). Different hysteresis functions can be used. In particular, the scale independent hysteresis switching logic [50] is described as follows:

$$H(\mathbf{q}, k, j^-) = \begin{cases} k & \text{if } (1+h)Q_k < Q_{j^-} \\ j^- & \text{elsewhere} \end{cases} \quad (3.101)$$

where h is the hysteresis constant. The discrete output l of the hysteresis is identically to their new state j^+

$$\begin{aligned} l &= \text{id}(j^+) = j^+ \\ \text{id} : \quad D_{\text{id}} &\longrightarrow \mathcal{I} \\ D_{\text{id}} &\subseteq \mathcal{I}. \end{aligned} \quad (3.102)$$

Instead of the hysteresis a dwell time switching logic [84] can be used. Switching is only allowed after a certain dwell time τ_D . This can be interpreted as a time hysteresis.

Thus the index j^+ of the best fitting model structure is determined.

Definition 3.5.2 (Decision logic) *The decision logic \mathfrak{E} is the nonlinear mapping*

$$\begin{aligned} j^+ &= \mathfrak{E}(\hat{\mathbf{X}}, \hat{\mathbf{Y}}, \mathbf{y}, \mathbf{x}_{\text{mea}}, j) \\ \mathfrak{E} : \quad D_{\mathfrak{E}} &\longrightarrow \mathcal{I} \\ D_{\mathfrak{E}} &\subseteq \mathbb{R}^{(n,N)} \times \mathbb{R}^{(p,N)} \times \mathbb{R}^p \times \mathbb{R}^{n_{\text{mea}}} \times \mathcal{I} \end{aligned} \quad (3.103)$$

with the discrete state

$$j^- \in \mathcal{I}, \quad (3.104)$$

the continuous state $\hat{\mathbf{X}}$ and the output $\hat{\mathbf{Y}}$ of the multiple observer (cf. definition 3.5.1), the output \mathbf{y} or the measurable states \mathbf{x}_{mea} of the original system 3.86/3.87. It applies

$$\mathfrak{E}(\hat{\mathbf{X}}, \hat{\mathbf{Y}}, \mathbf{y}, \mathbf{x}_{\text{mea}}, j) = H\left(\mathbf{q}(\hat{\mathbf{X}}, \hat{\mathbf{Y}}, \mathbf{y}, \mathbf{x}_{\text{mea}}), \underset{i \in \mathcal{I}}{\text{argmin}}(\mathbf{q}(\hat{\mathbf{X}}, \hat{\mathbf{Y}}, \mathbf{y}, \mathbf{x}_{\text{mea}})), j\right) \quad (3.105)$$

with the cost function \mathbf{q} (cf. Eq. 3.96), the argmin-operator (cf. Eq. 3.99) and the hysteresis H (cf. Eq. 3.100).

The discrete output is

$$l = \text{id}(j^+) \in \mathcal{I} \quad (3.106)$$

according to the identity 3.102.

3.5.3 Multiple model observer (MMO)

The multiple observer together with the decision logic define the multiple model observer (MMO). On the basis of the definitions 3.5.1 and 3.5.2 it becomes clear that the continuous inputs of the multiple observer result in a discrete output of the decision logic. Since the MMO consists of both continuous and discrete states, it is a hybrid system.

Definition 3.5.3 (Multiple model observer MMO) *Given a multiple observer \mathfrak{D} of definition 3.5.1 and the decision logic \mathfrak{E} of definition 3.5.2. The multiple model observer is the hybrid system*

$$MMO = (\mathcal{Z}, \mathcal{E}, \mathcal{O}, \mathfrak{D}, \mathfrak{E}, \text{id}) \quad (3.107)$$

where

- the hybrid states $(\hat{\mathbf{X}}, j) \in \mathcal{Z} \subseteq \mathbb{R}^{(n,N)} \times \mathcal{I}$,
- the continuous input $(\mathbf{y}, \mathbf{x}_{\text{mea}}, \mathbf{U}^*) \in \mathcal{E} \subseteq \mathbb{R}^p \times \mathbb{R}^{n_{\text{mea}}} \times \mathbb{R}^{(m',N)}$,
- the discrete output $l \in \mathcal{O} \subseteq \mathcal{I}$,

the continuous function \mathfrak{D} , the discrete function \mathfrak{E} and the discrete output function id .

The state $\hat{\mathbf{X}} \in \mathbb{R}^{(n,N)}$ of the multiple observer \mathfrak{D} is the continuous state of the overall MMO. The variable $j \in \mathcal{I}$ is the discrete state. The discrete state space is the index-set $\mathcal{I} = \{1, \dots, N\}$. All measurements are the inputs namely the system output $\mathbf{y} \in \mathbb{R}^p$, the measurable systems states $\mathbf{x}_{\text{mea}} \in \mathbb{R}^{n_{\text{mea}}}$ and other optional inputs $\mathbf{U}^* \in \mathbb{R}^{(m',N)}$. The discrete output is the estimate l , the index of the most suitable model structure.

3.5.4 Parameter estimation in the first order case

The special case of a multiple model observer for fast parameter estimation will be discussed based on the example of a first order system. Consider the first order system

where the parameter θ is treated as an augmented state

$$\begin{aligned}\dot{x}_1 &= \varphi_1(y)\theta + u \\ \dot{\theta} &= 0 \\ y &= x_1\end{aligned}\tag{3.108}$$

$$\varphi_1(y) > 0\tag{3.109}$$

It is assumed that the unknown constant parameter θ is contained in a closed interval $\theta \in \Theta = [\theta_{min}, \theta_{max}]$. The interval Θ is discretised using a set of N parameter values θ_i

$$\theta_{min} \leq \theta_i \leq \theta_{max} \quad i = 1, \dots, N\tag{3.110}$$

$$\mathcal{T} = \{\theta_i | i \in \mathcal{I} = \{1, \dots, N\}\},\tag{3.111}$$

Each of the N individual observers of the multiple model observer will be centered around one of the discrete parameter values θ_i .

$$\mathbf{O}_x = \{\mathbf{o}(\hat{x}_i, y, \mathbf{u}_i^*; \theta_i) | \theta_i \in \mathcal{T} = \{\theta_1, \dots, \theta_N\}, i \in \mathcal{I} = \{1, \dots, N\}\}\tag{3.112}$$

The set of individual observers constitutes the multiple observer \mathfrak{D} . Together with the decision logic \mathfrak{E} an estimate θ_i of the uncertain parameter θ is obtained.

For this purpose Eq. (3.108) is rewritten into

$$\begin{aligned}\dot{x}_1 &= \varphi_1(y)\theta_i + \varphi_1(y)x_{2i} + u \\ \dot{x}_{2i} &= 0 \\ y &= x_1\end{aligned}\tag{3.113}$$

where $x_{2i} = \theta - \theta_i$. Following the Lyapunov based observer design in [32] it is proposed to use the following individual nonlinear observer

$$\begin{aligned}\dot{\hat{x}}_{1i} &= \varphi_1(y)\theta_i + 2\omega\varphi_1(y)(y - \hat{y}_i) + u + \varphi_1(y)x_{2i} \\ \dot{\hat{x}}_{2i} &= \omega^2\varphi_1(y)(y - \hat{y}_i), \quad \omega > 0.\end{aligned}\tag{3.114}$$

Defining the error $e_i = [e_{1i}, e_{2i}]^T = [x_1 - \hat{x}_{1i}, x_{2i} - \hat{x}_{2i}]^T$ the observer will result in the bilinear error dynamics

$$\dot{e}_i = \varphi(y)Ae_i.\tag{3.115}$$

where the matrix

$$A = \begin{pmatrix} -2\omega & 1 \\ -\omega^2 & 0 \end{pmatrix}$$

is Hurwitz and $\varphi(y)$ represents the nonlinearity in the system output. The observer design renders the time derivative of the Lyapunov function

$$V_i(e_i) = \frac{1}{2} e_i^T \begin{pmatrix} 1 & 0 \\ 0 & \omega^{-2} \end{pmatrix} e_i \quad (3.116)$$

negative semidefinite

$$\dot{V}_i = -2\omega\varphi(y)e_{1i}^2 \leq 0. \quad (3.117)$$

Moreover, it follows from LaSalle's Invariance Theorem [66, 70] that e_2 converges as well. This means that the parameter estimate converges to its true value.

An important property of the error differential Eq. (3.115) is that its solution can be calculated. Defining

$$y^*(t-T, t) = \int_{t-T}^t \varphi_1(y(\tau)) d\tau > 0 \quad (3.118)$$

we obtain

$$e_i(t) = \exp(-\omega y^*(t-T, t)) \cdot \begin{pmatrix} 1 - \omega y^*(t-T, t) & y^*(t-T, t) \\ -\omega^2 y^*(t-T, t) & 1 + y^*(t-T, t) \end{pmatrix} e_i(0). \quad (3.119)$$

Knowing the measurable output error $e_{1i}(t-T)$ and $e_{1i}(t)$ at some time instant t Eq. (3.119) can be used to determine the parameter estimation error $e_{2i}(t)$ according to

$$e_{2i}(t) = h(y^*, e_{1i}(t), e_{1i}(0)) = \frac{1}{y^*} [(1 + \omega y^*) e_{1i}(t) - e^{-\omega y^*} e_{1i}(0)] \quad (3.120)$$

Thus, even under observer transients a parameter estimate

$$\hat{\theta}_i^* = \theta_i + \hat{x}_{2i}(t) + e_{2i}(t) \quad (3.121)$$

can be computed as shown in Fig. 3.7.

This is a prediction of the parameter estimation error while the observer has not converged yet and gives a further estimated value for the unknown parameter. The estimated value $\hat{\theta}_i^*$ is an approximation of the parameter θ . Without noise in the system the estimate $\hat{\theta}_i^*$ is equal to the parameter θ .

In cases where the solution of the error equation cannot be solved explicitly but the convergence behaviour is given by

$$\|e(t)\| \leq \kappa \|e^T(0)\| \exp(-\beta t), \quad (3.122)$$

an area where the true parameter value is situated can be calculated. Observers with exponential decreasing error dynamics are discussed in [15].

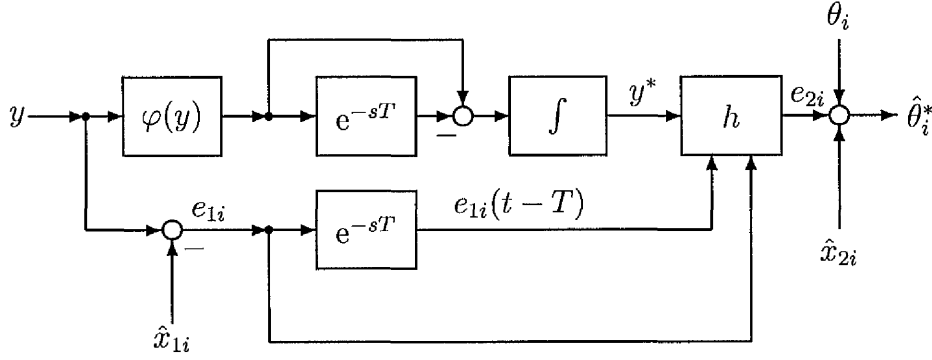


Figure 3.7: Parameter resetting law

The inequality (3.122) can be rewritten into:

$$\begin{aligned}
 \sqrt{e^T(t)e(t)} &\leq \kappa \sqrt{e^T(0)e(0)} \exp(-\beta t) \\
 \sqrt{e_1^2(t) + e_2^2(t)} &\leq \kappa \sqrt{e_1^2(0) + e_2^2(0)} \exp(-\beta t) \\
 e_1^2(t) + e_2^2(t) &\leq \kappa^2 \exp(-2\beta t)(e_1^2(0) + e_2^2(0)) \\
 e_2^2(t) &\leq \kappa^2 \exp(-2\beta t)(e_1^2(0) - e_1^2(t)) + \kappa^2 \exp(-2\beta t)e_2^2(0). \quad (3.123)
 \end{aligned}$$

The first part of Eq. 3.123 is known. Using the definition of $e_2 = \theta - x_2$

$$\begin{aligned}
 (\theta - x_2(t))^2 &\leq \kappa^2 \exp(-2\beta t)(e_1^2(0) - e_1^2(t)) + \kappa^2 \exp(-2\beta t)(\theta - x_2(0))^2 \\
 &\leq A + B(\theta - x_2(0))^2, \quad (3.124)
 \end{aligned}$$

is obtained where $A = \kappa^2 \exp(-2\beta t)(e_1^2(0) - e_1^2(t))$ and $B = \kappa^2 \exp(-2\beta t)$ are known. By solution of the quadratic inequality in θ one obtains an area where the true parameter is contained. This solution exists if $\frac{2x_2(t) - 2Bx_2(0)}{1-B} > 0$ and $x_2^2(t) - Bx_2^2(0) - A < 0$.

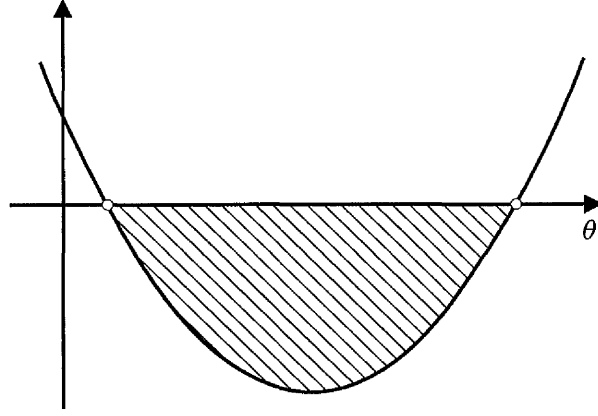
$$\theta^2 - 2\theta x_2(t) + x_2^2 \leq A + B\theta^2 - 2B\theta x_2(0) + Bx_2^2(0)$$

$$(1 - B)\theta^2 - (2x_2(t) - 2Bx_2(0))\theta + x_2^2(t) - Bx_2^2(0) - A \leq 0 \quad (3.125)$$

The solution of the inequality (3.125) is depicted in Fig. 3.8. For an approximation of θ this additional information can already be used while the observer is still in transient mode.

Anti-windup is introduced for the observer state \hat{x}_{2i} by defining the local bounds

$$\bar{\theta}_i = \begin{cases} \theta_{min} & \text{for } i = 0 \\ \frac{1}{2}(\theta_{i+1} + \theta_i) & \text{for } 1 \leq i \leq N - 1 \\ \theta_{max} & \text{for } i = N \end{cases} \quad (3.126)$$


 Figure 3.8: Estimated region of the true parameter θ

and setting the state equation

$$\dot{\hat{x}}_{2i} = \begin{cases} 0 & \text{for } (\theta_i + x_{2i}) \notin [\bar{\theta}_{i-1}, \bar{\theta}_i] \text{ and } \dot{x}_{2i}x_{2i} > 0 \\ \omega^2\varphi_1(y)(y - \hat{x}_{1i}) & \text{elsewhere} \end{cases} \quad (3.127)$$

The tolerance around θ_i is denoted by $[\bar{\theta}_{i-1}, \bar{\theta}_i]$. If the partitioning of the parameter space is uniform denote:

$$[\bar{\theta}_{i-1}, \bar{\theta}_i] = [\theta_i - \delta, \theta_i + \delta] \quad (3.128)$$

$$\theta_i + x_{2i} \notin [\bar{\theta}_{i-1}, \bar{\theta}_i] \Leftrightarrow x_{2i} \notin [-\delta, +\delta]. \quad (3.129)$$

The second observer state is stopped if it leaves the tolerated region.

The multiple observer for the first order system is as follows:

$$\dot{\hat{\mathbf{x}}}_i = \mathbf{o}(\hat{\mathbf{x}}_i, y, u; \theta_i) = \begin{pmatrix} \dot{\hat{x}}_{1i} \\ \dot{\hat{x}}_{2i} \end{pmatrix}, \quad (3.130)$$

where

$$\begin{aligned} \dot{\hat{x}}_{1i} &= \varphi_1(y)\theta_i + 2\omega\varphi_1(y)(y - \hat{y}_i) + u + \varphi_1(y)x_{2i} \\ \dot{\hat{x}}_{2i} &= \begin{cases} 0 & \text{for } (\theta_i + x_{2i}) \notin [\bar{\theta}_{i-1}, \bar{\theta}_i] \text{ and } (y - \hat{y}_i)x_{2i} > 0 \\ \omega^2\varphi_1(y)(y - \hat{y}_i) & \text{elsewhere} \end{cases} \end{aligned}$$

and the output is

$$\hat{y}_i = h(\hat{\mathbf{x}}_{1i}) = \hat{x}_{1i}. \quad (3.131)$$

Each of the N parallel observers has the same structure \mathbf{o} and the same output function h . The state matrix of the multiple observer $\dot{\hat{\mathbf{X}}} = \mathfrak{D}(\hat{\mathbf{X}}, y, u)$ is as follows

$$\hat{\mathbf{X}} = \begin{pmatrix} \hat{x}_{11} & \cdots & \hat{x}_{1N} \\ \hat{x}_{21} & \cdots & \hat{x}_{2N} \end{pmatrix} \in \mathbb{R}^{(2,N)}, \quad (3.132)$$

with the output vector

$$\hat{\mathbf{y}} = (\hat{x}_{11}, \dots, \hat{x}_{1N}). \quad (3.133)$$

When \hat{x}_{2i} is in saturation then e_{2i} will be constant and the error dynamics equation Eq. (3.115) simplifies to the stable first order system

$$\dot{e}_{1i} = \varphi_1(\mathbf{y}) [-2\omega e_{1i} + e_{2i}] \quad (3.134)$$

driven by a constant input e_{2i} . The solution to this equation

$$e_{1i} = \frac{1}{2\omega} [(2\omega e_{1i}(0) - e_{2i}) e^{-2\omega y^*} - e_{2i}] \quad (3.135)$$

will eventually converge to the finite value

$$e_{1i}(\infty) = -\frac{e_{2i}}{2\omega} \quad (3.136)$$

Hence, only one individual observer will have an output error converging to zero and consequently a cost index Q_i converging to zero independently of the particular cost index that is used.

The anti-windup keeps the parameter estimate within specified bounds. Consequently, each observer of the MMO will cover a specified region of the parameter space only. Observers that are in anti-windup mode will show a nonzero estimation error e_{1i} . This indicates that the corresponding model is not valid. A fast decision can be made which of the observer is not valid because \hat{x}_{2i} is in anti-windup mode.

For that reason, the quality index is defined on the basis of the observation errors. The only measurable error of observation is $e_{1i} = y - \hat{x}_{1i}$. The second error $e_{2i} = x_2 - \hat{x}_{2i}$ is calculated from the first in Eq. 3.120. The following cost index is not based on e_{1i} and e_{2i} but on e_{1i} and \hat{x}_{2i} :

$$\mathbf{q} = \begin{pmatrix} Q(\hat{x}_{11}, \hat{x}_{21}, y) \\ \vdots \\ Q(\hat{x}_{1N}, \hat{x}_{2N}, y) \end{pmatrix} \quad (3.137)$$

where

$$Q(\hat{x}_{1i}, \hat{x}_{2i}, y) = c_1 (y - \hat{x}_{1i})^2 + c_2 (\hat{x}_{2i})^2. \quad (3.138)$$

The cost is calculated for each observer in the same way, i.e. as weighted sum of the squared estimation error $e_{1i} = y - \hat{x}_{1i}$ and the squared state \hat{x}_{2i} . The observer with the smallest error e_{1i} and the smallest state \hat{x}_{2i} (that one which is not in anti-windup) is taken as the best.

Normally there will be noise in the system. The state estimates \hat{x}_{1i} and \hat{x}_{2i} do not depend directly on the measurements. By reduction of the observer gain the noise will be reduced as well. The output error $e_{1i} = y - \hat{x}_{1i}$ however is not noise free due to the measurement y . This causes noise in the cost index that may lead to erroneous estimation. Therefore, the individual cost indexes $\mathbf{J} = (J_1, \dots, J_N)^T$ should be filtered with a low pass filter

$$\mathbf{J}(s) = H_{LP}(s) \mathbf{q}(s). \quad (3.139)$$

The filter needs to be tuned. Note that a filter having a large time constant would cause a large settling time of the cost indices and a reduced estimation speed.

The filtered cost vector \mathbf{J} (3.139) together with the argmin-operator (3.99) determines the current suggestion θ_k for the parameter candidate of the MMO estimation.

$$\theta_k = \left\{ \theta_l \mid l = \underset{i \in \mathcal{I}}{\operatorname{argmin}}(\mathbf{J}) \right\} \neq \emptyset. \quad (3.140)$$

In order to prevent chattering between the parameter candidates a hysteresis is introduced. For the parameter estimation case the hysteresis switching logic (3.101) and (3.100) become

$$\theta_m^+ = H(\mathbf{J}, \theta_k, \theta_m^-) = \begin{cases} \theta_k & \text{if } (1+h)J_k < J_m^- \\ \theta_m^- & \text{elsewhere} \end{cases} \quad (3.141)$$

with the cost vector $\mathbf{J} = (J_1, \dots, J_N)^T$ (3.139), the current parameter suggestion θ_k (3.140) and the old estimate θ_m^- of the MMO. The new estimate for the unknown parameter θ of the system (3.108) is θ_m^+ . The state θ_j of the hysteresis is only set if the observer having the parameter $\theta_j^+ = \theta_k$ reduces the cost significantly. The hysteresis constant h can be used for tuning.

How to tune the MMO depends on the noise and on the required convergence rate of the observer. A slow converging MMO gives a slow estimate. The estimation error e_{1i} in Eq. (3.136) is smaller for faster observer and the estimation becomes more difficult. For fast observer the decision on θ_i needs to be made on \hat{x}_{2i} only because it does not depend on the systems output. If the cost index \mathbf{q} depends on e_{1i} it depends directly on the noisy systems output.

The time window T in equation (3.118) needs to be tuned properly. A speed up of the estimation can only be achieved if T is chosen smaller than the convergence time of the observer. A large T gives a small speed up of the estimation while a small T is noise sensitive. A detailed discussion of the MMO tuning can be found in [103].

3.6 Parameter resetting

The properties of the MME and MMO approaches (cf. Sec. 3.4 and 3.5) will be used for the Lyapunov function based parameter resetting outlined in Section 3.2 of a nonlinear adaptive controller (cf. Sec. 3.1.3).

The main objective is to improve the transient performance of the closed loop system (3.25) in particular with respect to the unknown parameter vector θ .

In order to evaluate the sufficient parameter resetting condition (3.41) one needs to deal with the fact that θ in the second term of Eq. (3.41) is unknown. Hence, other strategies counteracting the uncertainty are needed.

3.6.1 Multiple model parameter estimate used for resetting

A method for computing an estimate for the uncertain term by filtering is given by the multiple model approach in Sec. 3.4 [62].

Substituting (3.85) into (3.41) leads to

$$\Delta V(t) = \Delta \hat{\theta}^T \Gamma^{-1} \Delta \hat{\theta} - 2 \left(R^{-1}(t) (d_i(t) - \delta(t-)) \Delta \hat{\theta} \right)^T \Gamma^{-1} \Delta \hat{\theta} - (z^-)^T (z^-) \quad (3.142)$$

This means that resetting only causes negative jumps in $V(t)$. If there exists several θ_i such that $\Delta V_{ni}(t) < 0$, the one which minimizes $\Delta V_{ni}(t)$ (with respect to i) is selected since this will yield the largest negative jump in the Lyapunov function. If additional (possibly heuristic) reset conditions are introduced, they can not lead to instability since they will only lead to less frequent switching.

The reset criterion contains some monitoring of persistence of excitation. If the matrix $R(t)$ becomes close to singular (i.e. the system is poorly excited) the prediction error must be very small to justify a reset. In the singular case, no reset is allowed. The requirement of persistence of excitation is quite reasonable and natural since an instantaneous reset obviously requires that the data contains strong evidence about the parameters. This is not an unreasonable requirement since the purpose of the resetting is only to improve transient performance, and the persistence of excitation condition will typically hold during transients. On the other hand, it will not hold during close to steady-state conditions, but then there is no need for resetting.

For a first order system, if there is no uncertainty and only one parameter being estimated, it is easily seen that the reset condition $\Delta V_{ni}(t) < 0$ is equivalent to

$$\theta - |\hat{\theta}(t) - \theta| < \theta_i < \theta + |\hat{\theta}(t) - \theta| \quad (3.143)$$

since it requires that θ_i is closer to θ than $\hat{\theta}(t)$. Hence, minimization of $\Delta V_{ni}(t)$ is equivalent to minimizing $|\theta - \theta_i|$.

In the case when filters are used to produce $y(t)$ and $\zeta(t)$ in (3.77) and (3.78), there are some exponentially decaying terms in the following equations due to the filter's initial conditions that have been neglected in the analysis so far. These terms will, like the introduction of the integral in (3.80), prevent the reset algorithm from responding instantaneously. Thus, the filters should be tuned to address the tradeoff between response time and sensitivity to uncertainty. Furthermore, it might be beneficial to add a mechanism that inhibits resetting during the time interval where it is known that transients due to the filters are significant. This aspect will be discussed in detail in example 3.6.1.

Other performance signals can also be used to compute θ similar to (3.85). For example, one might use a nonlinear observer. In this case, the reset delay will be related to the speed of the observer error dynamics. This will be discussed in the following section.

Obviously uncertainty may lead to undesirable resetting that may increase the Lyapunov function. As an alternative, one might introduce some assumptions on the uncertainty and design a robust reset criterion that guarantees that the Lyapunov function does not increase due to uncertainty when resets occur. There are several alternative uncertainty characterizations that can be applied without too much additional complexity, but here it is simply assumed that the uncertainty $\epsilon(t)$ (cf. Eq: 3.77) belongs to some known bounded set

$$-\bar{E} \leq \epsilon(t) \leq \bar{E} \quad (3.144)$$

where $\bar{E} \in \mathbb{R}^n$ is a vector with positive elements. One may then derive an upper bound $\Delta \bar{V}_{ni}(t)$ that satisfies

$$\Delta \bar{V}_{ni}(t) \geq \sup_{-\bar{E} \leq \epsilon(\tau) \leq \bar{E}} \Delta V_{ni}(t) \quad (3.145)$$

and use this bound in the reset condition. One such bound is given in the next theorem:

Theorem 1 *Let*

$$\Delta \bar{V}_{ni}(t) = \rho_i(t) + \Delta \hat{\theta}^T \Gamma^{-1} \Delta \hat{\theta} - 2 \left(R^{-1}(t) d_i(t) - \Delta \hat{\theta} \right)^T \Gamma^{-1} \Delta \hat{\theta} - (z^-)^T (z^-) \quad (3.146)$$

and

$$\xi^i(t) = R^{-1}(t)\Gamma^{-1}(\hat{\theta}_i - \hat{\theta}(t)) \quad (3.147)$$

$$\rho_i(t) = T \sum_{j=1}^p \sum_{l=1}^n \overline{E}_l |\xi_j^i(t)| \sup_{\tau \in [t-T, t]} |\zeta_{j,l}(\tau)| \quad (3.148)$$

Suppose the parameter estimate is reset at time t to $\hat{\theta}(t^+) = \hat{\theta}_i$ only if $\Delta \overline{V}_{ni}(t) \leq 0$ and $R(t) > 0$. Then the adaptive control system with estimator resetting satisfies sufficient stability conditions given in Sec. 2.2. ■

Proof. It is straightforward to see that (3.146) satisfies (3.145). ■

Introducing the noise bound and relying on worst-case considerations effectively leads to a hysteresis that prevents resets due to the uncertainty, since $\rho_i(t) > 0$ for all t . If it is required that $\Delta \overline{V}_{ni}(t) \leq -\eta < 0$ for some $\eta > 0$, it follows that there will only be a finite number of resets, since otherwise the Lyapunov function would eventually be negative.

Example 3.6.1 (first order system) *A simple nonlinear system example (cf. (3.43)):*

$$\dot{x}_1 = \varphi(x_1)\theta + u + \nu \quad (3.149)$$

The control input is u and ν is due to noise and uncertainty. The nonlinear function $\varphi = x_1^2$ is a quadratic nonlinearity, and the parameter θ is highly uncertain and can change instantaneously (as a piecewise constant function of time). The backstepping design leads to the adaptive controller

$$u = -c_1 z_1 - \varphi(x_1)\hat{\theta} - \dot{y}_r \quad (3.150)$$

$$\dot{\hat{\theta}} = \gamma \varphi(x_1) z_1 \quad (3.151)$$

$$z_1 = x_1 - y_r \quad (3.152)$$

For the multi-model predictors the same model, with $y(t) = H(s)(sx_1(t) - u(t))$ and $\zeta(t) = H(s)\varphi(x(t))$, with the lowpass filter $H(s) = 1/(1 + \tau s)$ and time constant $\tau = 0.085$ is applied. Other parameters are $T = 0.085$, $c_1 = 20$ and $\Gamma = 100$. The controller and adaptation gain is chosen very low to clearly suppress noise. This causes relatively large transients. There are five parameter hypotheses $\theta_i \in \{-10, -5, 0, 5, 10\}$. In the simulation there is uniformly distributed white noise. Furthermore, unmodelled actuator dynamics as a first order system with unit gain and time constant 0.040 is introduced in the simulator. Using trial and error, the hysteresis threshold is chosen as $\rho = 0.01$.

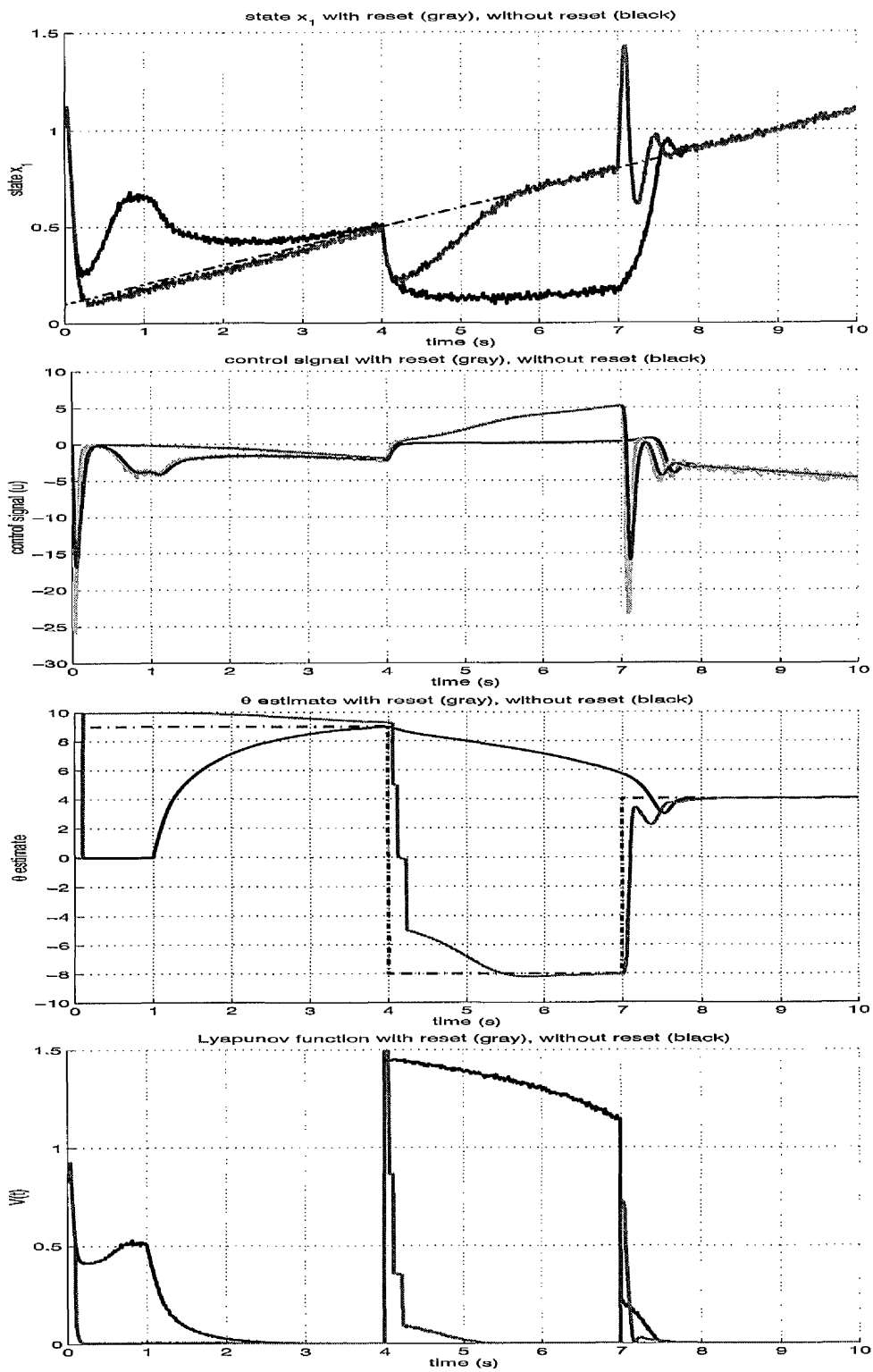


Figure 3.9: Simulation results.

Consider a simulation scenario where parameter θ changes instantaneously at times $t = 4$ and $t = 7$. Simulation results, with (grey lines) and without (black lines) estimator resetting, are shown in Fig. 3.9. It was verified that the persistence of excitation condition $R(t) > 0$ was satisfied with a large margin at all time. It can be observed both from the control error and the values of the Lyapunov function that the performance improved by the resets.

Note that this scenario differs slightly from the above theoretical setting where the parameter θ is assumed to be time-invariant. However, these are equivalent if one takes into account the transient generated by the step in θ , as done in the additional analysis below. From Figure 3.9 it can be observed that the filters and thresholds are tuned such that no erroneous resets are made. Certainly, the filters add transients to the performance signals $\Delta \bar{V}_{ni}(t)$, but these transients have been neglected in the reset algorithm. The rationale for this is shown below.

Consider the instantaneous jump from $\theta = 9$ to $\theta = -8$ at time $t = 4$, i.e.

$$\theta(t) = 9 - 17\mu(t - 4) \quad (3.153)$$

where $\mu(t)$ is the unit step function. This step generates a transient, such that (3.77) becomes

$$y(t) = 9\zeta(t) - 17H(s) (\varphi(x(t))\mu(t - 4)) + \epsilon(t) \quad (3.154)$$

It is assumed (for the purpose of simplicity in the analysis) that $\varphi(x(t)) \approx 1$ and consequently $\zeta(t) \approx 1$. Hence,

$$y(t) \approx 9 - 17 \left(1 - \exp \left(-\frac{t - 4}{0.085} \right) \right) \quad (3.155)$$

and

$$e_i(t) \approx (9 - \theta_i) - 17 \left(1 - \exp \left(-\frac{t - 4}{0.085} \right) \right) \quad (3.156)$$

where the uncertainty $\epsilon(t)$ is neglected. For $t < 4.0$ it was clear that $\theta_1 = 10$ gave smallest prediction error. For $t > 4$ it is clear that $\theta_5 = -5$ is the most accurate estimate. However, compare $e_2(t)$, $e_3(t)$, $e_4(t)$, and $e_5(t)$ (corresponding to $\hat{\theta}_2 = 5$, $\hat{\theta}_3 = 0$ and $\hat{\theta}_4 = -5$, respectively):

$$\begin{aligned} e_4(t) &\approx 14 - 17 \left(1 - \exp \left(-\frac{t - 4}{0.085} \right) \right) \\ e_3(t) &\approx 9 - 17 \left(1 - \exp \left(-\frac{t - 4}{0.085} \right) \right) \\ e_2(t) &\approx 4 - 17 \left(1 - \exp \left(-\frac{t - 4}{0.085} \right) \right) \end{aligned}$$

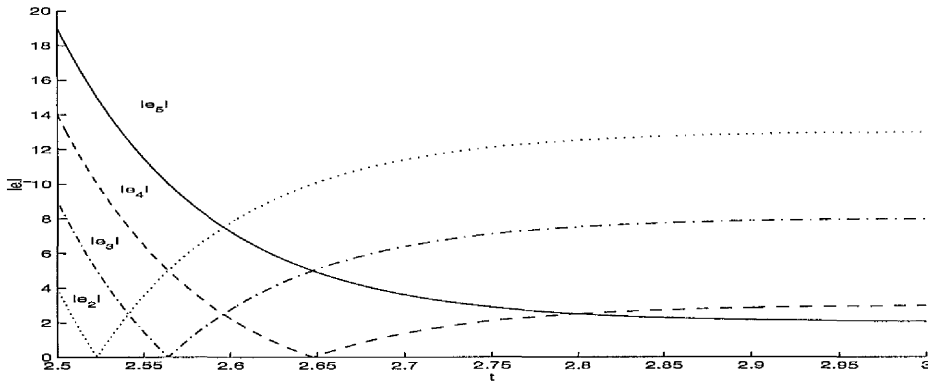


Figure 3.10: Absolute value of prediction errors after parameter step change ($|e_2(t)|$ (dotted), $|e_3(t)|$ (dash dot), $|e_4(t)|$ (dashed), $|e_5(t)|$ (solid)).

Initially, for $2.5 > t > 2.52s$ it is clear that $|e_2(t)| < |e_3(t)| < |e_4(t)| < |e_5(t)|$ since the first positive term of $e_2(t)$ (due to the parameter estimate error) counteracts the negative value of the second term (due to the filter transient) in Eq. (3.156), see figure 3.10 which illustrates the approximate terms e_2, e_3 and e_4 . Consequently, as seen in figure 3.11, the value of $\Delta\bar{V}_2(t)$ goes negative first, and then $\Delta\bar{V}_3(t)$ goes negative until finally $\Delta\bar{V}_4(t)$ goes negative. This can be observed from the plot of $\theta(t)$ where it is seen that after $t = 2.5s$ there is a sequence of three resets to $\theta_2 = 5, \theta_3 = 0$ and $\theta_4 = -5$, all in the right direction. Without filtering and noise, instead a single reset directly to the best value, namely of $\theta_4 = -5$ would happen. To summarize, the filters and their associated transients have the effect that resets are made in several smaller steps rather than in a single big step. One can argue that this is reasonable from a robustness point of view, and thus the filter transient does not necessarily need to be explicitly taken into consideration in the reset algorithm. Although the filter transients will reduce the transient performance, they improve the robustness of the algorithm.

3.6.2 Using the properties of the MMO for a first order system

The multiple model observer (cf. Sec. 3.5) provides additional information on parameter uncertainties which can be used to instantaneously reset the parameter estimate $\hat{\theta}$ of a nonlinear adaptive tuning function controller (3.44). Suppose the best estimate of the multiple model observer with respect to *modelling performance* is

$$\hat{\theta}^+ = \theta_i.$$

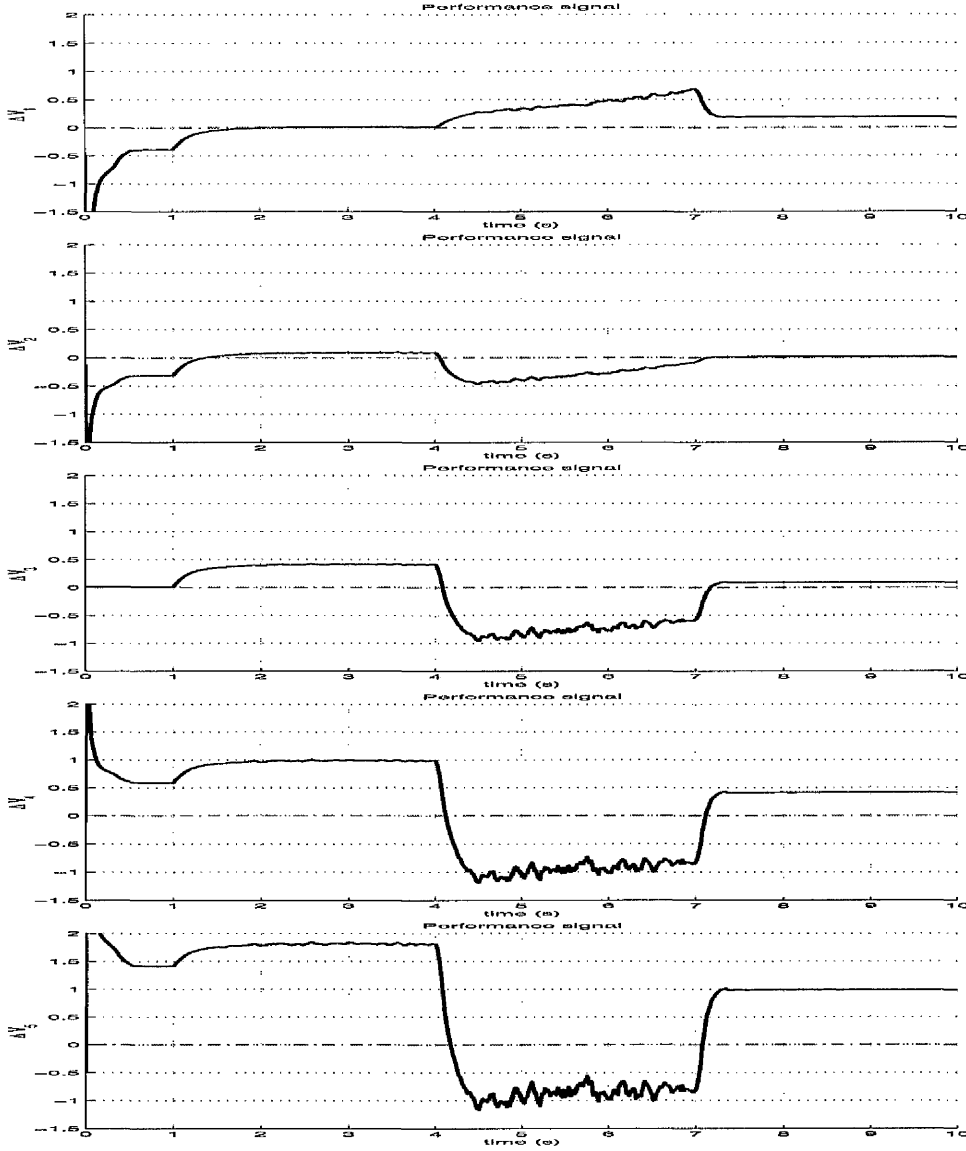


Figure 3.11: Performance signals ΔV_1 , ΔV_2 , ΔV_3 , ΔV_4 and ΔV_5 of the five models.

Additional information on the uncertain parameter θ is given by the transient estimate $\hat{\theta}_i^* \approx \theta$ in Eq. 3.121. Assume a noise free system and furthermore assume exact matching between the system and the observer dynamics. Then $\hat{\theta}_i^*$ is equal to the true parameter.

The properties of the MMO can be used to derive the following resetting law:

Theorem 3.6.1 Consider the control system (3.43) together with the control law (3.44), the parameter update law (3.45) and the MMO (3.114). Suppose that o_i is the observer that has been selected as the optimal one according to the decision logic \mathfrak{E} . Then,

setting $\hat{\theta}^+ = \theta_i$ will result in a negative step of the Lyapunov function (3.47) if

1. $x_{2i}(\tau)$ does not saturate within the time intervall $\tau \in [t - T, t]$.

2. the transient estimate is in the admissible region $[\bar{\theta}_{i-1}, \bar{\theta}_i]$

$$\bar{\theta}_{i-1} < \hat{\theta}_i^* < \bar{\theta}_i \quad (3.157)$$

3. either

$$\hat{\theta} - \bar{\theta}_i > \bar{\theta}_i - \theta_i \quad (3.158)$$

or

$$\bar{\theta}_{i-1} - \hat{\theta} > \theta_i - \bar{\theta}_{i-1} \quad (3.159)$$

4. either

$$((e > \varepsilon_1) \wedge (\Delta\hat{\theta} > \varepsilon_2)) \quad (3.160)$$

or

$$((e < -\varepsilon_1) \wedge (\Delta\hat{\theta} < -\varepsilon_2)). \quad (3.161)$$

If all conditions hold simultaneously the switching function 3.54 is set $S = 1$.

Proof If condition 1 of the theorem holds, according to Eqs. (3.120) and (3.121) we have

$$\hat{\theta}_i = \theta_i + \hat{x}_{2i}(t) + h(y^*(t, t - T), e_{1i}(t), e_{1i}(t - T)). \quad (3.162)$$

If in addition to this, condition 2 is satisfied, then it can be implied that the real parameter is contained in

$$\bar{\theta}_{i-1} < \theta < \bar{\theta}_i. \quad (3.163)$$

From condition 3 follows that either (3.158) is satisfied in which case we obtain by adding $\hat{\theta}$ to both sides and rearranging and employing (3.163)

$$-\Delta\hat{\theta} = \hat{\theta} - \theta_i < 2(\hat{\theta} - \bar{\theta}_i) \leq 2(\hat{\theta} - \theta) = -2\tilde{\theta} \quad (3.164)$$

If on the other hand (3.159) is satisfied then by subtracting $\hat{\theta}$ from both sides and employing (3.163)

$$\Delta\hat{\theta} = \theta_i - \hat{\theta} < 2(\bar{\theta}_{i-1} - \hat{\theta}) \leq 2(\theta - \hat{\theta}) = 2\tilde{\theta}. \quad (3.165)$$

Consequently, conditions (3.56) and (3.58) are satisfied which is sufficient for stability. ■

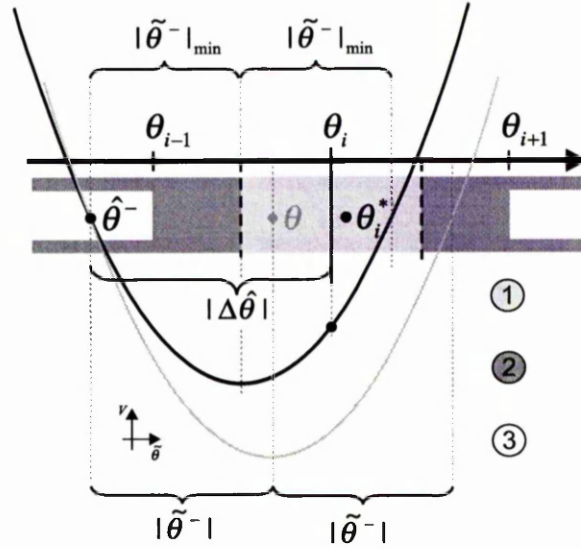


Figure 3.12: Worst case stability analysis

Fig. 3.12 shows the stability test. The MMO-estimate θ_i with its neighbours θ_{i-1} and θ_{i+1} is depicted. The axis is split in three areas ① to ③ marked by coloured stripes. Two parabolas depict the Lyapunov function like in Fig. 3.3.

The MMO-estimate θ_i is trusted only if the transient estimate $\hat{\theta}_i^*$ is in the respective zone. This is depicted by the light grey area ①.

The stability test consists of three steps:

1. The absolute value condition (3.52) requires small jumps $\Delta\hat{\theta}$ for small adaptation error $\tilde{\theta}^- = \theta - \hat{\theta}^-$. The smaller the jump the less the danger of destroying stability. The bounds $[\bar{\theta}_{i-1}, \bar{\theta}_i]$ can be used for a worst case admissible region estimation. The worst case approximation uses that $\theta' \in [\bar{\theta}_{i-1}, \bar{\theta}_i]$ which leads to the minimal $|\tilde{\theta}^-|_{min}$. This is depending upon $\hat{\theta}^-$ the upper or lower bound of the valid parameter space ①, i.e. $\bar{\theta}_i$ and $\bar{\theta}_{i-1}$ respectively.

$$\begin{aligned} \theta' &= \operatorname{argmin}_{\theta \in [\bar{\theta}_{i-1}, \bar{\theta}_i]} |\theta - \hat{\theta}^-| \\ &= \begin{cases} \bar{\theta}_{i-1}, & \text{if } \hat{\theta}^- < \theta_i \\ \bar{\theta}_i, & \text{if } \hat{\theta}^- > \theta_i \end{cases} \end{aligned} \quad (3.166)$$

$$|\tilde{\theta}^-|_{min} = |\theta' - \hat{\theta}^-|. \quad (3.167)$$

In Fig. 3.4 the MMO-estimate θ_i is larger than $\hat{\theta}^-$. Therefore the lower bound $\theta' = \bar{\theta}_{i-1}$ is taken as the worst case assumption.

2. The sign condition (3.51) requires the same sign of the estimated worst case adaptation error $\theta' - \theta_i$ and the parameter jump $\Delta\hat{\theta}$. This is correct in the dark

grey zone ②):

$$\text{sgn}(\Delta\hat{\theta}) = \text{sgn}(\theta' - \theta_i). \quad (3.168)$$

The zone is limited by the valid parameter zone ① and is open in the other direction.

If the sign condition (3.51) is fulfilled the parameter jumps towards the minimum of the Lyapunov parabola. The respective Lyapunov function is black and has its minimum at $\tilde{\theta} = 0$. The adaptation error $\tilde{\theta}$ vanishes for $\hat{\theta} = \theta'$.

3. The parameter not only needs to jump into the right direction but also the absolute value condition (3.52) must hold. This holds inside zone ③. With uniformly partitioned parameter space zone ③ is limited by θ_{i-1} or θ_{i+1} respectively. Inside ③ applies

$$|\Delta\hat{\theta}| \leq 2|\tilde{\theta}^-|_{\min}. \quad (3.169)$$

Together with the worst case estimation of $|\tilde{\theta}^-|$ (cf. number 1) a worst case maximum jump is found.

A jump $\hat{\theta}^-$ to θ_i results in a decrease of the Lyapunov function. The jump could even be larger. The limit is $|\Delta\hat{\theta}| = 2|\tilde{\theta}^-|_{\min}$. If the true parabola (grey line) was known the jump size could be enlarged to $2|\tilde{\theta}^-|$ without increasing the Lyapunov function but condition (3.167) gives only the worst case estimation.

In addition to the above considerations, the resetting should be done according to the control error $e = y - y_r$ as well as to the difference between the MMO-estimate θ_i and the continuous adaptation $\hat{\theta}$ because of a remaining uncertainty in the estimation. Switching is proposed only if the control error e and $\Delta\hat{\theta}$ are bigger than some threshold

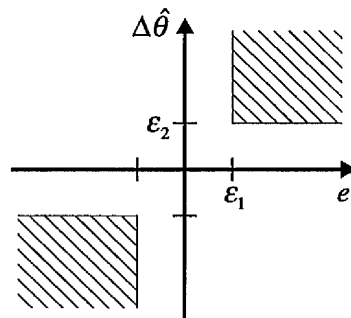


Figure 3.13: Switching Areas

as in the hatched areas depicted in Fig. 3.13. This introduces a hysteresis.

The resetting of the continuous adaptive controller is as follows:

$$\begin{aligned}\hat{\theta} &= \hat{\theta}^- + (\hat{\theta}^+ - \hat{\theta}^-)S \\ &= \hat{\theta}^- + \Delta\hat{\theta}S.\end{aligned}\tag{3.170}$$

with $S = 0$ or $S = 1$. When $S = 1$ the continuous adaption will be resetted using the MMO-estimate θ_i . In between the resetting events the parameter estimate will still be governed by the adaptation law and it will thus be piecewise continuous.

Example 3.6.2 (first order system) *The same simple nonlinear system example and the same controller settings as in example 3.6.1 will be used to show the advantages of the Multiple Model Observer and the resetting.*

A multiple observer (3.130) is designed for that system. The multiple observer dynamics has been chosen according to Eq. (3.114) with $\omega = 1000$. Five individual observer have been designed for five parameter hypotheses $\theta_i \in \{-10, -5, 0, 5, 10\}$. Each observer state \hat{x}_{2i} is confined to the tolerance interval $[-\delta, \delta]$ with $\delta = \frac{5}{2}$ (cf.(3.129)). Equal weighting $c_1 = 1$ and $c_2 = 1$ of the cost index (3.138) is chosen. A first order low pass filter (3.139 $H(s) = 25/(s + 25)$) is used to reduce the noise in the cost function. The time in the integral (3.118) is $T = 0.02$. For robustness the thresholds (3.160) in the switching law are chosen to $\epsilon_1 = 0.1$ and $\epsilon_2 = 6$ in order to prevent from erroneous switching due to uniformly distributed white noise and actuator dynamics.

Consider a simulation scenario where parameter θ changes instantaneously at times $t = 4$ and $t = 7$. Simulation results, with (grey lines) and without (black lines) estimator resetting, are shown in Fig. 3.14. The light grey line in the second lowest plot shows the MMO-estimate. It can be seen both from the control error and the values of the Lyapunov function that the performance is indeed improved by the resets.

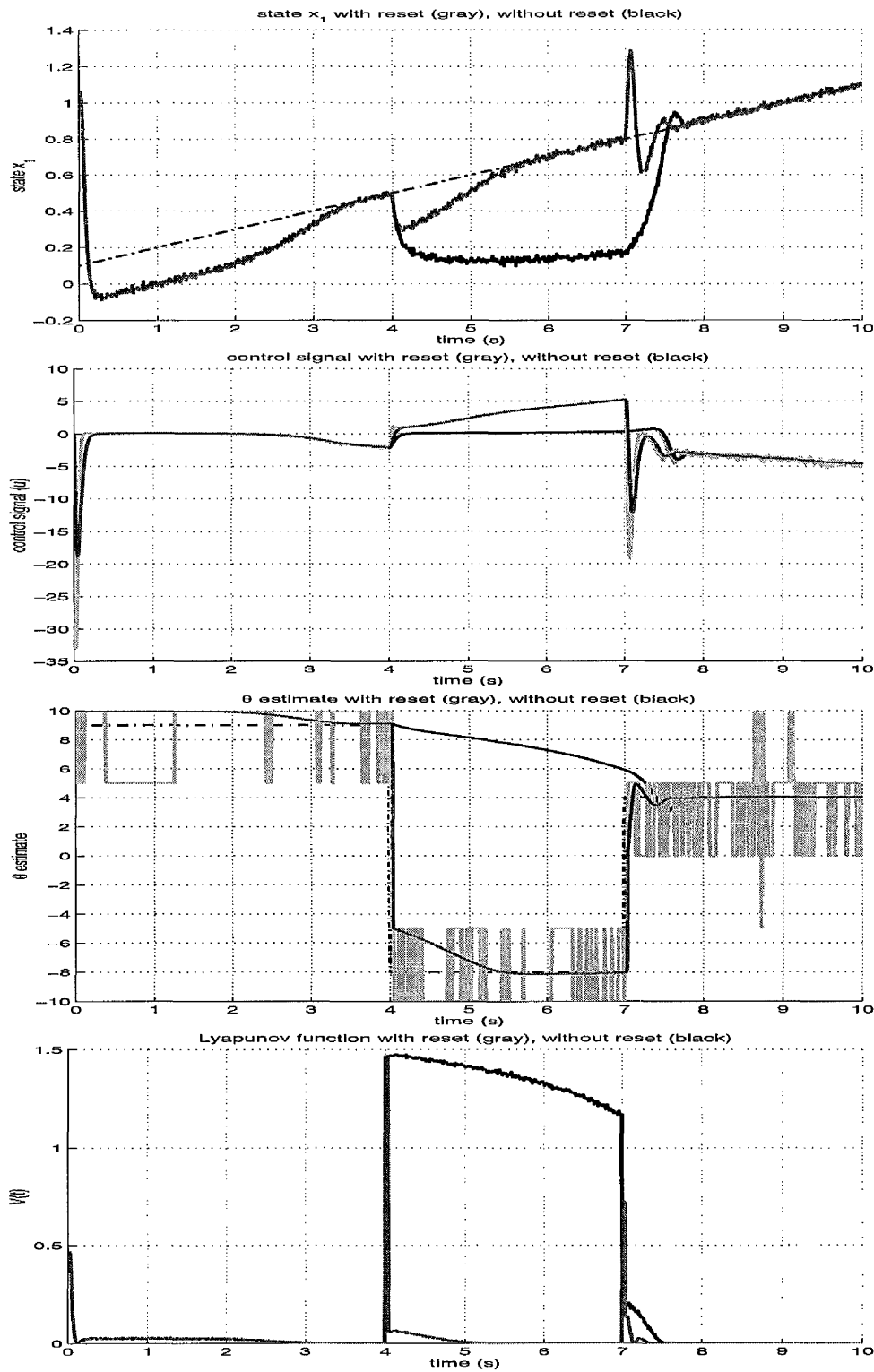


Figure 3.14: Simulation results.

Part II

Application

4 The ABS Control Problem

The complexity of automotive control systems is increasing. In production automobiles each controller has its own device and no communication between the individual controllers is implemented. In order to keep the complexity on a manageable level the different subsystems cannot be viewed as independent anymore. Thus, future control systems need a hierarchical and modular structure where information can be shared between subsystems.

Novel drive-by-wire systems without any hydraulic or mechanical connection between the brake pedal and the brakes or steering wheel and the front axle offer new options for car safety. With such systems the drive dynamics of a car can be significantly improved without expensive hardware modifications. Furthermore, the drive dynamics can be adapted to the requirements of the individual driver.

The lateral and vertical forces will be the control task. The coordination of active suspension, four-wheel steering and braking becomes a bigger issue leading to better driving pleasure, driveability, ride comfort, vehicle handling and safety. New electrically-driven actuators with better performance are increasing the overall system's stability and safety. Today's ESP controls the yaw rate of the car only by braking. Additional redundancy can be achieved if the car is steered by braking as done in production ESP but also with braking by steering where the wheels are used as a snowplough. The sliding of the wheels that moves not in their longitudinal direction results in braking forces.

For novel approaches consider a car equipped with:

- four independent steerable wheels
- four independent brakes (one at each wheel)
- no mechanical connections between the wheels

The advantages of such a hardware configuration are

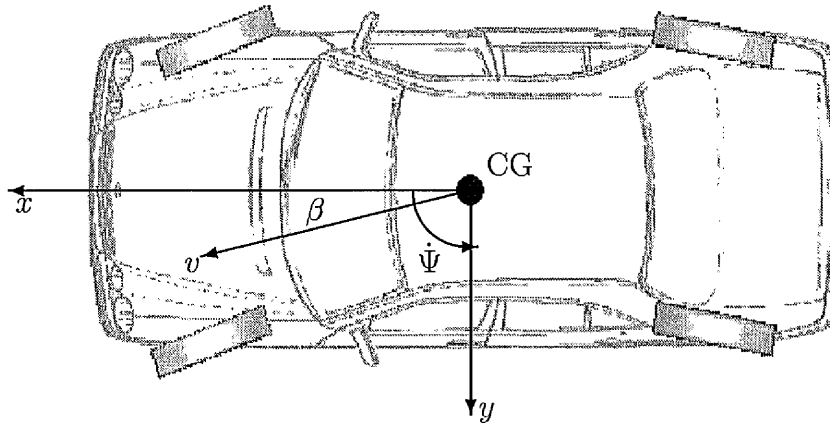


Figure 4.1: Vehicle dynamics

- increased manoeuvrability (e.g. in narrow lanes and for parking);
- the handling dynamics of the car can be changed almost arbitrarily;
- redundancy of the actuator set up can be used to compensate for faults in the system.

Since the driver cannot be made responsible for steering each wheel independently, such a car requires a control system which steers the wheels according to the driver command input (steering wheel angle). In the case when there are no actuator faults in the system the control problem consists of:

- Generation of a desired trajectory in terms of yaw velocity $\dot{\Psi}_d$ and side slip angle β_d from the driver command input signal. This is essentially an open loop control problem (following a path). With at least two independent inputs (front and rear wheel steering) it is possible to keep the side slip angle equal to zero $\beta_d = 0$.
- The second task is the disturbance attenuation with respect to modelling errors, side wind, tilted road, μ -split¹ conditions. This is a closed loop control problem [25].

If a fault occurs, the system has to be fault tolerant without mechanical redundancy. This means that if one steering mechanism is broken, the control system has to react in such a way that normal driving is influenced as little as possible and the driver can stop the car in a safe way [86]. The fault has to be detected and localized. If e.g. one

¹Under μ -split conditions the friction coefficient is different on each side of the vehicle

steering wheel is stuck at a particular steering angle, this angle has to be detected and the car can be driven safely with side slip angle.

The features are based on a modular model based structure and switching between controllers. All systems need information on the highly uncertain, possibly fast-changing road conditions. The friction between tyre and road has a high influence on the drive dynamics because it can change abruptly. There is the need for a fast estimation algorithm that communicates the characteristic to all drive dynamics control system.

The main focus in this thesis is on a model based ABS system with a hybrid tyre friction estimation algorithm for an electro mechanical brake actuator. Current ABS systems are designed in a heuristic manner with extensive tests. The model based ABS focuses on novel nonlinear and hybrid control algorithms [55] for a fast systematic development process.

The outline of the chapter is as follows: Sec. 4.1 gives an introduction to the background of the ABS control with related models and specifications. Also the main ideas of the conventional ABS are presented. Sec. 4.2–4.5 presents four different novel hybrid wheel slip controller namely a nonlinear PI controller, an inverse optimal nonlinear controller based on “Sontag’s” formula, a SSP controller as well as a sub-optimal constrained LQ controller. All controllers will be applied to the test vehicle. Sec. 4.6 discusses how the presented ABS system are switched on or off. The developed multiple model adaptive control ideas of Chapter 3 will be applied to wheel slip control in Sec. 4.7. Before implementing and testing the controller in the experimental vehicle preliminary simulations will be discussed in Sec. 4.8.

4.1 Anti-lock Brake System

Antilock brakes were first developed to help aircraft stop straight and quickly on slippery runways. The first use of antilock brakes was in 1947 on B-47 bombers. In 1954, the first automotive use of ABS was on a limited number of Lincolns. In the late 60’s, Ford, Chrysler, and Cadillac offered ABS on a few vehicles. These first systems used analog computers and vacuum-actuated modulators that cycled so slowly that they actually increased a vehicle’s stopping distance. In the late 70’s, Mercedes and BMW introduced electronically-controlled ABS systems in Europe. By 1985, Mercedes, BMW, and Audi introduced Bosch ABS systems, and Ford introduced its first Teves system. By the late-80’s, ABS systems were offered on many high-priced luxury and sports cars. Today, braking systems on most passenger cars and many light-duty

vehicles have become complex, computer-controlled systems. Since the mid-80s, vehicle manufacturers have introduced dozens of antilock braking systems. These systems differ in their hardware configurations as well as in their control strategy [2, 25].

Recently, there has been an increasing interest in automotive brake-by-wire technologies. Brake-by-wire means that there is no hydraulic connection between the brake pedal and the brake actuators. The driver's brake command results in an electric signal that will be communicated via micro-controllers to the actuator. Such technologies will require new types of brake actuators such as electro-mechanical or electro-hydraulic brakes. A main feature of electro-mechanical and electro-hydraulic brakes is that they allow adjustment of the brake force much more accurately than conventional brakes with solenoid valves. A major issue of future automotive control concepts is that the ABS will interact with other systems such as cruise control and anti-skid-control. This can only be achieved by using brake-by-wire technologies and requires novel ABS concepts. Moreover, the application of modern hybrid and heterogeneous control approaches can contribute to a more systematic, model based ABS design.

4.1.1 Problem description

Anti-lock brake systems (ABS) control the brake torque to prevent the wheels from getting locked in the process of braking. Current production ABS systems are highly sophisticated hybrid controllers[25, 4]. Initially the hybrid nature of the controller arose from the requirement to use cheap and simple hydraulic valves with three-point-characteristics as actuators. Furthermore, the hybrid nature of these controllers facilitates an adaptive behaviour with respect to

- the highly uncertain tyre characteristics and
- the fast changing road surface properties.

Such a behaviour cannot be achieved by conventional adaptive approaches.

ABS controllers tend to grow during the design process by including control strategies for a large variety of special cases which are analysed by extensive experimentation. An ABS system also includes a strategy for activating and deactivating the controller since it should only be active if the tyre slip exceeds a certain threshold and the wheel is likely to be locked.

4.1.2 Conventional Approach

The basic control philosophy [25, 135, 4] of conventional ABS systems is a combination of

- slip control and
- wheel acceleration control.

The control objective is to keep wheel slip at a specified set point or to maintain a specified wheel acceleration. Slip control works satisfactorily for non-decreasing tyre force characteristics (e.g. wheel with side-slip) while wheel acceleration control tends to work better for tyre characteristics that have a pronounced maximum. In conventional ABS systems the actuators are hydraulic solenoid valves which have three modes

- brake pressure increase
- brake pressure hold and
- brake pressure reduction

The controller is switched on when the acceleration of the wheel drops below -14 m/s for a period of time greater than ca. 30 ms. As long as the ABS is active the switching between the different actuator modes is controlled either using several slip and acceleration thresholds or by defining a switching surface using a weighted sum of slip and acceleration. The different algorithms show that an ABS is a genuinely hybrid controller. In practice ABS controllers have been shown to be highly adaptive since they can tolerate a considerable amount of uncertainty in the tyre force characteristics and the friction coefficient. This seems to be mainly due to their hybrid nature. It has been pointed out in [87, 88, 89, 90] that a switching type control strategy in general enhances adaptivity in a highly uncertain fast changing environment. There have been attempts to develop a non-hybrid approach for wheel-slip control [12] but such controllers have not been successful in practice.

Different theories were tested for their usefulness in ABS. The model based approach in [34] applies a search of the optimum brake torque via sliding modes. Because the approach requires the tyre force a sliding-mode observer is used to estimate it. The approach is tested in a very simplified simulation environment. Another theoretical approach is presented by Freeman [41]. Freeman designs an adaptive Lyapunov based nonlinear wheel slip controller. This controller has been extended in the following by introducing speed dependence of the Lyapunov function. A similar robust Lyapunov

based adaptive controller is presented in [138]. Neither of the approaches has been tested in simulation or in a real vehicle.

Taheri and Law [121] design a simple PD wheel slip controller by Ziegler-Nichols rules. The concentration is more on the desired slip value. A desired slip is estimated by evaluation of the switching of a conventional ABS. Additionally a modification of the desired slip according to the steering angle is proposed.

Some of the theories have been applied to real vehicles. Sliding mode control has been tested in a hardware in the loop simulator [65] and in a vehicle. A derivative part depending on the rotational acceleration is introduced in order to reduce the chattering of the sliding controller. The controller oscillates due to a very high desired slip. The sliding controller proposed by [28] is mainly used to show the advantage of a PWM controlled actuator.

Pettit [135] formulates a conventional ABS controller as a piecewise linear controller and analyses the switching cycles. Investigations on a variable desired slip can be found in [37]. The desired slip is varied according to the side slip angle.

Conventional ABS control is compared against PID, sliding and fuzzy controllers in [60]. The PID algorithm adapts very slowly on different road surfaces. A combination of the model based approaches should give good performance; but this has not been tested. The simulation analysis shows that a fast adaptation to the road condition is necessary.

Any production ABS incorporates a number of subsystems apart from the wheel slip controller[25, 4]. Among these systems the logic responsible for coordinating the four wheel slip controllers is of particular importance. The wheel slip controllers for each wheel are (as safety devices) only active in critical situations. Thus, each controller is switched off and the brake is set to manual operation when the wheel is no longer in danger of being locked. On the other hand, the slip controller has to be switched on early enough to prevent the wheel from locking. The corresponding switching logic is crucial for the functionality of the ABS and constitutes an inherently hybrid control design task.

4.1.3 Modular ABS system

The novel ABS system consists of modules, which communicate via well defined interfaces and exchange information as shown in Fig. (4.2). The interface between the driver and the wheel slip controller is the brake torque and a maximum wheel slip if the desired brake torque is too large. On the other hand, other drive dynamic systems

can provide a desired slip according to a desired deceleration. Estimation algorithms provide additional state and parameter estimates for the controller and can be communicated to other systems. The proposed ABS has the following modules:

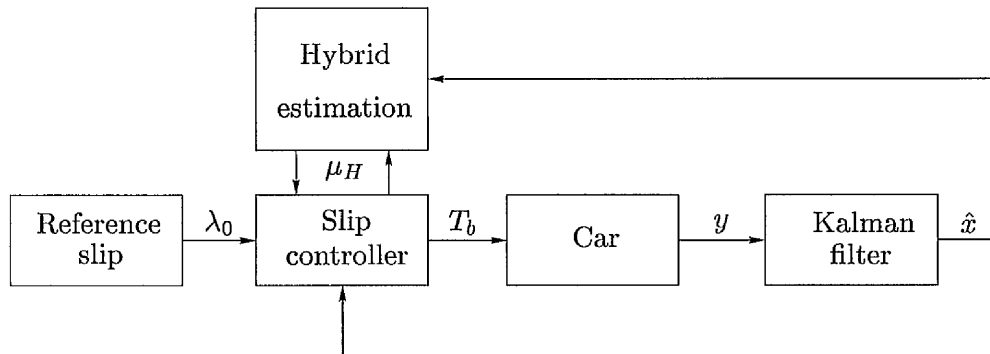


Figure 4.2: Modular structure of the ABS system

- Slip reference: The setpoint or desired slip λ_0 of the control system is calculated to guarantee the desired deceleration while maintaining steerability. An important feature is that other drive dynamic systems like ESP have direct access to the setpoint slip.
- Slip controller: The clamping force (clamping torque T_b respectively) is calculated by the controller in a way that each wheel is prevented from being locked. Four different control approaches are proposed:
 1. A Lyapunov based nonlinear adaptive PI controller,
 2. a nonlinear adaptive controller derived from the inverse optimal approach and “Sontag’s” formula,
 3. a simple gain scheduled PI controller designed by using SSP,
 4. a constrained LQ-controller.

Internal controller states such as the tyre friction coefficient can be provided to other modules.

- Kalman filter: For wheel slip control it is essential to know the velocity of the vehicle, side slip angle and the normal force. Since these variables cannot be measured (measurement of y) they need to be estimated. Heuristics are used in the production car ABS. The use of a Kalman filter has been frequently reported

in the literature [134, 127, 20, 43]. Here the vehicle states \hat{x} as well as the tyre road friction coefficient μ_H are estimated by the extended Kalman filter reported in [120]. The estimate of the possibly fast-changing road condition is somewhat slow. A faster estimation of friction is possible by separation of time scales having a relatively slow car body dynamics running in a different time scale than the fast wheel dynamics where the speed is assumed as a constant parameter.

- A hybrid multiple model and multiple observer based estimator introduced in Sec. 3.4 and Sec. 3.5 estimates the tyre friction characteristics. A fast estimator for the tyre friction characteristics is essential for ABS control since the tyre road friction depends on the surface condition that can change abruptly. The multiple model/observer based estimate is used to reset the parameter estimation of the Lyapunov based nonlinear adaptive wheel slip controller. The advantage of the estimator resetting is that the controller gain can be lowered. Transients due to adaptation can be damped out with resetting while the robustness and performance of the controller with respect to disturbances can be considerably improved. Other fast estimators or even qualitative observers [82, 77] could be used here. Several investigations on tyre road friction estimation can be found in [29, 45, 32]

It is easy to add new modules for a better functionality. The slip controller can be replaced by another one without influencing the other modules.

Similar modular structures have been proposed by the ITT electronic stabilisation program [38]. A superordinated system coordinates the individual functions of an ESP system. A modular system configuration with several functionalities such as wheel-individual slip control and steering combines the advantages of the different single systems to a novel drive dynamic control system [19]. Also BOSCH's novel system architecture "CARTRONIC" deals with integration of controllers in a hierarchical structure in order to have systems on a manageable level and for reuse and exchange of single components.

4.1.4 Equations of motion of a quarter car

The problem of wheel slip control is best explained by looking at a quarter car model shown in Fig. 4.3. The model consists of a single wheel attached to a mass m . While the wheel moves driven by the inertia of the mass m in the direction of the velocity vector v a tyre reaction force F_x is generated by the friction between the tyre surface

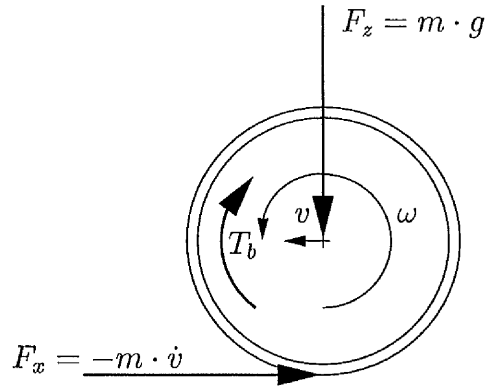


Figure 4.3: Quarter car slip model

and the road surface. The tyre reaction force will generate a torque that initiates a rolling motion of the wheel causing an angular velocity ω . A brake torque applied to the wheel will act against the spinning of the wheel causing a negative angular acceleration. The equations of motion of the quarter car are

$$m\dot{v} = -F_x \quad (4.1)$$

$$J\dot{\omega} = r F_x - T_b \text{sign}(\omega) \quad (4.2)$$

where

- v horizontal speed at which the car travels
- ω angular speed of the wheel
- F_z vertical force
- F_x tyre friction force
- T_b brake torque
- r wheel radius
- J wheel inertia

4.1.5 Tyre friction characteristics

The tyre friction force F_x is given by

$$F_x = F_z \cdot \mu(\lambda, \mu_H, \alpha, F_z) \quad (4.3)$$

where the friction coefficient μ is a nonlinear function of

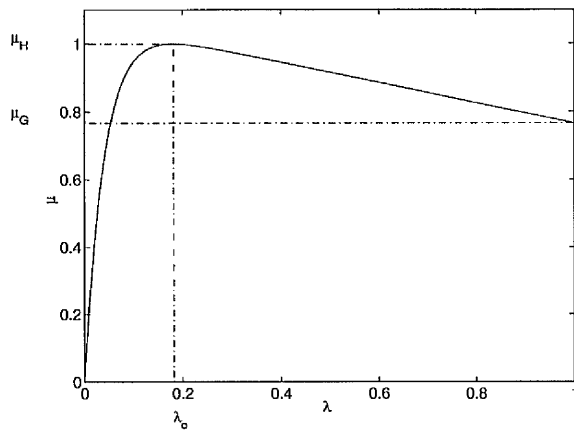
- λ tyre slip
- μ_H friction coefficient between tyre and road
- α slip angle of the wheel (cf. Appendix A)
- F_z the normal force

The slip λ is described by

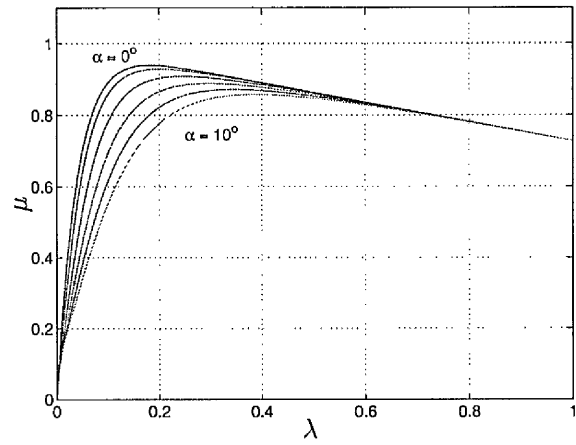
$$\lambda = \frac{v - \omega r}{v} \quad (4.4)$$

and describes the normalised difference between horizontal speed v and speed of the wheel perimeter ωr . The slip value of $\lambda = 0$ characterises the free motion of the wheel where no friction force F_x is exerted. If the slip attains the value $\lambda = 1$ the wheel is locked which means that it has come to a standstill.

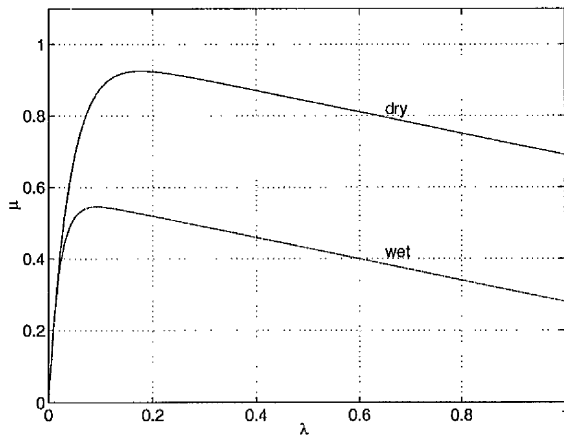
The friction μ can vary in a very wide range. Its qualitative dependence on slip λ is shown in Fig. 4.4.



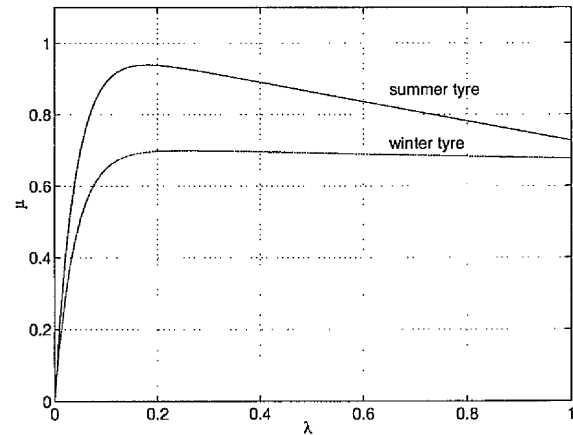
(a) Friction maximum and minimum



(b) Dependence on wheel slip angle α as a parameter



(c) Dependence on surface conditions



(d) dependence on tyre brand

Figure 4.4: Tyre friction curves

In Fig. 4.4(a) is shown how the friction μ will usually increase with slip λ up to a value $\lambda_0 \approx 0.14\mu_H$ where it attains its maximum μ_H . For higher slip values the friction coefficient will decrease down to a minimum μ_G where the wheel is locked and only sliding friction will act on the wheel.

The dependence of friction on the road condition is shown in Fig. 4.4(c). For wet or icy roads the maximum friction μ_H will decrease rapidly.

The tyre friction curve will also depend on the brand of tyre as shown in Fig. 4.4(d). In particular for winter tyres the curve will cease to have a pronounced maximum.

If the motion of the wheel is extended to two dimensions then the lateral slip of the tyre must also be considered. The definition of the slip angle α is shown in Fig. 4.5 where the wheel moves with velocity v_x in longitudinal direction and with velocity v_y in lateral direction.

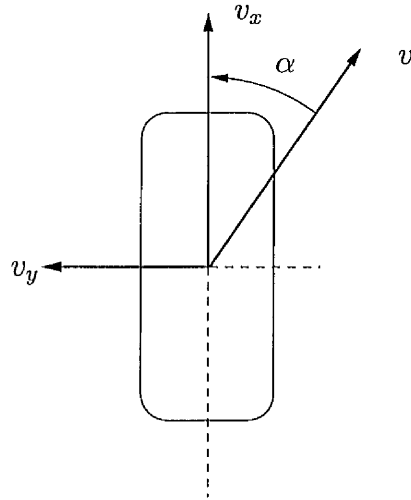


Figure 4.5: Definition of wheel slip angle

In this case longitudinal slip

$$\lambda_x = \frac{v_x - \omega r}{v} \quad (4.5)$$

and lateral slip

$$\lambda_y = \frac{v_y - \omega r}{v} = \sin \alpha \quad (4.6)$$

are distinguished as well as the corresponding friction coefficients μ_x and μ_y . Fig. 4.4(b) shows the dependence of the friction coefficient μ_x on the wheel slip angle α . The side force $F_y = F_z \mu_y$ depends on the wheel slip angle α as shown in Fig 4.6. For big slip angles the force gets smaller. In the sequel unless stated otherwise the slip angle will

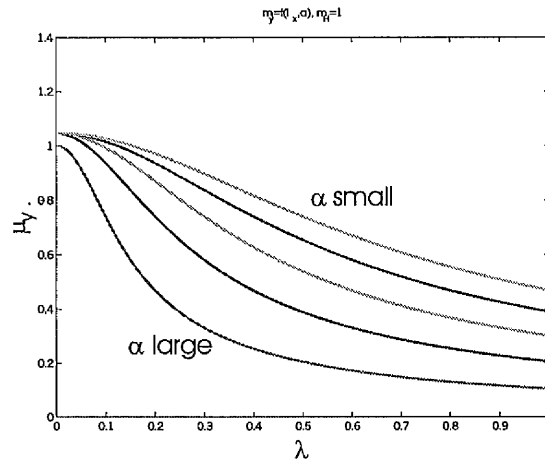


Figure 4.6: Definition of friction lateral force μ_y in dependence of wheel slip angle α

be considered to be zero for simplification with

$$\mu_x = \mu \quad \text{and} \quad v_x = v.$$

Tyre Friction Model

The qualitative dependence of the tyre reaction forces on slip, type of tyre and road condition has been explained. Here a typical mathematical model of the tyre friction characteristics will be given.

Numerous models that describe the nonlinear behaviour are reported in the literature. One can find static models as well as dynamic models, models that are built heuristically as well as ones derived from physical behaviour. Pacejka [96] derive a static heuristic model known as “magic formula” from experimental data where the friction is a function of slip. Burckhardt [25] presents a similar analytical model. Daiß and Kiencke [29] simplified Burckhard’s model. The result is a model that depends linear on the parameters. De Wit [32] proposes a dynamical tyre friction model.

Apart from the nonlinear behaviour of the slip the tyre friction depends on some other uncertainties like road condition, tyre pressure, brand of tyre, temperature etc. One special model is presented that will be used due to a low computational complexity and some other advantages.

The model has been originally reported in [120] and has the following advantages:

- it models longitudinal as well as lateral slip,
- the side slip angle is part of the model,

- relatively low computational complexity that make the model usable for real time implementation,
- invertibility $\mu_H = f(\mu, \lambda)$.

Other models can be found in e.g. [25, 68]. We denote the tangential and lateral forces on the contact surface between tyre and road by

$$\begin{aligned} F_x &= \mu_x F_z \\ F_y &= \mu_y F_z. \end{aligned} \quad (4.7)$$

The model used here describes the steady state tangential and lateral friction coefficients μ_x and μ_y using the following set of equations:

$$\mu_x = \begin{cases} \frac{\lambda_x}{(\xi_U - 1)^2 + C_U^* \xi_U} \cdot \frac{C_{U0}}{F_N} & \text{for } \xi_U \leq 1 \\ \frac{\lambda_x}{\lambda_R} \mu_U & \text{for } \xi_U > 1 \end{cases} \quad (4.8)$$

$$\mu_y = \begin{cases} \frac{\lambda_y}{(\xi_S - 1)^2 + C_S^* \xi_S} \cdot \frac{C_S}{F_z} & \text{for } \xi_S \leq 1 \\ \frac{\lambda_y}{\lambda_R} \mu_S & \text{for } \xi_S > 1 \end{cases} \quad (4.9)$$

where

$$C_U^* = \frac{\lambda_U \max C_{U0}}{F_N \mu_U} \quad C_S^* = \frac{\lambda_S \max C_S}{F_z \mu_S} \quad (4.10)$$

are the normalised stiffnesses and

$$\xi_U = \frac{\lambda_R}{\lambda_{U \max}} \quad \xi_S = \frac{\lambda_R}{\lambda_{S \max}} \quad (4.11)$$

are normalised slips. The definition of slip is given by

$$\lambda_x = -\frac{\omega r - v_x}{v_R} \quad (4.12)$$

$$\lambda_y = \sin \alpha \quad (4.13)$$

$$\lambda_R = \sqrt{\lambda_x^2 + \lambda_y^2} \quad (4.14)$$

where the symbols λ_x , λ_y and λ_R denote tangential, lateral and resulting slip respectively. The variable ω is the angular speed of the wheel, r its radius, v_x is the longitudinal speed of the footprint of the wheel, v_y the lateral speed of the foot print of the wheel and v_R the resultant speed.

For large values of slip the tyre friction characteristic becomes highly uncertain. Since the slip dynamics is unstable in this region it is, in fact, difficult to determine this part of the curve from experiments.

The parameters of the model:

μ_S coefficient of lateral friction

μ_U coefficient of tangential friction

C_S cornering stiffness

C_U tangential stiffness

λ_{Smax} slip where lateral friction approaches its maximum

λ_{Umax} slip where tangential friction approaches its maximum

depend on the vertical force F_z (load on tyre) and the friction coefficient μ_H of the road:

$$\mu_U = \left(\mu_{U0} + \mu_{U1} \frac{F_z}{F_N} \right) \mu_H \quad (4.15)$$

$$\mu_S = \left(\mu_{S0} + \mu_{S1} \frac{F_z}{F_N} \right) \mu_H \quad (4.16)$$

$$C_U = C_{U0} \frac{F_z}{F_N} \quad (4.17)$$

$$C_S = C_{S0} \sin \left[2 \arctan \left(\frac{F_z}{F_N} \right) \right] \quad (4.18)$$

$$\lambda_{Umax} = \lambda_{U0} \mu_H \quad (4.19)$$

$$\lambda_{Smax} = \mu_h \sin \left(\lambda_{S0} + \lambda_{S1} \frac{F_z}{F_N} \right) \quad (4.20)$$

The inverse model $\mu_H = f(\mu, \lambda)$ can be calculated for $\xi_U \leq 1$ by solving the quadratic equation

$$0 = \left(\mu_x - \frac{\lambda_x C_{U0}}{F_N} \right) \mu_H^2 - \mu_x \lambda_R \left(\frac{2}{\lambda_{U0}} - \frac{C_{U0}}{F_N \mu_{U0} + F_z \mu_{U1}} \right) \mu_H + \mu_x \frac{\lambda_R^2}{\lambda_{U0}}. \quad (4.21)$$

4.1.6 Dynamics of the uncontrolled system

To analyse the dynamics of system (4.1)–(4.2) a change of variables is carried out where the angular speed of the wheel ω is replaced by the slip λ . It is assumed that ω , v and T_b are positive. By calculating the derivative of Eq. (4.4) with respect to time we obtain

$$\dot{\lambda} = \frac{d}{dt} \left(1 - \frac{\omega r}{v} \right) \quad (4.22)$$

$$= -\frac{\dot{\omega} r}{v} + \underbrace{\frac{\omega r}{v}}_{1-\lambda} \cdot \frac{\dot{v}}{v} \quad (4.23)$$

Inserting the equations of motion results in the two equations

$$\dot{\lambda} = -\frac{1}{v} \left\{ \frac{1}{m} (1 - \lambda) + \frac{r^2}{J} \right\} F_z \mu(\lambda, \mu_H) + \frac{1}{v} \cdot \frac{r}{J} T_b \quad (4.24)$$

$$\dot{v} = -\frac{1}{m} F_z \mu(\lambda, \mu_H) \quad (4.25)$$

It can be seen that the time scale of the slip dynamics (4.24) scales with speed v . The qualitative dynamic behaviour of slip is not affected by speed.

When considering the slip as the output $y = \lambda$ and the brake torque as an input $u = T_b$ then Eq (4.25) describes the zero dynamics of the system since the speed dynamics can be made unobservable with respect to the output λ using the feedback

$$T_b = \frac{Jv}{r} \left[\frac{1}{v} \left\{ \frac{1}{m}(1 - \lambda) + \frac{r^2}{J} \right\} F_z \mu(\lambda, \mu_H) + \nu \right]$$

where ν is a new control input.

Next, the stability of the slip dynamics (4.24) is analysed for fixed values of the parameters μ_H and F_z . Define

$$\varphi(\lambda) = \left\{ \frac{J}{mr}(1 - \lambda) + r \right\} F_z \mu(\lambda, \mu_H) \quad (4.26)$$

and rewrite Eq. (4.24) to

$$\frac{J}{r} v \cdot \dot{\lambda} = -\varphi(\lambda) + T_b. \quad (4.27)$$

In general

$$\frac{J}{mr}(1 - \lambda) \ll 1$$

and hence

$$\varphi(\lambda) \approx r \cdot F_z \mu(\lambda, \mu_H)$$

is a good approximation.

The function φ is bounded and continuous on the interval $[0, 1]$. Thus, there exists a maximum φ_{max} and any constant brake torque

$$T_b > \varphi_{max}$$

will result in

$$\dot{\lambda} > 0$$

No equilibrium point will exist for a slip less than one and the system will be unstable.

For the case

$$T_b^0 \leq \varphi_{max}$$

equilibrium points are obtained which will be stable or unstable nodes depending on the sign of the slope of φ and consequently of μ . In Fig. 4.7 a typical case for a tyre friction curve with a maximum is depicted. For a given constant value of $T_b = T_b^0$ a stable node λ_0^1 and an unstable node λ_0^2 is obtained, which means that if the brake torque is fixed at $T_b = \varphi(\lambda_0^1)$ and the slip exceeds the value λ_0^2 then the system will be unstable.

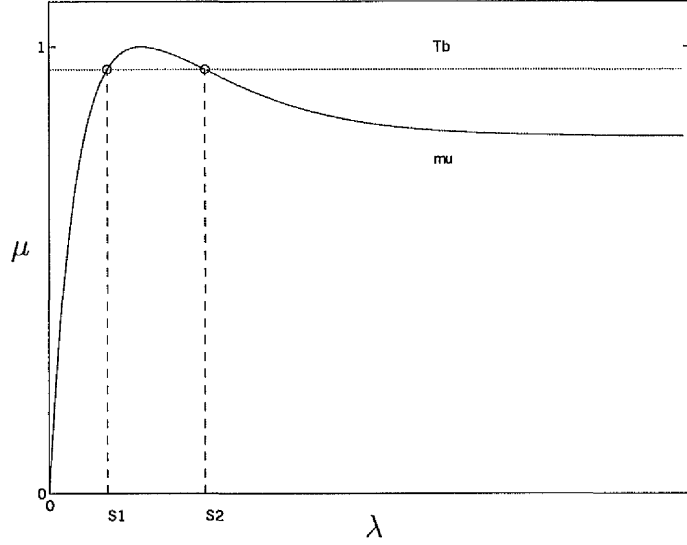


Figure 4.7: Slip equilibrium points

4.1.7 Mathematical Structure of the tyre slip dynamics

According to eq. (4.24) and (4.25) the equations of tyre slip have the following structure

$$\begin{aligned}\dot{x}_1 &= -\frac{1}{x_2}\varphi(x_1, \theta) + \frac{1}{x_2}u \\ \dot{x}_2 &= -\frac{\varphi(x_1, \theta)}{1 - x_1 + \frac{mr^2}{J}}\end{aligned}\quad (4.28)$$

where $\varphi(x_1, \theta) = \left\{ \frac{J}{mr} (1 - x_1) + r \right\} F_z \mu(x_1, \theta) > 0$, $0 < u \leq u_{max}$ and $\frac{\partial \varphi}{\partial \theta} \Big|_{x_1} > 0$. $x_1 = \lambda$ is the slip and $x_2 = \frac{Jv}{r}$. $\varphi(x_1, \theta)$ is a nonlinear function of slip and the uncertain tyre-road friction coefficient $\theta = \mu_H$, u is the brake torque. The first equation describes the tyre slip dynamics while the second equation is the equation of motion of the vehicle. In general the function φ depends nonlinearly on the parameter θ . The control problem consists in stabilising the slip around a constant set point x_1^0 where $\dot{x}_1 = 0$ hence $u^0 = \varphi(x_1^0, \theta) = \varphi_0$. With this the modified system is given by

$$\begin{aligned}\dot{\tilde{x}}_1 &= -\frac{1}{x_2}\tilde{\varphi}(x_1, \theta) + \frac{1}{x_2}\tilde{u} \\ \dot{x}_2 &= -\frac{\varphi(x_1, \theta)}{1 - x_1 + \frac{mr^2}{J}}\end{aligned}\quad (4.29)$$

where $\tilde{x}_1 = x_1 - x_1^0$ is the slip error, $\tilde{u} = u - u^0$ and $\tilde{\varphi} = \varphi(x_1^0 + \tilde{x}_1, \theta) - \varphi(x_1^0, \theta)$. The nonlinear system and input functions of the system $\tilde{\dot{x}} = \tilde{f}(x, \theta) + \tilde{g}(x)u$ are

$$\tilde{f} = \begin{pmatrix} -\frac{1}{x_2} \\ -\frac{\varphi(x_1, \theta)}{1 - x_1 + \frac{mr^2}{J}} \end{pmatrix}\quad (4.30)$$

and

$$\tilde{g} = \begin{pmatrix} \frac{1}{x_2} \\ 0 \end{pmatrix} \quad (4.31)$$

4.1.8 Specification of an ABS

From the previous considerations it is obvious that instabilities of the slip dynamics are likely to occur during uncontrolled braking in which case the angular speed of the wheel will eventually slow down to zero with the slip attaining a value of one and the wheel being locked. This is highly undesirable for several reasons:

- the wear of the tyre will be increased by uneven abrasion of rubber
- for cases where the tyre friction characteristics has a maximum, deceleration will be sub-optimal
- steerability of the car will be lost.

The problem of controlling the slip of a quarter car is considered. The control objective is to keep the slip at a specified set point value λ_0 while braking, thus preventing a wheel lock and maintaining steerability.

The specification includes the following requirements [25, 12]:

- no wheel lock allowed to occur for speeds above $4\frac{\text{m}}{\text{s}}$ and $\mu_H = 0.1$
- wheel lock for a period of less than 0.2 seconds is allowed for speeds in the range of $0.8 \dots 4\frac{\text{m}}{\text{s}}$
- for speeds below $0.8\frac{\text{m}}{\text{s}}$ the wheels are allowed to lock.
- The control system should be robust with respect to other unmodelled dynamics:
 - actuator dynamics,
 - suspension,
 - tyre relaxation dynamics.
- Since the controller will be implemented on a microprocessor in a TTP architecture it should be robust with respect to an additional time delay of 14 milliseconds caused by sampling.

4.2 A nonlinear PI tyre slip controller

A PI-type nonlinear adaptive tyre slip controller is presented. The tyre slip controller is designed to serve as a low-level controller in the ABS system. A control Lyapunov function approach (Sec. 3.1) for the relative degree one slip dynamics subsystem is taken to fix the structure of the controller and to calculate a lower bound on the controller gain necessary to achieve global stability. The control Lyapunov function is scaled with vehicle speed in order to avoid excessive high gain which could not be implemented. Gain scheduling techniques are used to determine the ultimate transient behaviour of the closed loop system and to accommodate for robustness against unmodelled (actuator) dynamics and sampling.

4.2.1 Design of a globally stabilising control law

Following the approach in [41, 61] the slip Eq. (4.24) is given the form

$$\dot{\lambda} = \frac{\chi r}{Jv} \sigma_1 \left[\frac{u}{\sigma_1} - \frac{\mu}{\chi} \right] \quad (4.32)$$

$$\dot{v} = -\frac{1}{m} \mu F_z \quad (4.33)$$

where σ_1 is a function of the slip λ and the vertical force F_z

$$\sigma_1(\lambda) = \left(1 + \frac{J}{mr^2} (1 - \lambda) \right) r F_z \quad (4.34)$$

which has the dimension of a torque. The control input into the system is the brake torque.

$$u = \chi T_b \quad (4.35)$$

where χ denotes the gain of the brake actuator which is uncertain due to changes in the friction coefficient between brake pads and brake disk. Its nominal value is assumed to be $\chi_0 = 1$ and its range

$$\chi_{min} \leq \chi \leq \chi_{max}$$

is assumed to be known.

In contrast to [41] a modified control Lyapunov function is used here

$$V = \frac{1}{2} v^2 \cdot (\lambda - \lambda_0)^2 + \frac{1}{2} \frac{\chi}{\gamma} \left(\frac{\mu(\lambda_0)}{\chi} - \eta \right)^2 \quad (4.36)$$

where λ_0 is the set point slip, γ is a positive number and η is an estimate of the set point value of the offset term $\frac{\mu}{\chi}$ in (4.32) which varies with road condition, tyre brand,

actuator gain etc. The weight v^2 of the first term in the Lyapunov function is necessary to prevent the controller from having excessively high gain. Due to the scaling of the slip dynamics with speed the gain of the plant will increase with decreasing v . This has to be compensated by lowering the controller gain. As will be shown later a high gain controller cannot be implemented since additional actuator dynamics and time sampling impose an upper bound on the loop gain.

Taking the time derivative of the Lyapunov function (4.36) and substituting (4.32) and (4.33) respectively one obtains

$$\begin{aligned}\dot{V} &= v^2(\lambda - \lambda_0)\dot{\lambda} + v(\lambda - \lambda_0)^2\dot{v} - \frac{\chi}{\gamma} \left(\frac{\mu(\lambda_0)}{\chi} - \eta \right) \dot{\eta} \\ &= v \left\{ \frac{\chi r}{J} \sigma_1 \left[\frac{u}{\sigma_1} - \frac{\mu(\lambda)}{\chi} \right] - \frac{1}{m} \mu(\lambda) F_z(\lambda - \lambda_0) \right\} (\lambda - \lambda_0) - \frac{\chi}{\gamma} \left(\frac{\mu(\lambda_0)}{\chi} - \eta \right) \dot{\eta}\end{aligned}\quad (4.37)$$

Using the definition of σ_1 in (4.34) and defining

$$\sigma_1(\lambda_0) = \sigma_0 \quad (4.38)$$

the derivative the first term of the Lyapunov function can be simplified further obtaining

$$\dot{V} = v \frac{\chi r}{J} \sigma_0 \left[\frac{u}{\sigma_0} - \frac{\mu(\lambda)}{\chi} \right] \cdot (\lambda - \lambda_0) - \frac{\chi}{\gamma} \left(\frac{\mu(\lambda_0)}{\chi} - \eta \right) \dot{\eta} \quad (4.39)$$

Finally, the identity

$$\begin{aligned}\mu(\lambda) &= \mu(\lambda_0) + \mu(\lambda) - \mu(\lambda_0) \\ &= \chi\eta + \mu(\lambda) - \mu(\lambda_0) + \chi \left(\frac{\mu(\lambda_0)}{\chi} - \eta \right)\end{aligned}\quad (4.40)$$

is used to yield

$$\begin{aligned}\dot{V} &= v \frac{\chi r}{J} \sigma_0 \left[\frac{u}{\sigma_0} - \eta - \frac{\mu(\lambda) - \mu(\lambda_0)}{\chi} \right] \cdot (\lambda - \lambda_0) \\ &\quad - \chi \left\{ \frac{1}{\gamma} \dot{\eta} + v \frac{r}{J} \sigma_0 (\lambda - \lambda_0) \right\} \cdot \left(\frac{\mu(\lambda_0)}{\chi} - \eta \right)\end{aligned}\quad (4.41)$$

The second term of Eq. (4.41) can be rendered zero by use of the update law (cf. Sec. 3.1 [70])

$$\dot{\eta} = -\gamma v \frac{r}{J} \sigma_0 (\lambda - \lambda_0) \quad (4.42)$$

where the design parameter γ will be specified later. The remaining part of the control Lyapunov function

$$\dot{V} = v \frac{\chi r}{J} \sigma_0 \left[\frac{u}{\sigma_0} - \eta - \frac{\mu(\lambda) - \mu(\lambda_0)}{\theta} \right] \cdot (\lambda - \lambda_0) \quad (4.43)$$

has to be made negative semidefinite by choosing an appropriate control law for u . The variable η is a known quantity and can be eliminated by the control whereas the uncertain term $\frac{\mu(\lambda) - \mu(\lambda_0)}{\chi}$ has to be dominated rather than cancelled. In the worst case this term has the opposite sign with respect to $(\lambda - \lambda_0)$ which happens when the tyre friction characteristics μ has a negative slope. However, the slope of μ will usually be bounded from below with the Lipschitz condition (cf. Eq. 2.14)

$$\frac{\mu(\lambda) - \mu(\lambda_0)}{\lambda - \lambda_0} \geq -\beta_{min}, \quad \beta > 0. \quad (4.44)$$

Using this condition, an upper bound on \dot{V} is

$$\dot{V} \leq v \frac{\chi^r}{J} \sigma_0 \left[\frac{u}{\sigma_0} - \eta + \frac{\beta_{min}}{\chi_{min}} (\lambda - \lambda_0) \right] \cdot (\lambda - \lambda_0) \quad (4.45)$$

and, using the PI control law

$$u = \sigma_0 \cdot [\eta - k_p(\lambda - \lambda_0)] \quad (4.46)$$

the condition

$$\dot{V} \leq v \frac{\chi^r}{J} \sigma_0 \left[\frac{\beta_{min}}{\chi_{min}} - k_p \right] \cdot (\lambda - \lambda_0)^2 < 0 \quad (4.47)$$

for closed loop stability is obtained. This condition can be satisfied by selection of the controller gain

$$k_p > \frac{\beta_{min}}{\chi_{min}} \quad (4.48)$$

which renders the closed loop system globally stable. In order to improve robustness with respect to unmodelled nonlinearities a nonlinear term can be added to the control law (4.46) e.g.:

$$u = \sigma_0 \cdot [\eta - k_p(\lambda - \lambda_0) - k_3(\lambda - \lambda_0)^3] \quad k_3 \geq 0 \quad (4.49)$$

The cubic term in the control law can considerably speed up the transients of the closed loop system for large slip errors while vanishing quickly when this error becomes small. The corresponding derivative of the Lyapunov function is:

$$\dot{V} \leq v \frac{\chi^r}{J} \sigma_0 \left[\frac{\beta_{min}}{\chi_{min}} - k_p - k_3(\lambda - \lambda_0)^2 \right] \cdot (\lambda - \lambda_0)^2 < 0 \quad (4.50)$$

It is worth noting that apart from the stability condition (4.48) one is completely free in the choice of the design parameters k_p and γ . This freedom can be used to accommodate additional performance and robustness requirements on the closed loop system. In accordance with classical control, performance and robustness conditions will be derived from the linearisation of the open loop system and the closed loop system about the set point λ_0 .

4.2.2 Linear Analysis

Define the control errors

$$e_1 = \lambda - \lambda_0 \quad (4.51)$$

$$e_2 = \eta - \frac{\mu(\lambda_0)}{\chi} \quad (4.52)$$

Then the closed loop error dynamics is given by

$$\dot{e}_1 = \frac{\chi r}{Jv} \left[\sigma_0 \{e_2 - k_p e_1\} + \frac{J\mu(\lambda_0)}{mr} F_z e_1 - \sigma_1 \frac{\mu(\lambda) - \mu(\lambda_0)}{\chi} \right] \quad (4.53)$$

$$\dot{e}_2 = -\gamma v \frac{r}{J} \sigma_0 e_1 \quad (4.54)$$

which results in the linearisation

$$\begin{aligned} \dot{e}_1 &= \frac{\chi r}{Jv} \left[\sigma_0 \{e_2 - k_p e_1\} + \frac{J\mu(\lambda_0)}{mr} F_z e_1 - \frac{\sigma_0}{\chi} \left. \frac{d\mu(\lambda)}{d\lambda} \right|_{\lambda=\lambda_0} e_1 \right] + \mathcal{O}(e_1^2) \\ \dot{e}_2 &= -\gamma v \frac{r}{J} \sigma_0 e_1 \end{aligned} \quad (4.55)$$

The structure of the linearised error dynamics equation suggests a choice of the controller gain of the form

$$k_p = \frac{\beta_{min}}{\chi_{min}} + \frac{1}{\sigma_0} \frac{J}{mr} F_z \eta + \frac{1}{\sigma_0} \frac{J}{r\chi_{min}} v \kappa \quad (4.56)$$

with a new design parameter κ and the resulting error dynamics

$$\begin{aligned} \dot{e}_1 &= -\frac{\chi}{\chi_{min}} \kappa e_1 - \frac{\chi r}{Jv} \sigma_0 \left\{ \frac{1}{\chi} \left. \frac{d\mu(\lambda)}{d\lambda} \right|_{\lambda=\lambda_0} + \frac{\beta_{min}}{\theta_{min}} \right\} e_1 + \frac{\theta r \sigma_0}{Jv} e_2 + \mathcal{O}(e_1^2, e_2^2) \\ \dot{e}_2 &= -\gamma v \frac{r}{J} \sigma_0 e_1 \end{aligned} \quad (4.57)$$

First the nominal error dynamics is designed where the the Lipschitz constant β_{min} is assumed to take the value

$$\beta_{min} = - \left. \frac{d\mu(\lambda)}{d\lambda} \right|_{\lambda=\lambda_0}$$

and

$$\chi_{min} = \chi$$

such that the bracketed term is cancelled. The corresponding error dynamics is

$$\dot{e} = \hat{A} e \quad (4.58)$$

where

$$e = \begin{pmatrix} e_1 \\ e_2 \end{pmatrix} \quad \text{and} \quad \hat{A} = \begin{pmatrix} -\frac{\chi}{\chi_{min}} \kappa & \frac{\chi r \sigma_0}{Jv} \\ -\gamma v \frac{r}{J} \sigma_0 & 0 \end{pmatrix} \quad (4.59)$$

which leads to the characteristic equation

$$\det(sI - \hat{A}) = s^2 + \kappa s + \gamma \left[\frac{r}{J} \sigma_0 \right]^2 \quad (4.60)$$

The design parameters can now be fixed to

$$\kappa = \frac{2\hat{D}}{T} \quad (4.61)$$

$$\gamma = \frac{1}{T^2} \left[\frac{J}{r\sigma_0} \right]^2 \quad (4.62)$$

where the closed loop dynamics is given by the rise time T and the nominal damping \hat{D} of the step response. Next, the perturbed closed loop system is analysed. It has the characteristic equation

$$\det(sI - A) = s^2 + \frac{2D}{T}s + \frac{1}{T^2} \quad (4.63)$$

where

$$D = \frac{\chi}{\chi_{min}} \hat{D} + \frac{T}{2} \cdot \frac{\theta r}{Jv} \sigma_0 \left\{ \frac{1}{\chi} \frac{d\mu(\lambda)}{d\lambda} \Big|_{\lambda=\lambda_0} + \frac{\beta_{min}}{\chi_{min}} \right\} \quad (4.64)$$

First, the case $\chi_{min} = \theta$ is analysed i.e. there is now uncertainty in the actuator gain. In this case

$$D = \hat{D} + \frac{T}{2} \cdot \frac{r}{Jv} \sigma_0 \left\{ \frac{d\mu(\lambda)}{d\lambda} \Big|_{\lambda=\lambda_0} + \beta_{min} \right\} \quad (4.65)$$

The perturbed damping coefficient scales with the inverse of the speed. Thus, the largest deviation from the nominal case will occur when the speed is low ($v = v_{min}$) and the slope of the tyre friction characteristics attains its maximum value

$$\max \left[\frac{d\mu(\lambda)}{d\lambda} \right]_{\lambda=\lambda_0} = \beta_{max} \quad (4.66)$$

Hence, an upper bound on D is given by

$$D \leq \hat{D} + T \cdot \frac{r}{Jv_{min}} \sigma_0 \cdot \frac{\beta_{min} + \beta_{max}}{2}. \quad (4.67)$$

Thus the perturbed closed loop system is stable.

4.3 Sontags's universal formula used for ABS

Another Lyapunov based nonlinear adaptive tyre slip controller is presented [74]. The inverse optimal design introduced in Sec. 3.1 is applied.

The advantage of the inverse optimal approach is that it relies on domination of the destabilising nonlinearities and it does not cancel stabilising nonlinearities. Furthermore the knowledge of nonlinearities is not used for cancellations. A worst case

approximation of the uncertain nonlinearity can be used instead. The stability margins of this approach are better with respect to static modelling errors. Thus this approach is robust against unmodelled dynamics without having high gain.

Again, consider the slip Eq. (4.29). In contrast to the control Lyapunov approach in Sec. 4.2 the control Lyapunov function (clf) is given by:

$$V = \frac{1}{2}\tilde{x}_1^2x_2^2 + \frac{1}{2\gamma}\tilde{\theta}^2 \quad (4.68)$$

where $\tilde{\theta} = \theta - \hat{\theta}$. The time derivative is given by

$$\begin{aligned} \dot{V} &= x_2^2\tilde{x}_1\dot{\tilde{x}}_1 + \tilde{x}_1^2x_2\dot{x}_2 - \frac{1}{\gamma}\tilde{\theta}\dot{\tilde{\theta}} \\ &= -\tilde{x}_1x_2 \left(\tilde{\varphi}(x_1, \theta) + \frac{\tilde{x}_1}{1-x_1 + \frac{mr^2}{J}}\varphi(x_1, \theta) - \tilde{u} \right) - \frac{1}{\gamma}\tilde{\theta}\dot{\tilde{\theta}} \end{aligned} \quad (4.69)$$

where $\varphi(x_1, \theta)$ is the tyre slip nonlinearity, linearised at the estimated parameter $\hat{\theta}$,

$$\varphi(x_1, \theta) = \varphi(x_1, \hat{\theta}) + \left. \frac{\partial \varphi}{\partial \theta} \right|_{x_1, \hat{\theta}} \tilde{\theta} + \varepsilon. \quad (4.70)$$

The error ε is related to the higher order terms in the Taylor series expansion. This error is small for large slip. The friction depends nearly linearly on the parameter θ for large slip and nonlinearly for very small slip where the system is stable (see Fig. 4.8). This

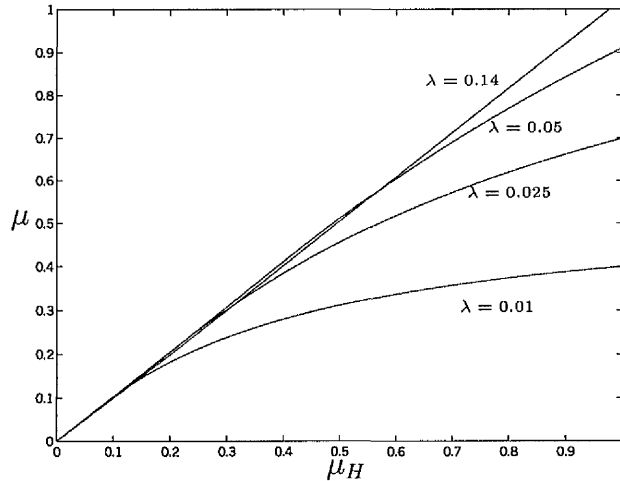


Figure 4.8: Friction as a function of μ_H with slip as parameter

gradient approach has been reported in [91]. An approach for systems with nonlinear but convex/concave parametric uncertainty is discussed in [14].

The time derivative becomes, after sorting with respect to $\tilde{\theta}$,

$$\begin{aligned} \dot{V} = & -\tilde{x}_1 x_2 \left(\tilde{\varphi}(x_1, \hat{\theta}) + \varepsilon + \frac{\tilde{x}_1}{1 - x_1 + \frac{mr^2}{J}} \varphi(x_1, \hat{\theta}) + \frac{\tilde{x}_1}{1 - x_1 + \frac{mr^2}{J}} \varepsilon + u \right) \\ & - \left(\left(\frac{\partial \tilde{\varphi}}{\partial \theta} \Big|_{x_1, \hat{\theta}} + \frac{\tilde{x}_1}{1 - x_1 + \frac{mr^2}{J}} \frac{\partial \varphi}{\partial \theta} \Big|_{x_1, \hat{\theta}} \right) \tilde{x}_1 x_2 + \frac{1}{\gamma} \dot{\tilde{\theta}} \right) \tilde{\theta} \end{aligned} \quad (4.71)$$

The tuning function

$$\dot{\tilde{\theta}} = -\gamma \left(\frac{\partial \tilde{\varphi}}{\partial \theta} \Big|_{x_1, \hat{\theta}} + \frac{\tilde{x}_1}{1 - x_1 + \frac{mr^2}{J}} \frac{\partial \varphi}{\partial \theta} \Big|_{x_1, \hat{\theta}} \right) \tilde{x}_1 x_2 \quad (4.72)$$

renders the second part of the time derived Lyapunov function (4.71) negative semidefinite. The part of (4.71) that depends on the uncertain parameter θ is cancelled.

A particular optimal stabilising control law \tilde{u} that renders the remaining part of the Lyapunov function negative definite is given by Sontag's formula (3.7):

$$\tilde{u} = \begin{cases} - \left(c_0 + \frac{a(x) + \sqrt{a^2 + (b^T(x)b(x))^2}}{b^T(x)b(x)} \right) b(x) & \text{for } b(x) \neq 0 \\ 0 & \text{for } b(x) = 0. \end{cases} \quad (4.73)$$

The application of Sontag's universal formula to the slip control system (4.29) and the first part of the Lyapunov function $V_{aclf} = \frac{1}{2} \tilde{x}_1 x_2$ yields:

$$\begin{aligned} a &= L_f V = - \underbrace{\tilde{x}_1 x_2}_b \left[\tilde{\varphi}(x_1, \hat{\theta}) + \frac{\tilde{x}_1}{1 - x_1 + \frac{mr^2}{J}} \varphi(x_1, \hat{\theta}) \right] \\ b &= (L_g V)^T = \tilde{x}_1 x_2 \end{aligned} \quad (4.74)$$

Since $b = 0$ implies $a = 0$ the control law can be simplified to

$$\begin{aligned} \tilde{u} = & -c_0 \tilde{x}_1 x_2 + \tilde{\varphi}(x_1, \hat{\theta}) + \frac{\tilde{x}_1}{1 - x_1 + \frac{mr^2}{J}} \varphi(x_1, \hat{\theta}) \\ & - \text{sgn}(\tilde{x}_1) \cdot \sqrt{\left(\tilde{\varphi}(x_1, \hat{\theta}) + \frac{\tilde{x}_1}{1 - x_1 + \frac{mr^2}{J}} \varphi(x_1, \hat{\theta}) \right)^2 + \tilde{x}_1^2 x_2^2}. \end{aligned} \quad (4.75)$$

The first term of the Lyapunov function is rendered negative definite by the control law (4.75) while the second is stabilised by the adaptation law (4.72). The parameters c_0 and $\gamma \in \mathbf{R}^+$ can be used to accommodate performance and robustness requirements of the closed loop system. Note that the ‘‘Sontag’’ controller adapts to the tyre friction coefficient μ_H . The adaptation can be interpreted as the integral part of the controller [70].

4.4 SSP wheel slip controller

The design of an ABS controller using the SSP-approach [133] is based on linearisation of the non-linear slip model (4.24) of a braking quarter car. Here a change of the time domain will be proposed to relax the speed dependence of the slip dynamics. The slip differential equation

$$v\dot{\lambda} = -\left\{\frac{1}{m}(1-\lambda) + \frac{r^2}{J}\right\} F_z\mu(\lambda, \mu_H) + \frac{r}{J}T_b \quad (4.76)$$

is modified using the transformation $\frac{v}{dt} = \frac{1}{d\tau}$. This results in a transformed slip dynamics

$$\frac{d\lambda}{d\tau} = -\left\{\frac{1}{m}(1-\lambda) + \frac{r^2}{J}\right\} F_z\mu(\lambda, \mu_H) + \frac{r}{J}T_b \quad (4.77)$$

in the new time domain $\tau = \frac{t}{v}$.

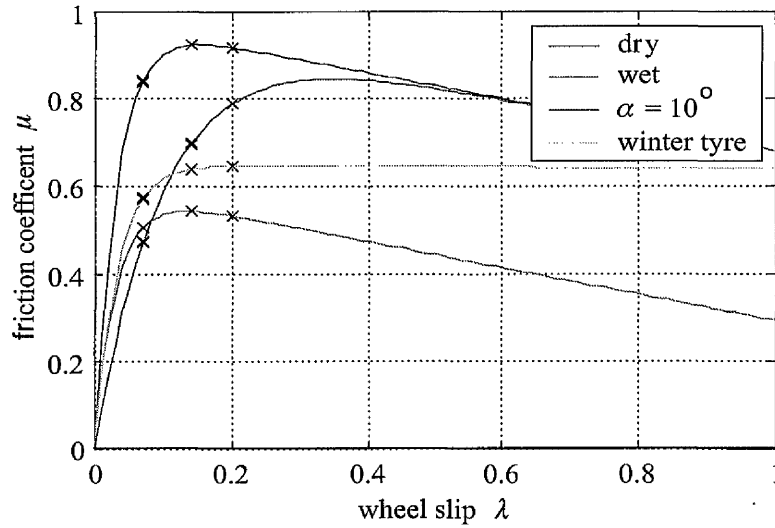


Figure 4.9: Tyre friction curves with 12 linearisation points

Linearisation of the modified slip equation (4.77) using four different road conditions and three different wheel slips, as depicted in Fig. 4.9, results in an array of 12 (9 stable and 3 unstable) transfer functions:

$$G_i(s^*) = \frac{0.32}{s^* + k_i} \quad (4.78)$$

where

$$-k_i = -\{1649, 69.84, -114.1, 861.1, -26.65, -130.1, 11.70, 138.9, 18.77, 2287, 1060, 513.8\}$$

are the poles of the individual plant transfer functions. The operator s^* stands for the modified Laplace operator in the time domain τ .

Solving the set of equations and inequalities described in [133] yields the following linear PI controller

$$G_c(s^*) = \frac{621s^* + 10248}{s^*} \quad (4.79)$$

$$= 621 + \frac{10248}{s^*}. \quad (4.80)$$

Bode plots (cf. Fig. 4.10 and 4.11) and closed loop step responses are shown for each linear plant. The plant transfer function as well as the phase margin [30, 110] are displayed. The minimal phase margin is $\Phi(\omega_{GC}) = 43.2^\circ$ at $\omega_{GC} = 21.5\text{Hz}$.

Using the inverse transformation $s^* = \frac{s}{v}$ in order to get the controller in the time domain t one gets

$$G_c(s) = 621 + \frac{10248v}{s}. \quad (4.81)$$

This gain scheduled controller shifts the D-region for velocities $v > 1$ towards the left hand side. Thus, the stability is preserved if the system is time invariant.

4.5 LQRC wheel slip controller

Recently algorithms have been developed for efficient real-time implementation of constrained LQ controllers (LQRC) [57]. The handling of constraints is important since for example actuator rate constraints will constitute fundamental performance limitations. They are also considered to be a useful design parameter to avoid excitation of resonant suspension modes. Nonlinearities such as the dependence on the speed are handled by gain-scheduling and local linearisations.

The discrete-time slip dynamics (4.24), with sampling interval Δ is:

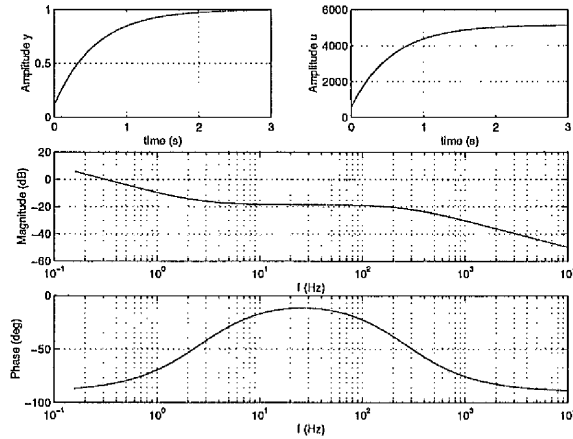
$$\lambda(k+1) = \lambda(k) - \frac{\Delta}{v(k)} \left(\frac{1}{m}(1 - \lambda(k)) + \frac{r^2}{J} \right) F_z \mu(\lambda(k), \mu_H(k), \alpha(k)) + \frac{\Delta}{v(k)} \frac{r}{J} T_b(k) \quad (4.82)$$

Let $(\lambda_0, T_{b,0})$ be an equilibrium point for (4.24) defined by the constants $v_0, \alpha_0, F_{z,0}$ and $\mu_{H,0}$. For a given λ_0 one gets

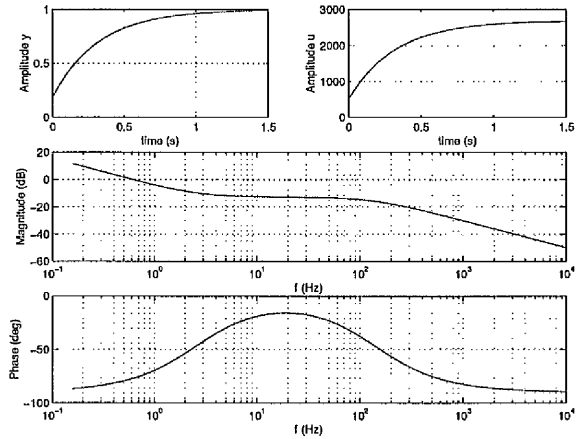
$$T_{b,0} = \left(\frac{J}{mr}(1 - \lambda_0) + r \right) F_z \mu(\lambda_0, \mu_{H,0}, \alpha_0). \quad (4.83)$$

A linear model, valid near some equilibrium state is

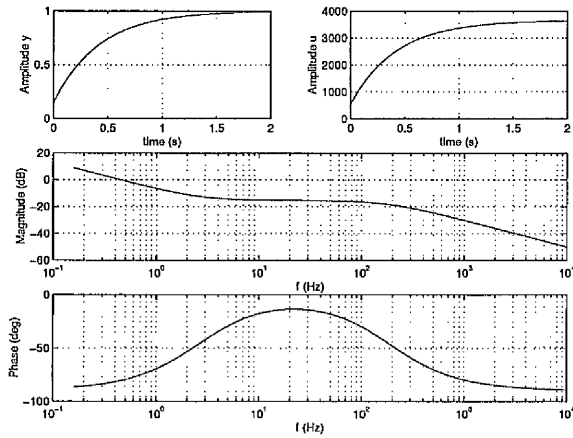
$$\lambda(k+1) = \lambda_0 + \alpha_1(\lambda(k) - \lambda_0) + \beta_1(T_b(k) - T_{b,0}) \quad (4.84)$$



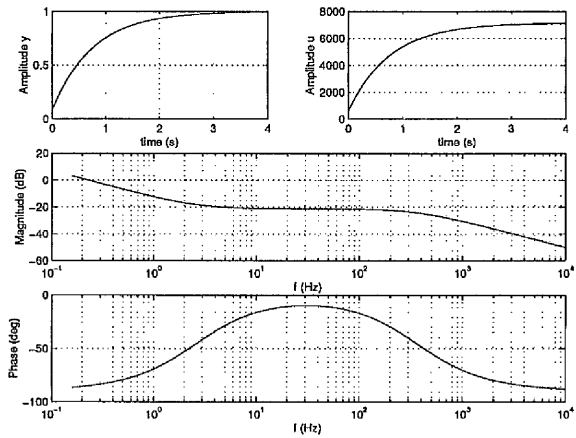
(a) $G(s^*) = \frac{0.3}{s^*+1649}$; Phase margin = 96.85



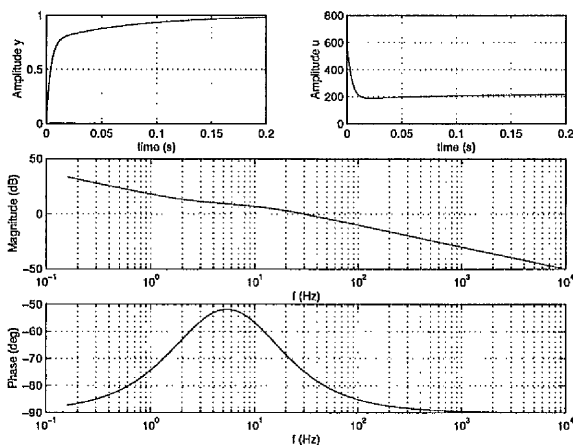
(b) $G(s^*) = \frac{0.3}{s^*+861.1}$; Phase margin = 103



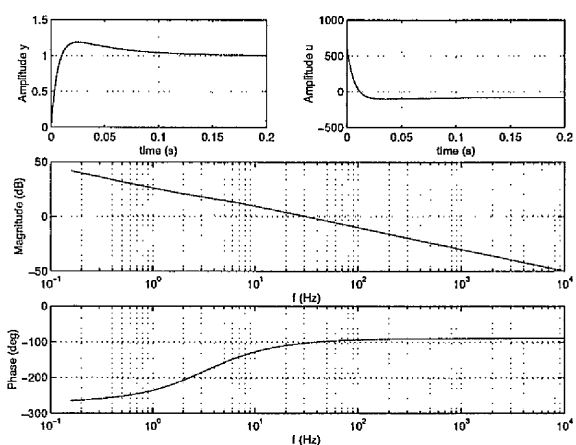
(c) $G(s^*) = \frac{0.3}{s^*+1170}$; Phase margin = 100



(d) $G(s^*) = \frac{0.3}{s^*+2287}$; Phase margin = 95

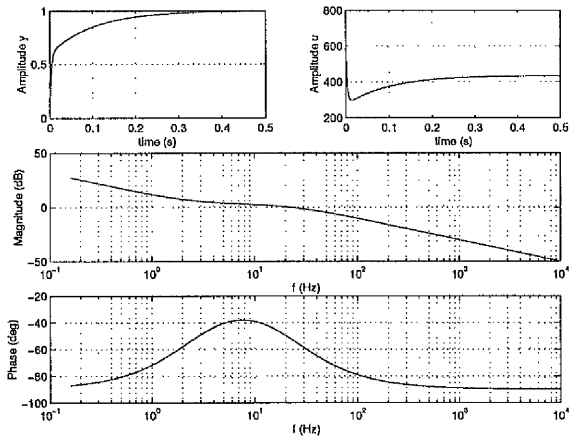


(e) $G(s^*) = \frac{0.3}{s^*+69.84}$; Phase margin = 105

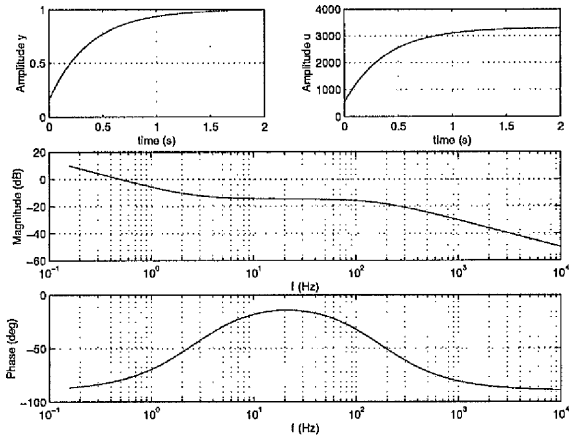


(f) $G(s^*) = \frac{0.3}{s^*-26.65}$; Phase margin = 77.5

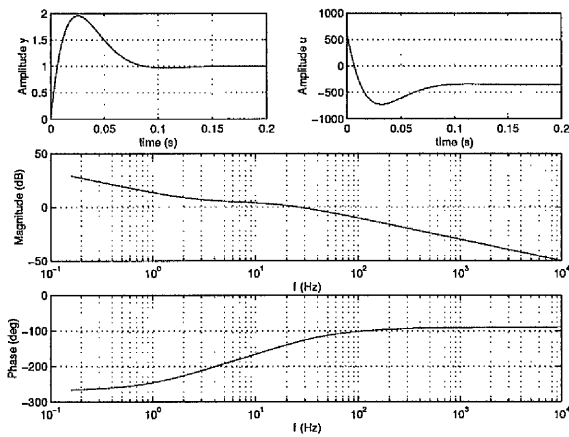
Figure 4.10: Bode plots (I) and closed loop step responses (SSP controller)



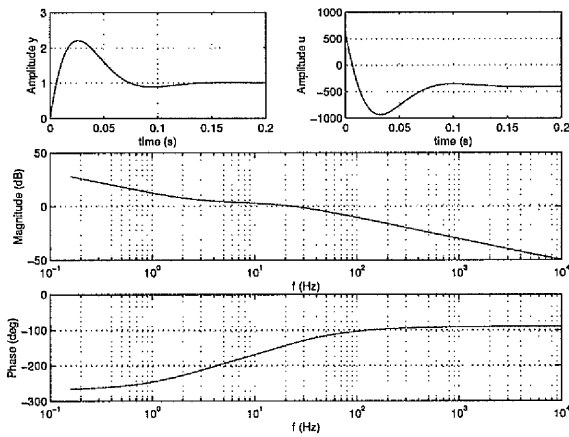
(a) $G(s^*) = \frac{0.3}{s^* + 138.9}$; Phase margin = 127.4



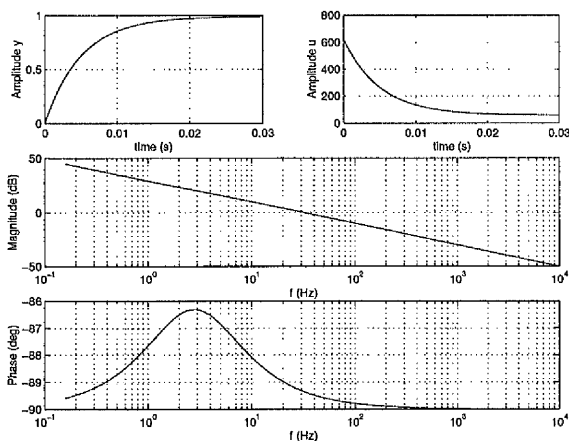
(b) $G(s^*) = \frac{0.3}{s^* + 1060}$; Phase margin = 100



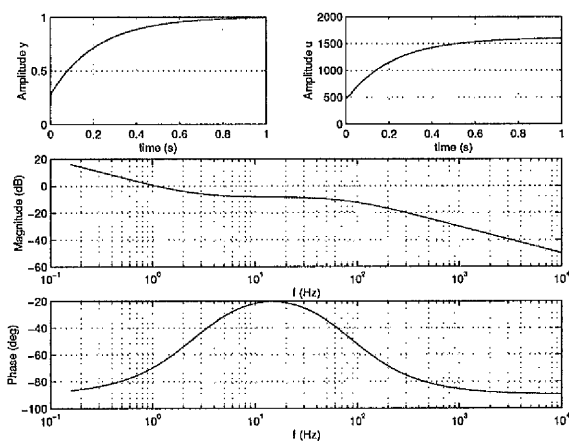
(c) $G(s^*) = \frac{0.3}{s^* - 114.1}$; Phase margin = 49.4



(d) $G(s^*) = \frac{0.3}{s^* - 130.1}$; Phase margin = 43.2



(e) $G(s^*) = \frac{0.3}{s^* + 18.77}$; Phase margin = 90.6



(f) $G(s^*) = \frac{0.3}{s^* + 513.8}$; Phase margin = 112

Figure 4.11: Bode plots (II) and closed-loop step responses (SSP controller)

where α_1 and β_1 are linearization constants given by

$$\begin{aligned}\alpha_1 &= 1 + F_{z,0} \frac{\Delta}{v_0} \left(\frac{1}{m} \mu(\lambda_0, \mu_{H,0}, \alpha_0) - \left(\frac{1}{m} (1 - \lambda_0) + \frac{r^2}{J} \right) \frac{\partial \mu}{\partial \lambda}(\lambda_0, \mu_{H,0}, \alpha_0) \right) \\ \beta_1 &= \frac{r \Delta}{v_0 J}\end{aligned}\quad (4.85)$$

In order to introduce integral action in the controller, an additional state associated with the integral of the slip error is introduced

$$i_e(k+1) = i_e(k) + \Delta(\lambda(k) - \lambda^*(k)) \quad (4.86)$$

where λ^* is the desired slip. The control $u(t)$ computed by the LQRC controller [56] is defined as the change in the commanded brake torque $u(t) = \tilde{T}_b(t) - \tilde{T}_b(t-1)$, which leads to the additional state equation

$$\tilde{T}_b(k) = \tilde{T}_b(k-1) - u(k) \quad (4.87)$$

From (4.84) it follows that

$$\lambda(k+1) - \lambda^* = \alpha_1(\lambda(k) - \lambda^*) + \beta_1(T_b(k) - T_{b,0}) + c \quad (4.88)$$

where c is a constant that can be neglected due to the integral action.

A state-space realization of the 1st order actuator dynamics (discussed in Sec.5.1) is

$$T_b(k) = 0.6T_b(k-1) + 0.4u(k-1) \quad (4.89)$$

The linearised control-oriented model of the slip dynamics including 1st order actuator dynamics and a time delay is:

$$\begin{pmatrix} i_e(k+1) \\ \lambda(k+1) - \lambda^* \\ T_b(k+1) - T_{b,0} \\ \tilde{T}_b(k+1) - T_{b,0} \end{pmatrix} = A \begin{pmatrix} i_e(k) \\ \lambda(k) - \lambda^* \\ T_b(k) - T_{b,0} \\ \tilde{T}_b(k) - T_{b,0} \end{pmatrix} + Bu(k) \quad (4.90)$$

where

$$A = \begin{pmatrix} 1 & \Delta & 0 & 0 \\ 0 & \alpha_1 & \beta_1 & 0 \\ 0 & 0 & 0.6 & 0.4 \\ 0 & 0 & 0 & 1 \end{pmatrix} \quad (4.91)$$

$$B = \begin{pmatrix} 0 \\ 0 \\ 0 \\ 1 \end{pmatrix} \quad (4.92)$$

The gain-scheduled constrained LQR controller [98] is given by:

$$u(k) = u_{LQRC}(i_e(k), \lambda(k) - \lambda^*, T_b(k), \tilde{T}_b(k); v(k)). \quad (4.93)$$

The function u_{LQRC} is a piecewise linear function with 3 linear parts. One part is the linear classical LQ controller that is active near the setpoint. The two other parts correspond to the minimum and maximum constant values of the actuator rate and are active when the classical LQ violates the rate constraints.

Gain scheduling on both speed v and slip λ has been applied. The space (v, λ) is divided into rectangles with scheduling for $v = 1, \sqrt{2}, 2, 2\sqrt{2}, 4, 4\sqrt{2}, 8, \dots$ m/s and $\lambda = 0.14$ and $\lambda = 0.06$. The motivation for the scheduling strategy is the significant modelling error for small values of λ that leads to very slow transient response of the controller when the slip increases.

The constrained LQR is designed for fixed A and B matrices (for a number of values of v and possibly λ) based on (4.90).

The actuator rate constraint leads to the following input constraint:

$$-\dot{T}_b^{max} \Delta \leq u_{LQRC}(k) \leq \dot{T}_b^{max} \Delta \quad (4.94)$$

Maximum braking forces with the EMB 4.0 actuator (cf. Sec. 5.1) are 30 kN at front wheels and 15 kN at rear wheels. In order to avoid an air gap between the brake pads and the brake disk, a minimum brake force of 50N is applied. This leads to the constraints for the front wheels

$$T_b^{min} = 0.1056\text{m} \cdot 50\text{N} = 5.3\text{Nm} \quad (4.95)$$

$$T_b^{max} = 0.1056\text{m} \cdot 30\text{kN} = 3017\text{Nm} \quad (4.96)$$

$$\dot{T}_b^{max} = 150\text{kNm/s} \quad (4.97)$$

and for the rear wheels

$$T_b^{min} = 0.1056\text{m} \cdot 50\text{N} = 5.3\text{Nm} \quad (4.98)$$

$$T_b^{max} = 0.1056\text{m} \cdot 15\text{kN} = 1584\text{Nm} \quad (4.99)$$

$$\dot{T}_b^{max} = 150\text{kNm/s} \quad (4.100)$$

There is an anti-windup mechanism on the integrator i_e . Due to the switching, we have in addition bumpless transfer where $i_e(t)$ is recalculated for the new controller such that $u(t) = 0$ for those t where the controller is switched. Then $i_e(t)$ solves

$$0 = u_{LQRC}(i_e(k), \lambda(k) - \lambda^*, T_b(k), \tilde{T}_b(k-1), \hat{v}(k)) \quad (4.101)$$

The stability of the LQRC wheel slip controller has been analysed in [98].

4.6 Activation and Bumpless Transfer

As a safety device the ABS is only active in critical situations when the driver commanded brake force results in higher slips than the setpoint of the controller. The maximal applied brake force is limited to the drivers commanded brake force. The slip controller is only allowed to lower the brake force in order to prevent the tyre from locking. For safety reasons this is an important issue. When the driver releases the brake pedal the brake force should be lowered accordingly.

Figure 4.12 shows the on/off switching of the overall controller. An operation mode f is only set when the controller is switched on manually, the gear g is set to forward (not reverse) and the reference speed v_r of the vehicle is higher than the minimum speed. The controller will be switched off when the velocity drops below a minimum ($v_{min} = 1\text{m/s}$).

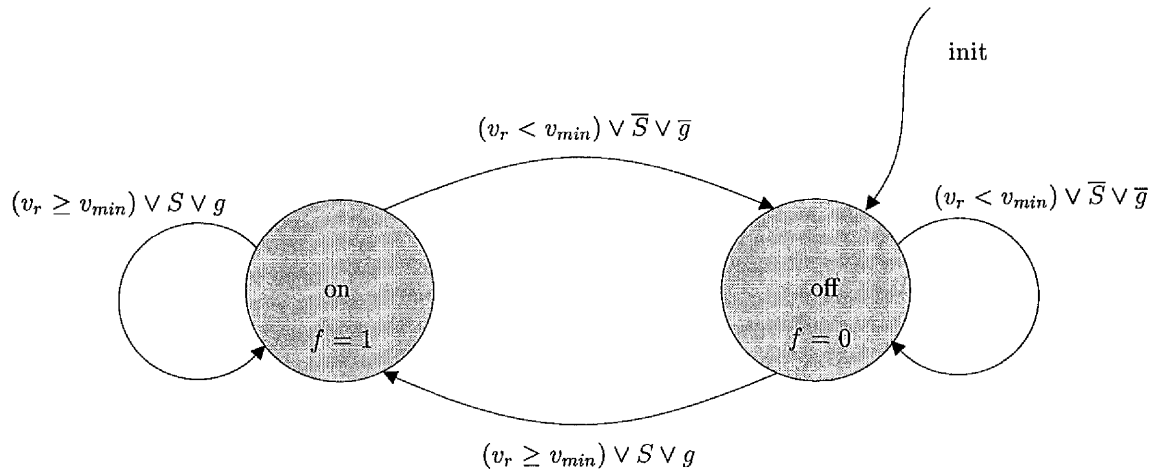


Figure 4.12: On/Off automaton

Normally the brake demand by the driver is higher than the brake torque applied by the controller. A bumpless transfer to the manual mode is necessary to avoid a jerk when the full brake force is applied. The increase of the clamping force is limited by a rate limiter. The maximum rate is chosen as 20kN/sec. Figure 4.13 shows the mode-switching automaton having three states. The controller remains in manual mode when f is off. The automatic mode is active when f is off and the driver requests a brake force F_d that is higher than minimal brake force F_{min} . That means that the driver brakes. If the driver releases the brake pedal and f is off the controller switches to manual mode. If the driver does not release the brake pedal and f is off, the controller switches into bumpless transfer mode where the gradient of the brake force is limited

until the output of the rate limiter reaches the desired clamping force F_d . Then it switches back into manual mode.

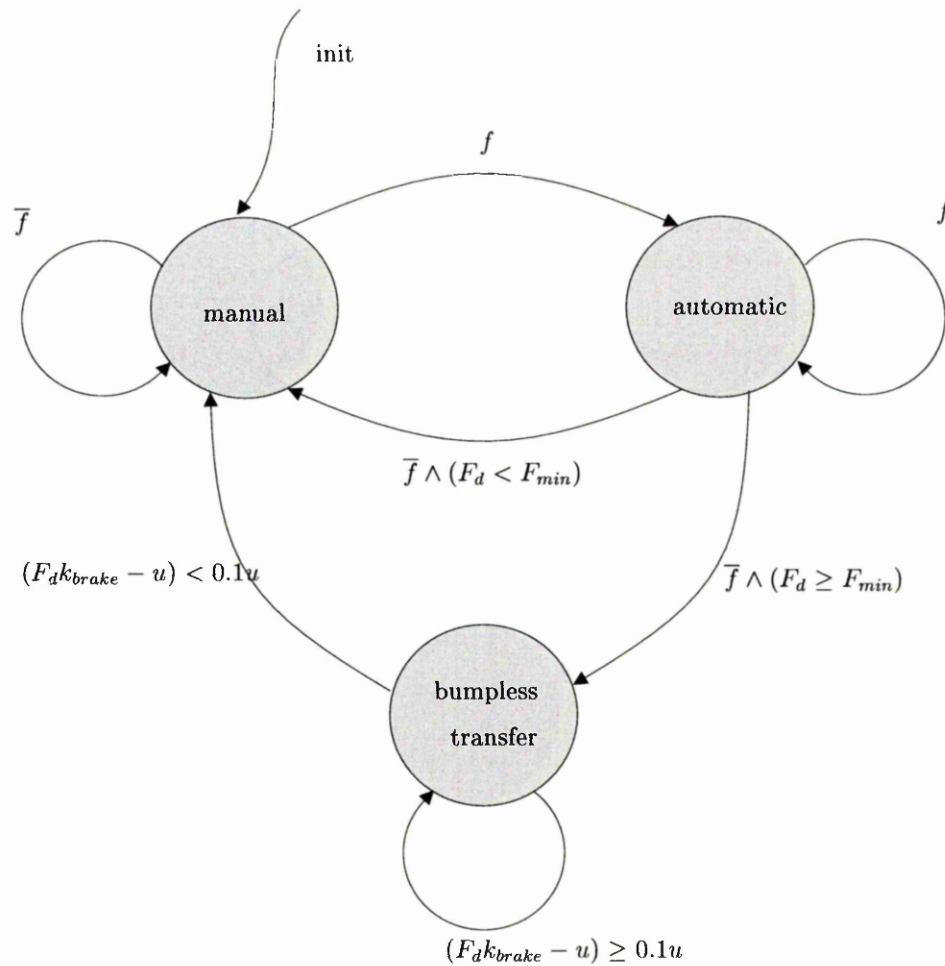


Figure 4.13: Mode changes automaton

These additional features have been realised in the anti-windup routines of the controller.

4.7 Tyre friction estimate resetting

As mentioned in previous sections there is a need for a fast tyre friction estimate to improve the transient performance of the wheel slip controller. The friction estimate in the adaptive controller converges only slowly. With a fast estimation algorithm the transient behaviour can be improved. It is shown that the transient behaviour of a nonlinear Lyapunov based adaptive controller can be improved by resetting the parameter estimate without loss of stability.

For production cars no tyre force sensor is available. Observer or estimation algorithms (cf. Sec. 3.3) are proposed in the literature.

Different road conditions (dry, wet, ice) are estimated by Gustafsson [45] by assuming different slopes of the friction curve $\mu(\lambda)$ for the different surfaces at low slip. A Kalman filter and least squares algorithms for estimation are applied. Kiencke [67] determines first the friction μ and uses a tyre model which is linear in the parameters. The proposed estimation algorithms depend very much on the tyre model used. The approach of De Wit et al. [32] is similar to the following approach. De Wit et al. uses one dynamic tyre friction model and an observer. They augment the system equations by an additional state θ that represents the uncertain road condition. This state is assumed to be constant, $\dot{\theta} = 0$.

The following approach uses observers that have an additional state representing the tyre friction coefficient of a steady state tyre friction model. This state is assumed to be constant. Instead of one observer a finite number of parallel observers as proposed in Sec. 3.5 is used, each parameterised with one parameter for one road condition.

4.7.1 Friction coefficient estimation using MMO

Observers with bilinear error dynamics

Let $M : \{\mu_{Hi}, \quad i = 1, \dots, n\}$ be a finite set of parameter values. A set of n single disturbance observers $o_i, \quad i = 1, \dots, n$ each having a fixed value of μ_{Hi} is designed. This multiple observer \mathfrak{D} together with the decision logic \mathfrak{E} results in a multiple model observer (MMO) for tyre friction coefficient estimation.

According to Eq. (4.2) the equation of motion of a single rotating wheel is given by

$$J\dot{\omega} = rF_x(\omega, v, \mu_H) - T_b \quad (4.102)$$

The dynamics depend on the uncertain tyre friction parameter μ_H . Hence, the tyre friction force F_x is uncertain. Denote the angular velocity $x_1 = \omega$, the brake torque $u =$

T_b . The measured outputs of the system are $y = \omega$ and v . Furthermore, we assume that a nominal friction torque $r\hat{F}_x(y, \mu_{Hi})$ as a function of y and a fixed μ_{Hi} is known. The friction error $x_{2i} = r\mu_H - \mu_{Hi}$ between real friction and nominal friction is assumed to be an unknown but constant disturbance and will be considered as an additional state. Consequently, the resulting modified system is given by

$$\begin{aligned}\dot{x}_1 &= \frac{r}{J} (F_x(x_1, v, \mu_{Hi}) + F_x(x_1, v, x_{2i} - \mu_{Hi}) - F_x(x_1, v, \mu_{Hi})) - \frac{1}{J}u \\ \dot{x}_{2i} &= 0\end{aligned}\quad (4.103)$$

The equation for the friction error $F_x(x_1, v, x_{2i} - \mu_{Hi}) - F_x(x_1, v, \mu_{Hi})$ can be linearised according to the parameter μ_H by Taylor approximation giving the sensitivity function:

$$F_x(x_1, v, x_{2i} - \mu_{Hi}) - F_x(x_1, v, \mu_{Hi}) = \left. \frac{\partial F_x(x_1, v, \mu_H)}{\partial \mu_H} \right|_{\mu_{Hi}} x_{2i} + \delta \quad (4.104)$$

where δ is comparatively small. Fig. 4.14 shows the three dimensional plot of the sensitivity function (4.104). Each individual observer is only valid in one of the regions indicated by the thick lines.

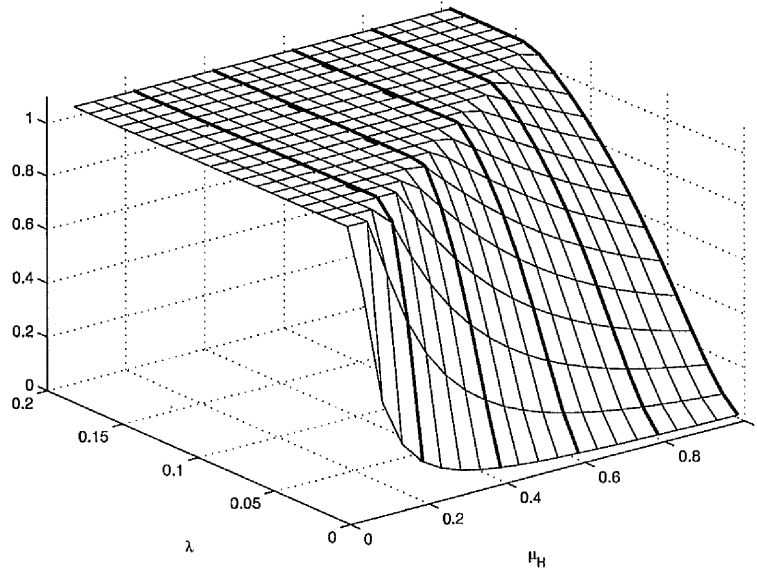


Figure 4.14: Normalised derivative of the tyre friction force $\frac{\partial F_x(x_1, v, \mu_H)}{\partial \mu_H}$

Having nonlinearities only as functions of the outputs, the extended system (4.103) is linearisable by output injection and thus, an observer with bilinear error dynamics can be designed. This property is preserved after Euler discretisation of the system

with a sampling interval T_s which leads by using the following abbreviations

$$\begin{aligned} B &:= T_s \frac{r}{J} \\ F_i &:= F_x(\mu_{Hi}) \\ \partial F_i &:= \left. \frac{\partial F_x(x_1, \nu, \mu_H)}{\partial \mu_H} \right|_{\mu_{Hi}} \\ \partial F_{max} &:= \left. \frac{\partial F_x(x_1, \nu, \mu_H)}{\partial \mu_H} \right|_1 \end{aligned}$$

to the state equation

$$x_1[k+1] = x_1[k] + B \left(F_i[k] + \partial F_i[k] x_{2i}[k] \right) - r B T_b[k] \quad (4.105)$$

$$x_{2i}[k+1] = x_{2i}[k] \quad (4.106)$$

The corresponding observer o_i is

$$\begin{aligned} \hat{x}_{1i}[k+1] &= \hat{x}_{1i}[k] + B \left(F_i[k] + \partial F_i[k] \hat{x}_{2i}[k] \right) - \frac{1}{r} B T_b[k] \\ &\quad + k'_1 \left(x_1[k] - \hat{x}_{1i}[k] \right) \end{aligned} \quad (4.107)$$

$$\hat{x}_{2i}[k+1] = \hat{x}_{2i}[k] + \nu_i \quad (4.108)$$

with the respective error equations $e_i = x_i - \hat{x}_i$

$$\begin{aligned} e_1[k+1] &= (1 - k'_1) e_1[k] + B \partial F_i e_2[k] \\ e_2[k+1] &= e_2[k] + \nu[k] \end{aligned} \quad (4.109)$$

Following the Lyapunov based design where in the continuous case the time derivative $\dot{V} = \dot{e}_1 e_1 + \frac{1}{\varrho} \dot{e}_2 e_2$ has to be made negative definite the Euler discretised Lyapunov function derivative results in

$$\frac{1}{T_s} (V[k+1] - V[k]) = \frac{1}{T_s} (e_1[k+1] - e_1[k]) e_1[k] + \frac{1}{\varrho T_s} (e_2[k+1] - e_2[k]) e_2[k], \quad (4.110)$$

or

$$\Delta V = -k'_1 (e_1[k])^2 + B \partial F_i[k] e_1[k] e_2[k] - \frac{1}{\varrho} \nu[k] e_2[k]. \quad (4.111)$$

For stability it is sufficient that $\Delta V \leq 0$ (cf. Sec. 2.2). The second observer error cannot be measured. Thus, it follows that

$$\nu[k] = \varrho B \partial F_i[k] e_1[k] \quad (4.112)$$

with the appropriate error dynamics

$$\mathbf{e}[k+1] = \underbrace{\begin{pmatrix} 1 - k'_1 & B \partial F_i[k] \\ -\varrho B \partial F_i[k] & 1 \end{pmatrix}}_{\phi_e[k]} \mathbf{e}[k]. \quad (4.113)$$

Note that the error introduced by the discretisation of the Lyapunov function may lead to instability of the system. Thus for stability the design parameter of the observer need to be chosen carefully. The error dynamics can be designed by choosing the observer coefficient

$$k'_1 = k_1 \partial F_i \quad (4.114)$$

and placing the eigenvalues of

$$A = \begin{pmatrix} 1 - k'_1 & B\partial F_i[k] \\ -\rho B\partial F_i[k] & 1 \end{pmatrix}. \quad (4.115)$$

The poles are placed at

$$z_{1,2} = 1 - \frac{k_1 \partial F_i}{2} \pm \sqrt{\frac{k_1^2 \partial F_i^2}{4} - \rho B^2 \partial F_i^2}. \quad (4.116)$$

For the choice of the two design parameters k_1 and ρ the time variant nonlinearity $\partial F_i[k]$ needs to be taken into account. Fig. 4.14 shows that the sensitivity function $\partial F_i[k]$ is limited to

$$0 \leq \partial F_i \leq \max \left(\frac{\partial F_x}{\partial \mu_H} \right). \quad (4.117)$$

For all ∂F_i , $|z_{1,2}| < 0$ must hold. The maximum value ∂F_{max} only depends on $F_{z,max}$. By setting

$$k_1 = \frac{2}{\partial F_{max}} \quad (4.118)$$

we end up with a pole placement of ²

$$z_{1,2} = 1 - \frac{\partial F_i}{\partial F_{max}} \pm \frac{\partial F_i}{\partial F_{max}} \sqrt{1 - \rho B^2 \partial F_{max}^2}.$$

By setting

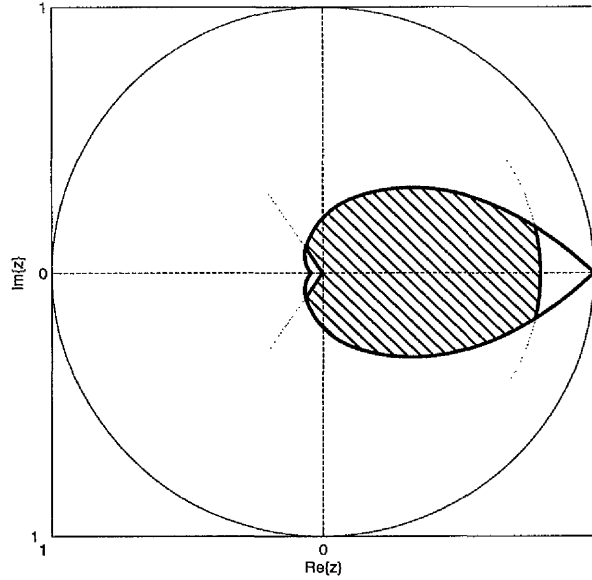
$$\rho = \frac{1}{B^2 \partial F_{max}^2} = \frac{k_1^2}{4B^2}, \quad (4.119)$$

the root in Eq. (4.119) is set to zero. Consequently, real poles are placed in a region of “nice” stability [16] (cf. Fig. 4.15(hatched region)). The position of the poles depends on the relative derivative of the tyre force $0 \leq \frac{\partial F_i}{\partial F_{max}} \leq 1$.

$$z_{1,2} = 1 - \frac{\partial F_i}{\partial F_{max}}, \quad (4.120)$$

The more the poles move towards the circle the slower the system becomes. A small $\frac{\partial F_i}{\partial F_{max}}$ implies a small slip and a slower observer settling time.

²Note that $\frac{\partial F_i}{\partial F_{max}}$ is used for the ratio $\frac{\left. \frac{\partial F_x(x_1, v, \mu_H)}{\partial \mu_H} \right|_{\mu_H i}}{\left. \frac{\partial F_x(x_1, v, \mu_H)}{\partial \mu_H} \right|_1}$.

Figure 4.15: Region of “nice” stability in the z -plane

Performance Signal Generator and Switching logic

Next, a performance index $J(\hat{x}_i[k], y[k])$ is defined for each observer of the set \mathfrak{D} . A switching logic L is used to determine the estimate $\hat{\mu}_H$ of the multi-observer \mathfrak{D} . L satisfies two purposes:

1. selecting the coefficient μ_{Hi} corresponding to the observer o_i with the best performance index.
2. providing a mechanism that prevents the MMO from chattering.

The performance index is calculated from each wheel speed error e_{1i} and the friction torque error x_{2i}

$$Q_i[k] = \sum_{j=0}^{\infty} W_j (c_1 e_{1i}[k-j]^2 + c_2 x_{2i}[k-j]^2) \quad (4.121)$$

where W_j are the weights of a discrete low-pass filter.

In order to prevent chattering the switching logic has a hysteresis. Let o_p be the valid observer at time $k-1$ then a switch to a new observer o_i occurs only if $Q_i[k](1+h) < Q_p[k]$ where $Q_p[k]$ is the current performance of the observer o_p at the previous time instant and $h > 0$ is the hysteresis. Otherwise no switching will occur and o_p will remain valid.

4.7.2 Estimation of the friction coefficient using MME

Multiple model estimation as in Sec. 3.4 cannot be implemented directly since it is based on the assumption that the system is linear in the unknown parameter. The algorithm is modified for the problem of friction coefficient estimation and resetting of the adaptive wheel slip controller.

Consider the equation of motion of the wheel (4.2). The friction could be calculated, if the wheel acceleration were measurable as:

$$\mu_x = \frac{J}{F_z r} \dot{\omega} + \frac{T_b}{F_z J} \quad (4.122)$$

Since the acceleration $\dot{\omega}$ can not be measured directly and our system is sampled, a predictor will be designed. Discretising Eq. (4.122) using Euler discretisation one gets

$$\mu_x[k] = \frac{J}{F_z r} \frac{\omega[k] - \omega[k-1]}{T_s} + \frac{T_b[k]}{F_z J}. \quad (4.123)$$

In order to reduce the influence of noise in the system FIR-filters will be used.

$$\sum_{i=0}^{n_f} w_i \mu_x[k-i] = \sum_{i=0}^{n_f+1} \nu_i \omega[k-i] + \sum_{i=0}^{n_f} \iota_i T_b[k-i]. \quad (4.124)$$

Suppose the tyre friction coefficient μ_H is constant for n_f steps. Substitution of (4.124) with respect to $\mu_H[k]$ results in

$$\mu_x[k] = \sum_{i=0}^{n_f+1} \frac{\nu_i}{w_o} \omega[k-i] + \sum_{i=0}^{n_f} \frac{\iota_i}{w_o} T_b[k-i] - \sum_{i=1}^{n_f} \frac{w_i}{w_o} \mu_x[k-i].$$

By solving the quadratic equation (4.21) a parameter estimate $\hat{\mu}_H$ is obtained. This friction value is considered as the best parameter estimate.

Let $M : \{\mu_{H_i}, | i \in \mathcal{I} = \{1, \dots, N\}\}$ be a finite set of parameter values as in Sec. 4.7.1. The minimal value $\operatorname{argmin}_{i \in \mathcal{I}} \Delta \bar{V}_{ni}[k]$ of equation (3.146) in theorem 1 gives the parameter μ_{H_i} that is used for resetting the parameter estimate of the adaptive controller if

$$\Delta \bar{V}_{ni}[k] = \Delta \bar{V}_{ni}[k-1] - \left(\rho_i + \frac{1}{\gamma} \Delta \hat{\mu}^2[k] - \frac{2}{\gamma} (\hat{\mu}_H[k] - \mu_{H_i}[k]) \Delta \hat{\mu}[k] - (\lambda[k])^2 \right) \quad (4.125)$$

is negative. The difference between the controller estimate μ_{H_c} and $\hat{\mu}_{H_i}$ is denoted as $\Delta \hat{\mu}$.

4.8 Simulation

A simulation environment for testing ABS (and steering) controllers has been developed. The simulation is based on the nonlinear four wheel car model described in Appendix A. The model parameters have been adapted to that of the real test vehicle (Mercedes E-class) to make the simulation as realistic as possible. The software satisfies the following requirements:

- The low complexity of the model makes it accessible to control design.
- The model captures the essential dynamics of the vehicle.
- The interface for the ABS controller is identical to that of the real test vehicle.

The simulation software is written in ANSII-C and produces log-Files that can be processed in MATLAB. In principle the simulation software can also be used to test other vehicle dynamic control systems.

In the simulation the behaviour of four different wheel slip controllers is tested. The controllers will be evaluated against each other on different road surface conditions.

The test manoeuvre for simulation is a straightforward panic stop which starts at $t = 0.2\text{s}$ with an initial speed of 35m/s . The applied brake demand is a large clamping force of 20000N . For safety reasons only half the brake wish is applied at the rear wheels because a locked rear wheel will result in instability of the vehicle. The road condition changes at several time steps $t = 1.5, 3[\text{s}]$ to different tyre-road friction coefficients. The considered friction coefficient is $\mu_H = 0.2$ in the first 1.5 seconds, changes to $\mu_H = 0.9$ and at $t = 3\text{sec}$ changes to $\mu_H = 0.5$. The desired wheel slip is set to 0.14 . Note that by using the high setpoint slip of $\lambda_0 = 0.14$ also for lower tyre/road friction coefficients the controller needs to stabilise the system in the unstable part of the tyre friction curve. In order to test the robustness, noise is added to the wheel speed measurement ω . Results are presented only for one front wheel. The regulation of the rear wheels is less critical and better results can be obtained.

The following sections are organised as follows: Each wheel slip controller has been tested in simulation and will be discussed separately. For each controller wheel slip, clamping force, friction and velocity will be displayed in Fig. 4.16–4.22. At the end of the section all controllers will be compared.

4.8.1 PI wheel slip controller simulation

Fig. 4.16 shows the simulation plots of the wheel slip λ , the clamping force F_b , the tyre/road friction and the wheel speed using the nonlinear adaptive wheel speed controller introduced in Sec. 4.2. Three simulations have been performed. One without parameter resetting (black lines), another with estimator resetting by using the estimate of the MME derived in Sec. 4.7.2 (grey lines) and the PI controller using the properties of the multiple model observer derived in Sec. 4.7 (light grey lines).

The controller stabilises the system. After the period of time necessary for the controller to adapt to the current friction coefficient, the slip converges to the desired slip. Large slip transients, when the road condition changes instantaneously are undesirable. This is due to the relatively slow adaptation and the low gain. The low gain is required due to uncertainty, noise and unmodelled dynamics of the real test vehicle. As long as the estimate of the friction μ does not converge the control error remains large. The transients could be damped out by using higher controller gain and a higher adaptation speed. However, enlarging the controller gain is not feasible, because it causes instability that is due to the sampled data system and a time delay of 14ms between sensor measurements and control output. Note that the controller is designed for the continuous time system. Analysis of the Lyapunov function is only valid for the continuous time system. The discretisation of the continuous controller may cause instabilities. The robustness is only achieved by tuning the parameters of the controller. Furthermore, the controller is designed for the system without taking any actuator dynamics since the actuator is very fast and time delays into account but the simulation contains an actuator model. Using a low gain controller the slip error remains large until the adaptation converges. This can be seen in the upper plot when the time $1.5\text{s} < t < 3\text{s}$.

The transients can be damped out by using estimator resetting. By doing this the maximum peak of slip is smaller than without switching. A very large peak of slip can be observed in the grey slip curve (MME) at $t = 3\text{s}$. Note that the MME estimate is not displayed. No resetting occurs. The tuning parameter ρ_i in the reset condition (4.125) is adjusted in a way that no erroneous switch occurs. This robustness is at the expense of helpful switches, which are sometimes suppressed. For $t > 6.2\text{s}$ the slip is not computed properly due to numerical problems. This does not matter because the slip controller is switched off at speeds less than 1m/s. When the controller is switched off the bumpless transfer (cf. Sec.4.6) of the brake force can be observed.

The relatively low gain of the controller can be seen in the smooth control signal F_b .

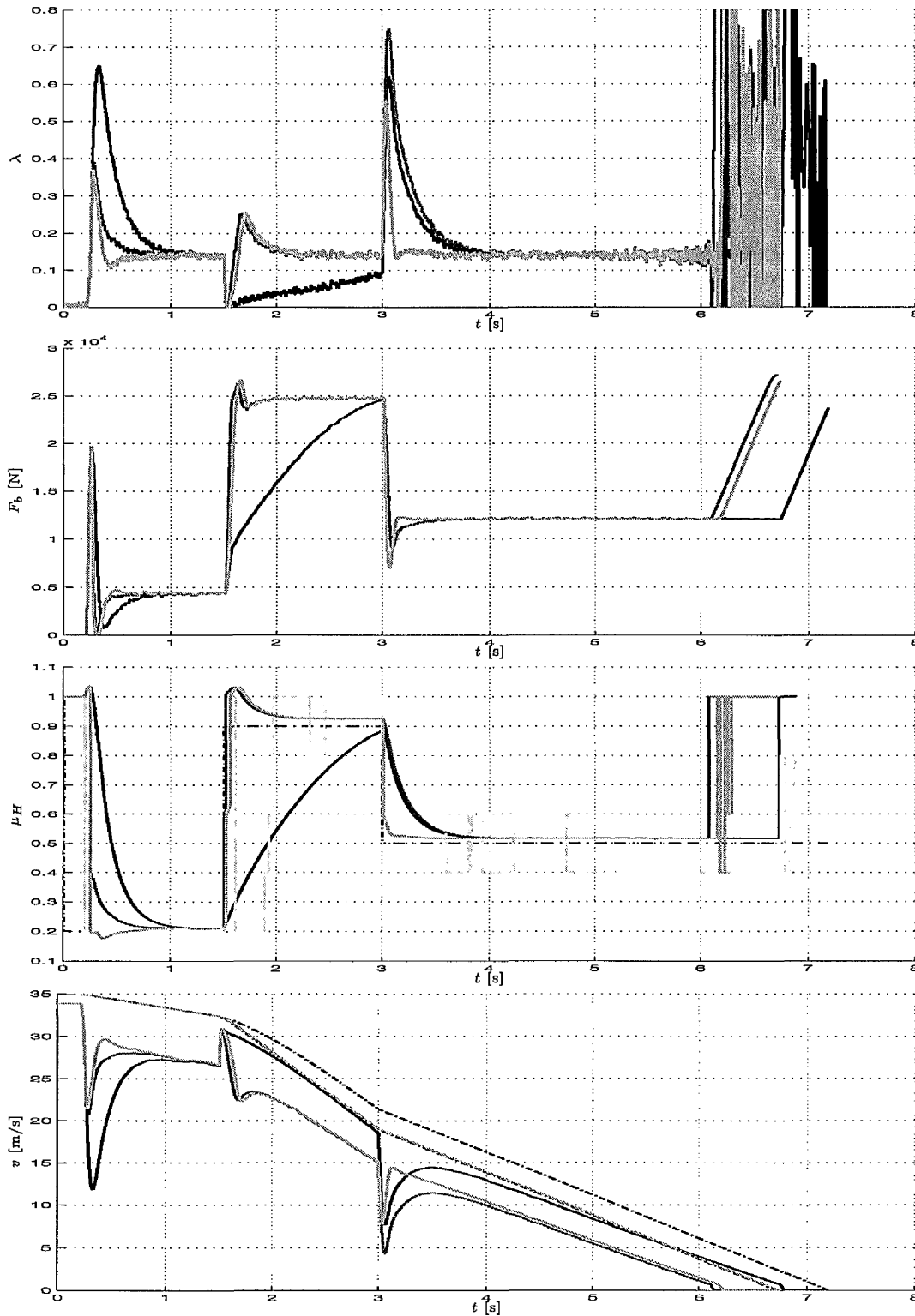


Figure 4.16: Wheel slip, clamping force, tyre friction and vehicle speed of the PI-wheel slip controller (without resetting: black, using MME: grey, using MMO: light grey).

Only at the resetting points the clamping force “jumps”.

The third plot shows the real tyre/road friction coefficient (dash dot) together with the continuous adaptation of the tyre friction that is reset at some point. The continuous adaptation depends on the wheel slip and is slower for lower slip. The light grey curve shows the output μ_{Hi} of the multiple model observer. At low slip ($t \approx 1.7\text{s}$), where the continuous adaptation is slow the MMO estimation is wrong since no information on the friction coefficient can be obtained because the tyre friction is less sensitive to the friction coefficient μ_H for low slip. Note that the wrong estimate does not cause erroneous switches. The switching of the MMO-estimate between 0.6 and 0.4 is because the real friction value of 0.5 is exactly between the discrete observers. Small disturbances cause variations in the cost function of the MMO and thus switching between adjacent observers.

The lowest plot of Fig. 4.16 shows the vehicle speed (dash dot line), given by an extended Kalman filter [120] and the circumferential wheel speed (solid lines). Note that the stopping time and thus the stopping distance is shorter by resetting the continuous parameter estimate. Also the slip transients will be damped out. This is a clear performance enhancement.

4.8.2 Simulation results of the “Sontag” controller

The results of wheel slip control using “Sontag’s” formula introduced in Sec. 4.3 are depicted in Fig. 4.17. They are very similar to that obtained by the nonlinear adaptive PI wheel slip controller (cp. Fig. 4.16). The performance of the combination of an adaptive controller and a stability preserving resetting strategy is as good as the performance of the pure adaptive controller.

The control signal and the slip oscillates a little more than the PI controller. Best results are obtained by resetting the continuous adaptation by the fast estimate given by a multiple model observer MMO. Transitions are clearly reduced by resetting. Switching does not lead to instabilities. Unnecessary switching is not observed. The true parameter is estimated very fast.

The stopping distance is shorter with estimator resetting. A clear performance improvement can be seen.

In Fig. 4.18 the controller gain of the “Sontag’s” wheel slip controller is modified to show the disadvantages of either increasing or decreasing the controller gain. The black curves show the results of the low gain controller while the grey curves are for the high gain controller. The nominal gain c_0 in Fig. 4.17 is set to 40 while the high gain

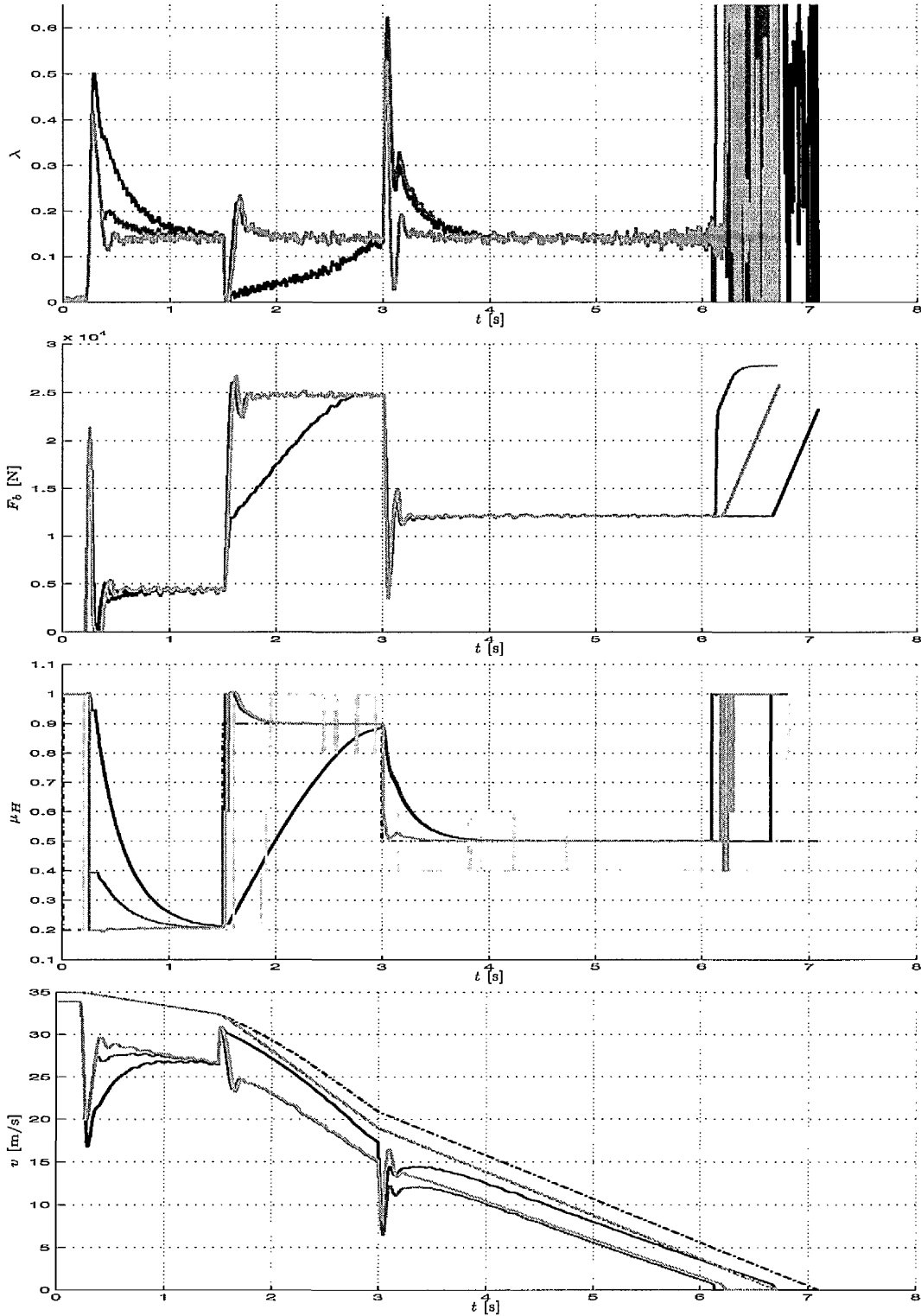


Figure 4.17: Wheel slip, clamping force, tyre friction and vehicle speed of the “Sontag”-wheel slip controller (without resetting: black, using MME: grey, using MMO: light grey).

controller uses $c_0 = 80$ and the low gain controller $c_0 = 15$. Increasing the gain results in oscillations of the wheel slip and the control signal. The robustness is reduced while no obvious performance benefit is obtained. The slip transients for the lowered gain are very large. Recovery of the wheel slip after road condition changes takes a long time.

Fig. 4.19 shows how the performance of the low gain controller can be improved by estimator resetting. A smooth control signal, a good transient performance and in the wheel slip case a shorter braking distance is achieved.

Fig. 4.20 shows that the fast multiple model observer is robust against oscillations of the control system. Also the performance of the high gain controller can be improved by resetting. No incorrect or erroneous switching operations can be observed.

4.8.3 Simulation of the SSP wheel slip controller

Fig. 4.21 shows the simulation of the SSP controller. This simple non-adaptive controller stabilises the slip dynamics. Large overshoot of the control variable indicates high controller gain. Because of this the controller is less robust. The integral part of the controller has only little influence. The slip dynamics become faster with decreasing speed. The noise in the slip becomes larger for lower speed. This results in a reduced robustness for lower speed.

The controller has no sufficient integral part to cancel the slip error for low speed.

An easy use of the MMO theory is not possible, since this automatic controller design is not Lyapunov function based.

4.8.4 Simulation of the LQRC wheel slip controller

Fig. 4.22 shows the simulation results of the sub-optimal constrained LQ-controller of Sec. 4.5. The results are very good except for large transients due to fast changing road conditions. These transients could be damped by using the multiple observers for resetting the integral part of the controller.

The controller actuator rate constraint modes are active between $t = 1.5\text{sec}$ and between $t = 1.7\text{sec}$ and $t = 3\text{sec}$ and $t = 3.1\text{sec}$.

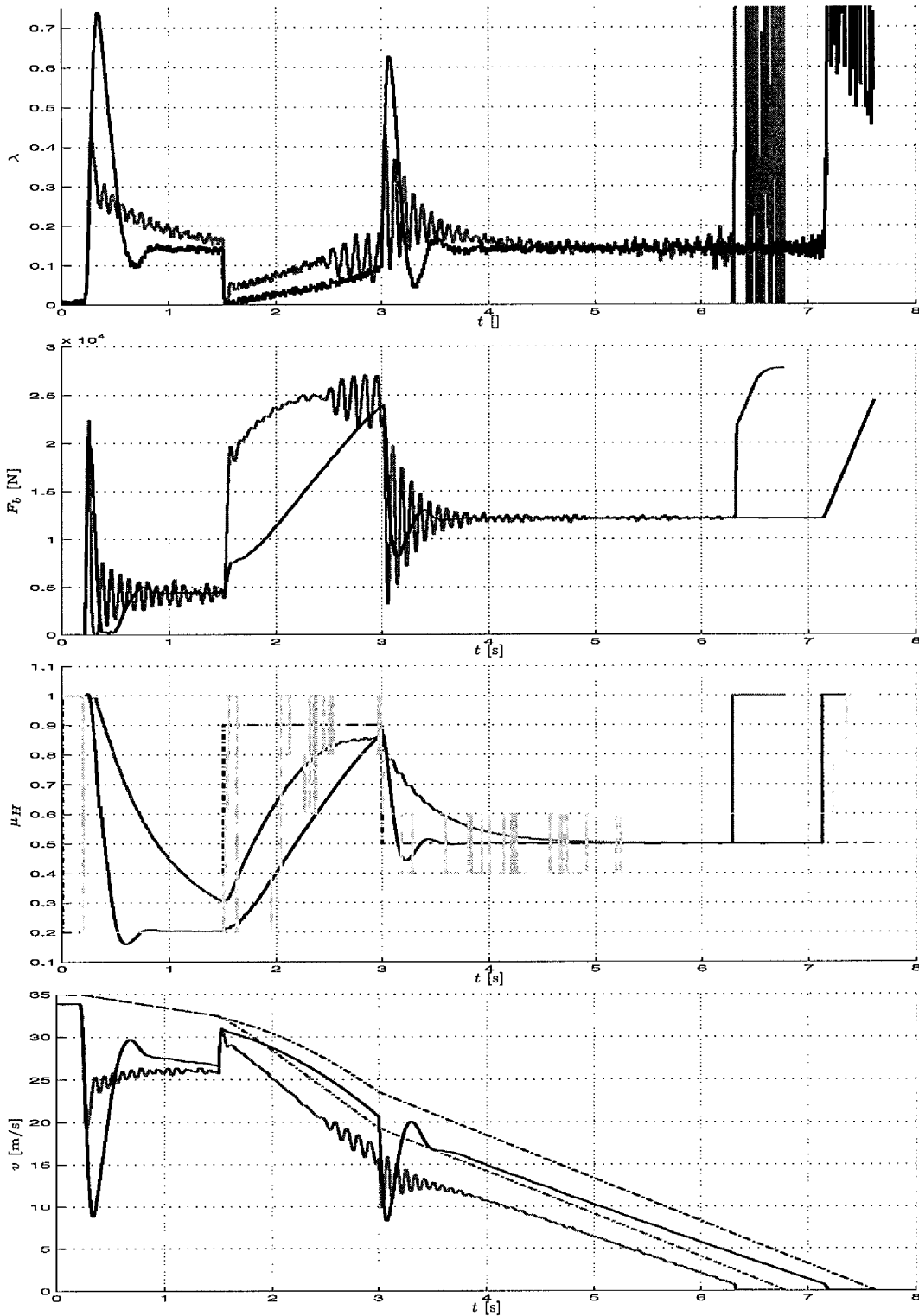


Figure 4.18: Wheel slip, clamping force, tyre friction and vehicle speed of the “Sontag”-wheel slip controller with low gain (black) and high gain (grey).

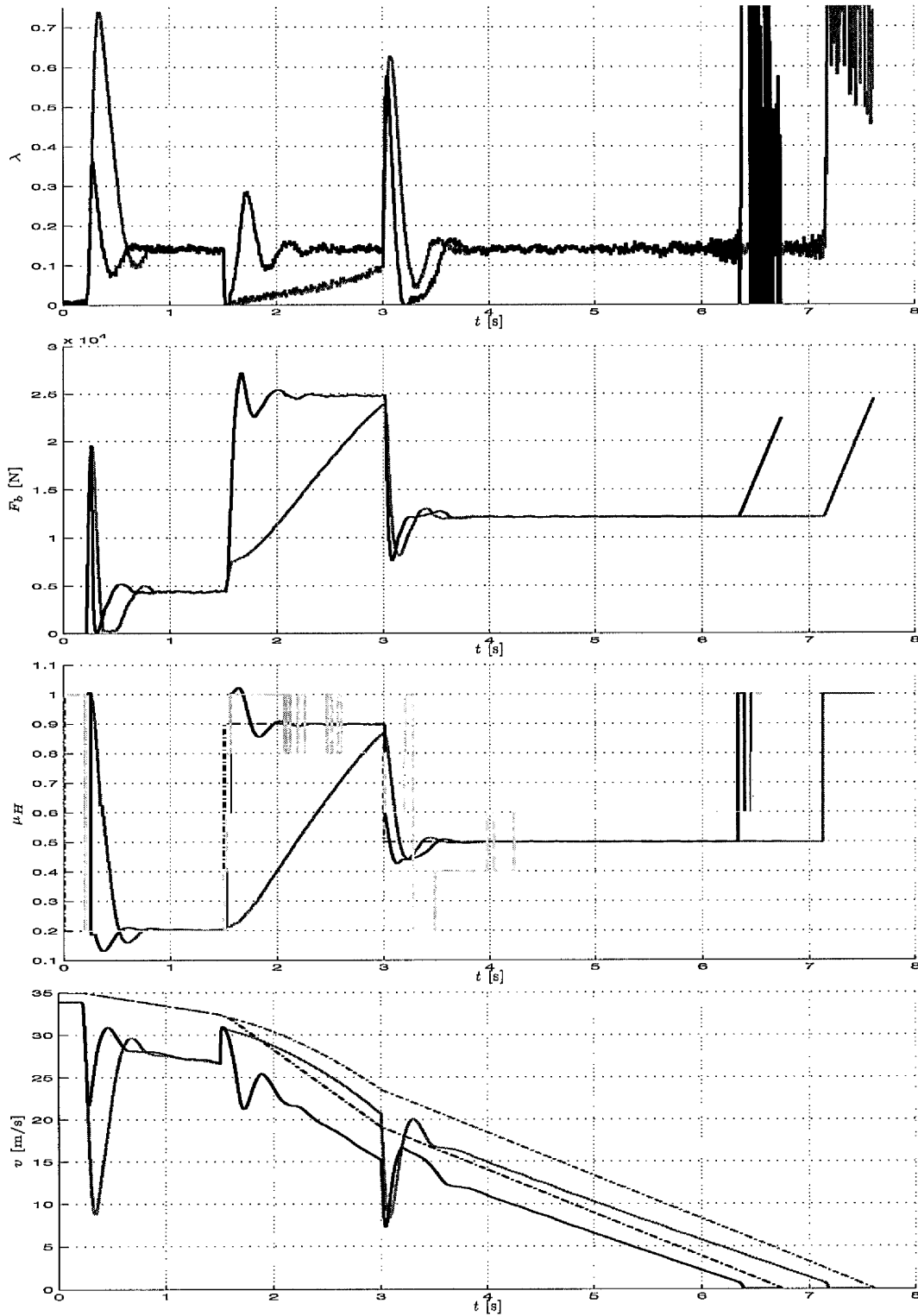


Figure 4.19: Wheel slip, clamping force, tyre friction and vehicle speed of the “Sontag”-wheel slip controller with low gain (with resetting: black, using MMO: grey).

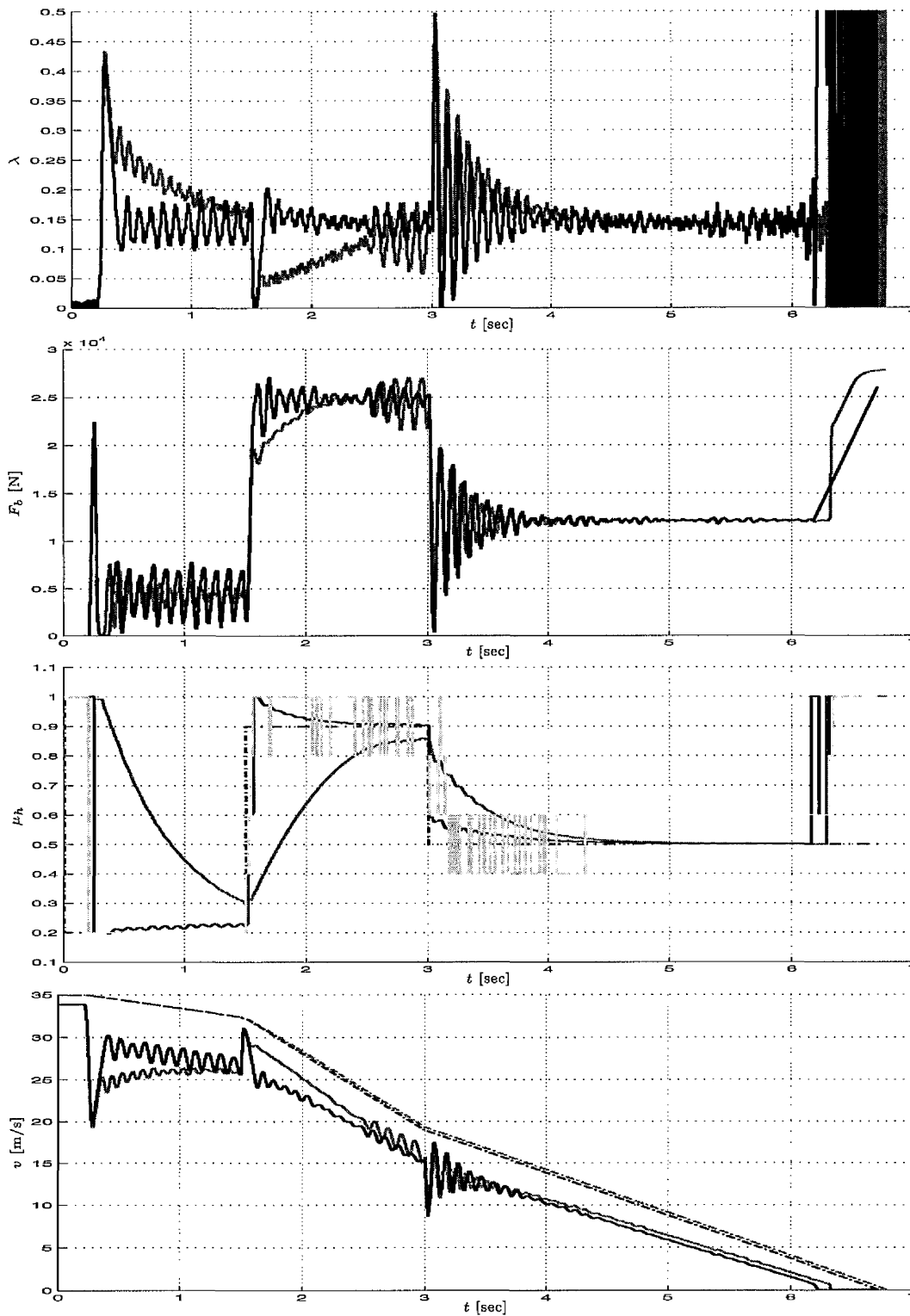


Figure 4.20: Wheel slip, clamping force, tyre friction and vehicle speed of the “Sontag”-wheel slip controller with high gain (with resetting: black, using MMO: grey).

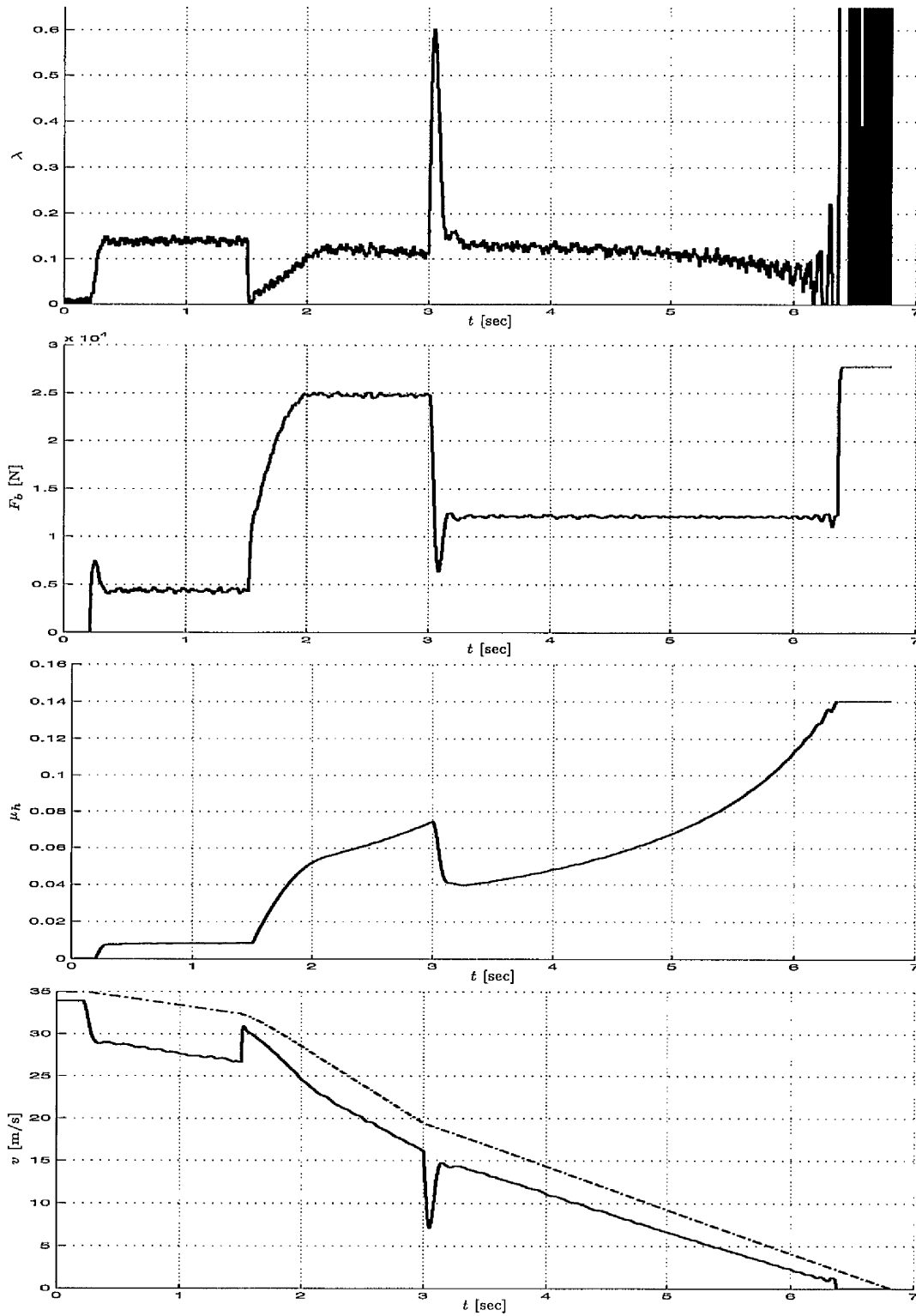


Figure 4.21: Wheel slip, clamping force and vehicle speed of the SSP-wheel slip controller.

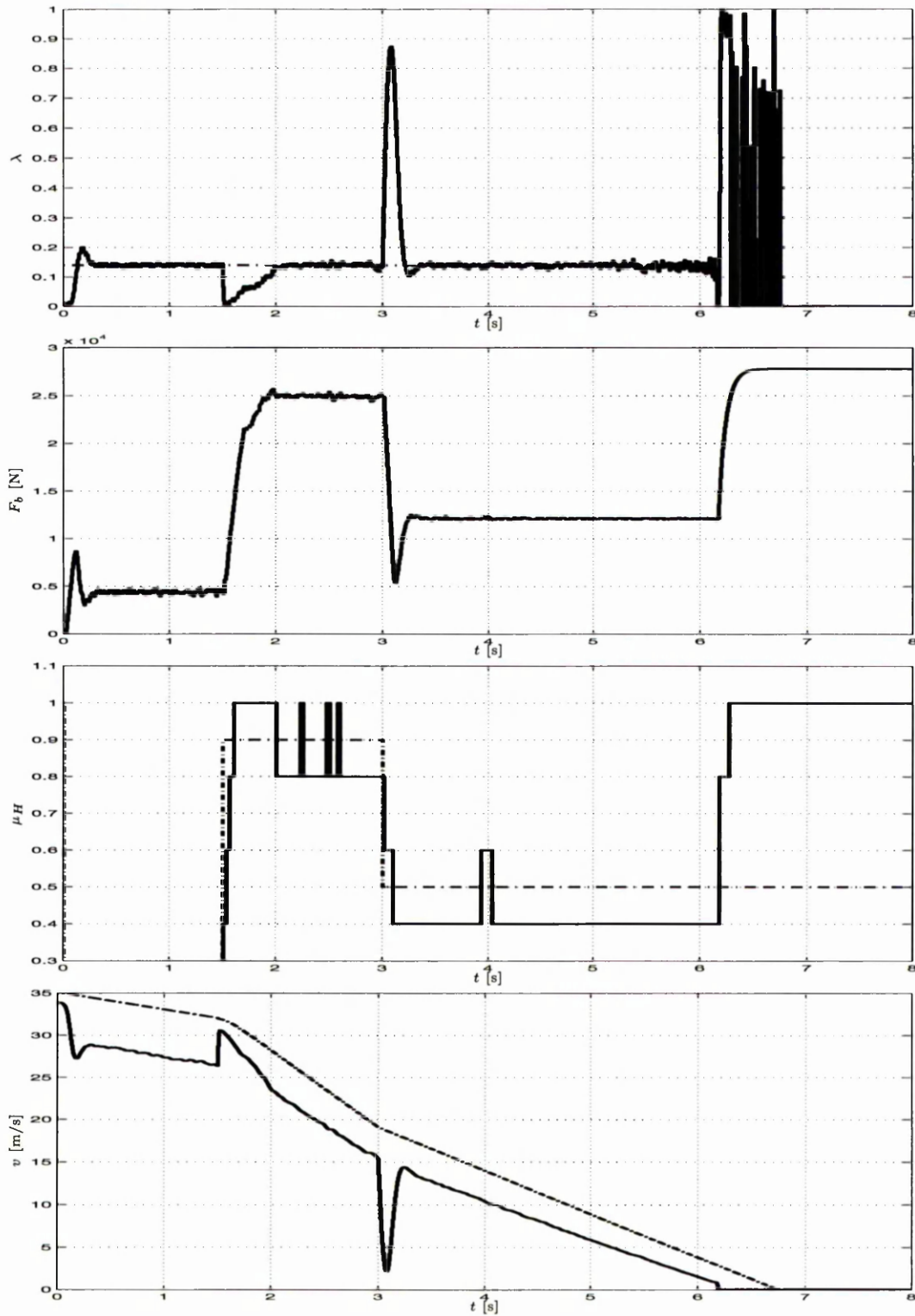


Figure 4.22: Wheel slip, clamping force, tyre friction and vehicle speed of the LQRC-wheel slip controller.

4.8.5 Four controllers compared

Comparing all four automatic controllers, it is noticeable that the two nonlinear controllers using parameter resetting exhibit similar behaviour, whereby the inverse optimal approach is somewhat better. Fig. 4.23 shows the nonlinear adaptive PI controller (black), the inverse optimal adaptive controller (grey) and the linear simultaneous stabilising controller (light grey). When the sub-optimal constrained LQ-controller (cf. Fig. 4.22) was combined with parameter resetting a very good control performance could be achieved.

By resetting the continuous parameter estimation with a fast parameter estimation algorithm a clear improvement of the regulation quality is obtained, without increasing the controller gain. Without parameter resetting it takes about 10m more braking distance to stop the car for both nonlinear controllers (cp. Fig. 4.17 and 4.16). The transients due to road surface changes are clearly reduced.

4.8.6 Conclusions

In the simulation the behaviour of four different wheel slip controllers has been tested. The controllers have been evaluated against each other on different road surface conditions. It has been shown that the inverse optimal adaptive wheel slip controller (cf. Sec. 4.3) has the best performance when using estimator resetting and a multiple model observer estimates the tyre/road friction coefficient. The second best controller is a nonlinear adaptive PI controller (cf. Sec. 4.2) which also uses the fast estimate of tyre/road friction for resetting the continuous friction estimation. Without resetting both controllers are insufficient to cover the transients when the road condition changes. The SSP wheel slip controller shows that even a simple controller can control the system, however it does not achieve the specified performance. The gain scheduled constrained LQ-controller is a good linear controller since it is optimal in some way. The limitation of this controller can be in the slow integral part and in the linear feedback.

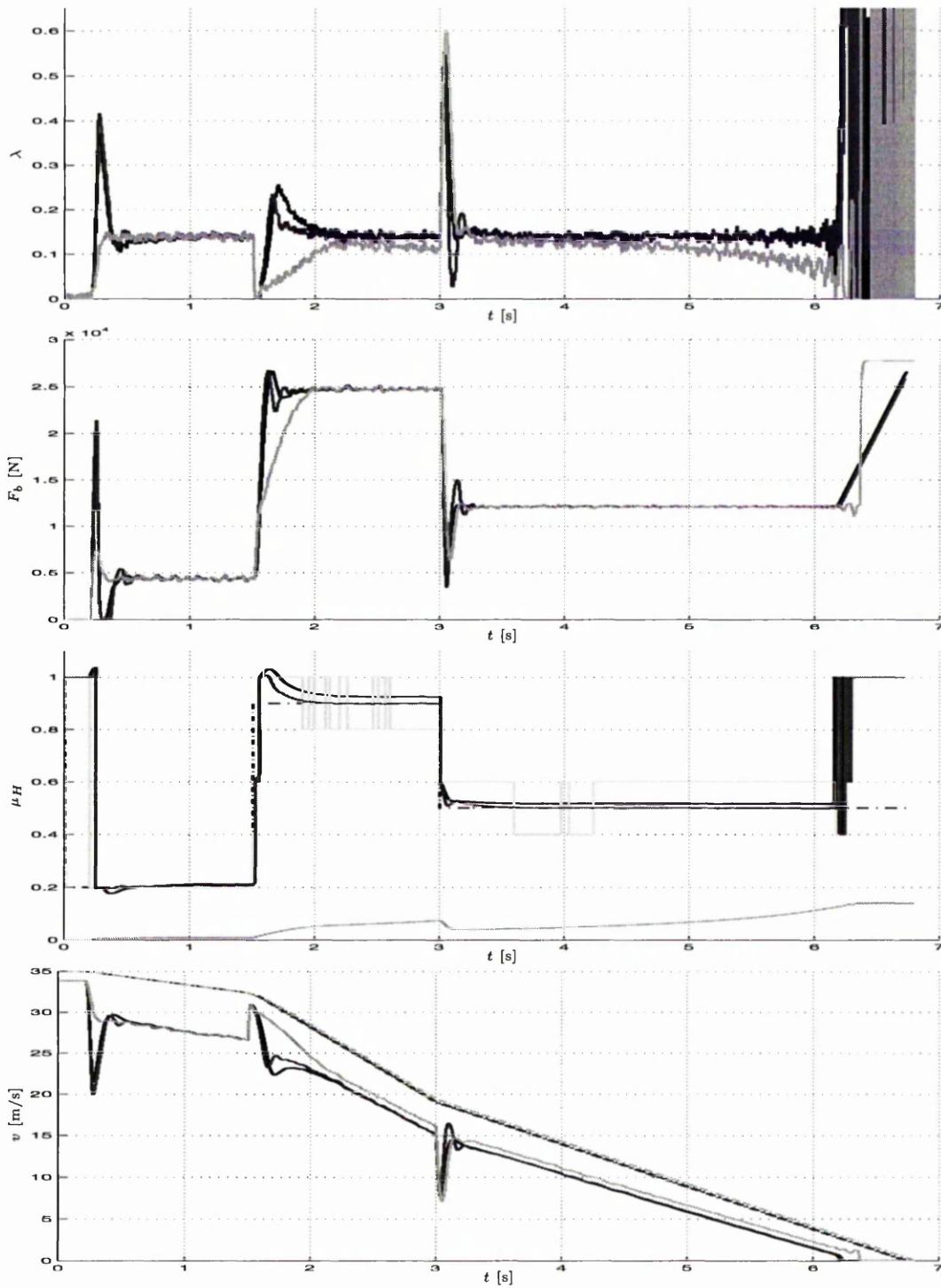


Figure 4.23: Wheel slip, clamping force, tyre friction and vehicle speed of three different Slip controller simulations (PI-controller with MMO (black), "Sontag's" controller with MMO (grey) and the SSP controller (light grey)).

5 Experimental results

In the previous chapter, hybrid control methods have been applied to wheel slip control. These four controllers and the multiple observer have been tested and evaluated in a real passenger car (cf. [75]). In the following section, first the test vehicle and the electro-mechanical brake actuators will be described in Sec. 5.1. Also a nonlinear model of the brake actuator will be developed. Some applicational viewpoints are given in Sec. 5.2. Vehicle braking tests under real life conditions (cf. Sec. 5.3 and Sec. 5.4) are presented. At the end of the section the tested controllers will be evaluated.

5.1 ABS test vehicle

The test vehicle is a Mercedes E220 passenger car equipped with four electro-mechanical disk brakes supplied by Continental Teves and a brake-by-wire system. Fig. 5.1 shows a photo of the test vehicle.

Fig. 5.2 shows the hardware architecture of the vehicle. It consists of four servo controllers for the brakes, a monitoring unit, a brake-by-wire control unit and a power supply unit. These systems communicate via a TTP (time-triggered protocol) bus. This bus is a synchronous bus. The vehicle is equipped with the following sensors:

- four wheel speed sensors,
- a sensor for the steering wheel angle,
- sensors for the position of the brake pedal and the force applied to the brake pedal,
- two accelerometers for longitudinal and lateral acceleration respectively,
- a yaw rate sensor and
- hall sensors for measuring the clamping forces at each brake.



Figure 5.1: Photo of the ABS test vehicle

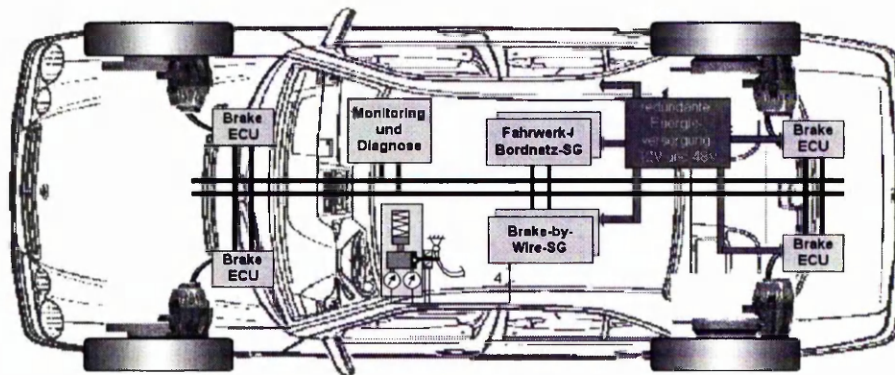


Figure 5.2: ABS test vehicle hardware architecture

The brake-by-wire software is written in C and provides an interface for the ABS controller. The interface gives access to the sensor signals and reads the command signals for the brakes provided by the ABS controller. From the brake pedal measurements (brakewish) the brake-by-wire system computes a desired clamping force F_d for each brake. In the anti-windup routine the limitation of the slip controller output F_b is realised. Thus, the control output F_s cannot become larger than the desired clamping force F_d . F_s is the reference clamping force signal supplied to the brake servo controllers of each wheel. The ABS controller runs at a sampling period of 7 milliseconds

and with a delay of two time steps between the control signal and the sensor output.

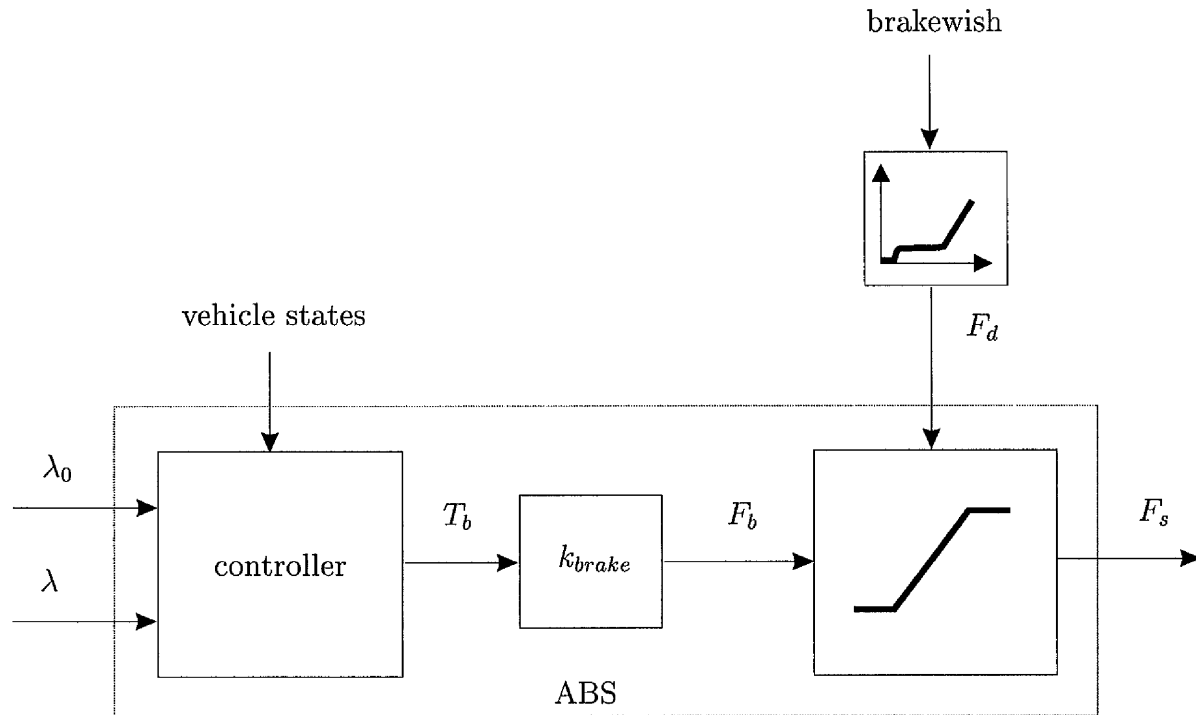


Figure 5.3: Slip controller interface

Electro-mechanical Brake Actuator

The electro-mechanical wheel brake by Continental Teves [109] is a disk brake working on the floating caliper-principle. Here, only the holding device is connected firmly to the vehicle's steering knuckle. Together with both brake pads the fist is fixed, with one degree of freedom towards the active line of the clamping force. Fig. 5.4 shows a photo of the electro-mechanic brake and the disk integrated in the vehicle.

Fig. 5.5 shows a sectional drawing of the brake. The electromechanic converter is a brushless DC motor. At the pads-sided end the rotor is geared and at the same time forms the sun wheel of the following planetary gear. The planet wheels of the planetary gear are in mesh with the internal-gear wheel, bolted in the brake cabinet, and power the planet carrier. A planetary roller gear applies for the transformation of the rotary motion into a translatory motion. The planetary gears spindle is hollow and contains a force measurement device as well as a pressure pin for the decoupling of bending movements acting on the spindle. When activating the brake the drive end

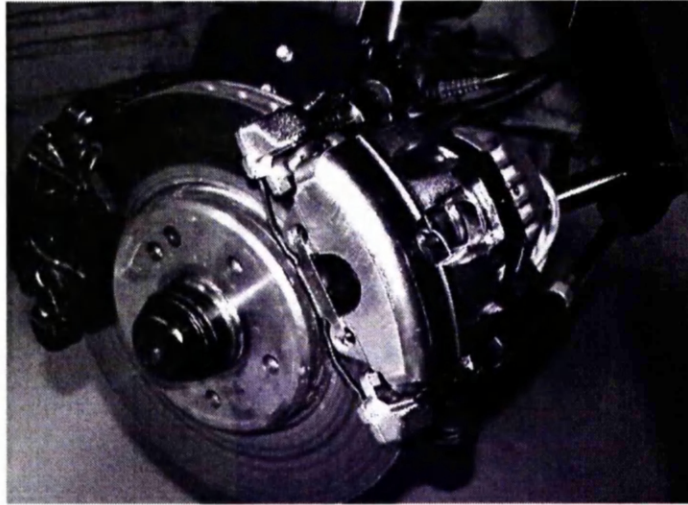


Figure 5.4: Photo of the electro-mechanical brake

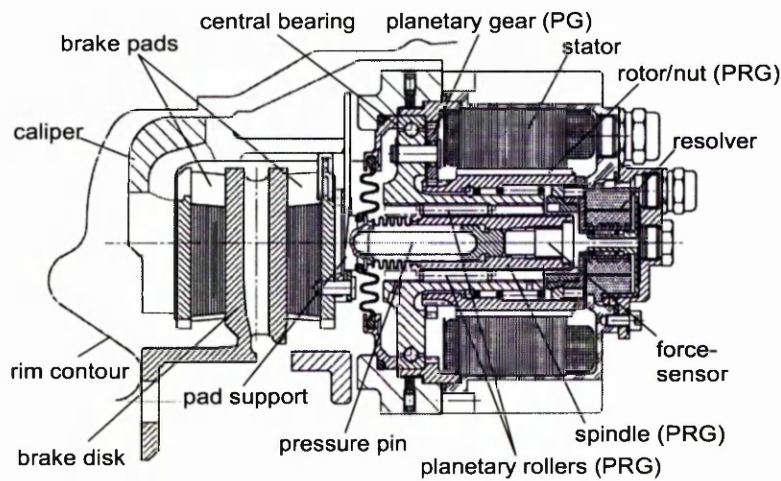


Figure 5.5: Electro-mechanical brake

brake pad will be moved through the pad support, whereas the pressure pin and the force sensor will be shifted towards the brake disk, caused by the spindle's motion.

The electro mechanical brake is servo controlled by a cascade PID-controller running with a sampling period of 2.33 milliseconds. This is later shown in Fig. 5.8

Model of the electromechanical brake

The model of the electromechanical brake consists of a model of an electric motor and a gearbox that transforms the rotational movement into a translatory movement. A

nonlinear characteristic for the conversion of the movement into a force as well as a nonlinear friction model is taken into account. Fig. 5.6 shows the structure of the physical model of the brake where the symbols have the following meaning:

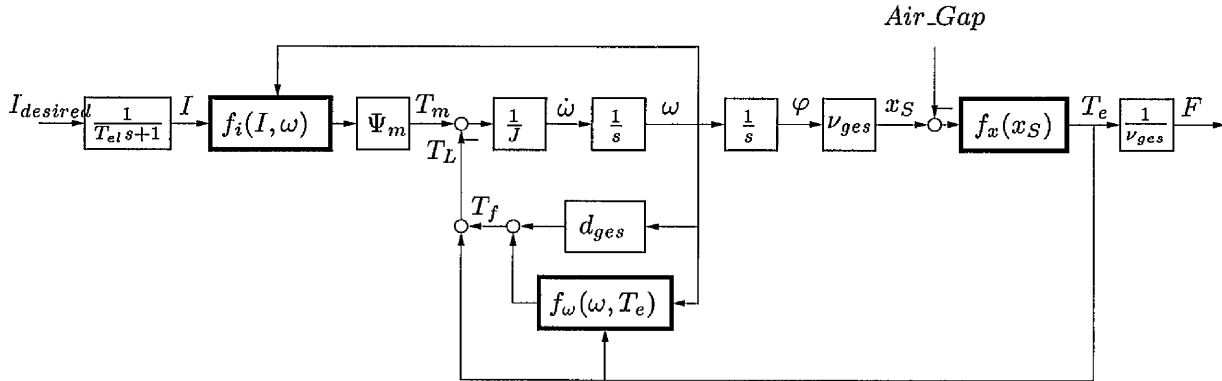


Figure 5.6: Physical EMB model

- Air_Gap : Air gap between brake disk and brake pads
- d_{ges} : Overall viscous friction
- $f_i(I, \omega)$: Feedback of the motor on the current
- $f_x(x_S)$: Transfer function between spindle position and clamping force
- $f_\omega(\omega, T_e)$: Transfer function between angle of rotation and friction torque
- F : Clamping force
- I : Motor current
- J : Overall inertia
- T_e : Available torque
- T_f : Friction torque
- T_L : Available load torque $T_L = T_e + T_f$
- T_m : Electric torque
- T_{el} : Electric time constant of the motor
- x_S : Spindle position
- ν_{ges} : Transmission factor
- φ : Rotation angle
- Ψ_m : Magnetic flux
- ω : Angular velocity

The feedback given by the motor on the current is modelled as follows:

$$f_i(I, \omega) = \begin{cases} \min(I, (1 - \frac{\omega}{\omega_0})I_{\max}) & \text{if } \omega \geq 0 \ \& \ I \geq 0 \\ \max(I, -I_{\max}) & \text{if } \omega \geq 0 \ \& \ I < 0 \\ \max(I, -(1 + \frac{\omega}{\omega_0})I_{\max}) & \text{if } \omega < 0 \ \& \ I \leq 0 \\ \min(I, I_{\max}) & \text{if } \omega < 0 \ \& \ I > 0. \end{cases}$$

where

ω_0 : maximum rotor speed for zero load [rad/s]

I_{\max} : maximum stator current $I_{\max} = 40A$.

The characteristic curve between the spindle position and the clamping force will be approximated by a polynomial with the degree of five and a hysteresis

$$f_x(x_S) = \begin{cases} 0 & \text{if } x \leq 0 \\ c_5x^5 + c_4x^4 + c_3x^3 + c_2x^2 + c_1x + c_0 & \text{if } x > 0. \end{cases}$$

The clamping force has a behaviour of a hysteresis $h(u)$ modelled as shown in Fig. 5.7.

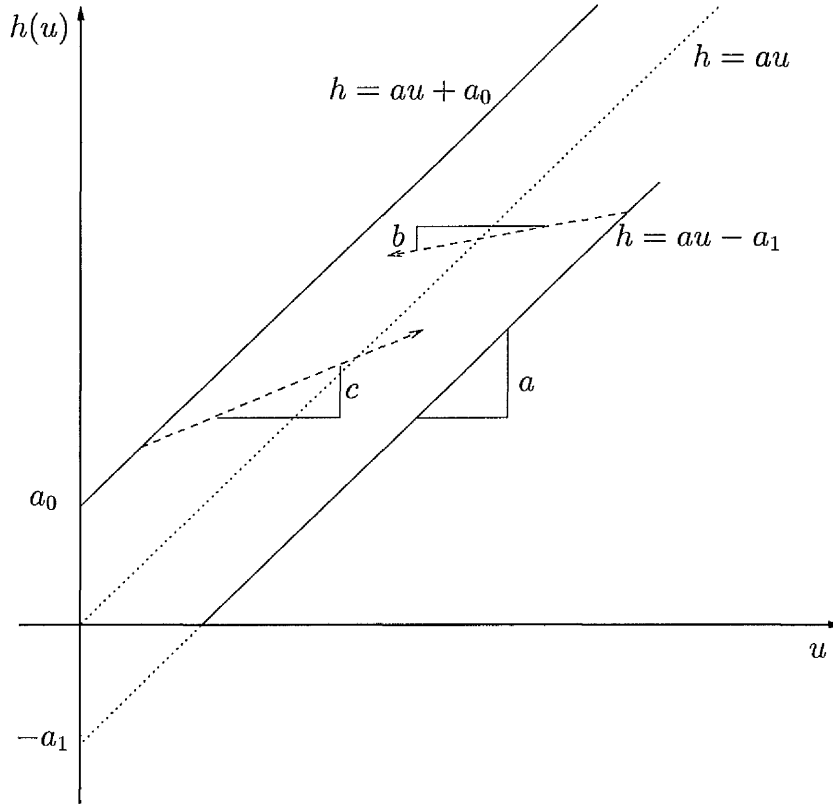


Figure 5.7: Clamping force hysteresis

Due to the positive clamping force, the hysteresis is defined only for the positive forces u and h . Increasing u results in a motion along the curve $h = au - a_1$. If u

decreases, h will decrease too. The decrease of h has the slope b until the curve $h = au + a_0$ is crossed. When u decreases continuously, h moves along the curve $h = au + a_0$. When u increases, h increases with the slope c until the curve $h = au - a_1$ is crossed.

The friction is described by the following function [31]:

$$f_\omega(\omega, T_e) = \gamma_0 + \gamma_1 \exp\{-\beta_0 |\omega|\} + \gamma_2(1 - \exp\{-\beta_1 |\omega|\}) |T_e + T_0| \operatorname{sgn}(\omega)$$

where

$$\begin{aligned} T_0 = \nu_{ges} Zero_Load. & : \text{Zero_Load is the zero load axial force offset for friction [N]} \\ \mu_0 & : \text{stiction force coefficient [1]} \\ \mu_1 & : \text{dry friction coefficient [1]} \\ \Omega = \omega_{min} & : \text{rotor velocity for minimum friction} \\ \omega_{low} & : \text{rotor velocity threshold for drop in stiction force [rad/s]} \\ \omega_{high} & : \text{rotor velocity threshold for speed dependent friction [rad/s]} \\ \beta_1 = 1/\omega_{low} & \\ \beta_2 = 1/\omega_{high} & \\ \kappa = e^{\Omega(\beta_1 - \beta_2) - \ln(\frac{\beta_1}{\beta_2})} & \\ \gamma_0 = \frac{\kappa\mu_1 - \mu_0}{\kappa - 1} & \\ \gamma_1 = \kappa \frac{(\mu_0 - \mu_1)}{\kappa - 1} & \\ \gamma_2 = \frac{(\mu_0 - \mu_1)}{\kappa - 1} & \end{aligned}$$

The electromechanical brake is servo controlled by a cascade PID-controller, which consists of a current controller, an angular velocity controller and a force controller as shown in Fig. 5.8. The index m denotes the measured values of the clamping force F_{sp} , the angular velocity ω and the current I . Index s indicates the reference signal.

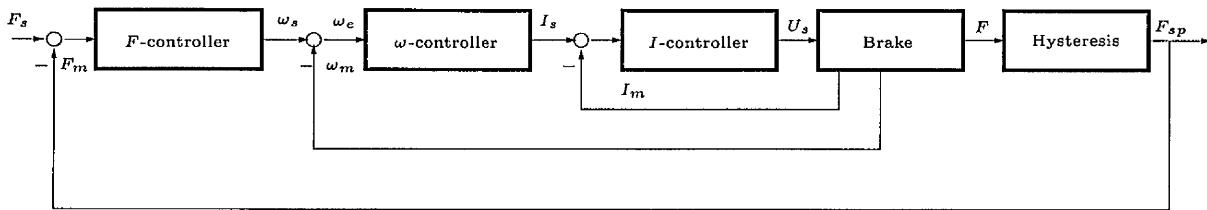


Figure 5.8: scheme of the cascade structure of the EMB servo controller

Simple EMB model The nonlinear brake model is used for simulation. A very simple brake model is applied for the controller design. A discretised first order transfer function

$$H(z) = \frac{0.4}{z - 0.6} \quad (5.1)$$

where the sampling time is $T_S = 2.33\text{ms}$ covers the main dynamic effects. At $f = 3\text{Hz}$, it has a phase of -18 degrees and at $f = 10\text{Hz}$, a phase of -53 degrees. Sinusoidal experimental results show that at $f = 3\text{Hz}$, the EMB actuator has a phase of approximately -20 degrees, while at $f = 10\text{Hz}$, the phase is -60 degrees. The step responses are similar (cf. Fig. 5.9) while the nonlinear model is better. Fig. 5.9 shows a step response of the brake as well as the same step responses of the linear and nonlinear model.

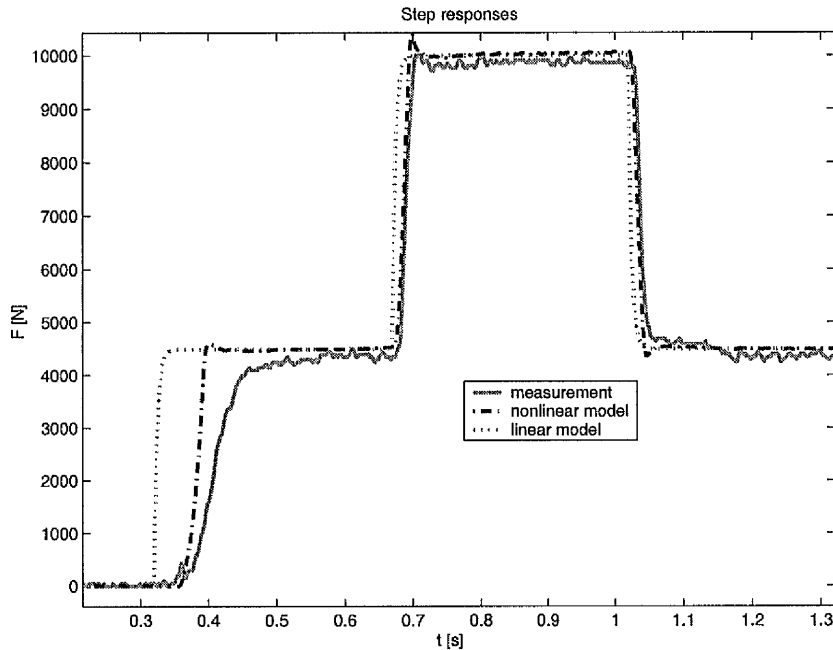


Figure 5.9: Validation of the brake models

5.2 Applicational viewpoint

The problem of implementing a controller on a digital computer is not very often discussed in the literature. It is necessary to take into account the interfaces to the sensors, actuators and the human operators into account. To obtain a good control system, it is also necessary to consider the following [16]:

- Pre-filtering and computational delay
- Actuator nonlinearities
- Operational aspects
- Numerics

- Realization
- Programming aspects

The controllers in Sec. 3.1 are based on the assumption that the controller can be implemented continuously. This is not possible when using a microcontroller. Therefore, the controllers have to be discretised. If the sampling rate is high enough and the controller design is robust, the discretisation does not lead to instability. Arcak [15] deals with unmodelled dynamics in robust nonlinear control but only dynamics that do not change the relative degree.

An additional time delay of 14ms between sensor output and control signal makes the control system less robust. Furthermore, the controller has been designed for the system neglecting actuator dynamics.

The free design parameters of the controllers are used, in order to make the implementation robust. For test and adjusting purposes simulations are necessary.

The computing time is limited on micro controllers. Therefore, in order to avoid runtime errors the Kalman filter has been split up in three parts. At each time step only a third part of the Kalman filter calculations are performed. Thus, the Kalman filter runs at a sampling period of 21ms.

5.3 Experimental Methods

The following section describes experiments that will be performed with the test vehicle in order to evaluate the slip controller.

The measurement of the braking performance of ABS systems are based on publications of the International Standard (ISO) for testing the anti lock braking systems on motor vehicles [5, 1, 6, 8] as well as on the standard literature on ABS [25] and publications of the Society of Automotive Engineers [3].

From the standard tests a subset of the most important experiments is taken to evaluate the performance of the ABS controllers developed within the thesis. The tests are described in Table 5.1. Due to logistical reasons a subset of the experiments was chosen namely test number 1,3,10. These tests show the major properties of the controller. Since the initial values of the controllers friction estimators is set to high values the test number six is also covered. The steerability has not been tested directly since the slip controller is a low level controller working independently for each wheel. Yaw accelerations have not been taken into account.

Table 5.1: Performance tests for ABS

Exp-eriment	Description	Initial Speed	Reference
1	Straight line panic braking (fast increase of brake force) test on high tyre friction coefficient (dry asphalt)	30 [m/s]	ISO 6597 [1, 25, 3]
2	The same test as described in Experiment 1 with constant medium tyre friction coefficient (wet asphalt)	30 [m/s]	ISO 6597 [1]
3	The same test as described in Experiment 1 with low tyre friction coefficient (ice)	10 [m/s]	ISO 6597 [1]
4	The same test as described in Experiment 1 while driving downhill	10 [m/s]	ISO 6597 [1]
5	The same test as described in Experiment 1 with slow increase of brake force (1-5 [kN/s])	30 [m/s]	[25]
6	Changing friction coefficient test (high \rightarrow low)	20 [m/s]	[25, 3]
7	Changing friction coefficient test (low \rightarrow high)	20 [m/s]	[25, 3]
8	μ -split friction test	20 [m/s]	[25, 3]
9	Lane change Test	30 [m/s]	ISO 3888-1 [25, 8, 3]
10	Braking in a turn Radius 100 [m], Lateral acceleration 5 [m/s]	22.5 [m/s]	ISO 7975 [6]

5.3.1 Presentation of the results

According to [1] the following information shall be recorded during each test stop:

- The actual speed of the vehicle at the initiation of braking;
- the control force (brake force);
- the deceleration or stopping distance;
- any locking of the wheels (wheel speed);

- deviation of the vehicle from its course or abnormal vibrations.

The following additional information shall also be recorded:

- the ambient conditions;
- the vehicle loading conditions;
- relevant tyre information.

All the test results may be presented in the form of a table as well as representative graphs.

In the test vehicle during the tests the following information is logged at a sampling period of 7ms:

1. The vehicle speed estimated by the Kalman Filter (one for each wheel) and measured by a correlation sensor (one for the vehicle),
2. the wheel speed for each wheel,
3. the wheel slip value for each wheel calculated from the vehicle- and wheel speed,
4. the desired and measured clamping force,
5. the estimate of the friction coefficient (Kalman filter, MMO),

Furthermore the setpoint slip and ambient conditions are logged.

5.3.2 Evaluation criteria

The essential performance criteria to be analysed are:

- deceleration,
- braking distance,
- maximum peaking of slip,
- steerability.

If the slip behaviour matches the controller specification (cf. Sec. 4.1.8) the minimum braking distance is guaranteed while the steerability is maintained. For that reason only the slip behaviour is used for evaluation of the control performance. Further logged details will be used to explain specific behaviour of the different controllers.

5.4 Car tests

The test vehicle has been described in Sec. 5.1. The tests have been made according to the experimental plan in Sec. 5.3.

For all tests the following measurements are displayed:

- **upper plot** the wheel slip (solid line), the setpoint slip (dash-dotted line) and the state of the mode switching automaton (grey line). The automaton mode is one for braking with ABS, 0.75 if no brake wish is applied by the driver but the ABS is switched on, 0.5 in bumpless transfer mode and zero in off mode.
- **second plot** the desired clamping force F_d (dash-dotted grey line), the control signal F_s (dashed grey) and the measured clamping force F_{sp} (solid black line),
- **third plot** different friction estimates:
 1. the estimation of the adaptive controller (the integrator) (solid black),
 2. the MMO-estimate (dash dotted grey) and
 3. the Kalman-filter estimate (dashed)
- **lower plot** the vehicle speed estimated by the Kalman filter (dash-dotted dark grey), the wheel speed (solid black) and the measured vehicle speed (fat light grey). Note that the measured vehicle velocity is measured by using a correlation sensor. It measures the speed near the right front wheel. Please note that the other displayed plots are for the left front wheel.

Furthermore the longitudinal (black) and lateral (grey) acceleration as well as the estimated lateral velocity is displayed.

5.4.1 Test 1: Straight ahead braking on dry road

Figures 5.10–5.23 show a straight ahead braking manoeuvre on dry asphalt. The tyre friction coefficient is approximately one. This experiment corresponds to the first entry in table 5.1 in section 5.3. The Sontag’s, the nonlinear PI, the LQRC and the SSP wheel slip controller as well as a production car ABS have been tested. The initial speed is about 80km/h. The vehicle is equipped with Continental summer type tyres (ContiEcoContact CP 215/55R16). These tyres have a pronounced maximum friction force at approximately $\lambda = 0.12$ and a higher stiffness than winter tyres. The setpoint slip is set to $\lambda_0 = 0.14$, that means in the unstable part of the friction curve.

Fig. 5.10 – 5.12 show the results for “Sontag’s” tyre slip controller. The upper plot of Fig. 5.10 shows the slip (black), the setpoint slip $\lambda_0 = 0.14$ (grey dash dot) and the flag of the mode change automaton of the controller (grey). Initially, the controller chatters between manual-mode and automatic-mode. This is a small bug and will be solved in later versions. When the driver hits the brake the controller switches into automatic mode at $t \approx 0.9\text{sec}$. The controller stays in automatic mode until the reference speed falls below $v_r = 1\text{m/s}$. Then it switches into bumpless transfer mode (0.5) and into off-mode.

The slip stays mostly below the setpoint slip. This is introduced by the slowly increasing integral part of the controller. The integrator (third plot black line) integrates constantly until time $t \approx 2.5\text{s}$. At this point the slip increases fast due to the negative slope of the friction curve until $\lambda_{max} = 0.37$. The integral part counteracts this high slip with decreasing its value. At $t = 2.7\text{s}$ the slip falls short of the setpoint and the integrator starts again. This is apparently a limit cycle and might be introduced by the time delays and a winter tyre model used in the controller. The integral part of the controller is very slow.

The second plot of Fig. 5.10 shows the commanded clamping force of the driver (grey dash dot), the controller output (grey) and the measured clamping force (black). A time delay between command and measurement can be observed. This is due to 14ms communication time delay, a phase shift according to the actuator dynamics and an air gap between brake pads and brake disk. The brake pads are applied to the disk when the driver hits the brake. Without braking there is an air gap between brake disk and brake pads. Apart from this, the clamping force is never higher than the driver’s wish. The clamping force increases quickly up to almost the steady state value and is quite smooth. The bumpless transfer can be observed when the controller mode flag in the upper plot is 0.5. In off-mode (mode flag eq. zero) the clamping force follows the drivers command.

The third plot shows the estimates of the friction of the MMO (grey dash dot), the Kalman filter (dashed) and the integral part of the controller (black). The initial value of the controller’s integral part is set to $\mu_H = 0.8$. It has been found out that the initial value for the integrator should be $\mu_H = 1.0$. This will result in higher slip peaking at the beginning when braking on a slippery surface. Nevertheless, a higher peaking of slip is more acceptable than a slow increase of the clamping force due to a slow integrator. The integral part converges very slowly probably to a limit cycle around one as described before. The MMO-estimate is wrong until $t = 0.8\text{s}$. This is initiated by the strong pitching of the vehicle that has not been considered in the model used

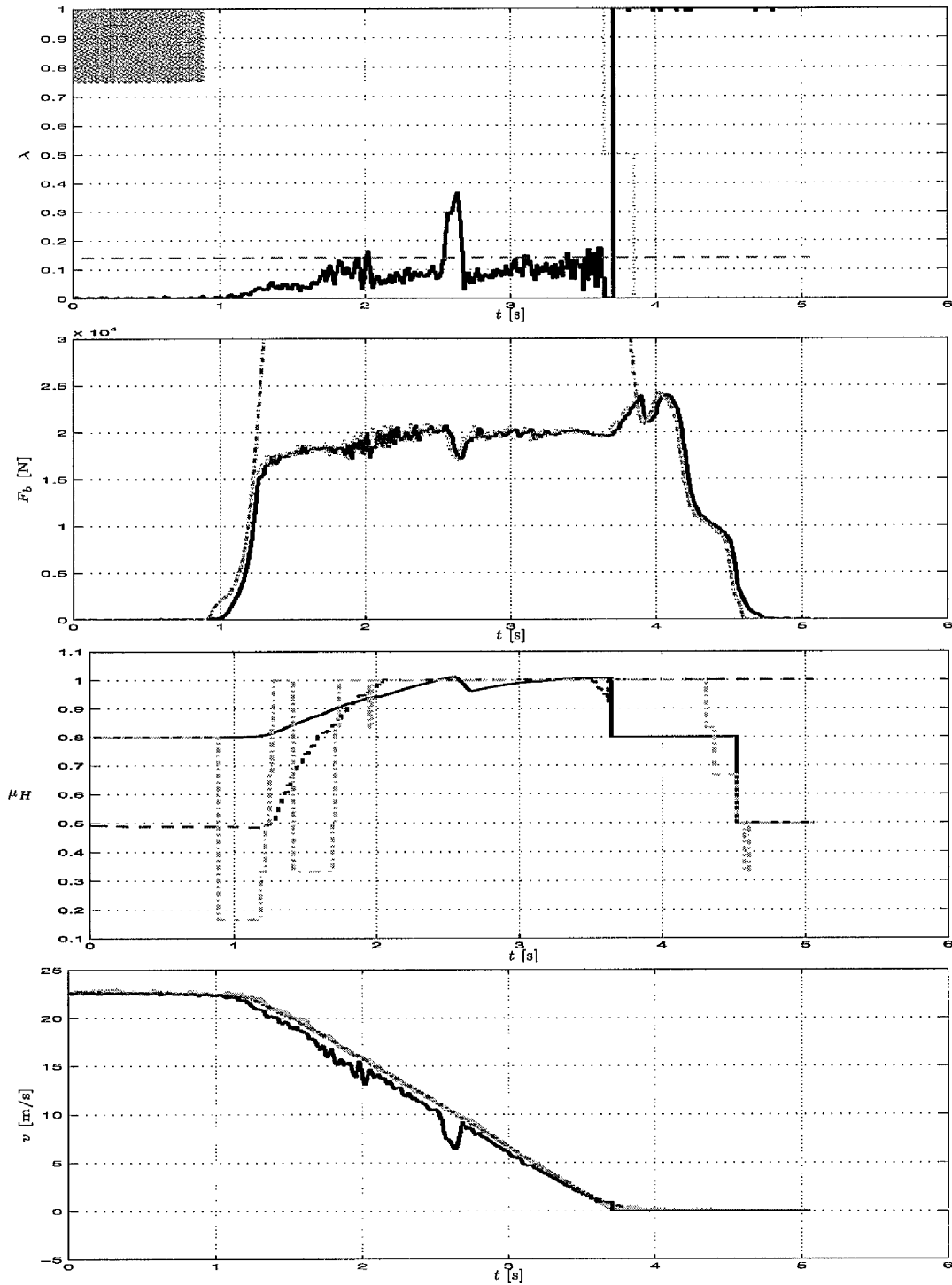
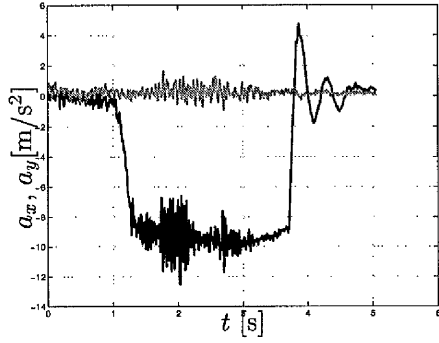
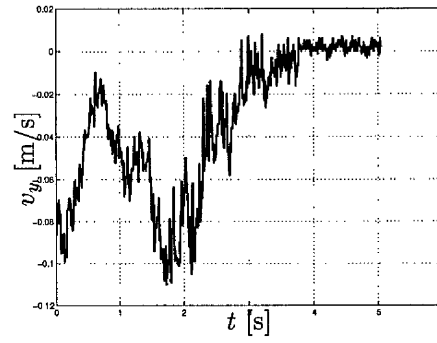


Figure 5.10: Test 1 results with “Sontag” tyre slip controller braking on dry road with reference slip $\lambda_0 = 0.14$.

Figure 5.11: Accelerations a_x and a_y Figure 5.12: Lateral speed v_y

for controller- and observer-design. The Kalman filter converges slowly to the friction coefficient of one.

Figure 5.11 shows a fast increasing deceleration a_x (black) and the constant zero lateral acceleration a_y (grey). Over the whole braking manoeuvre the deceleration is nearly constant $a_x = -9\text{m/s}^2$. Furthermore after the standstill of the vehicle between approx. $t = 3.8\text{s}$ and $t = 4.6\text{s}$ the pitching of the vehicle can be seen. This oscillation is relatively weakly damped. The lowest plot in Fig. 5.10 shows the reference and wheel speed. The noise in the a_x measurement gives feedback to the estimation of the vertical forces (cf. App. A.8) and thus to the controller. This can be observed at time $t \approx 2\text{s}$.

Figure 5.12 shows the lateral velocity of the vehicle estimated by the Kalman filter. A maximal lateral velocity of $v_{y_{max}} = -0.11\text{m/s}$ shows that there is not too much deviation from the normal course. This is confirmed by the lateral acceleration in Fig. 5.11.

Fig. 5.13 – 5.15 show the same experiment as in Fig. 5.10 – 5.12 with the nonlinear PI controller instead of the “Sontag’s” controller. The results are quite similar and can be explained in the similar way. A difference between “Sontag’s” controller and the nonlinear PI controller is that the “Sontag” controller uses a tyre model while the PI controller does not. Both controllers are nonlinear PI controllers with slow adaptation. Noise introduced by the deceleration measurement has weaker feedback to the control output for the PI controller. This can be seen by comparing the measurement plots Fig. 5.13 – 5.15 and Fig. 5.10 – 5.12. Please note that under real life conditions it is nearly impossible to achieve two exactly similar experiments. The controller does not depend only on the ambient conditions but also on the initial states and estimates of the Kalman filter.

Fig. 5.16 – 5.18 show the same experiment as shown in Fig. 5.10 – 5.12 by using the LQRC controller. This controller has very low gain. The upper plot in Fig. 5.16

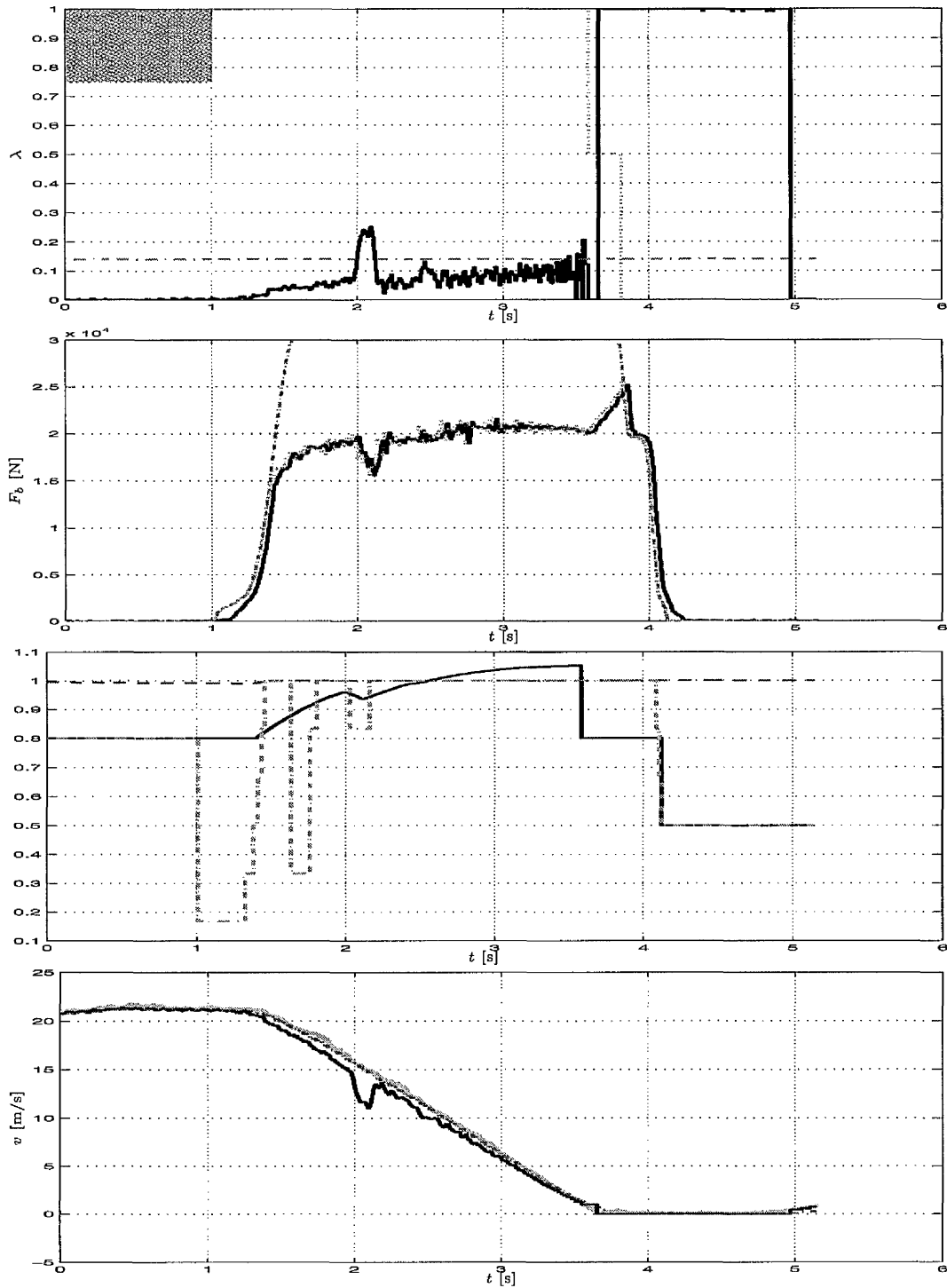
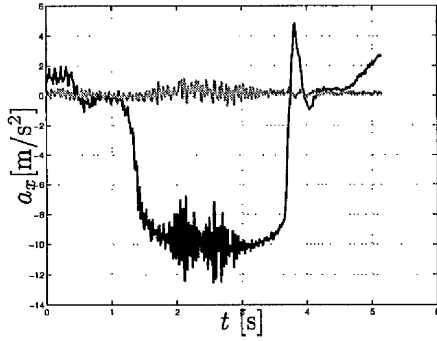
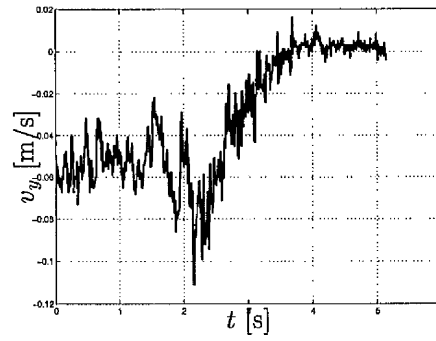


Figure 5.13: Test 1 results with nonlinear PI tyre slip controller braking on dry road with setpoint slip $\lambda_0 = 0.14$.

Figure 5.14: Accelerations a_x and a_y Figure 5.15: Lateral speed v_y

shows a very slow increase of the slip. This is due to the very slow increase of the clamping force which is very smooth and displayed in second plot of Fig. 5.16. This slow smooth clamping force comes from a very low proportional feedback. For that reason the controller is very comfortable but the braking distance is significantly longer than with the nonlinear controllers. This result is unacceptable because a panic braking manoeuvre needs to begin with a fast increase of the brake force until the maximum brake force is achieved. The upper plot of Fig. 5.16 shows a cyclic behaviour of the slip value. Two peaks can be observed. Once the slip has fallen under the setpoint value the time needed for increasing the clamping force and thus the slip is unacceptably high. The maximum peaking of slip is $\lambda_{max} = 0.44$. The peaks are slightly higher than those of the nonlinear controllers. The third plot of Fig. 5.16 shows the MMO estimate which is wrong for low slips. This behaviour is introduced by the tyre model used in the MMO design. The lowest plot shows the smoothly increasing retardation which correlates with the acceleration measurement in Fig. 5.17. The lateral velocity shown in Fig. 5.18 also very low. Its maximum is $v_{y_{max}} = -0.125\text{m/s}$.

Figure 5.19–5.21 shows a straight ahead braking manoeuvre with SSP tyre slip controller on dry asphalt. Please note that this experiment has been done with winter tyres (ContiTS790 215/55R16). For that reason the results cannot be directly related to the other braking manoeuvres shown in Figures 5.10–5.18. Furthermore, note that in this experiment the mode changes of the controller have not been implemented. The slip value converges very slowly to a value that is smaller than the setpoint slip. This is due to a small integral part. It can be seen that due to the winter tyres no cyclic behaviour is introduced. The clamping force (second plot) is very smooth and slow. It does not follow the drivers brake demand. Thus the controller does not fulfill the requirements for ABS. The controller gain is too small. The decreasing value of the clamping force after $t \approx 1.8\text{s}$ can be explained by a wrong slip estimation. It can

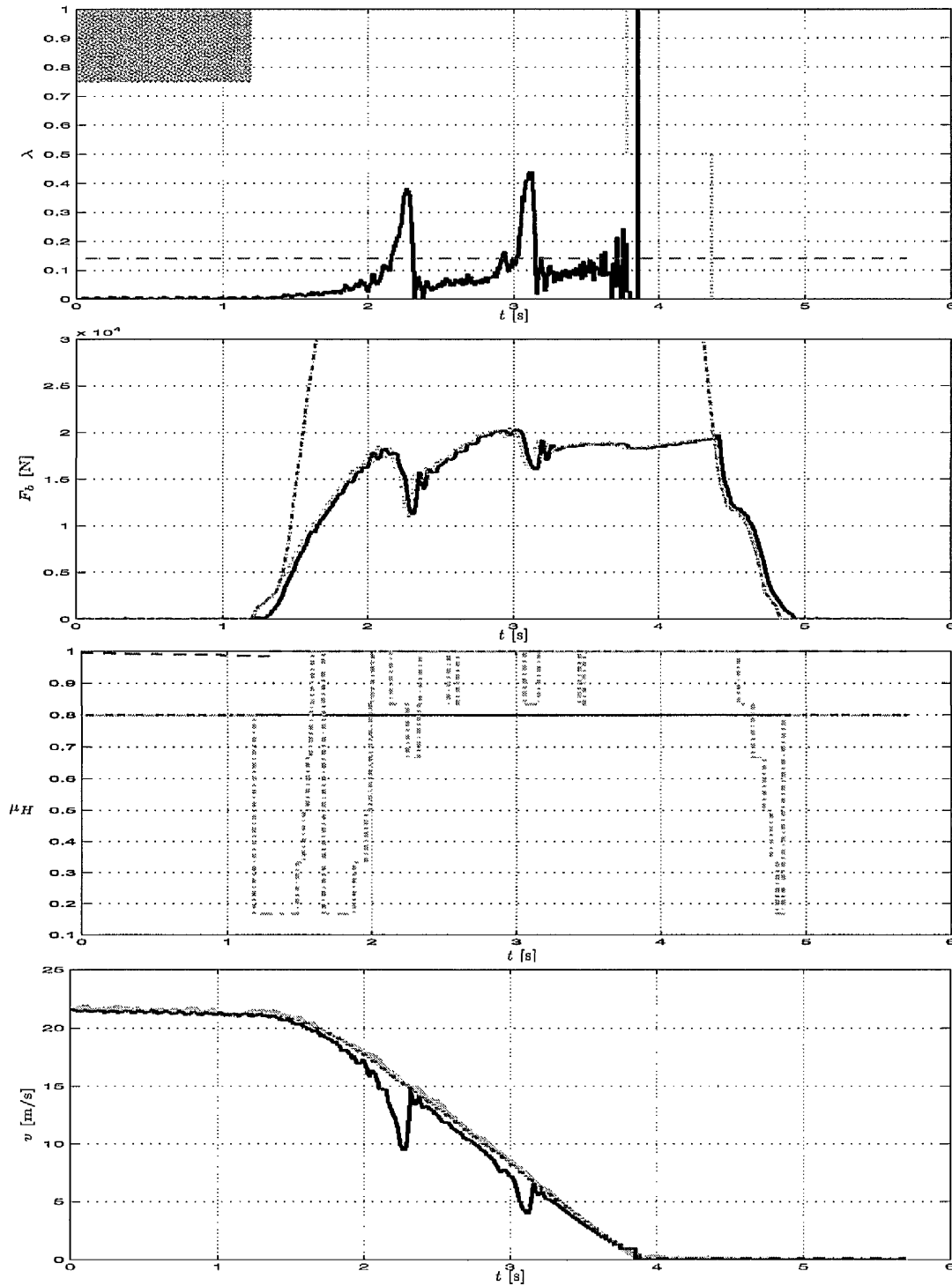
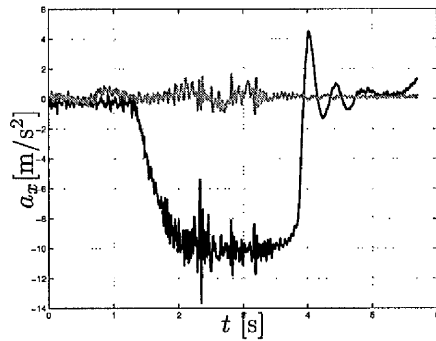
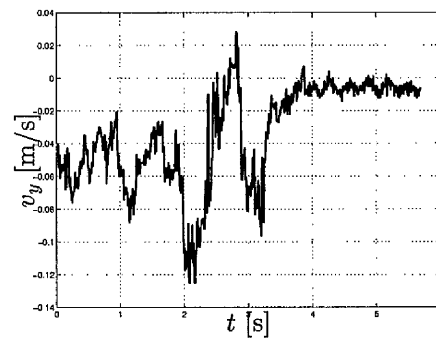


Figure 5.16: Test 1 results with LQRC tyre slip controller braking on dry road with setpoint slip $\lambda_0 = 0.14$.

Figure 5.17: Accelerations a_x and a_y Figure 5.18: Lateral speed v_y

be seen that the deceleration falls also after $t \approx 1.8\text{s}$ (cp. Fig 5.20) while the slip is constant. The third plot shows the MMO friction estimate. The MMO estimates a tyre friction coefficient $\mu_H = 0.8$ when the slip is high enough. The lowest plot shows that there is a difference between estimated (dashed) and measured (light grey) vehicle speed. This small error causes large slip estimation errors. Figure 5.20 shows a very smooth noiseless acceleration measurement and the brake jerk at low speed $t \approx 3\text{s}$ when the controller is switched off without bumpless transfer. No significant lateral speed can be observed in Fig. 5.21.

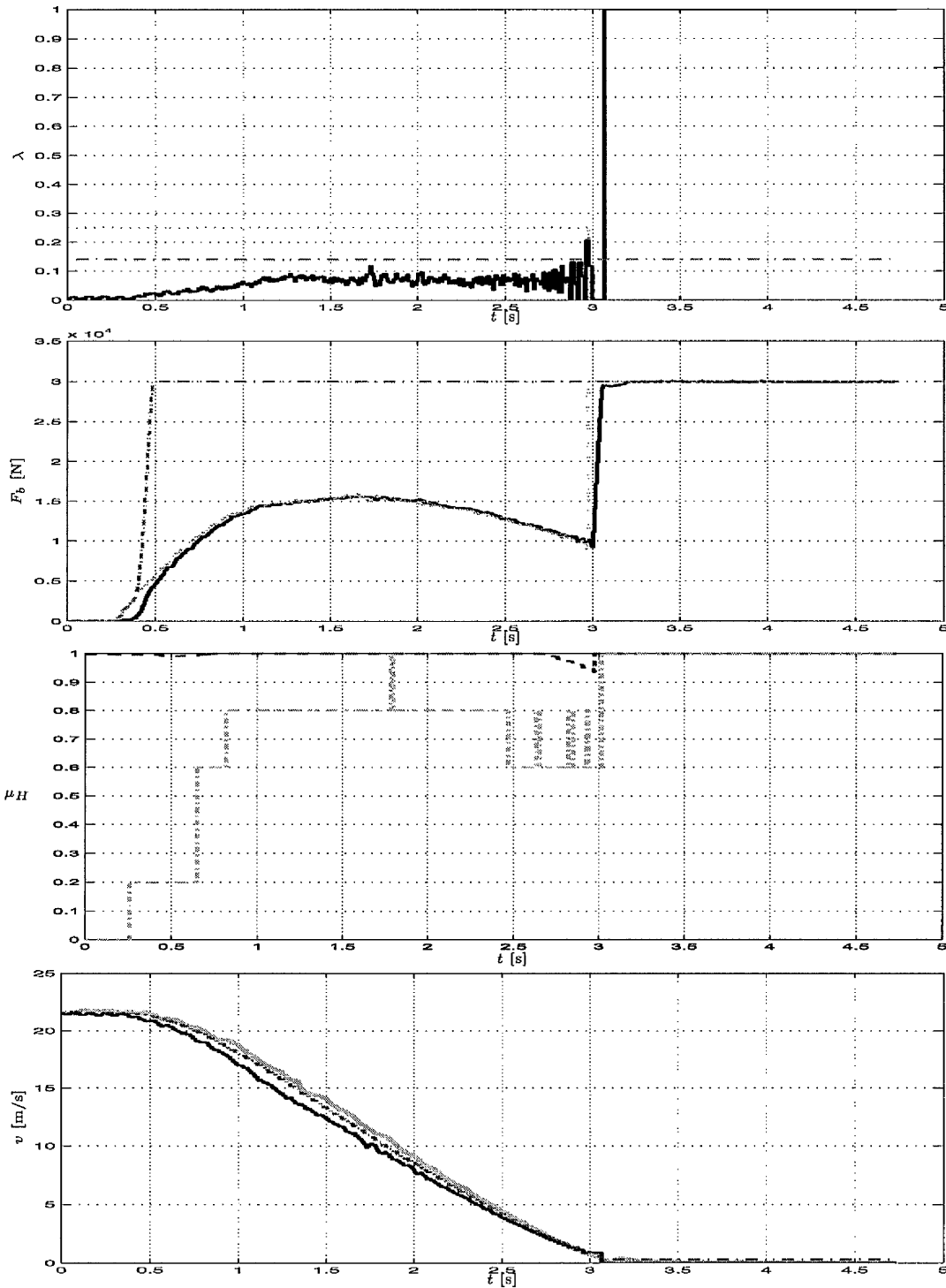


Figure 5.19: Test 1 results with SSP tyre slip controller braking on dry road with setpoint slip $\lambda_0 = 0.14$.

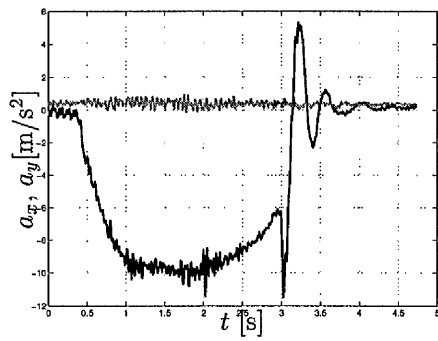


Figure 5.20: Accelerations a_x and a_y

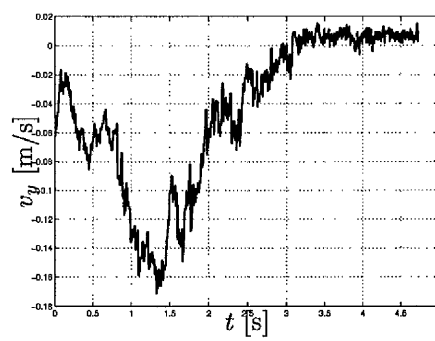


Figure 5.21: Lateral speed v_y

5.4.2 Conventional ABS on dry road

Fig. 5.22 and 5.23 show the slip, clamping force and speed of production car ABS brake-manoeuvres on high friction coefficient. In 5.22 the front wheels, and in 5.23 the rear wheels are displayed. The upper plot shows two slip values calculated from the wheel speed and the reference speed calculated by the ABS and displayed in the lowest plot. The control output (dashed), the desired clamping force (dash dot) as well as the measured clamping force (solid) are displayed in the second plot. Large slip transients can be observed and larger slip values can be seen at the front wheels. A limit cycle can be seen which is introduced by the control philosophy of conventional ABS described in sec. 4.1.2. The brake force increases until a certain slip value or wheel acceleration is approached. Then an amount of brake force is released and the brake force increases again. The brake force distribution can be seen by comparing the brake forces at the wheels. The slip peaking reduces the comfort of production car ABS significantly. The model based approaches are more comfortable and have a better performance. Nevertheless, note that the conventional ABS is very robust.

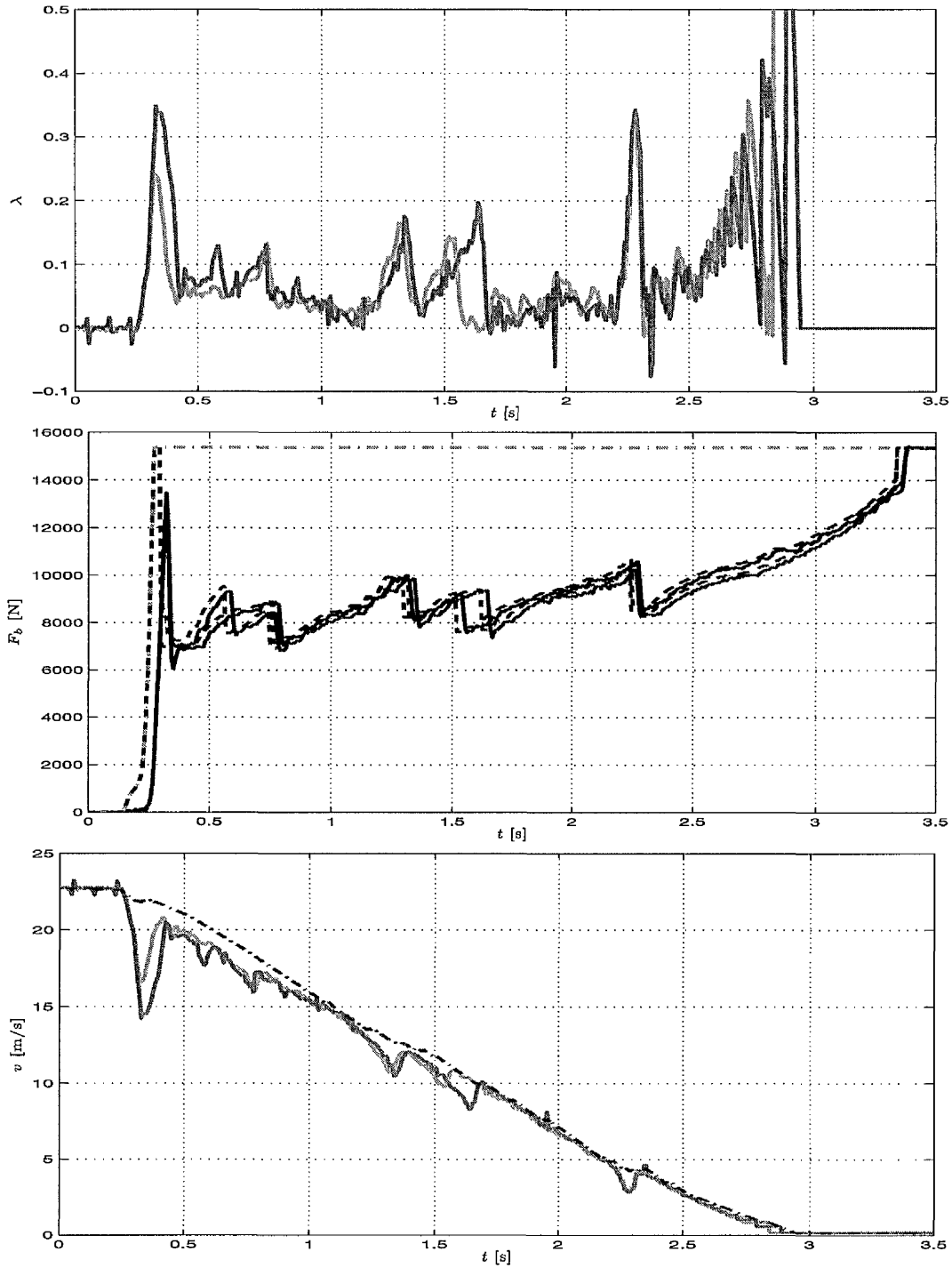


Figure 5.22: Conventional production car ABS on dry road (front wheels)

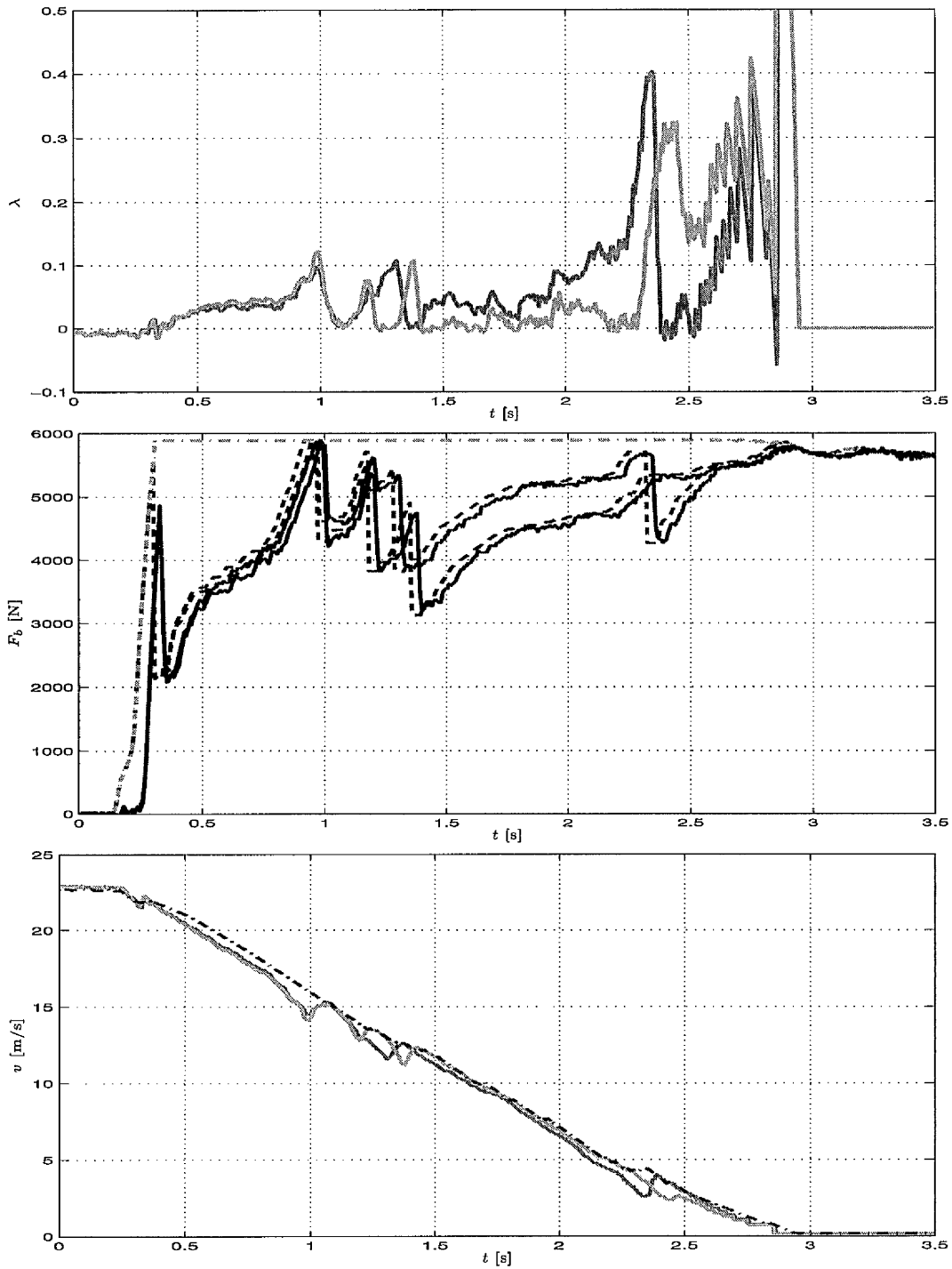


Figure 5.23: Conventional production car ABS on dry road (rear wheels)

5.4.3 Test 3: Straight ahead braking on ice

Figures 5.24–5.36 show a straight ahead braking manoeuvre on an icy road having a friction coefficient $\mu_H \approx 0.1$. The initial speed of the vehicle for all tests is $v_{init} \approx 50 - 60$ km/h. This experiment corresponds to the third experiment described in table 5.1. The experiments have been done without the full functionality of the bumpless transfer and the controller mode changes being implemented. The vehicle is equipped with winter tyres (ContiEcoContact CP 215/55R16) that have no pronounced maximum of the tyre friction curve. The setpoint slip is set to $\lambda_0 = 0.05$. Note that this low setpoint is at the unstable part of the slip curve for a low friction coefficient.

Figures 5.24–5.26 show the braking manoeuvre using the “Sontag” tyre slip controller. At the beginning of braking a large slip transient can be observed (upper plot black line). The clamping force (second plot) is immediately lowered due to a resetting of the integrator of the adaptive controller. The wheel is accelerated very slowly due to the low frictional force whereby the clamping force is nearly zero for a quarter of a second. Also the deceleration is only a tenth of the same manoeuvre done on dry road (cf. Fig. 5.25). The third plot shows the friction estimates. The integrator of the controller is reset to 0.2 at $t \approx 0.5$. This is the MMO estimate. The Kalman filter as well as the integrator converges to 0.1. Approximately a quarter second is needed to speed up the wheel by very low frictional force. After the transient the slip is controlled at the setpoint. For low speed the slip increases. This is because of a slightly too high estimate of the reference speed (cf. Fig. 5.24 lowest plot $t > 4$ s) that is due to an acceleration measurement that is very small (cf Fig. 5.25) and noisy. The acceleration measurement is at the same level as the noise. Furthermore the time constant of the slip problem becomes smaller for low speed. Thus for lower speed the control problem gets more difficult. Please note also that small disturbances have large effects. The bumpless transfer can be seen nicely between $t \approx 10.5$ and 12s.

Figure 5.26 shows the estimated lateral velocity that is not very high and can be handled easily by the driver. The lateral acceleration is very small (cf. Fig. 5.25). Due to that the lateral velocity estimation of the Kalman filter is not very reliable.

Figure 5.27–5.29 show the same experiment as shown in Figures 5.24–5.26 using the nonlinear PI slip controller. The results are quite similar. The maximum peaking of slip is higher for the PI controller. Note that it is very difficult do the same experiment under the same conditions twice with different controllers. The slip increases very fast and the controller performance of the PI controller is not worse than that of the “Sontag” controller. Both controllers behave quite similarly. The slip in the upper plot

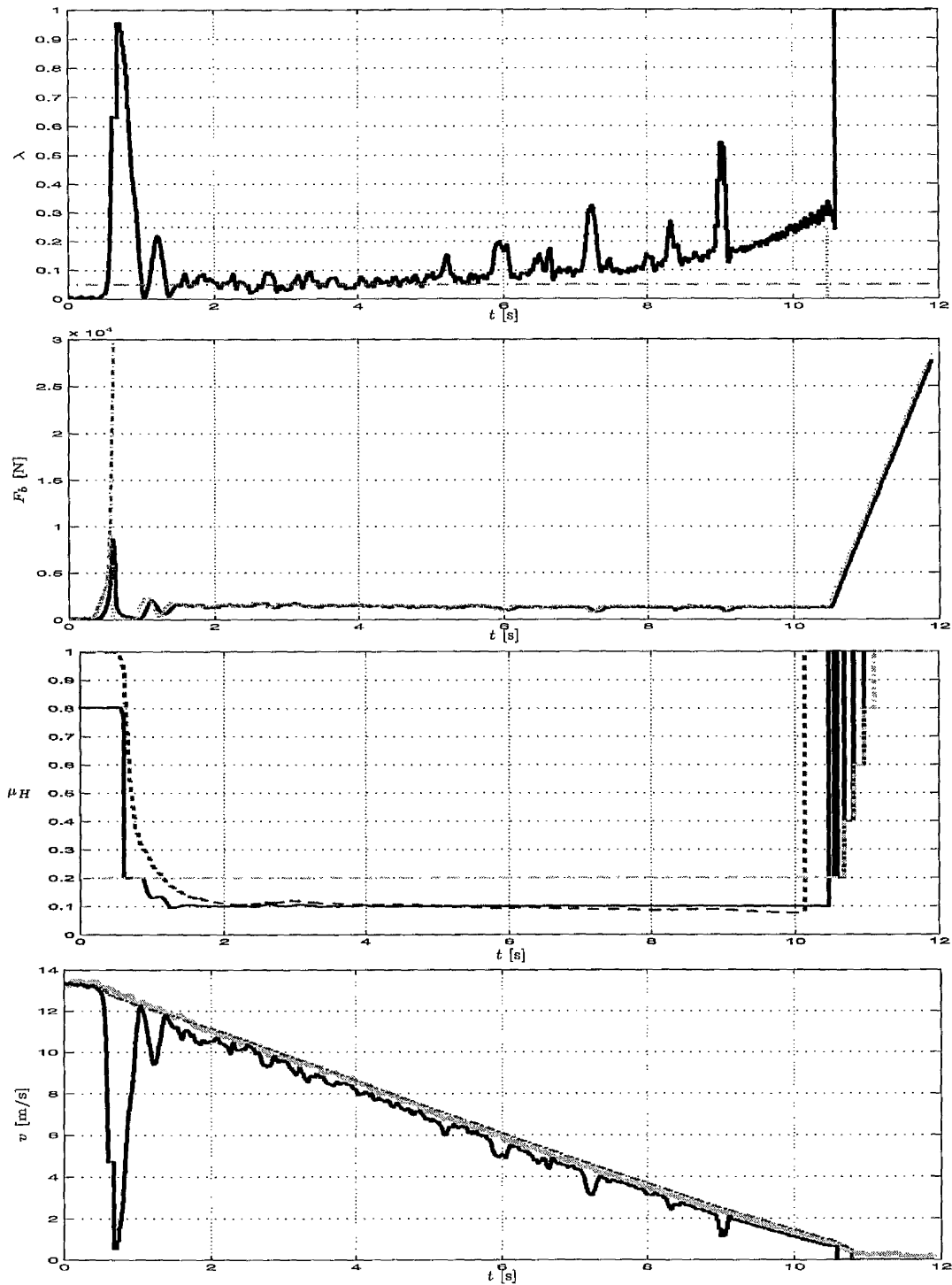
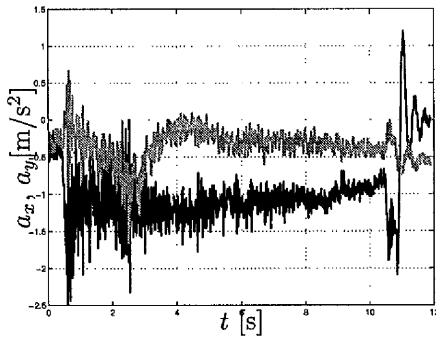
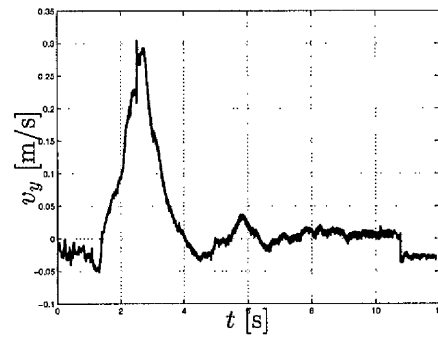


Figure 5.24: Test 3 results with “Sontag” tyre slip controller braking on ice with setpoint slip $\lambda_0 = 0.05$.

Figure 5.25: Accelerations a_x and a_y Figure 5.26: Lateral speed v_y

is very high while the clamping force is almost zero because of the low frictional forces and the control problem for low speed. Some peaks of the slip may be introduced by a slightly inhomogeneous icy surface. The ice was melting while doing the experiments. The retardation is very small (cf. Fig. 5.28) because of the very slippery surface.

In Figures 5.30–5.32 the braking on an icy road with the LQRC controller is displayed. The slip (upper plot) is not peaking because the controller is slower than the nonlinear ones. This has been shown in the experiments on high friction coefficient. The slip value does not increase for lower speed. The friction coefficient seems to be higher than in the other experiments. This can be seen in the friction estimates as well as in the acceleration measurements in Fig. 5.31. The Kalman filter speed estimate is wrong in the first three seconds.

Figures 5.33–5.35 show the results of the SSP controller. This simple linear PI controller has a reasonable performance. It is not able to hold the slip at the setpoint but it prevents the tyre from being locked. The deceleration measurement shown in Fig. 5.34 is not worse than that of the other controllers. Also in this experiment the Kalman filter speed estimate is wrong in the first three seconds. The Kalman filter estimate for the speed is based on acceleration measurements that is small and noisy.

Figure 5.36 shows production car ABS brake-manoeuvres on low friction coefficient. Only the slip values of all four wheels are displayed. Large slip peaks especially for the front wheels can be observed at the beginning of braking. The cyclic recurring slip peaking is due to the control philosophy explained in Sec. 4.1.2. The difference of the controllers on an icy road is smaller than on high friction. The model based approaches do not have the cyclic slip peaking but both the model based controllers and the conventional ABS have the large peaking of slip at the beginning.

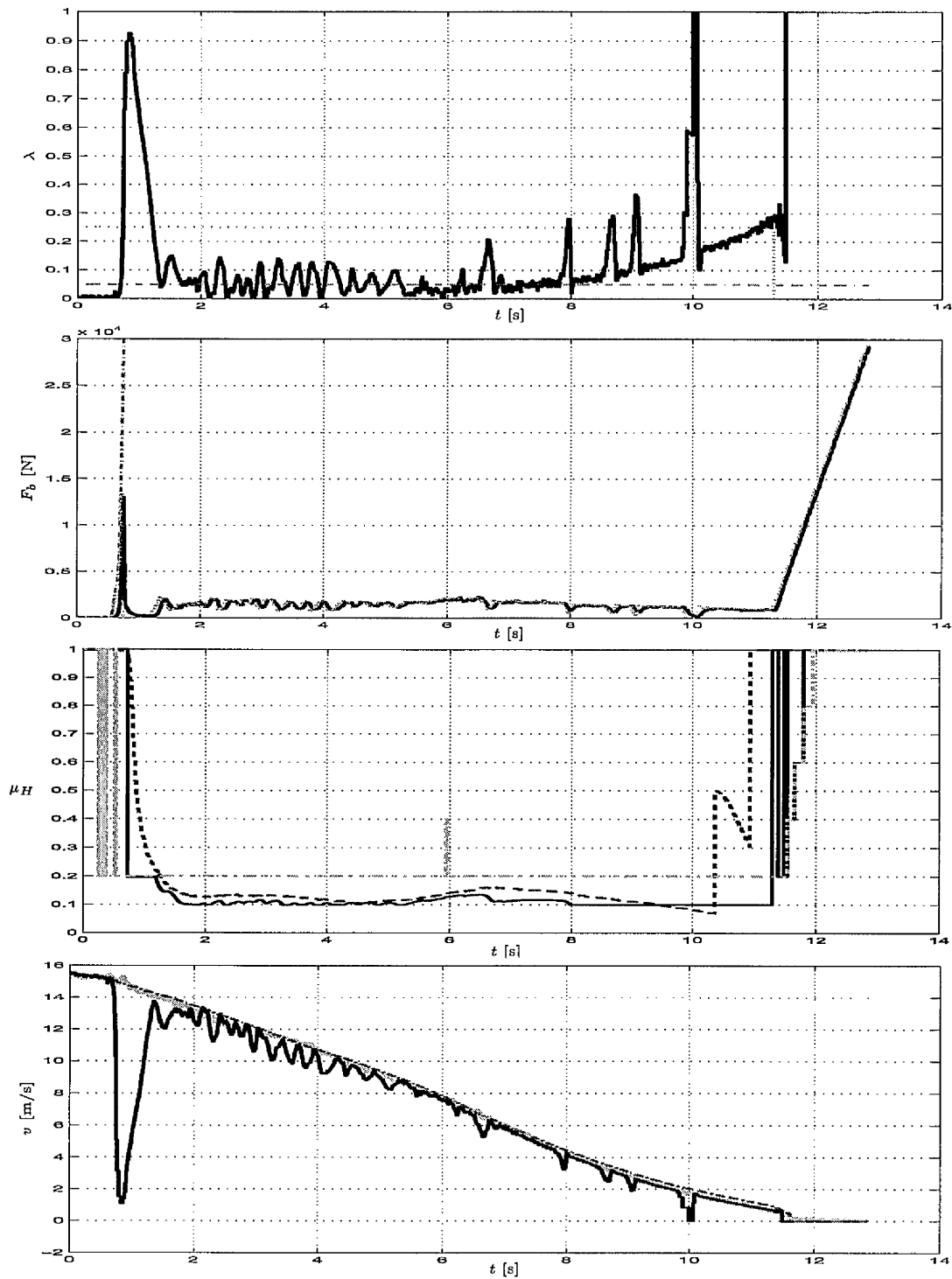


Figure 5.27: Test 3 results with nonlinear PI tyre slip controller braking on ice with setpoint slip $\lambda_0 = 0.05$.

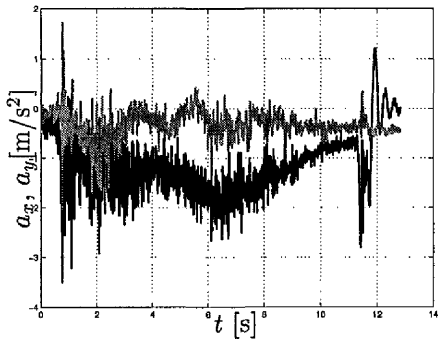


Figure 5.28: Accelerations a_x and a_y

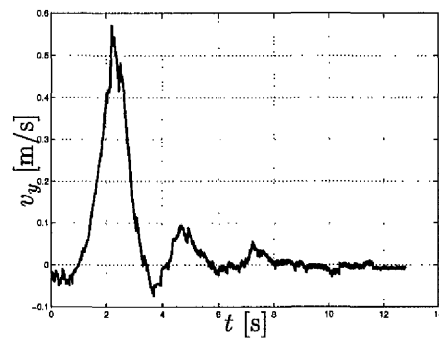


Figure 5.29: Lateral speed v_y

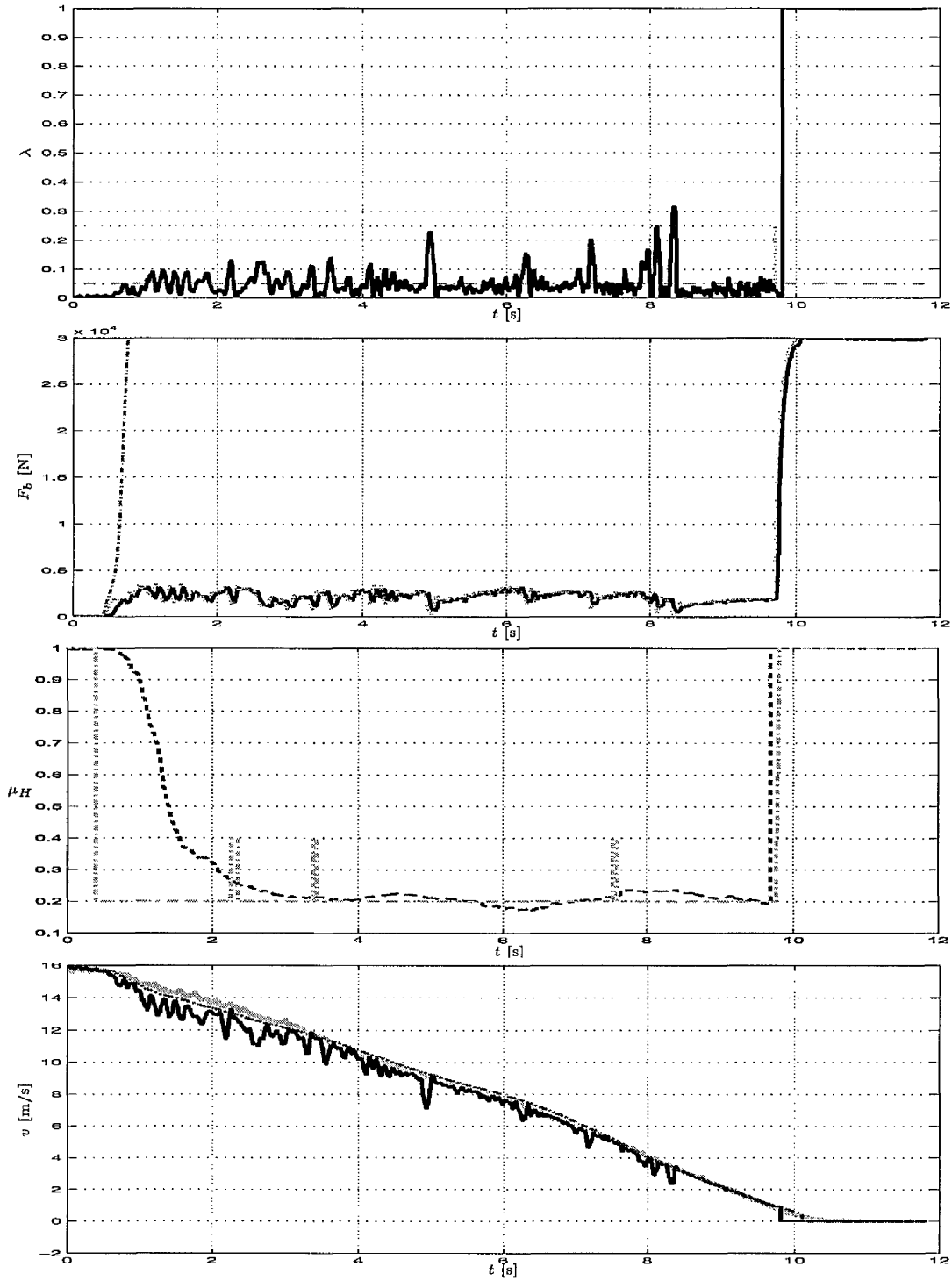


Figure 5.30: Test 3 results with LQRC tyre slip controller braking on ice with setpoint slip $\lambda_0 = 0.05$.

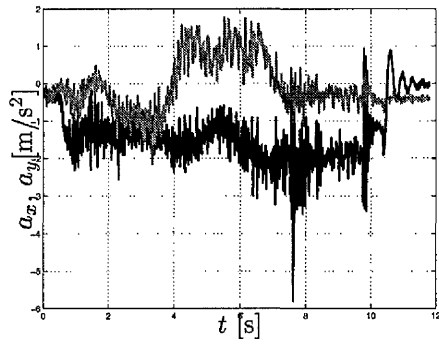


Figure 5.31: Accelerations a_x and a_y

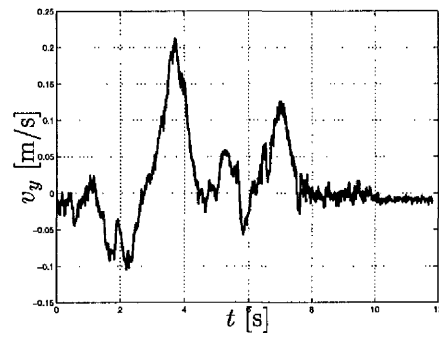


Figure 5.32: Lateral speed v_y

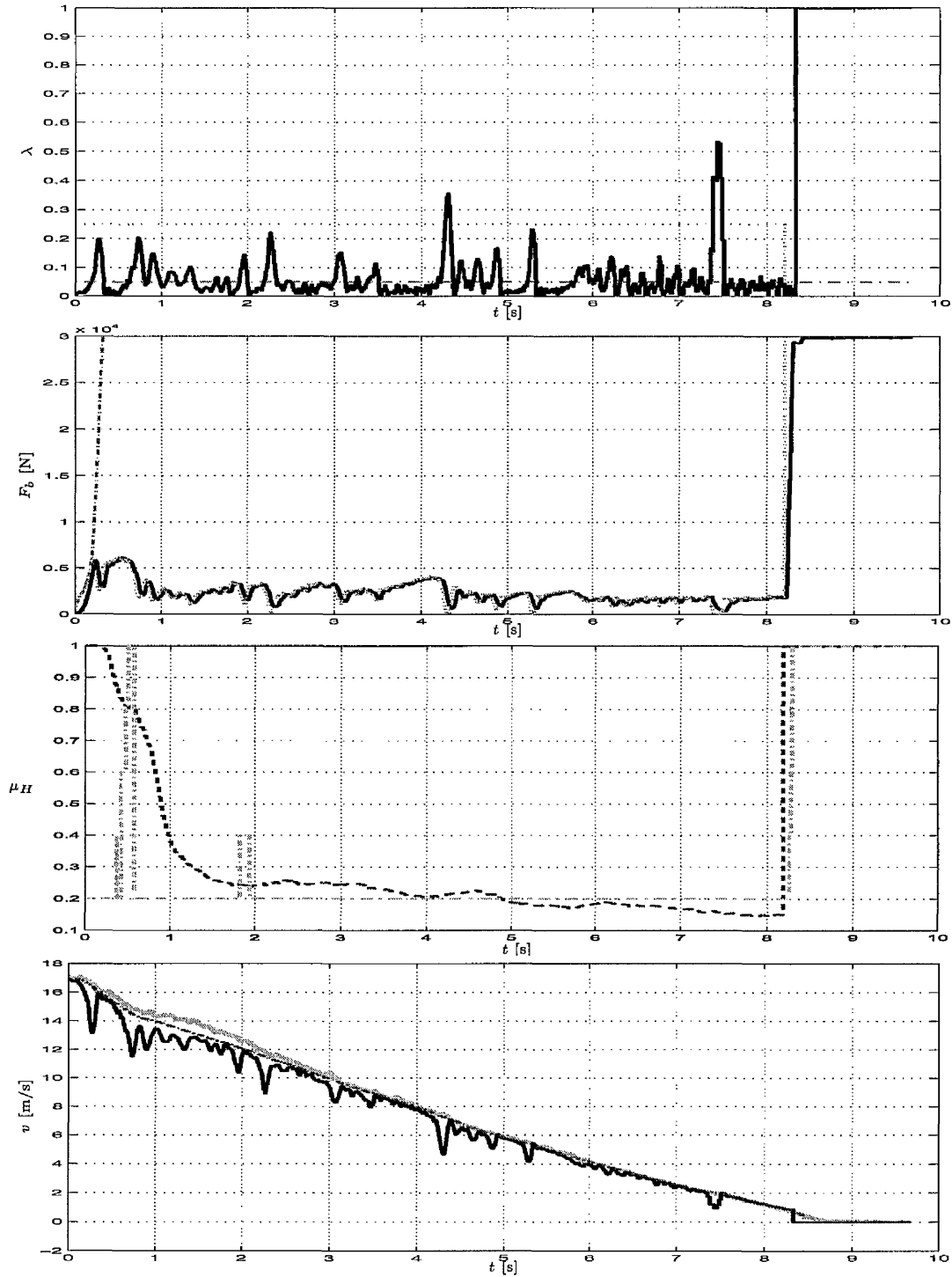


Figure 5.33: Test 3 results with SSP tyre slip controller braking on ice with setpoint slip $\lambda_0 = 0.05$.

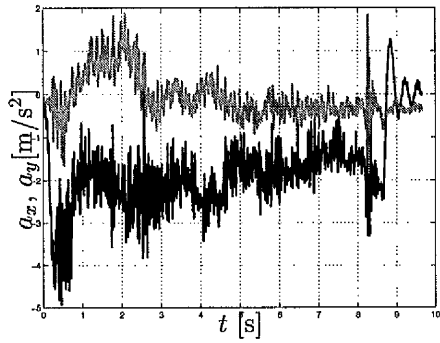


Figure 5.34: Accelerations a_x and a_y

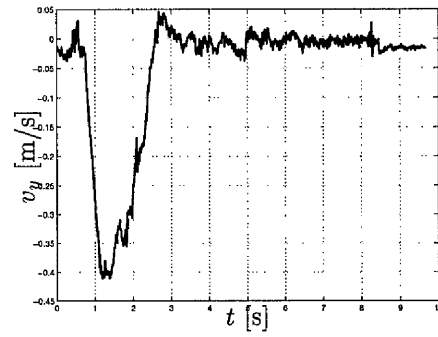


Figure 5.35: Lateral speed v_y

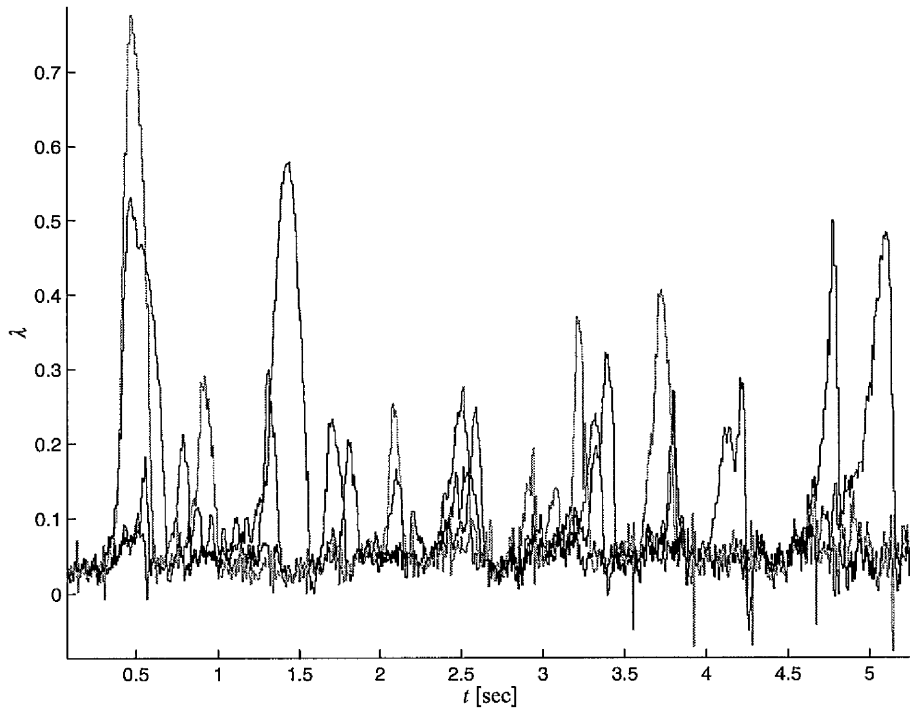


Figure 5.36: Conventional production car ABS on icy road

5.4.4 Conventional ABS on ice

Similar to Fig. 5.22 and 5.23 Fig. 5.37 and 5.38 show the slip, clamping force and speed of production car ABS brake-manoeuvres on medium friction coefficient. This test corresponds to test 2 in Table 5.1. The upper plot shows two slip values calculated from the wheel speed and the reference speed calculated by the ABS and displayed in the lowest plot. The control output (dashed), the desired clamping force (dash dot) as well as the measured clamping force (solid) are displayed in the second plot. Larger transients are to be observed than for dry road. For vehicle speed smaller than 10m/s wheel locking can be observed.

The production car ABS is very robust in general and it works reliably on different surfaces. The production car ABS is less comfortable than the model based approaches. Please note that the comfort is not the main interest during braking in a dangerous situation. Furthermore a reliable working braking system is the main focus in the context of ABS which is only active in critical situations.

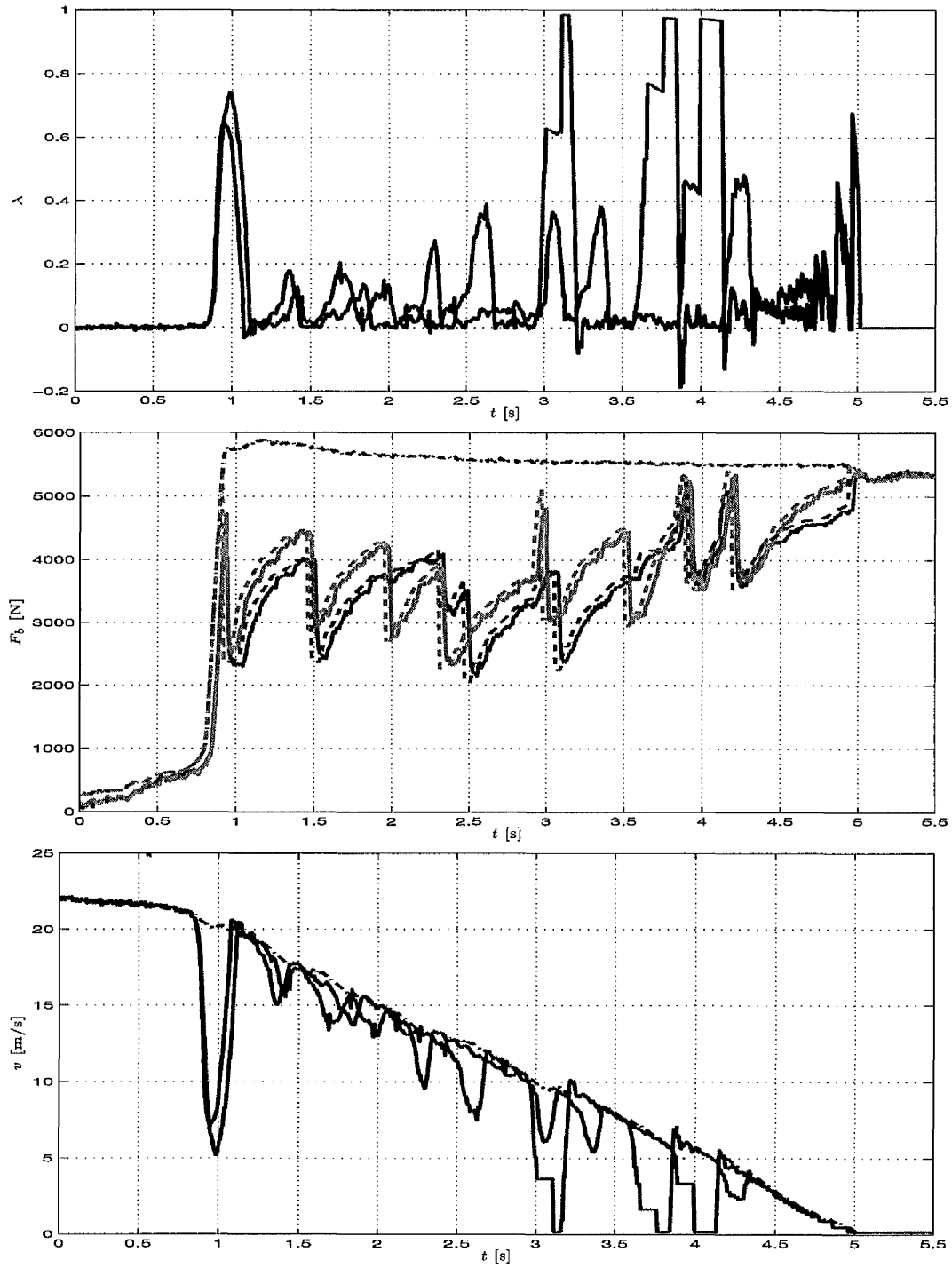


Figure 5.37: Conventional production car ABS on wet road (front wheels)

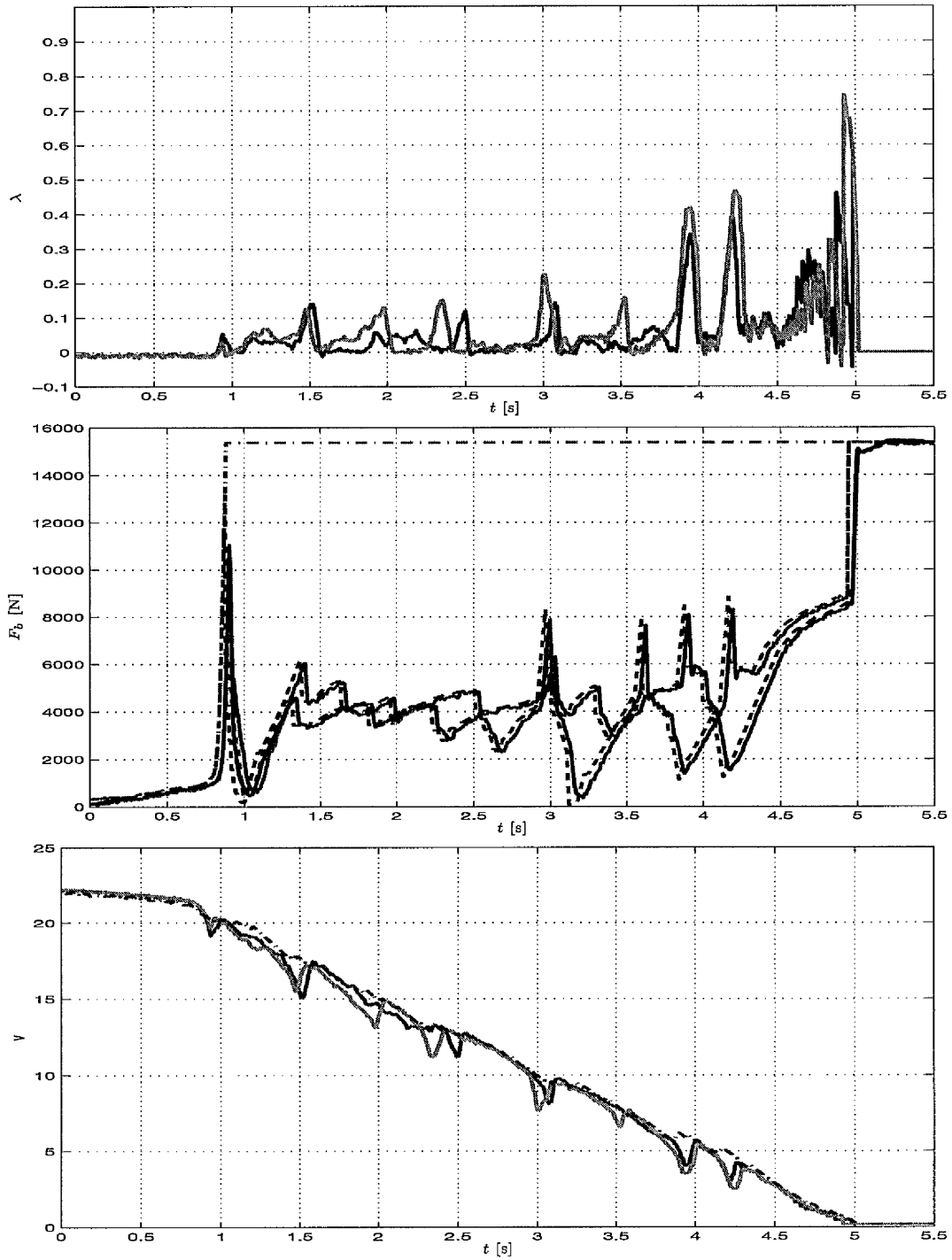


Figure 5.38: Conventional production car ABS on wet road (rear wheels)

5.4.5 Test 10: Braking in a turn

Figures 5.39–5.47 show a braking manoeuvre in a turn. The vehicle was driving in a circle having a radius of approximately 15m. The initial speed before the braking is $v \approx 40\text{km/h}$, the lateral acceleration $a_y \approx 6\text{m/s}^2$. The vehicle is equipped with Continental summer tyre (ContiEcoContact CP 215/55R16). The surface is wet asphalt having a frictional coefficient $\mu_H \approx 0.8$. This test corresponds to the test no. 10 in Table 5.1.

Figures 5.39–5.41 show the “Sontag” controller. The tyre slip is displayed in the upper plot of Fig. 5.39 (black). The Kalman filter estimate of the reference speed is 0.5m/s too low when the vehicle is not braking. Thus the slip estimate is wrong. The slip converges while braking. After converging the slip is controlled at the setpoint. The second plot shows the quickly increasing brake force at the beginning and the bumpless transfer between $t \approx 2.2\text{s}$ and 2.5s. The third plot shows the friction estimate of the controller (black) that has not been reset by the MMO (grey). The controller is initialised with a frictional coefficient $\mu_H = 0.8$ while not braking. This value is optimal for wet surface and gives a smaller overshoot for higher frictional values. The lowest plot shows the vehicle reference speed and the wheel speed. It can be seen that the value of wheel speed is constant over some time steps because of the gridding of the wheel speed sensor.

Fig. 5.40 shows the longitudinal acceleration a_x (black line) as well as the lateral acceleration a_y . The deceleration increases sharply up to a value of $a_x \approx -9\text{m/s}^2$ until the vehicle comes to a standstill. The lateral acceleration is continuously decreasing. The oscillations in a_x and also in a_y indicates the pitching and rolling of the vehicle. Fig. 5.41 shows the lateral velocity of the vehicle that is approximately constant over the braking manoeuvre. This confirms that the vehicle was still steerable.

Figures 5.42–5.44 show the nonlinear PI controller. This controller behaves quite similarly to the “Sontag” controller. A disturbance at $t \approx 1.3\text{s}$ excites oscillations in the wheel slip that are fed back to the controller via acceleration measurements (cf Fig. 5.43) and vertical force F_z .

Fig. 5.43 shows the decreasing lateral acceleration (grey) and the nearly constant deceleration a_x while braking. The lateral velocity in Fig. 5.44 estimate seems not to be very good while not braking.

Figures 5.45–5.47 show the LQRC controller. The results are similar to that of the other braking manoeuvres using that controller. The slip (Fig. 5.45 upper plot) increases very slowly, slower than while straight braking. This is due to the difference

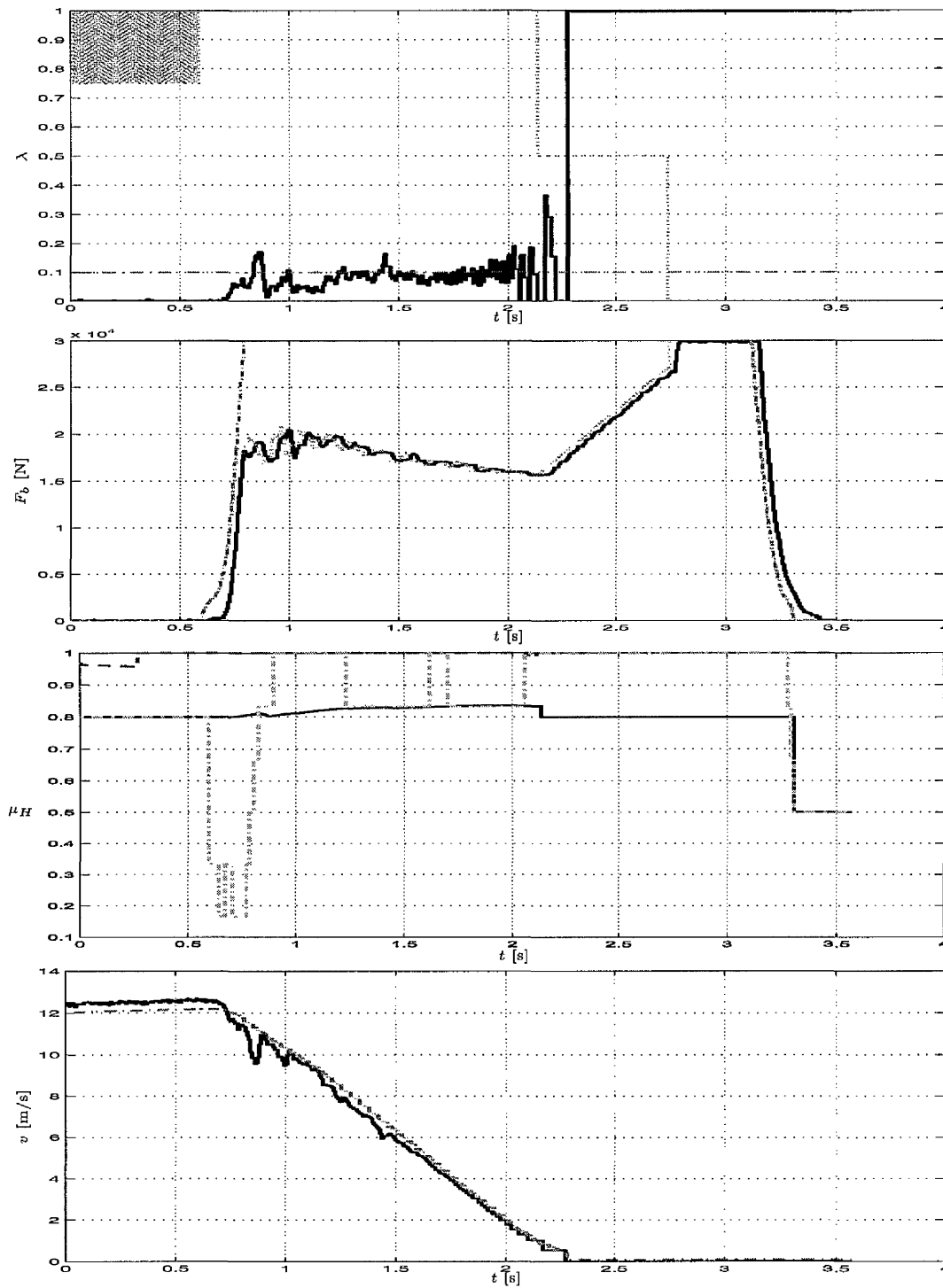
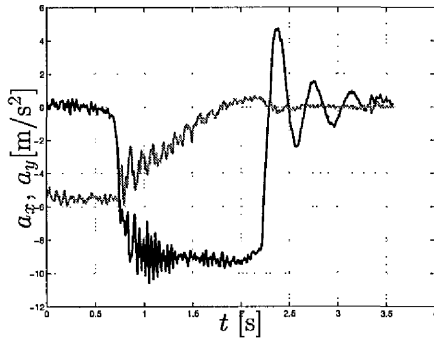
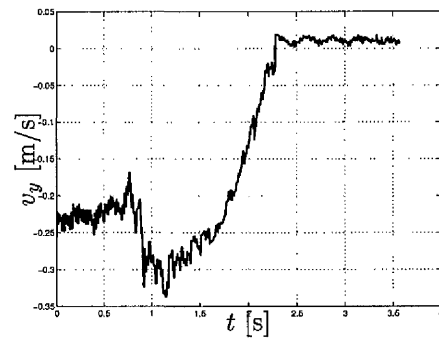


Figure 5.39: Test 10 results with “Sontag” tyre slip controller braking in a turn with setpoint slip $\lambda_0 = 0.1$.

Figure 5.40: Accelerations a_x and a_y Figure 5.41: Lateral speed v_y

between the assumed and the real tyre stiffness. This controller has been designed for a non-cornering tyre friction curve. The brake force is not following the driver's wish for low slips. The controller's integral part has too low gain.

Fig. 5.46 shows the slow increasing longitudinal deceleration a_x (black) as well as the decreasing lateral acceleration a_y . The estimation of the lateral velocity v_y in Fig. 5.45 is bad for small slips.

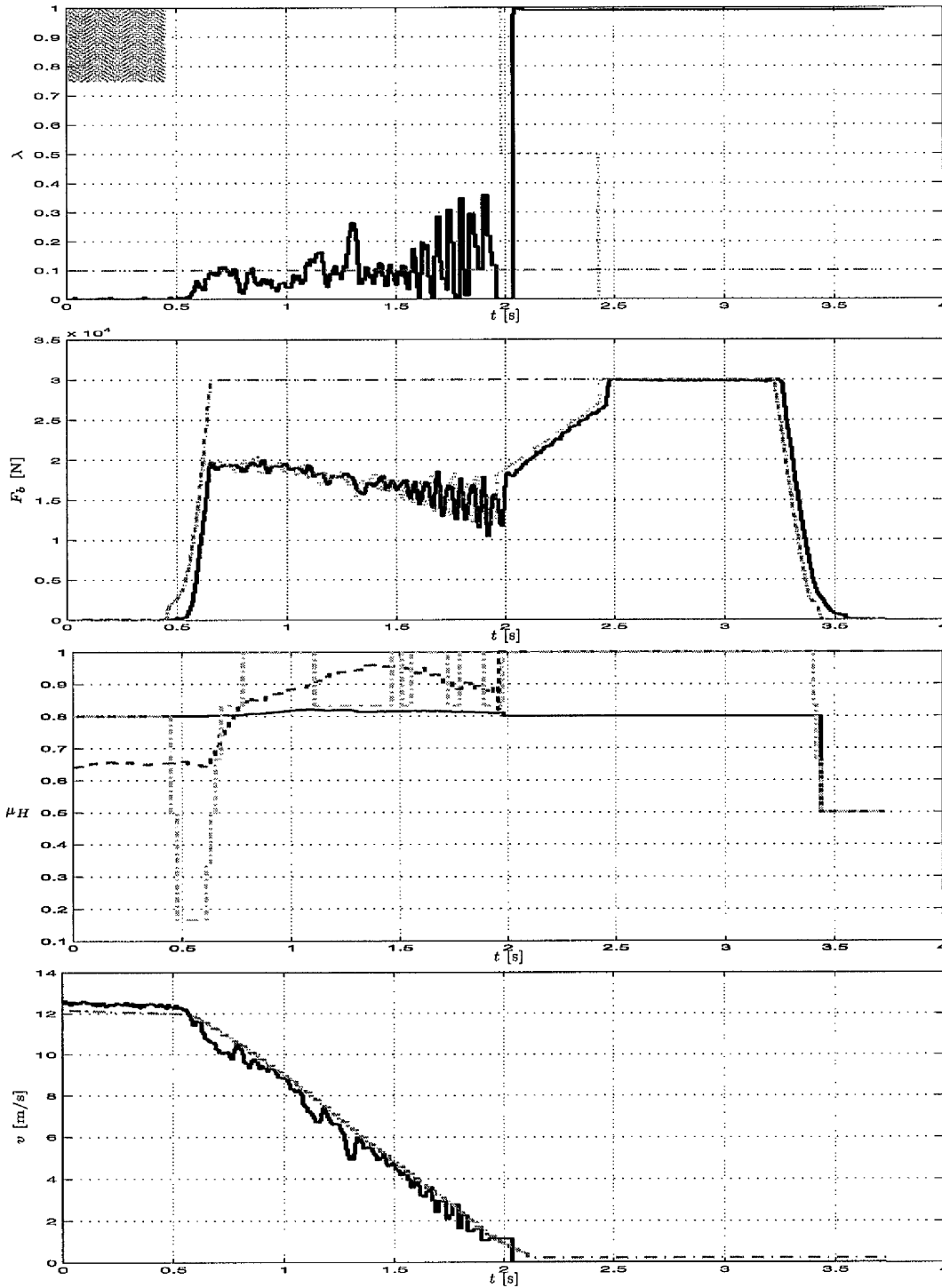


Figure 5.42: Test 10 results with nonlinear PI tyre slip controller braking in a turn with setpoint slip $\lambda_0 = 0.1$.

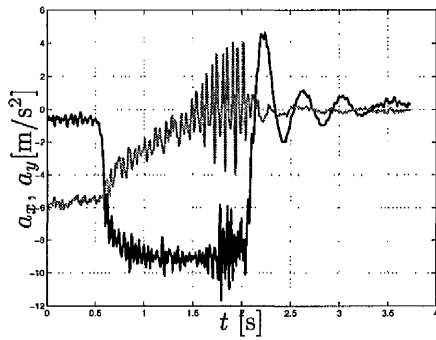


Figure 5.43: Accelerations a_x and a_y

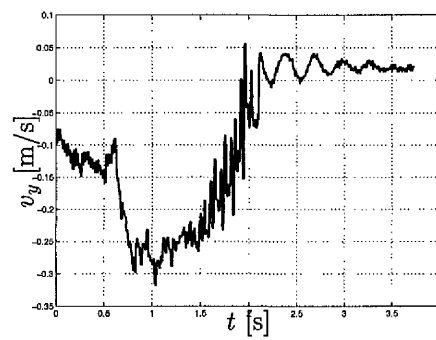


Figure 5.44: Lateral speed v_y

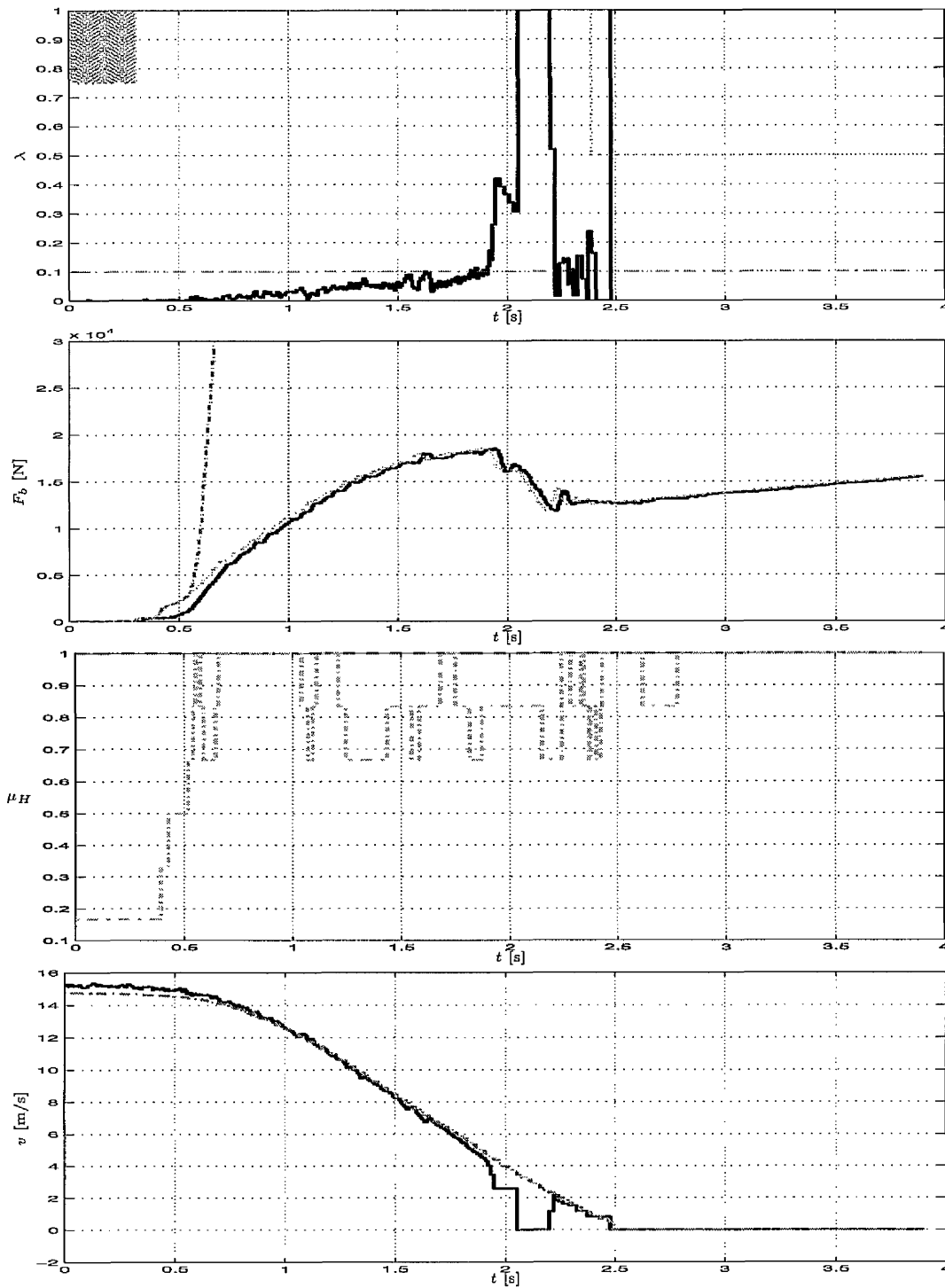


Figure 5.45: Test 10 results with LQRC tyre slip controller braking in a turn with setpoint slip $\lambda_0 = 0.1$.

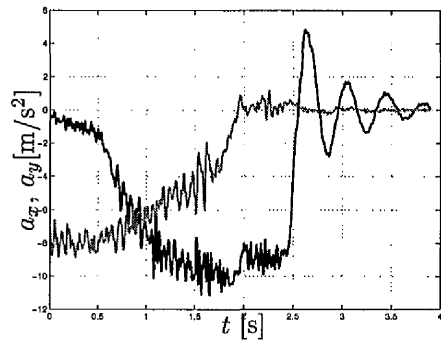


Figure 5.46: Accelerations a_x and a_y

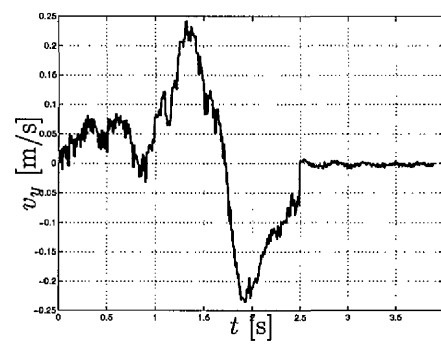


Figure 5.47: Lateral speed v_y

5.4.6 MMO verification tests

The described performance tests were mainly to show the individual results for each controller. In order to verify the MMO the following experiments show the benefits of the MMO in combination with the nonlinear adaptive controllers. The previous tests show that the MMO does not destroy the stability. Furthermore the transients are damped and the performance becomes better.

The following experiments have been done with winter tyres (ContiEcoContact CP 215/55R16) and a software version without the full functionality of controller mode changes. The controller modes are only on and off, the bumpless transfer mode is realised in off-mode.

Straight ahead braking on dry road

Fig. 5.48 shows a panic brake manoeuvre of the vehicle on a dry road. The setpoint slip is $\lambda_0 = 0.1$. The slip converges very fast to the setpoint. No overshoot of the slip can be observed. The clamping force follows the driver's brake demand sufficiently until the setpoint is reached. The initial estimate $\hat{\mu}_H$ of the adaptive controller is approximately 0.7. The estimate of the MMO is 0.8. No resetting of the controller occurs. This is quite reasonable because the slip error is small. Switching is only necessary when the slip error is large and the controller resetting helps to reduce slip transients. The multiple model observer converges to a friction value of $\mu_H = 0.8$. The problem of estimating the friction coefficient at the beginning is introduced by the pitching of the vehicle that has not been considered in the MMO design. Please note that also in simulation no dynamic pitching model has been used (cf. App. A.8). The Kalman filter reference speed estimation differs from the measured speed. For that reason the slip is higher than displayed.

The bumpless transfer can be seen in the clamping force plot at $3.75 \leq t \leq 4.5$ s. Fig. 5.49 shows a large fast increasing longitudinal deceleration measurement of approximately -10m/s^{-2} and a very small lateral acceleration measurement. The estimated lateral velocity is small (cf. Fig. 5.50).

Straight ahead braking on snow with and without MMO

Fig. 5.51 shows a straight brake manoeuvre without MMO on a road covered with 3cm fresh snow. The same manoeuvre with MMO parameter resetting will be shown in Fig. 5.54.

The setpoint slip is $\lambda_0 = 0.07$ which is in the unstable area of the slip curve. Without resetting the slip has a long transient of about one second. The relatively low maximum peaking of slip is due to the initial condition of the adaptation (integral part is 0.78 at the beginning). All three estimation methods estimate a friction value of approximately 0.4 whereby the Kalman filter as well as the integrator are slower than the MMO. Please note that no estimation is possible without braking.

The acceleration measurement increases quickly to a value of approximately -4m/s^{-2} in Fig. 5.52.

Allowing the resetting of the integral part of the adaptive controller the performance becomes significantly better (cf Fig. 5.54). The slip transient at the beginning takes only half a second though the integrator initial value of 1.0 is even worse. The clamping force has a strong undershoot after the switch at $t = 1.2\text{s}$. The reset can be seen in the third plot (black line). The Kalman filter estimates still slowly. Only one reset is to be observed. Other unnecessary switches cannot be seen. The slip is controlled at the setpoint for the rest of the manoeuvre.

The acceleration measurement in Fig. 5.55 is smaller than in Fig. 5.46 due to changed environmental conditions. Also a higher clamping force in Fig. 5.45 than in Fig. 5.54 results in smaller acceleration. Thus the surface must have been more slippery.

Figure 5.57 shows a brake manoeuvre on snow ($\mu_H \approx 0.5$) of the LQRC controller. No transient can be observed. The slip converges without any overshoot to the desired slip. Because of a slow increasing slip the controller is not optimal. The same behaviour has been already shown for braking on dry asphalt and icy road.

The relatively slowly increasing deceleration in Fig. 5.58 verifies the lower braking performance.

Straight ahead braking on ice with and without MMO

Figures 5.60 and 5.63 show a braking manoeuvre with Sontag's wheel slip controller on a very slippery icy road having a friction coefficient $\mu_H \approx 0.1$. A very large slip transient can be seen without resetting. Note that the re-acceleration of the wheel after a standstill is very low on ice.

Fig. 5.60 shows the manoeuvre without allowing the MMO to reset the adaptive controller. The slip transient takes approximately one second. A standstill of the wheel can be seen. Please note that though the clamping force is almost zero the wheel is accelerating very slowly. The controller does not control the slip exactly at the desired value. This is probably due to the very slippery road and small disturbances

acting on the wheel. The Kalman filter and the integral controller part converge slowly whereby the MMO estimates $\mu_H = 0.2$. Please note that the reference speed estimation is somewhat wrong. The wheel speed cannot be larger than the vehicle speed (cp. $t = 2\text{s}$). The speed estimation is mainly based on the acceleration measurement that is very low for small friction and in the range of noise.

Fig. 5.61 shows the very small longitudinal and lateral acceleration. Since the measurements are very noisy the speed estimation (cf. Fig. 5.60 and Fig. 5.62) is difficult.

Fig. 5.63 shows the same manoeuvre but allowing the MMO to reset the adaptive controller. The wheel is prevented from being locked. A small slip transient takes only a quarter of a second. After the switch the slip is controlled at the setpoint. The deviation in the slip plot is due to a slightly wrong reference speed estimation. Only one reset can be observed at the beginning when the slip error takes a value larger than the threshold. All three estimation methods estimate a frictional coefficient of $\mu_H \approx 0.2$. Please note that the friction estimate in Fig. 5.60 was only 0.1. The environmental conditions were not exactly the same. Nevertheless the improvement of the performance has been shown.

Fig. 5.64 shows the smooth but quickly increasing longitudinal acceleration. Since the acceleration measurement is noiseless the vertical force estimation is smooth and the control signal is smooth. The result is a smooth slip. The nearly constant measurement of longitudinal acceleration with an increasing slip also verifies the wrong reference speed estimate. Because of a small noise level in the lateral acceleration measurement the Kalman filter estimates a small lateral velocity. The MMO-estimation is fast but rough. Only when the slip is very low the estimation is wrong.

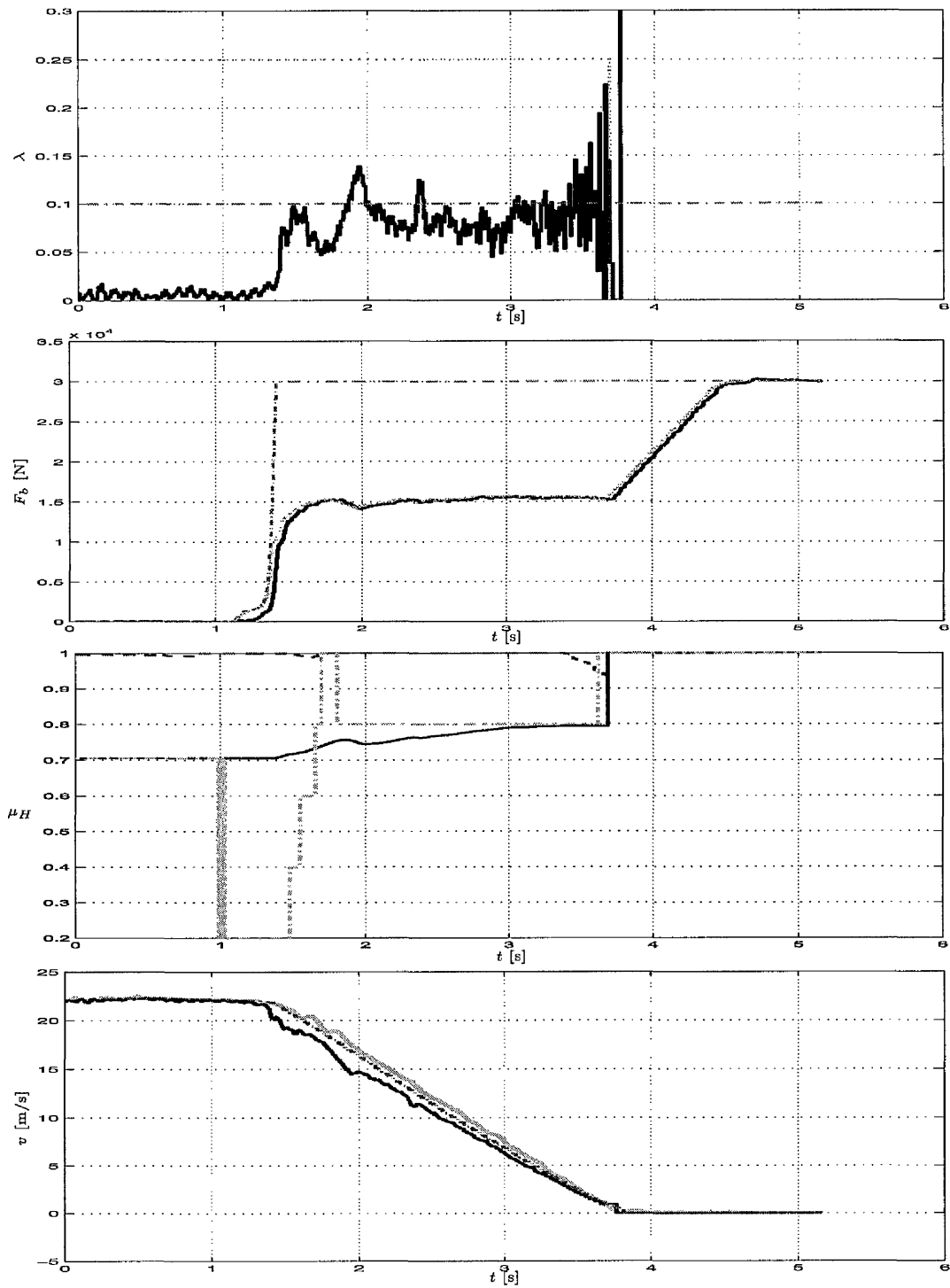


Figure 5.48: "Sontag" tyre slip controller with MMO braking on a dry road.

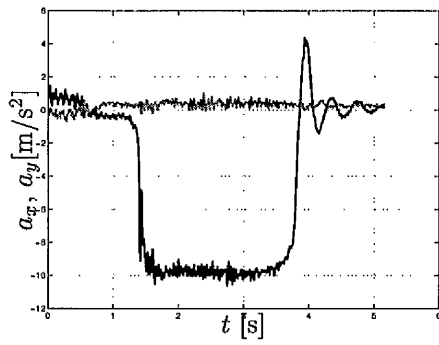


Figure 5.49: Accelerations a_x and a_y

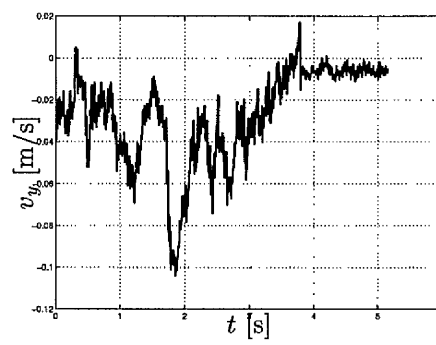


Figure 5.50: Lateral speed v_y

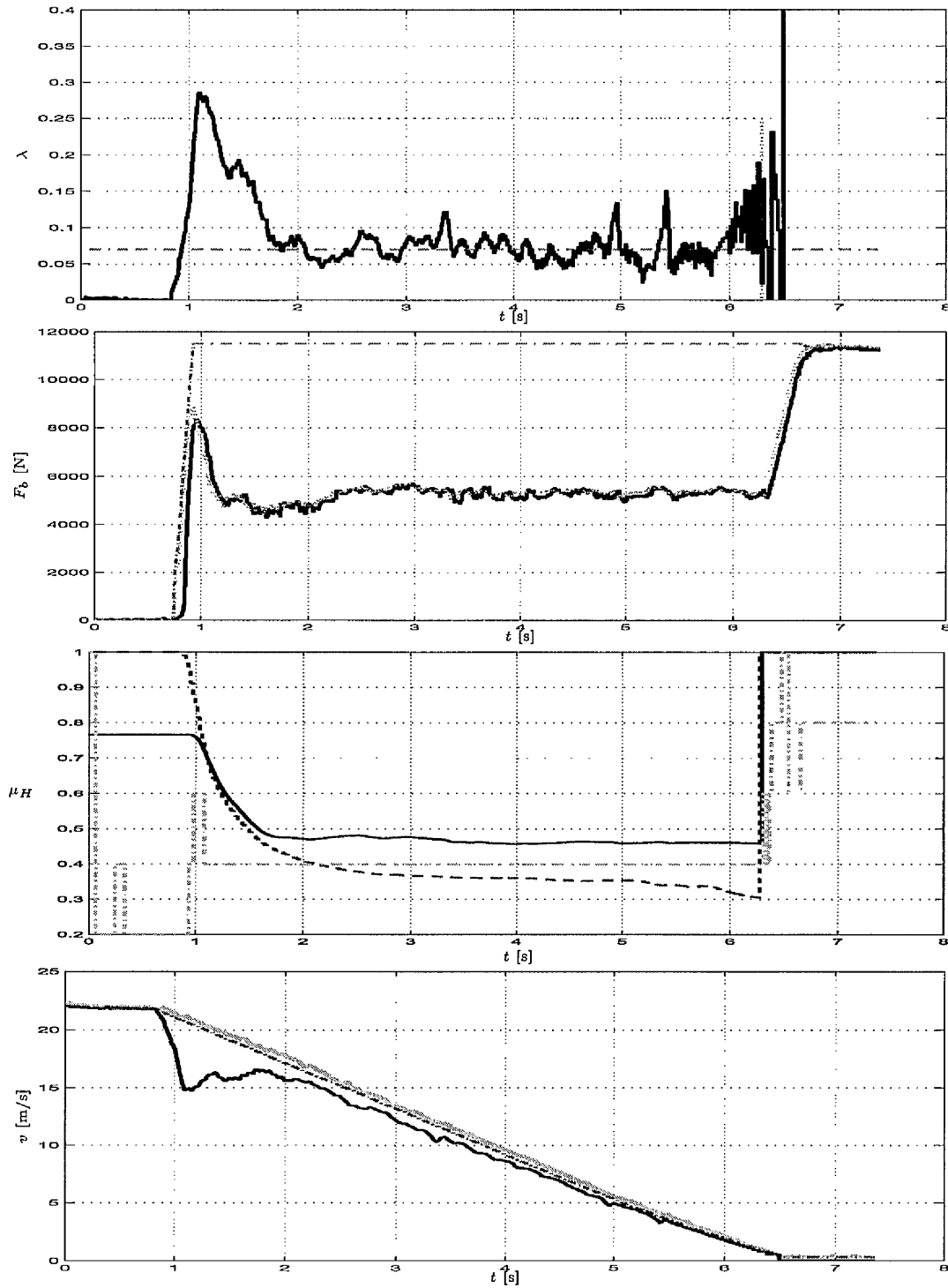


Figure 5.51: Nonlinear PI tyre slip controller without MMO braking on snow.

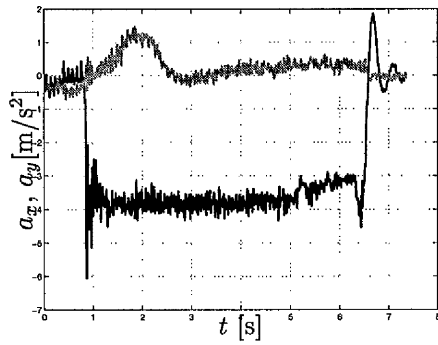


Figure 5.52: Accelerations a_x and a_y

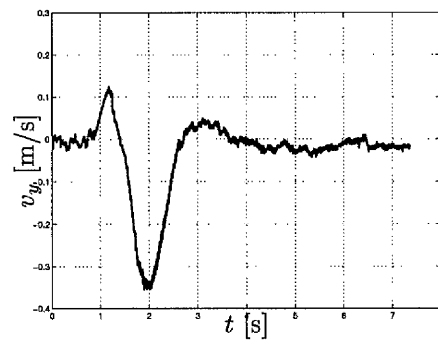


Figure 5.53: Lateral speed v_y

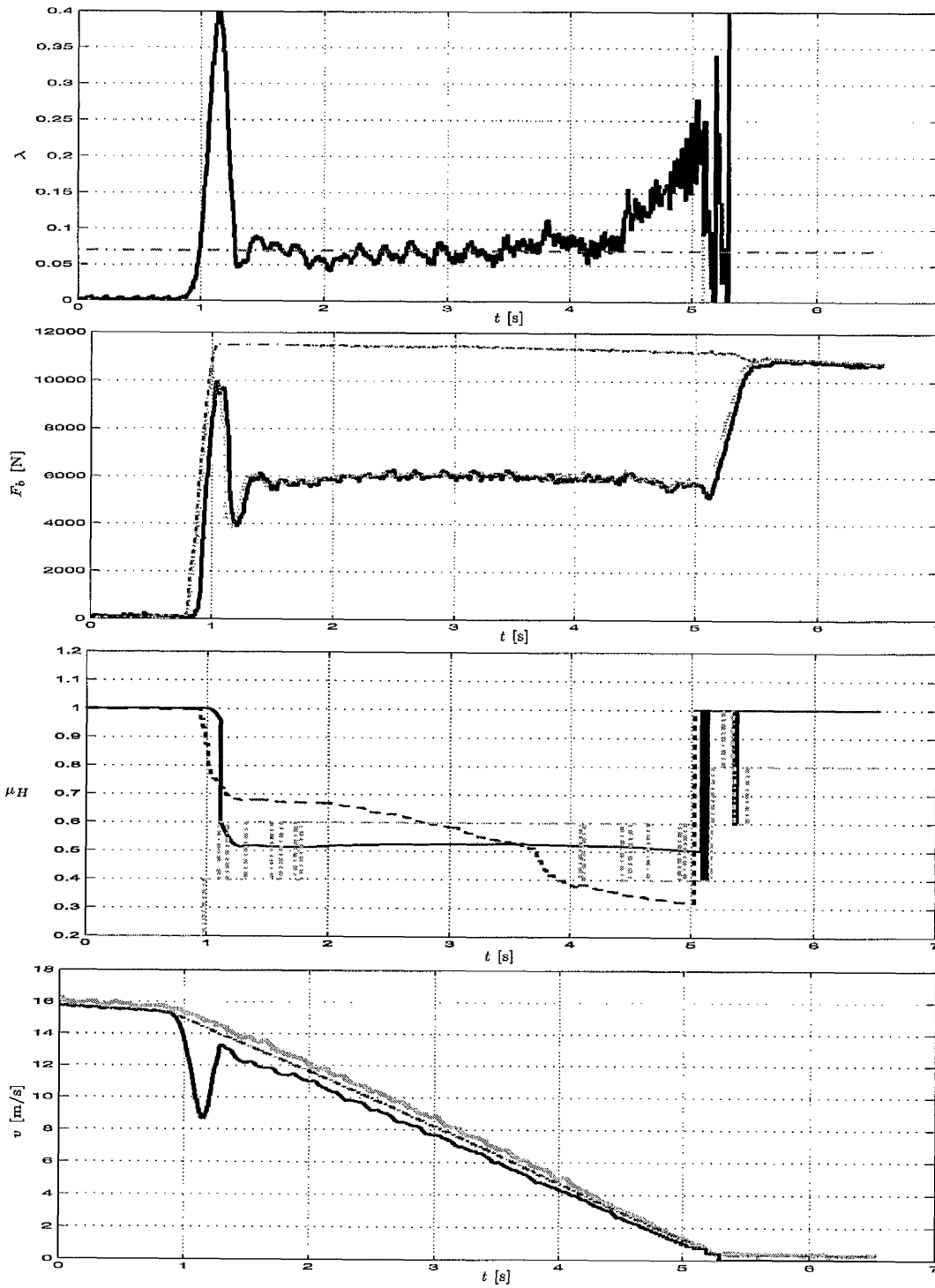


Figure 5.54: Nonlinear PI tyre slip controller with MMO braking on snow.

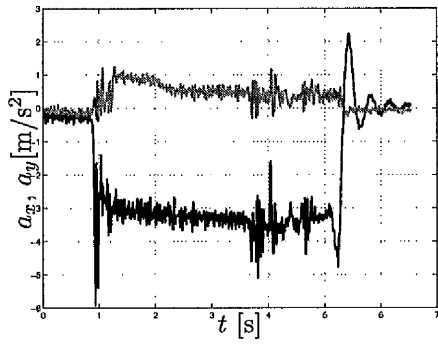


Figure 5.55: Accelerations a_x and a_y

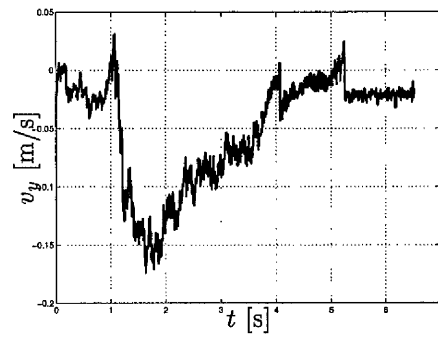


Figure 5.56: Lateral speed v_y

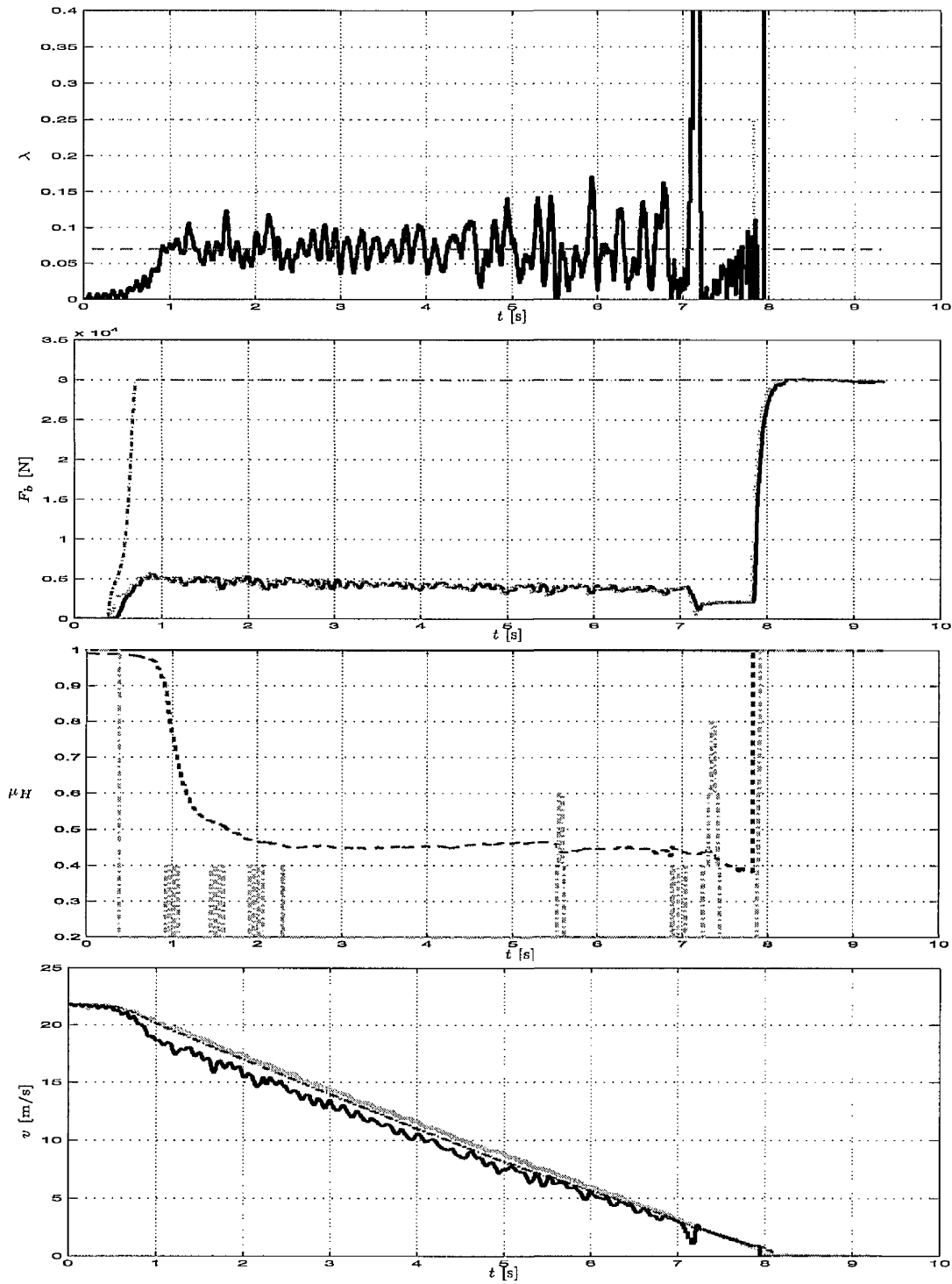


Figure 5.57: LQRC tyre slip controller without MMO braking on snow.

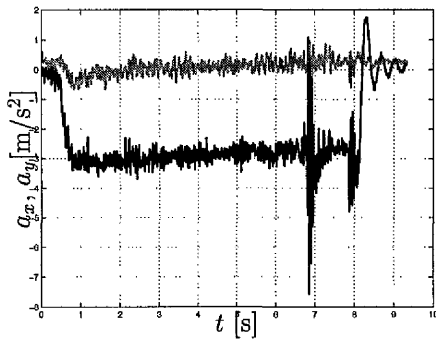


Figure 5.58: Accelerations a_x and a_y

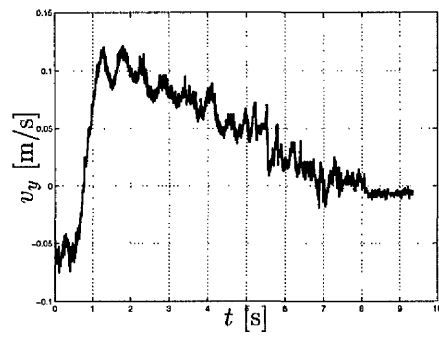


Figure 5.59: Lateral speed v_y

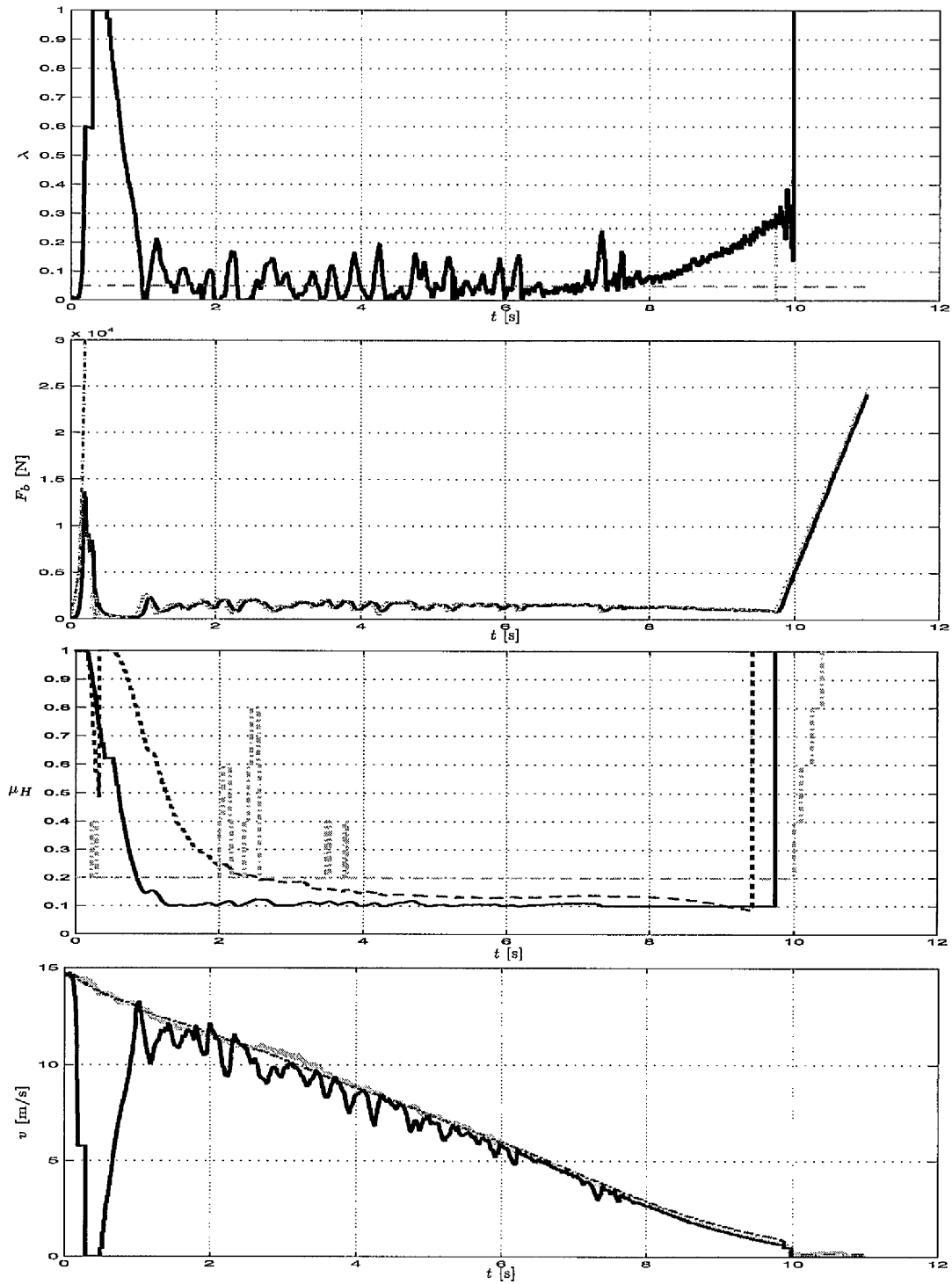


Figure 5.60: "Sontag" tyre slip controller without MMO braking on ice.

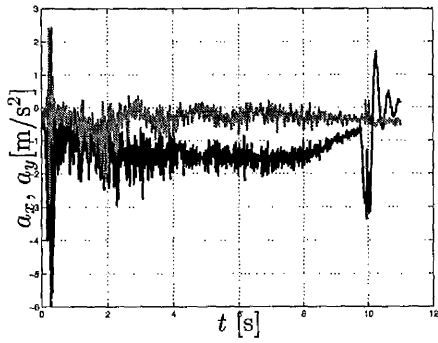


Figure 5.61: Accelerations a_x and a_y

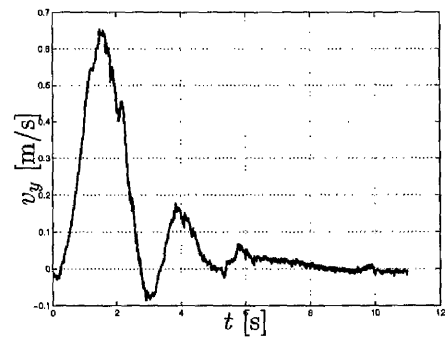


Figure 5.62: Lateral speed v_y

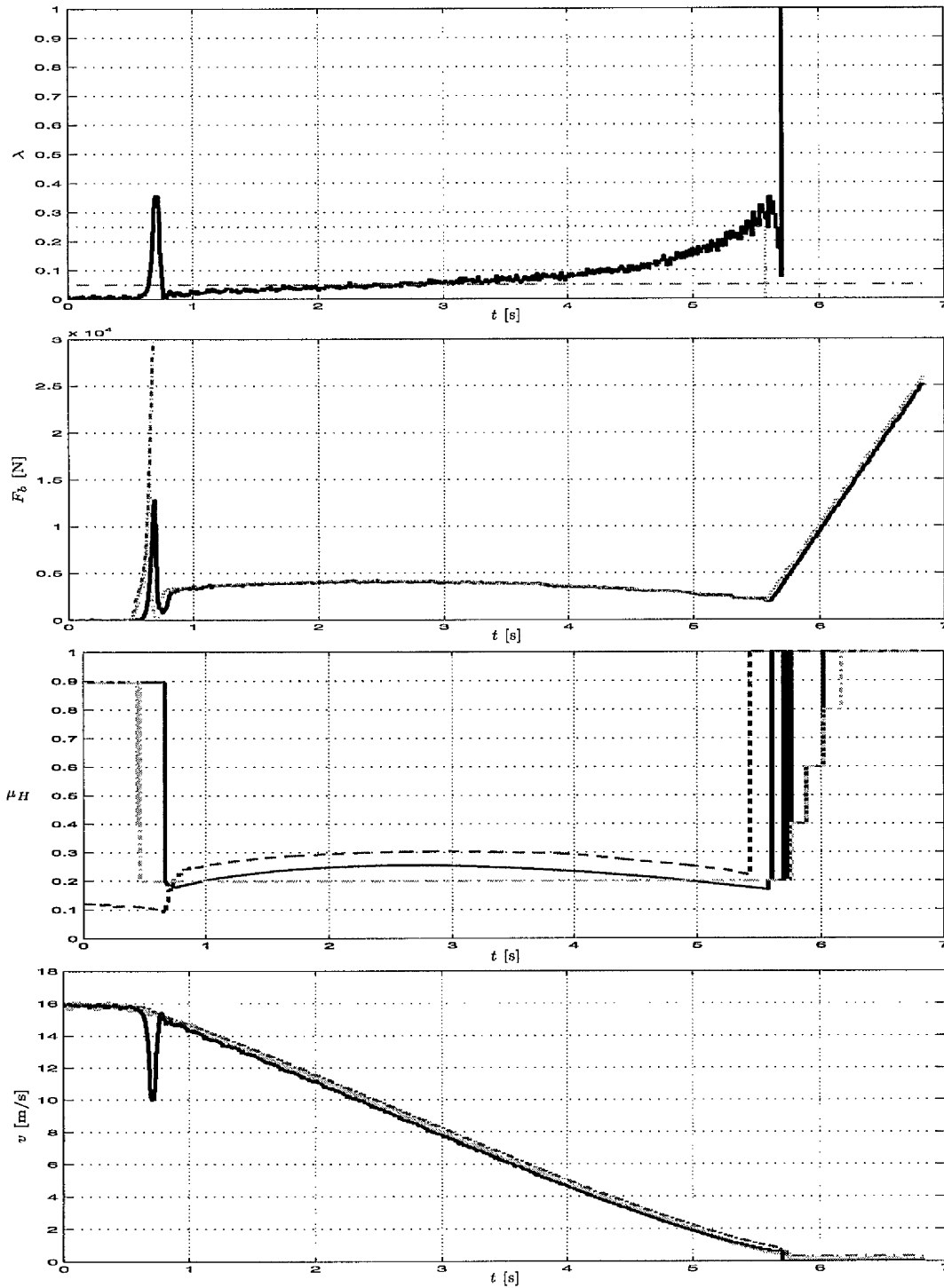


Figure 5.63: "Sontag" tyre slip controller with MMO braking on ice.

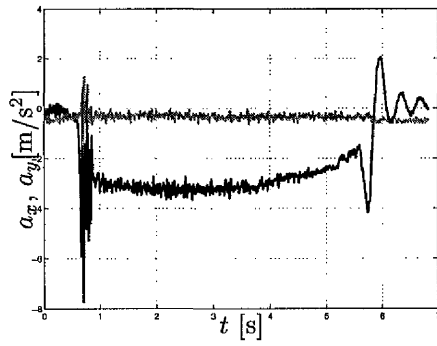


Figure 5.64: Accelerations a_x and a_y

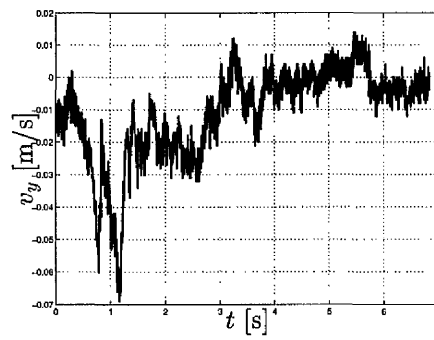


Figure 5.65: Lateral speed v_y

5.4.7 Discussion of results

The experiments carried out with the developed controllers have been shown in the preceding sections. A subset of the tests described in Table 5.1 has been taken to show the benefits and the performance of the model based approaches. Not all the tests described in the table have been done because of a limited time for vehicle tests and limited test facilities. Nevertheless the controllers have been evaluated against each other and against the production car ABS. Since there is additional demand on optimising the control performance some ideas for the improvement will be discussed.

All controllers (Sontag, nonlinear PI, LQRC, SSP) stabilise the system with each controller having a different performance. The nonlinear controllers have better performance than the linear ones. In the following each individual controller will be discussed:

- **“Sontag’s” wheel slip controller** The “Sontag’s” wheel slip controller is based on the application of Sontag’s formula to the wheel slip control problem. The controller design is based on an adaptive control Lyapunov function. Thus the controller adapts to different environments, in particular to different tyre friction coefficients. After having converged to the environmental condition the control performance is very good. The wheel slip is controlled correctly with a short rise time. The controller is robust against noise and time delays in the system. When the environment changes the controller needs some adaptation time and transients in the wheel slip can be seen. The adaptation time constant has been chosen relatively high to achieve robustness. The transient behaviour can be significantly improved by resetting the adaptive controller with an estimate given by a fast multiple model observer that estimates discrete values of the tyre friction. For the resetting stability conditions can be shown. The adaptive controller is reset only if the stability is preserved and the transient behaviour is improved.
- **nonlinear adaptive PI wheel slip controller** The nonlinear adaptive PI controller is also based on a similar adaptive control Lyapunov function. The controller structure is similar to the “Sontag’s” controller whereby the “Sontag’s” controller uses more information about the tyre friction behaviour. The nonlinear PI controller is based on domination of the unstable tyre slip dynamics while the “Sontag’s” controller uses full knowledge of the nonlinear tyre frictional behaviour. The control output of the proportional part of the “Sontag’s” controller (solid grey) and the nonlinear PI controller (solid black) versus the control error

$\tilde{\lambda}$ is displayed in Fig. 5.66. Also the nonlinearity $\tilde{\varphi}$ (grey dashed) as well as the inverted nonlinearity $-\tilde{\varphi}$ (as it would be used in a cancellation controller) are displayed. The control output of both (“Sontag’s” and nonlinear PI controller)

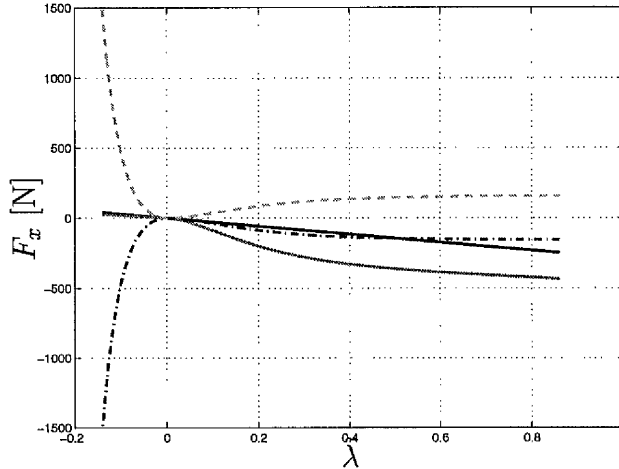


Figure 5.66: Nonlinearity and control

is quite similar in the stable part of the tyre friction curve. The control action of the “Sontag’s” controller is larger in the unstable part of the nonlinearity. Due to that the “Sontag’s” controller behaves slightly more robustly.

Also the nonlinear PI controller is reset by the external tyre friction estimate given by the multiple model observer with performance being improved by the resetting.

- **constrained LQ (LQRC) wheel slip controller** The LQRC controller is based on a realtime implementation of sub-optimal constrained LQ controllers. The idea is the scheduling of linear controllers. The LQRC wheel slip controller is somewhat slow but prevents the wheel from being locked. Nevertheless the performance is not sufficient for a real ABS application because the rise time of the controller is not high enough. The clamping force needs to follow directly the drivers demand until the wheel tends to lock. Potentially, the performance can be improved by further tuning of the controller or by applying the resetting strategy of the MMO and the nonlinear controllers to the LQRC approach. The integral part of the controller could be sped up in that way.
- **simultaneously stabilising (SSP) wheel slip controller** The SSP controller is a simple linear controller that stabilises the tyre slip dynamics. The nonlinear

wheel dynamics have been linearised for a number of different wheel slips as well as for different road surfaces. One single controller has been found that stabilises all linearised plants. But note that time invariance still can lead to instability of the system. This very simple controller control the system. Unfortunately the performance is different for different environmental conditions. On dry road the SSP controller is very slow in raising the brake force. This cannot be accepted for ABS control. Since the SSP controller design did not take the actuator dynamics and the time delay of 14ms into account the performance may be improved by considering this.

- **production car ABS** The conventional production car ABS is not a model based approach but a combination of wheel slip and wheel acceleration control. The control strategy consists mainly of a sequence of mode changes of the control signal. This is due to the solenoid-valve actuators in conventional hydraulic ABS. For that reason the conventional ABS has a cyclic overshoot of the slip. The slip value is not controlled at a specified value. Furthermore a limit cycle around the optimal slip value can be seen. Nevertheless the conventional ABS is very robust. Please note that several years of manpower were spent to develop such a system.

The best test results have been achieved by using the “Sontag” tyre slip controller in combination with the multiple model observer (MMO) and the resetting of the integrator in the case of fast changing road condition. The adaptation to new environmental conditions is very fast although the fast adaptation is not achieved by a high adaptation gain. Good results that are similar to that of the “Sontag” controller have been achieved by the nonlinear PI controller also in combination with the MMO. This is quite reasonable because the controller structure of both controllers is similar. Both controllers are nonlinear PI-type controllers whereby the “Sontag” controller fulfills optimality criteria and uses more information about the nonlinearity of the system.

The performance of the linear controllers (LQRC and SSP) does not fulfill the specification requirements for an ABS. Since the rise time is not sufficient the braking distance is longer which is unacceptable in practice. Nevertheless, both controllers prevent the tyre from being locked and stabilise the system.

The following detrimental effects on the control performance have been identified.

- The control performance depends very much on the accuracy of the Kalman filter speed estimation. No pitching and rolling have been taken into account. A small mis-estimation of the reference speed results in large slip errors. Since the slope

of the tyre curve is very high for low slips the effect of miss-estimation of the reference speed results in large excursion of the tyre slip and thus the frictional force.

Reasonably, the extended Kalman filter is a major candidate for improvements even though the Kalman filter is not a focus of the thesis. If it is possible to improve the Kalman filter the control performance of the slip controllers will be improved.

- The estimated distribution of vertical forces depends directly on the measured acceleration a_x without considering dynamics (cf. Appendix A.8). Since the measurement of a_x is very noisy the estimated vertical force is noisy as well and gives feedback to the controller. This can introduce parasitic oscillations in the controller that can be avoided if a dynamic pitching model is introduced. Another simpler option is to filter the acceleration measurements before applying the force distribution to the controller.

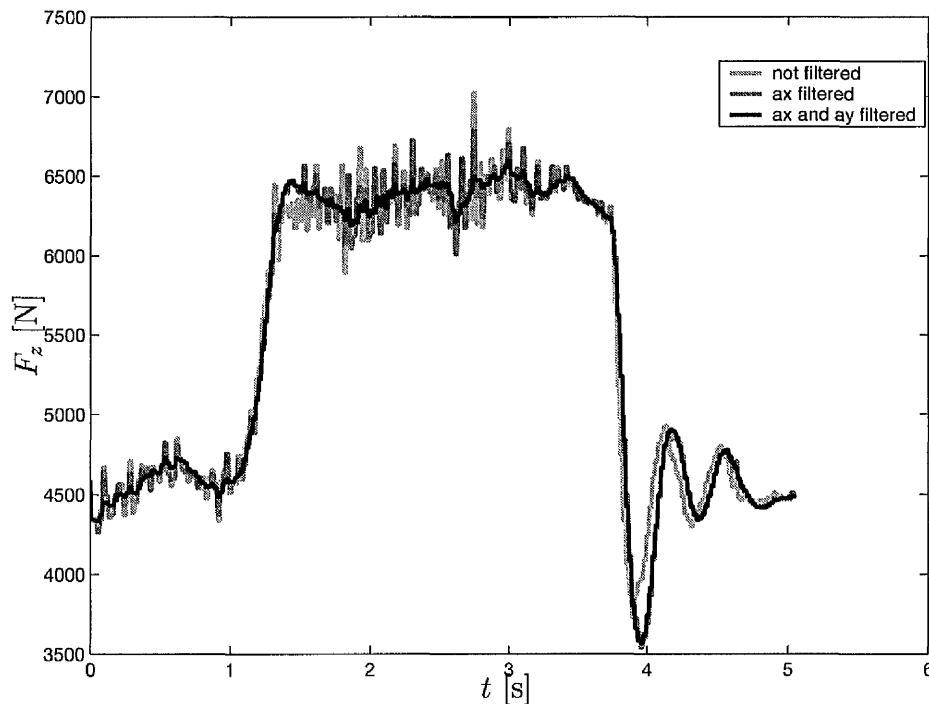


Figure 5.67: Filtered vertical force of one wheel

Figure 5.67 shows the vertical force for one wheel when the acceleration measurements are filtered and are not. Thus the vertical force gets smoother when filters for both accelerations a_x and a_y are introduced.

- Since tests have been made with two different tyre brands, winter (ContiEcoContact CP 215/55R16) and summer (ContiEcoContact CP 215/55R16), the robustness of the controllers has been tested. The controllers have been designed for winter (ContiEcoContact CP 215/55R16) tyres. The controller performance was found to be better for winter tyres than for summer tyres. This is due to the tyre stiffness. Summer tyres (ContiEcoContact CP 215/55R16) have a stiffness that is approximately double than of the winter tyres. Also, the maximum of the slip curve is reached at rather lower slip values, $\lambda_{u0} \approx 0.06$. Fig. 5.68 shows seven cubic spline estimates of the tyre friction curve. The grey curves show the approximation for seven measurements, while the black curve is an average over the experiments. Winter tyres have their maximum at $\lambda_{u0} \approx 0.1$. A cubic spline approximation is shown in Fig. 5.69.

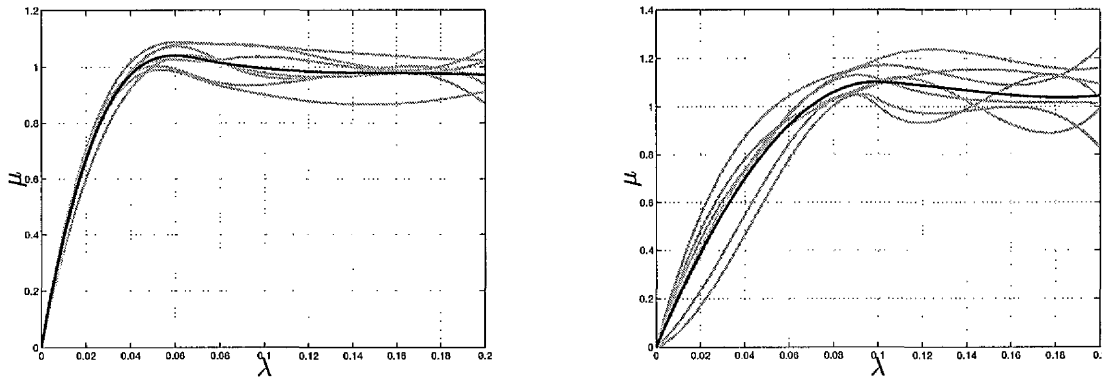


Figure 5.68: Tyre friction spline approximation (summer) Figure 5.69: Tyre friction spline approximation (winter)

In order to do the spline approximations the following has been considered. First, from the acceleration measurements, a_x and a_y , a vertical force distribution for the four wheels has been calculated. The rolling motion and air resistance have also been taken into account. In order to reduce the effect of noise, the acceleration measurement has been low pass filtered. Secondly, with the slip estimate, a cubic spline approximation has been found for the longitudinal force versus slip. The spline approximation has been heuristically optimised to get similar results for different braking manoeuvres.

Note that these friction curves are not very accurate. Normally, tyre curves are measured under defined conditions on a test bed where the tyre slip is known exactly. Since the curves in Fig. 5.68 and Fig. 5.69 are results from real vehicle tests and the vehicle velocity is estimated by an extended Kalman filter, the slip

values are uncertain, but the spline approximation assumes correct slip values. Unfortunately, the estimation of the slip value around its maximum is very sensitive to small slip variations. Nevertheless, conclusions from the curves can be made.

In Fig. 5.70 the tyre friction curves for both summer and winter tyres are displayed. It can be seen that the summer tyres have a higher stiffness and a more pronounced maximum peak of the curve than the winter tyres. The winter tyres have lower stiffness and a less pronounced maximum. The negative slope right of the maximum is lower for winter tyres than for summer tyres. Please note that the displayed curves are approximations taken from a limited number of experiments. Furthermore, note that the controller design and the simulation

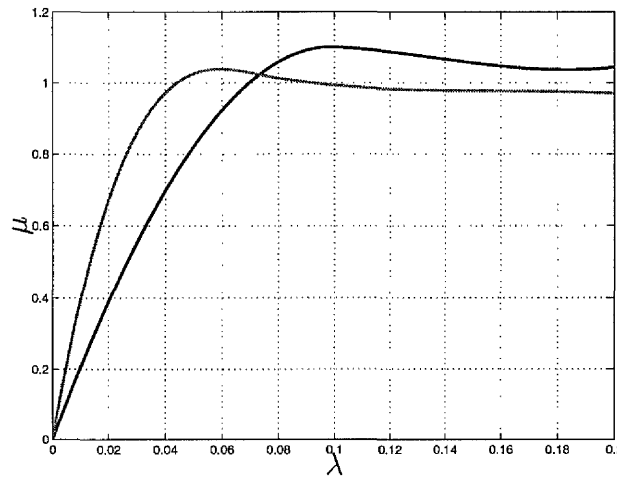


Figure 5.70: Tyre friction spline approximation (summer(grey)/winter(black) compared)

were made for different tyre friction curves. The tyre friction curves used in the controller design have a maximum friction value peak at $\lambda_{u0} \approx 0.14$ and a tyre stiffness that is between the spline approximations of summer and winter tyres. The considered curves had no decrease of the friction behind that maximum.

5.4.8 Conclusions

The car tests show the benefits of model based and hybrid control. A model based wheel control system is able to fulfill the requirements of the ABS specification. Namely, to prevent the tyre from being locked and to maximise the frictional force. The slip can be controlled at a specified value which is not possible with conventional production

car ABS. Further work is needed to optimise the controllers. Please note that neither of the presented approaches is an explicit heterogeneous controller since the order of the controllers and of the plant does not change.

6 Conclusions

Automobiles are complex systems for which a multitude of individual control systems, for instance ABS and ESP, are at present implemented independently from each other. Each of these controllers has its own electronic device. By this approach, it is possible to achieve a high standard of functionality and safety. But the material and development costs of these systems are immense. With regard to an extension of the performance such a structure proves not to be useful anymore. For the development of new interacting controllers new technologies are required. In fact, a systematic modular design of the overall system is useful since redundancies can be avoided. Supplementary sensors and a common state estimation lead to a new interface for ESP and ABS. The interface for ABS is no longer the braking force but the desired slip, adjusted by ESP.

In the future, more sensors will be provided in a vehicle. Thus, it is possible to design systems based on physical models. By means of these models, specific and problem-adapted control design methods can be applied. In this particular project, a model-based ABS control system has been developed. Because of safety-relevant functions the ABS controllers have to be robust with respect to disturbances. On the other hand, models are always a simplification of the physical reality and therefore inaccurate. Thus, controllers also have to be robust with respect to modelling errors. Because of the fact that disturbances should be counteracted quickly, the application of hybrid control approaches is useful. Road conditions, as an example, can change very quickly. The ABS control has to react immediately to these changes.

Since the field of hybrid control is very large and diverse only a small subset of related technologies has been discussed. The multiple model ideas in the literature have been combined with recent developments in the field of Lyapunov function based adaptive nonlinear control. A hybrid multiple model observer consists of several parallel state observers each parameterised with a discrete value of an uncertain parameter. Via a cost index for each of the models (observer) it is possible to obtain a discrete parameter estimate. This estimate can be used for resetting the continuous parameter estimation

of the nonlinear adaptive controller. Special care is taken to preserve stability in the process of switching.

A clearly specified practically relevant automotive control problem has been chosen and was solved by means of hybrid control. It has been shown that the controller performance can be significantly improved by hybrid control while the stability is maintained. In the special case of anti-lock-brake systems the transients due to fast changing road conditions can be damped by resetting a tyre friction estimate. Thus, the controller and the adaptation gain can be lowered without losing performance. This is important in order to counteract uncertainty (modelling and noise) in the system.

The hybrid ABS controller presented in this thesis has not only been tested in simulation but also in real life. The application of new theories in industry has to entail a shortening and a simplification of the product development and has to improve the quality of the product. For these reasons, the usability and the benefit of new algorithms have to be tested and verified on the product under real conditions. Also, a testing of the controllers under real conditions is very important because in simulation reality is highly simplified. The road, for instance, with its rough and uneven surface is modelled only insufficiently by steps in the friction coefficient and by adding white noise. Also, a discrete time implementation, the behaviour of the TTP-bus system, and real actuators, all have a strong influence on the overall control behaviour and are not included in the model. Nevertheless, simulations are necessary in order to estimate the control systems behaviour and to initialize possible design-parameters.

The contribution of this thesis can be summarised as follows:

- The multiple model ideas in the literature have been combined with recent developments in the field of Lyapunov function based nonlinear control. The convergence rate of a nonlinear adaptive backstepping control law can be sped up by use of multiple models or multiple observers to reset the parameter estimate. Such resetting is of particular importance in any applications where the environment or system parameters change rapidly or even instantaneously.
- A set of sufficient closed loop stability conditions have been formalised for resetting tuning function based nonlinear adaptive controllers. It is not only shown that stability is preserved, but also that the local convergence-rate is increased.
- A fast multiple model observer based parameter estimation algorithm combined with the stability condition guarantees a negative jump of the Lyapunov function and, consequently, an increased performance. Even under transient conditions

a parameter estimate can be obtained by the observer. The multiple model observer cannot only be used for parameter estimation but also for estimation of structural changes in the system. The parameter estimation is only one specific application.

- The development of theoretical results has been driven by the practical problems which arose from the hybrid nature of the tyre-road dynamics. The four wheel slip controllers together with the parameter resetting have been implemented and tested in a real Mercedes E-class car equipped with a brake-by-wire system and electromechanical brake actuators. Preliminary simulations with a simulation environment that has the same interfaces as the real vehicle have been done with a nonlinear simulator. The controllers have been compared to each other and evaluated against a production car ABS.
- Two adaptive nonlinear wheel slip controllers have been developed. The wheel slip controllers serve as low level controllers in a novel model based ABS system. It has been shown that a simple linear PI controller can be found that stabilises the wheel slip system. The simultaneously stabilising controller does not have sufficient performance to fulfill the requirements of the ABS control system. Also a sub-optimal constrained LQ-controller has been implemented and tested.
- The resetting technique has been applied to friction estimation in wheel slip control. The transient performance is improved in the case of fast-changing road conditions by means of resetting the estimate of the adaptive tyre slip controller.
- The full-scale experimental trial has been carried out on the basis of the evaluation criteria for conventional ABS systems and the ISO-norms for testing ABS systems. Furthermore, the major experimental infrastructure was used to evaluate the developed controller under real life conditions that cannot be established in any simulation environment. The real vehicle tests show the benefits of the algorithms. The developed control algorithms gives very good results compared to conventional controllers by a reduced development time.

The future theoretical work should be continuously driven by the practical application. The following issues can be of major interest for the future:

- Other fast converging observers can be developed and implemented in the framework of the multiple models/observers and the parameter resetting. By doing

this the quality of the observer can be enhanced specifically for the respective problem.

- Since the proposed resetting strategy is based on the control Lyapunov function approach for nonlinear systems, resetting of non-CLF based adaptive controllers is of interest.
- The stability investigation is based on the uncertainty of the estimated parameter. A further reduction of the uncertainty in the Lyapunov approach can provide an improvement of the transient behaviour.
- Large transients of the LQRC wheel slip controller could be damped out by resetting the integrator of the controller with a fast estimate. Then, the MMO resetting strategies need to be adapted to the LQRC controller representation.
- Since most drive dynamic control systems are safety devices they need to be robust against failures and damage of the system. The safety of the system needs to be designed in a proper way. Hybrid control could be used here as well.
- The quickly estimated tyre friction coefficient can be applied to other related problems like ESP. This can lead to a better performance.
- The influences of unmodelled dynamics like suspension and pitch dynamics in wheel slip control should be analysed since there is still space for improvements.
- Since the reference speed estimation of the Kalman filter sometimes is not reliable and the slip calculation depends on the reference speed an improvement of the Kalman filter would be beneficial.

Within the thesis it has been shown that hybrid control technologies can improve the control performance of a real life application. Furthermore, by means of model based control the automotive ABS control problem can be solved whereby the design process is reduced. Thus, the practical relevance of model based hybrid control has been proven.

Bibliography

- [1] ISO6597 Road vehicles – Hydraulic braking systems–Measurement of braking performance, 1991.
- [2] SAE J2246 Antilock Brake System Review, 1992.
- [3] SAE J46 Wheel-Slip Brake-Control System Road test code, 1993 (1973).
- [4] *Bremsanlagen für Kraftfahrzeuge*. Robert Bosch GmbH, Stuttgart, 1994.
- [5] ISO11835 Road vehicles – Motor vehicles with antilock braking system – Measurement of braking performance, 1995.
- [6] ISO7975 Passenger cars – Braking in a turn – Open-loop test procedure, 1996.
- [7] *Special Issue on Hybrid Dynamical Systems*, volume 43. IEEE Transactions on Automatic Control, 1998.
- [8] ISO3888-1 Passenger cars – Test track for a severe lane-change manoeuvre, 1999.
- [9] *Special Issue on Hybrid Dynamical Systems*, volume 88. Proceedings of the IEEE, 2000.
- [10] Jürgen Ackermann. *Robuste Regelung*. Springer, 1993.
- [11] R. Alur, C. Courcoubetis, T.A. Henzinger, and P.-H. Ho. The algorithmic approach to the specification and verification of hybrid systems. In Robert L. Grossmann, Anil Nerode, Anders P. Ravn, and Hans Rischel, editors, *Hybrid systems Lecture Notes in Computer Science*. Springer-Verlag, 1993.
- [12] Dieter Ammon. *Modellbildung und Systementwicklung in der Fahrzeugdynamik*, volume 73 of *Leitfäden der angewandten Mathematik und Mechanik*. B. G. Teubner, Stuttgart, 1. edition, 1997.

-
- [13] Mats Andersson. *Object-Oriented Modeling and Simulation of Hybrid Systems*. PhD thesis, Department of Automatic Control Lund Institute of Technology, December 1994.
- [14] Anuradha M. Annaswamy, Fredrik P. Skantze, and Ai-Poh Loh. Adaptive control of continuous time systems with convex/concave parameterisation. *Automatica*, 34(1).
- [15] Murat Arcak and Petar Kokotović. Robust output-feedback design using a new class of nonlinear observers. In *Proceedings of the 39th IEEE Conference on Decision and Control, Sydney, Australia*, pages 752–755, 2000.
- [16] Karl J. Åström and Björn Wittenmark. *Computer-Controlled Systems*. Prentice-Hall, Inc., Englewood Cliffs, N.J., 2 edition, 1990.
- [17] Karl J. Åström and Björn Wittenmark. *Adaptive Control*. Addison Wesley, 2 edition, 1995.
- [18] P.I. Barton and C.C. Pantelides. Modelling of combined discrete/continuous processes. *Process System Engineering*, 40(6):966–979, 1994.
- [19] Sven Beiker and Manfred Mitschke. Verbesserungsmöglichkeiten des Fahrverhaltens von PKW durch zusammenwirkende Regelsysteme. *ATZ Automobiltechnische Zeitschrift*, 103:38–43, 2001.
- [20] Matthew C. Best and Timothy J. Gordon. Real time state estimation of vehicle handling dynamics using an adaptive Kalman filter. In *Proceedings of the 4th International Symposium on Advanced Vehicle Control*, pages 183–188, September 1998.
- [21] Michael S. Branicky. *Studies in Hybrid Systems: Modeling, Analysis, and Control*. PhD thesis, Massachusetts Institute of Technology, 1995.
- [22] Michael S. Branicky. Multiple Lyapunov functions and other analysis tools for switched and hybrid systems. *IEEE Transactions on Automatic Control*, 43(4), 1998.
- [23] Roger W. Brockett. Hybrid models for motion control systems. In Trentelmann and Willems, editors, *Essays on Control: Perspectives in the Theory and its Application*. Birkhäuser, 1993.

- [24] I. N. Bronstein, K. A. Semendjajew, G. Musiol, and H. Mⁿuhlig. *Taschenbuch der Mathematik*. Verlag Harri Deutsch, Frankfurt am Main, 1 edition, 1993.
- [25] Manfred Burckhardt. *Radschlupf-Regelsysteme*. Vogel Buchverlag, Würzburg, 1993.
- [26] Ch.G. Cassandras and S. Lafortune. *Introduction to discrete event systems*. Kluwer Academic Publishers, 1999.
- [27] G.W. Chang, J.P. Hespanha, A.S. Morse, M.S. Netto, and R. Ortega. Supervisory field-oriented control of induction motors with uncertain rotor resistance. submitted for publication, 2000.
- [28] Seongho Choi and Dong-Woo Cho. Control of wheel slip ratio using sliding mode controller with pulse width modulation. In *Proceedings of the 4th International Symposium on Advanced Vehicle Control*, pages 629–635, September 1998.
- [29] A. Daiß and U. Kiencke. Estimation of tyre slip during combined cornering and braking observer supported fuzzy estimation. In *13th Triennial World Congress*, pages 41–46, San Francisco, 1996.
- [30] John J. D’Azzo and Constantine H. Houpis. *Linear control system analysis and design*. McGaw-Hill, 1995.
- [31] Canudas de Wit, C., Noël, P., and B. Brogliato. Adaptive friction compensation in robot manipulators: low velocities. *The Int. J. Robot Research*, 10(3):189–199, 1991.
- [32] Canudas de Wit, Roberto Horowitz, and P. Tsiotras. Model-based observers for tyre/road contact friction prediction. In Nijmeier and T.I. Fossen, editors, *New Directions in Nonlinear Observer Design*, number 244 in Lecture Notes on Control and Information Science, pages 23–42. Springer-Verlag, 1999.
- [33] M. Doêgruel and Ü. Özgüner. Stability of hybrid systems. In *IEEE International Symposium on Intelligent Control*, pages 129–134, 1994.
- [34] Sergeji Drakunov. ABS control using optimum search via sliding mode. *IEEE Transactions on Control Systems Technology, Special Issue on Automotive Control*, 3(1):79–85, 1995.
- [35] Sergey Drakunov and Vadim Utkin. Sliding mode observers. tutorial. In *Proceedings of the 34th IEEE CDC, New Orleans*, pages 3376–3378, 1995.

- [36] S. W. Emeljanow. *Automatische Regelsysteme mit veränderlicher Struktur*. Oldenbourg Verlag, München, 1967.
- [37] M. Fajdiga and N. Janičijević. A hybrid driving and braking system with wheel slip control. In *24th FISITA Congress, Total Vehicle Dynamics*, pages 1–6, June 1992.
- [38] H. Fennel, G. Gutwein, A. Kohl, M. Latarnik, and G. Roll. Das modulare Regler- und Regelkonzept beim ESP von ITT Automotive. In *7. Aachener Kolloquium Fahrzeug und Motorentechnik*, pages 409–431, 1998.
- [39] A. F. Filippow. Differential equations with discontinuous righthand sides. volume 51. *Mathematicheskii Sbornik*, 1960.
- [40] A. F. Filippow. *Differential Equations with Discontinuous Righthand Sides*. Kluwer Academic Publishers, Dordrecht, Boston, London, 1988.
- [41] R. Freeman. Robust slip control for a single wheel. Research Report CCEC 95-0403, University of California, Santa Barbara, 1995.
- [42] Bernard Friedland. *Advanced Control System Design*. Prentice-Hall, Inc., Englewood Cliffs, N.J., 1996.
- [43] Takehiko Fujioka and Torahiko Yamanouchi. Estimation system for vehicle position by use of Kalman filter and disturbance observer. In *Proceedings of the 4th International Symposium on Advanced Vehicle Control*, pages 189–194, September 1998.
- [44] P.W. Glynn. A GSMP formalism for discrete event. *Proceedings of IEEE*, 77(1):14–23, 1989.
- [45] Fredrik Gustafsson. Monitoring tyre-road friction using the wheel slip. *IEEE Control Systems Technology Magazine*, 18(4):42–49, 1998.
- [46] Peter D. Hanlon and Peter S. Maybeck. Characterization of Kalman filter residuals in the presence of mismodeling. In *Proceedings of the IEEE CDC, Tampa, Florida*, 1998.
- [47] David Harel. Statecharts: A visual formalism for complex systems. *Science of Computer Programming*, 8:231–274, 1987.

-
- [48] I. Hartmann and Ch. Landgraf. *Grundlagen der linearen Regelungstechnik*. Technische Universität Berlin, 1994. Skriptreihe Regelungstechnik und Bildverarbeitung.
- [49] Sven Hedlund and Anders Rantzer. Optimal control of hybrid systems. In *Proceedings of IEEE Conference of Decision and Control*, December 1999.
- [50] J.P. Hespanha. *Logic-Based Switching Algorithms in Control*. Dissertation, Graduate School, Yale University, December 1998.
- [51] J. Hochermann-Frommer, S. R. Kulkarni, and P. Ramadge. Controller switching based on output prediction errors. *IEEE Transactions on Automatic Control*, 43(5):596–607, 1998.
- [52] J.E. Hopcroft and J.D. Ullman. *Introduction to Automata Theory, Languages, and Computation*. Addison-Wesley, 1979.
- [53] A. Isidori. *Nonlinear Control Systems*. Communication and Control Engineering Series. Springer-Verlag, Berlin, third edition, 1995.
- [54] Tor A. Johansen. Computation of Lyapunov functions for smooth nonlinear systems using convex optimization. 1999.
- [55] Tor A. Johansen, Jens Kalkkuhl, Idar Petersen, and Jens Lüdemann. Hybrid control strategies in ABS. In *Proceedings of the IEEE ACC*, 2001.
- [56] Tor A. Johansen and Idar Petersen. ABS with tyre slip control - an LQRC approach. 2001. Unpublished.
- [57] Tor A. Johansen, Idar Petersen, and Olav Supplhaug. On explicit suboptimal LQR with state and input constraints. In *Proceedings of the IEEE CDC*, 2000.
- [58] Mikael Johansson. *Piecewise Linear Control Systems*. PhD thesis, Department of Automatic Control, Lund Institute of Technology, 1999.
- [59] Mikael Johansson and Anders Rantzer. A stability analysis for nonlinear and hybrid systems. Technical report, Department of Automatic Control, Lund Institute of Technology, September 1996.
- [60] Cheng Jun. The study of ABS control system with different control methods. In *Proceedings of the 4th International Symposium on Advanced Vehicle Control*, pages 623–628, Nagoja, Japan, September 1998.

-
- [61] Jens Kalkkuhl, Dennis Giesa, and Jens Lüdemann. A nonlinear adaptive tyre slip controller. Tech. report, DaimlerChrysler Research and Technology, 1999.
- [62] Jens Kalkkuhl, Tor A. Johansen, and Jens Lüdemann. Improved transient performance of nonlinear adaptive backstepping using estimator resetting based on multiple models. *IEEE Transactions on Automatic Control*, 47(1):136–140, 2002.
- [63] Jens Kalkkuhl, Tor A. Johansen, and Jens Lüdemann. Nonlinear adaptive backstepping with estimator resetting using multiple observers. In *Nonlinear and Hybrid Control in Automotive Applications*. Springer-Verlag, 2002.
- [64] Jens Kalkkuhl, Tor A. Johansen, Jens Lüdemann, and Andreas Queda. Nonlinear adaptive backstepping with estimator resetting using multiple observers. In *Proceedings of the HSCC2001*, pages 319–332, Rome, Italy, 2001.
- [65] Taketoshi Kawabe, Masao Nakazawa, Ikuro Notsu, and Yoshito Watanabe. A sliding mode controller for wheel slip ratio control system. *Vehicle system dynamic*, (27):393–408, 1997.
- [66] Hassan K. Khalil. *Nonlinear Systems*. Macmillan Publishing Company, 1992.
- [67] U. Kiencke. Realtime estimation of adhesion characteristic between tyres and road. In *Proceedings of the IFAC World Congress*, 1993.
- [68] W. Kortüm and P. Lugner. *Systemdynamik und Regelung von Fahrzeugen*. Springer-Verlag, Berlin, 1994.
- [69] A. J. Krener and A. Isidori. Linearisation by output injection and nonlinear observers. *Systems and Control Letters*, 3:47–52, 1983.
- [70] Miroslav Krstić, I. Kanellakopoulos, and Petar Kokotović. *Nonlinear Adaptive Control Design*. John Wiley & Sons Inc., 1995.
- [71] Bengt Lennartsson, Michael Tittus, Bo Eghardt, and Stefan Petterson. Hybrid systems in process control. *IEEE Control Systems*, 16(5):45–56, 1996.
- [72] Daniel Liberzon and Stephen Morse. Benchmark problems in stability and design of switched systems. Technical report, Yale University, 1999.
- [73] Yong Liu. Switching observer design for uncertain nonlinear system. In *Proceedings of the 34th IEEE CDC, New Orleans*, pages 1756–1761, 1995.

- [74] Jens Lüdemann, Jens Kalkkuhl, and Tor Arne Johansen. Nonlinear adaptive slip control using sontag's formula. *IEEE Transactions on Automatic Control*, 2002. Unpublished.
- [75] Jens Lüdemann, Jens Kalkkuhl, Tor Arne Johansen, Idar Petersen, Kenneth J. Hunt, Tilmann Schmitt-Hartmann, Anders Rantzer, and Stefan Solyom. Model based wheel slip control - an experimental benchmark. *Control Eng. Practice*, 2002. Unpublished.
- [76] Jan Lunze. Ein Beispiel für den Entwurf schaltender Beobachter. *Automatisierungstechnik*, (11):556–562, 2000.
- [77] Jan Lunze and J. Schroder. Process diagnosis based on a discrete-event description. *Automatisierungstechnik*, 47(8):358–365, 1999.
- [78] J. Malmberg, B. Bernhardsson, and K.J. Åström. A stabilizing switching scheme for multi controller systems. *IFAC World Congress*, 1996.
- [79] A. Matveev and A. Savkin. *Qualitative theory of hybrid dynamical systems*. Birkhaeuser, 2000.
- [80] A.N. Michel, K. Wang, and B. Hu. *Qualitative theory of dynamical systems: The role of stability preserving mappings*. Marcel–Decker, 2001.
- [81] Richard H. Middleton, Graham C. Goowin, David J. Hill, and David Q. Mayne. Design issues in adaptive control. *IEEE Transactions on Automatic Control*, 33(1):50–58, 1 1988.
- [82] Manfred Morari, Alberto Bemporad, and D. Mignone. A framework for control, state estimation fault detection and verification of hybrid systems. *Automatisierungstechnik*, 47(8):374–381, 1999.
- [83] A. Stephen Morse. Towards a unified theory of parameter adaptive control–PartII: Certainty equivalence and implicit tuning. *IEEE Transactions on Automatic Control*, 37(1):15–29, January 1992.
- [84] A. Stephen Morse. Supervisory control of families of linear set-point controllers–part 1: Exact matching. *IEEE Transactions on Automatic Control*, 41(10):1413–1431, October 1996.

- [85] A. Stephen Morse. Supervisory control of families of linear set-point controllers—part 2: Robustness. *IEEE Transactions on Automatic Control*, 42(11):1500–1515, October 1997.
- [86] Vijay Narayanan and Giorgio Rizzioni. Fault diagnosis in advanced vehicle steering. *Automotive Engineering International*, 106:35–37, 1998.
- [87] K. S. Narendra and J. Balakrishnan. Improving transient response of adaptive control systems using multiple models and switching. *IEEE Transactions on Automatic Control*, 39(9):1861–1866, 1994.
- [88] K. S. Narendra and J. Balakrishnan. Intelligent control using fixed and adaptive models. In *Proceedings on the 33rd CDC, Lake Buena vista, Florida*, pages 1680–1685, December 1994.
- [89] K. S. Narendra, J. Balakrishnan, and M. K. Ciliz. Adaption and learning using multiple models, switching and tuning. *IEEE Control Systems Magazine*, 15(3):37–51, 1995.
- [90] K. S. Narendra and C. Xiang. Adaptive control of discrete-time systems using multiple models. In *Proceedings on the 37th CDC Tampa, Florida*, pages 3978–3983, December 1998.
- [91] Kumpati S. Narendra and Anuradha M. Annaswamy. *Stable Adaptive Systems*. Prentice-Hall, Inc., Englewood Cliffs, N.J., 1989.
- [92] Kumpati S. Narendra and J. Balakrishnan. A common Lyapunov function for stable lti systems with commuting A-matrices. *IEEE Transactions on Automatic Control*, 39(12):2469–2470, 1994.
- [93] Kumpati S. Narendra and Cheng. Adaptive control of discrete-time systems using multiple models. *IEEE Transactions on Automatic Control*, 45(9), 2000.
- [94] A. Nerode and W. Kohn. Models for hybrid systems: automata, topologies, stability, observability. Tech. report, Mathematical Sciences Institute, Cornell University, 1992.
- [95] Henk Nijmeijer and Arjan van der Schaft. *Nonlinear Dynamical Control Systems*. Springer Verlag, 1990.

- [96] H. B. Pacejka and R. S. Sharp. Shear force developments by pneumatic tyres in steady-state conditions: A review of modeling aspects. *Vehicle Systems Dynamics*, 29:409–422, 1991.
- [97] P. Peleties and R. DeCarlo. Asymptotic stability of m-switched systems using lyapunov-like functions. In *Proceedings of the American Control Conference, Boston*, pages 1679–1984, 1991.
- [98] Idar Petersen, Tor A. Johansen, Jens Kalkkuhl, and Jens Lüdemann. Wheel slip control in ABS brakes using gain scheduled constrained LQR. In *Proceedings of the IEEE ECC*, 2001.
- [99] C. A. Petri. *Kommunikation mit Automaten*. PhD thesis, Institut für Instrumentelle Mathematik, Universität Bonn, 1962.
- [100] S. Pettersson. *Analysis & Design of Hybrid Systems*. PhD thesis, Chalmers University of Technology, 1999.
- [101] S. Pettersson and B. Lennartson. Modelling, analysis & synthesis of hybrid systems. In *Reglermöte'96, Luleå*, pages 150–154, June 1996.
- [102] William F. Powers and Paul R. Nicastrì. Automotive vehicle control challenges of the 21st century. *Control engineering practice*, 8:605–618, 2000.
- [103] Andreas Queda. Hybride Parameterschätzung mit Anwendung auf ein modellbasiertes ABS-Regelsystem, Diplomarbeit, Technische Universität Dortmund, 2001.
- [104] S. Raghavan and J. K. Hendrick. Observer design for a class of nonlinear systems. *International Journal of Control*, 59:515–528, 1994.
- [105] R. Rajamani. Observers for Lipschitz nonlinear systems. *IEEE Transactions on Automatic Control*, 43:397–401, 1998.
- [106] Herbert E. Rauch. Intelligent fault diagnostics and control reconfiguration. *IEEE Control Systems*, 14(3):6–11, 1994.
- [107] Keith Redmill, Ümit Özgüner, Jeff Musgrave, and Walter Merrill. Intelligent hierarchical trust vector control for a space shuttle. *IEEE Control Systems*, 14(3):13–24, 1994.

- [108] P. Rieckert and T. Schnuck. Zur Fahrmechanik des gummbereiften Kraftfahrzeugs. *Ingenieur Archiv*, 11:210–224, 1940.
- [109] Ralf Schwarz, Rolf Isermann, Jürgen Böhm, Joachim Nell, and Peter Rieth. Clamping force estimation for a brake-by-wire actuator. In *SAE Technical Paper Series*, number 1999-01-0482, 1999.
- [110] R. Sepulchre, M. Janković, and P. Kokotović. *Constructive Nonlinear Control*. Springer–Verlag, London, 1997.
- [111] Daniel Shevitz and Brad Paden. Lyapunov stability theory of nonsmooth systems. *IEEE Transactions on Automatic Control*, 39(9):1910–1914, 1994.
- [112] Robert N. Shorten and Kumpati S. Narendra. Investigating the stability of a class of hybrid system. *Computing & Control Engineering Journal*, 9(2):1910–1914, 1998.
- [113] Gy. Simon and G. Péceli T. Kovács házy. Transients in reconfigurable control loops. In *IEEE Instrumentation and Measurement Technology Conference IMTC/2000 Baltimore, Maryland, U.S.A.*, May 2000.
- [114] Jean-Jaques E. Slotine. *Applied Nonlinear Control*. Prentice-Hall, Inc., 1991.
- [115] Eduardo D. Sontag. A "universal" construction of Artstein's theorem on nonlinear stabilization. 1989.
- [116] Eduardo D. Sontag. *Mathematical Control Theory*. Springer–Verlag, 1998.
- [117] Eduardo D. Sontag and G.A. Lafferriere. Remarks on control Lyapunov functions for discontinuous stabilizing feedback. In *Proceedings of the 32nd CDC*, pages 306–308, 1993.
- [118] Eduardo D. Sontag and Hector Sussmann. Remarks on continuous feedback. In *Proceedings of the CDC Albuquerque*, pages 916–921, 1980.
- [119] James A. Stiver and Panos J. Antsaklis. Modelling and analysis of hybrid control systems. In *Proceedings of the 31st CDC Tucson, Arizona*, pages 966–979, December 1992.
- [120] Avshalom Suissa and Fritz Böttiger. Ein robustes Kalman-Filter zur indirekten Bestimmung des Schwimmwinkels und anderer Fahrdynamikgrößen eines Fahrzeuges. Technischer Bericht F1M-93-100, DaimlerChrysler AG, 1994.

-
- [121] S. Taheri and E.H. Law. Slip control braking of an automobile during combined braking and steering manoeuvres. In *Advanced Automotive Technologies*, volume 40, pages 209–227, 1991.
- [122] G. Tao, X. L. Ma, and S. M. Joshi. Adaptive state feedback control of systems with actuator failures. In *Proceedings of the 2000 American Control Conference*, pages 3069–3070, 2000.
- [123] Lucio Taverini. Differential automata and their discrete simulators. *Nonlinear Analysis, Theory, Methods and Applications*, 11(6):665–683, 1987.
- [124] Didier Theilliol, Hassan Noura, and Dominique Sauter. Fault-tolerant control method for actuator and component faults. In *Proceedings of the 37th IEEE CDC, Tampa, Florida*, pages 604–609, 1998.
- [125] Vadim I. Utkin. Variable structure systems with sliding modes. *IEEE Transactions on Automatic Control*, 22(2):212–222, 1977.
- [126] Arjan van der Schaft and Hans Schumacher. *An Introduction to Hybrid Dynamical Systems*. Springer-Verlag, London, 2000.
- [127] Paul J. Th. Venhovens and Karl Naab. Vehicle dynamics estimation using Kalman filter. In *Proceedings of the 4th International Symposium on Advanced Vehicle Control*, pages 195–206, September 1998.
- [128] M. Vidyasagar. New directions of research in nonlinear systems theory. In *Proceedings of the IEEE*, volume 74, pages 1060–1091, 1986.
- [129] M. Vidyasagar. *Nonlinear systems analysis*. Prentice-Hall, 1993.
- [130] Yongji Wang and Kenneth J. Hunt. A general framework for the calculation of stability radius for a parametrically uncertain system via non-linear optimisation. *Automatica*, 1999. Submitted for publication.
- [131] Yongji Wang and Kenneth J. Hunt. Simultaneous stabilisation and strong simultaneous stabilisation of r-tuple plants with D stability: a constrained optimisation approach. *Trans. IEEE on Automatic Control*, 1999. Submitted for publication.
- [132] Yongji Wang and Kenneth J. Hunt. The calculation of stability radius with D stability region and nonlinear coefficients. In *Proceedings of the 3rd IFAC Symposium on Robust Control Design*, Prague, Czech Republic, 2000.

- [133] Yongji Wang, Tilmann Schmitt-Hartmann, Kenneth J. Hunt, and Michael Schinkel. A new approach to simultaneous stabilisation with D stability and its application to control of antilock braking systems. In *Proceedings of the European Control Conference (ECC)*, pages 612–617, Porto, Portugal, 2001.
- [134] Kajiro Watanabe, Kazuyuki Kobayashi, and Ka C. Cheok. Absolute speed measurement of automobile from noisy acceleration and erroneous wheel speed information. In *SAE Technical Paper Series*, number 920644, 1992.
- [135] P. E. Wellstead and N.B.O.L. Pettit. Analysis and redesign of an antilock brake system controller. In *IEE Proceedings of Control Theory Application*, pages 413–426, September 1997.
- [136] H. Ye, N. Michel, and L. Hou. Stability theory for hybrid dynamical systems. In *Proceedings of the 34th IEEE CDC, New Orleans*, pages 2679–2684, 1995.
- [137] H. Ye, N. Michel, and L. Hou. Stability analysis of discontinuous systems with applications. In *Proceedings of the 13th IFAC*, pages E:461–466, 1996.
- [138] J. S. Yu. A robust adaptive wheel-slip controller for antilock brake system. In *Proceedings of the 36th IEEE CDC*, 1997.
- [139] Hans Joachim Zander. *Logischer Entwurf binärer Systeme*. VEB Verlag Technik Berlin, 1982.
- [140] Peter V. Zhivoglyadov, Richard H. Middleton, and Minyue Fun. Localisation based switching adaptive control for time-varying discrete time systems. *IEEE Transactions on Automatic Control*, 45(4):752–755, 2000.

Appendix

A Four wheel car model

A.1 Geometry of the Vehicle

Figure A.1 shows the definition of the body fixed coordinate system. The origin of the system is located at the centre of gravity of the vehicle (CG).

x is positive in forward direction

y is positive to the left

z is positive in upward direction

The numbers $1, \dots, 4$ indicate the tyre footprints with respect to the centre of gravity. $\dot{\Psi}$ indicates the yaw velocity.

After choosing γ_i and h_i for $i = 1, \dots, 4$, the whole geometric system is defined by

$$b_i = h_i \sin \gamma_i \quad (\text{A.1})$$

$$l_i = h_i \cos \gamma_i \quad (\text{A.2})$$

The calculation will be done for a generalized quarter-car (c.f. figure A.2) where x_i , y_i , h_i and θ_i substitute the geometric quantities l_i , b_i , h_i and γ_i respectively.

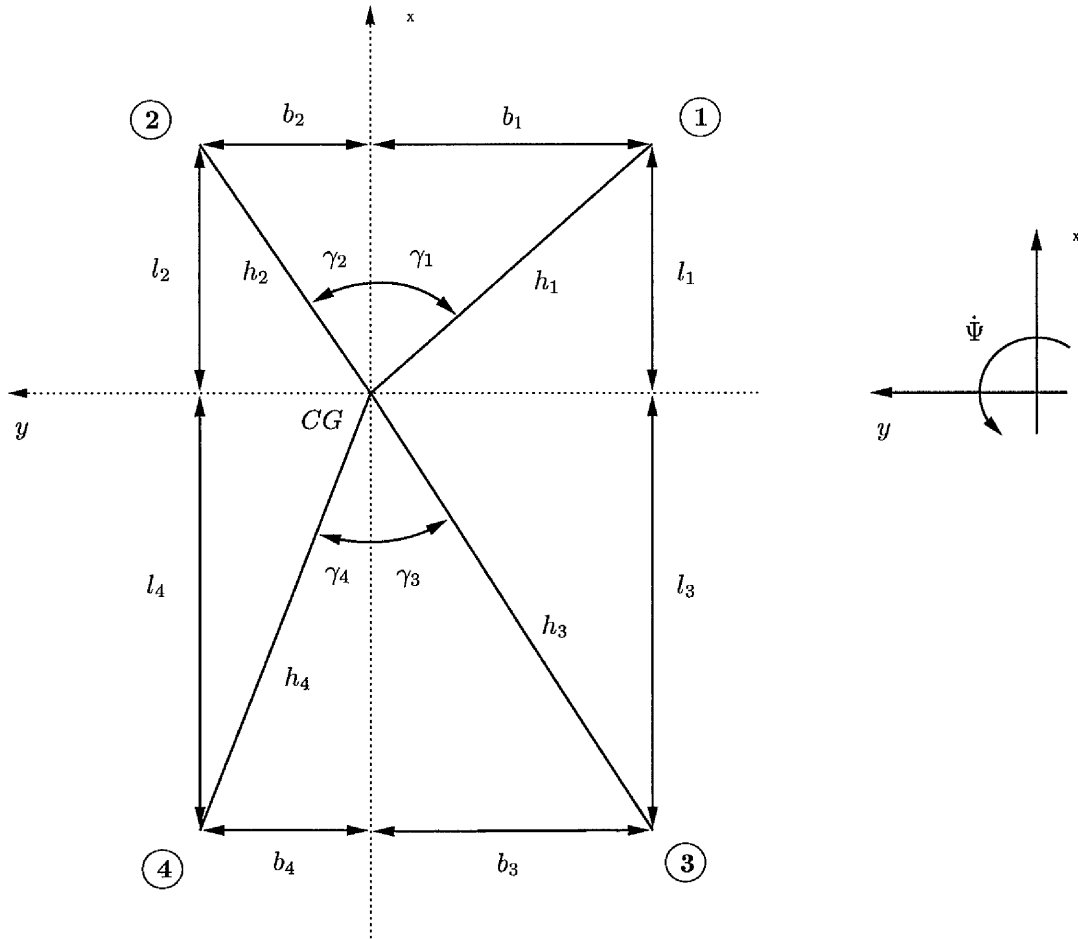


Figure A.1: Vehicle axis system and geometric definitions

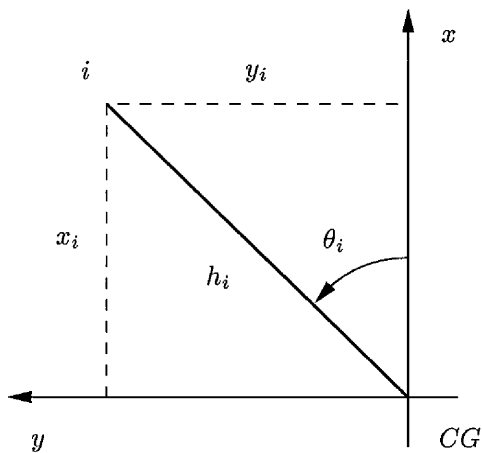


Figure A.2: Generalized quarter-car

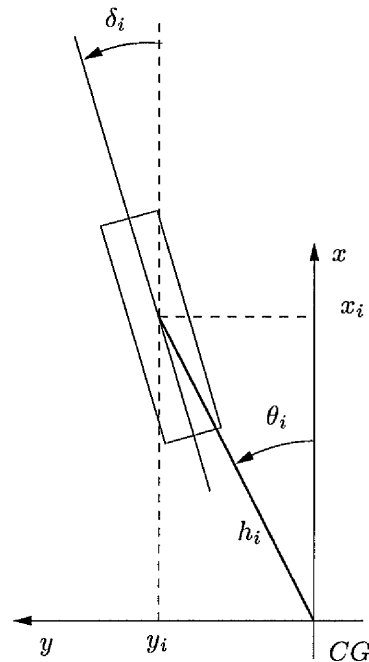


Figure A.3: Definition of the steer angle

From figure A.2 we get the following relations

$$\theta_1 = -\gamma_1 \quad (\text{A.3}) \quad x_1 = l_1 \quad (\text{A.7}) \quad y_1 = -b_1 \quad (\text{A.11})$$

$$\theta_2 = \gamma_2 \quad (\text{A.4}) \quad x_2 = l_2 \quad (\text{A.8}) \quad y_2 = b_2 \quad (\text{A.12})$$

$$\theta_3 = \pi + \gamma_3 \quad (\text{A.5}) \quad x_3 = -l_3 \quad (\text{A.9}) \quad y_3 = -b_3 \quad (\text{A.13})$$

$$\theta_4 = \pi - \gamma_4 \quad (\text{A.6}) \quad x_4 = -l_4 \quad (\text{A.10}) \quad y_4 = b_4 \quad (\text{A.14})$$

The steer angle δ_i is defined as angle between the x -axis of the vehicle and the longitudinal axis of the tyre.

$$\delta_i \in \left[-\frac{\pi}{2}; \frac{\pi}{2} \right] \quad (\text{A.15})$$

A.2 Forces at the Wheel

The coordinate system of the tyre is defined in the same way as for the vehicle: x -axis in longitudinal direction, y -axis in lateral direction.

The tyre longitudinal force F_{x_i} and the tyre lateral force F_{y_i} are defined in the local coordinate system of the wheel.

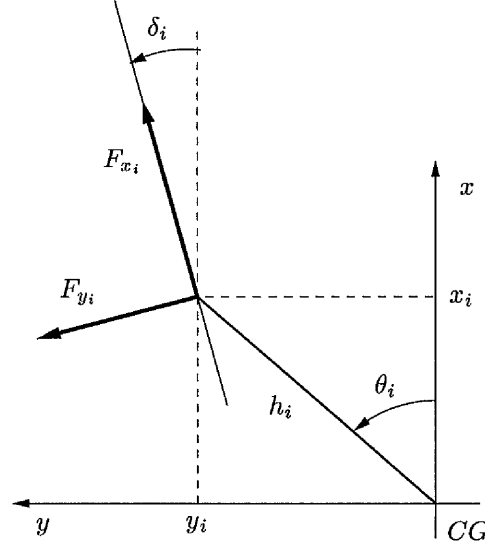


Figure A.4: Definition of the tyre forces

The quantities f_{x_i} and f_{y_i} indicate the components of the forces generated by the

tyres in the body fixed coordinates:

$$f_{xi} = F_{xi} \cos \delta_i - F_{yi} \sin \delta_i \quad (\text{A.16})$$

$$f_{yi} = F_{xi} \sin \delta_i + F_{yi} \cos \delta_i \quad (\text{A.17})$$

To abbreviate this expression we introduce the rotation-matrix $\mathbf{D}(\delta_i)$

$$\mathbf{D}(\delta_i) = \begin{pmatrix} \cos \delta_i & -\sin \delta_i \\ \sin \delta_i & \cos \delta_i \end{pmatrix} \quad (\text{A.18})$$

and the force vector \mathbf{f}_i

$$\mathbf{f}_i = \begin{pmatrix} f_{xi} \\ f_{yi} \end{pmatrix} = \mathbf{D}(\delta_i) \begin{pmatrix} F_{xi} \\ F_{yi} \end{pmatrix} = \mathbf{D}(\delta_i) \cdot \mathbf{F}_i \quad (\text{A.19})$$

A.3 Torque Caused by the Forces at the Wheel

The torque generated by the tyre forces will be called m_i and the force acting on the lever arm h_i is then $\frac{m_i}{h_i}$.

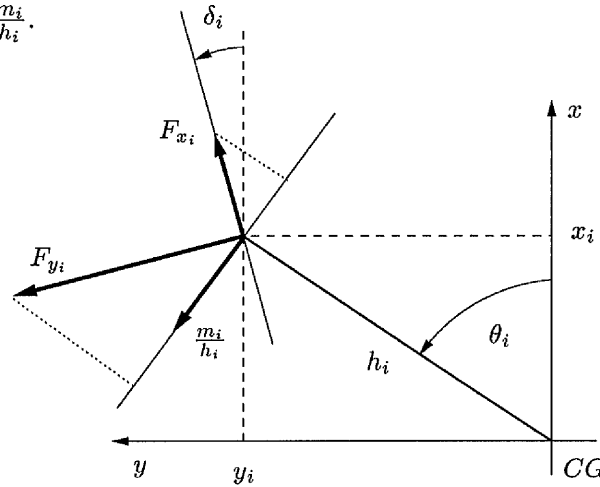


Figure A.5: Torque generated by the tyre forces

Because of

$$\begin{pmatrix} f_{xi} \\ f_{yi} \end{pmatrix} = \mathbf{D}(\delta_i) \mathbf{F}_i \quad (\text{A.20})$$

$$= \mathbf{D}(\delta_i) \begin{pmatrix} F_{xi} \\ F_{yi} \end{pmatrix} \quad (\text{A.21})$$

we can represent $\frac{m_i}{h_i}$ as shown in figure A.6.

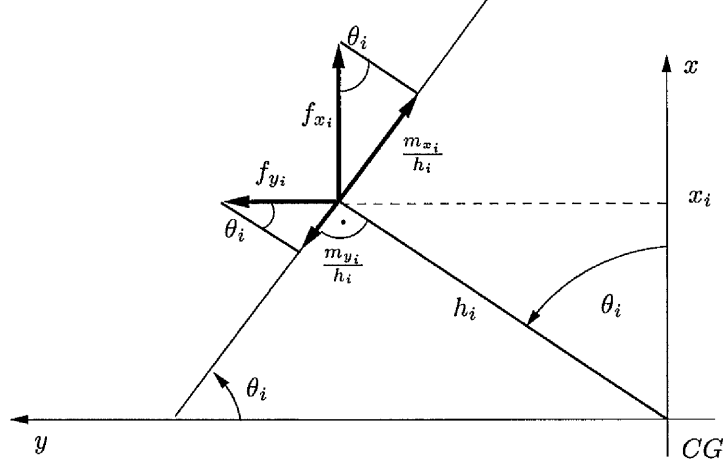


Figure A.6: Tyre forces in body fixed coordinates

That leads to

$$\begin{aligned} \frac{m_i}{h_i} &= \frac{m_{x_i} + m_{y_i}}{h_i} \\ &= -f_{x_i} \sin \theta_i + f_{y_i} \cos \theta_i \end{aligned} \quad (\text{A.22})$$

Introducing the geometry vector

$$\mathbf{g}_i(h_i, \theta_i) = \begin{pmatrix} -\sin \theta_i \\ \cos \theta_i \end{pmatrix} \cdot h_i \quad (\text{A.23})$$

we can express the torque as

$$m_i = \mathbf{g}_i^T(h_i, \theta_i) \cdot \mathbf{f}_i \quad (\text{A.24})$$

and with Eq.(A.19) we get

$$m_i = \mathbf{g}_i^T(h_i, \theta_i) \mathbf{D}(\delta) \mathbf{F}_i \quad (\text{A.25})$$

The sum of all tyre forces at the centre of gravity is given by

$$\mathbf{f} = \begin{pmatrix} f_x \\ f_y \end{pmatrix} = \sum_{i=1}^4 \mathbf{D}(\delta_i) \begin{pmatrix} F_{x_i} \\ F_{y_i} \end{pmatrix} \quad (\text{A.26})$$

And the sum of all torques at the centre of gravity is

$$M = \sum_{i=1}^4 \mathbf{g}_i^T \mathbf{D}(\delta_i) \mathbf{F}_i \quad (\text{A.27})$$

$$M = \sum_{i=1}^4 \mathbf{g}_i^T \mathbf{D}(\delta_i) \begin{pmatrix} F_{xi} \\ F_{yi} \end{pmatrix} \quad (\text{A.28})$$

A.4 Dynamic Equations for the Forces

A.4.1 Expression in Body Fixed Coordinates

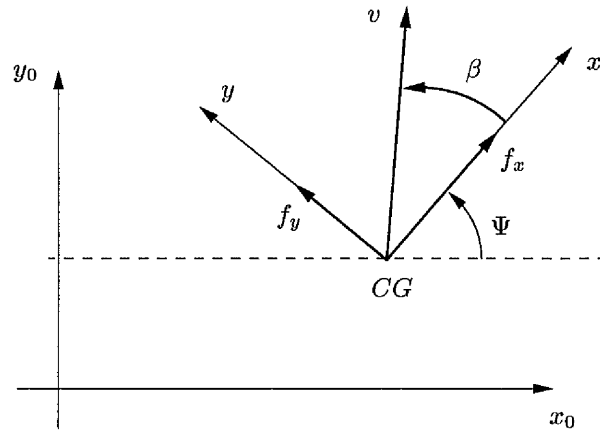


Figure A.7: The body fixed coordinate system in the inertial system

The components of the force acting on the centre of gravity can be expressed in inertial coordinates:

$$f_{x0} = f_x \cos \Psi - f_y \sin \Psi \quad (\text{A.29})$$

$$f_{y0} = f_x \sin \Psi + f_y \cos \Psi \quad (\text{A.30})$$

Using the rotation matrix

$$\mathbf{D}(\Psi) = \begin{pmatrix} \cos \Psi & -\sin \Psi \\ \sin \Psi & \cos \Psi \end{pmatrix} \quad (\text{A.31})$$

we get

$$\mathbf{f}_0 = \mathbf{D}(\Psi)\mathbf{f} \quad (\text{A.32})$$

According to Newton's law the expression

$$\begin{aligned}
 m \cdot \frac{d}{dt} \begin{pmatrix} v_{x0} \\ v_{y0} \end{pmatrix} &= \mathbf{D}(\Psi) \mathbf{f} \\
 m \cdot \frac{d}{dt} \left[\mathbf{D}(\Psi) \begin{pmatrix} v_x \\ v_y \end{pmatrix} \right] &= \mathbf{D}(\Psi) \mathbf{f} \\
 m \cdot \left[\mathbf{D}(\Psi) \begin{pmatrix} \dot{v}_x \\ \dot{v}_y \end{pmatrix} + \frac{d\mathbf{D}(\Psi)}{dt} \begin{pmatrix} v_x \\ v_y \end{pmatrix} \right] &= \mathbf{D}(\Psi) \mathbf{f} \tag{A.33}
 \end{aligned}$$

is obtained.

Differentiating the rotation matrix $\mathbf{D}(\Psi)$ we get

$$\frac{d}{dt} \mathbf{D}(\Psi) = \begin{pmatrix} -\sin \Psi & -\cos \Psi \\ \cos \Psi & -\sin \Psi \end{pmatrix} \dot{\Psi} = \mathbf{D}(\Psi) \begin{pmatrix} 0 & -1 \\ 1 & 0 \end{pmatrix} \dot{\Psi} \tag{A.34}$$

Thus,

$$m \cdot \left[\frac{d}{dt} \begin{pmatrix} v_x \\ v_y \end{pmatrix} + \underbrace{\begin{pmatrix} -v_y \\ v_x \end{pmatrix} \dot{\Psi}}_{\text{Coriolis Term}} \right] = \mathbf{f} \tag{A.35}$$

Inserting Eq.(A.26) leads to

$$m \cdot \begin{pmatrix} \dot{v}_x - v_y \dot{\Psi} \\ \dot{v}_y + v_x \dot{\Psi} \end{pmatrix} = \sum_{i=1}^4 \mathbf{D}(\delta_i) \begin{pmatrix} F_{xi} \\ F_{yi} \end{pmatrix} \tag{A.36}$$

A.4.2 Expression in Velocity and Side Slip Angle

Regarding figure A.8, the following relations are between speed and side slip angle given

$$v_x = v \cos \beta \quad (\text{A.37})$$

$$v_y = v \sin \beta \quad (\text{A.38})$$

and

$$\dot{v}_x = \dot{v} \cos \beta - v \dot{\beta} \sin \beta \quad (\text{A.39})$$

$$\dot{v}_y = \dot{v} \sin \beta + v \dot{\beta} \cos \beta \quad (\text{A.40})$$

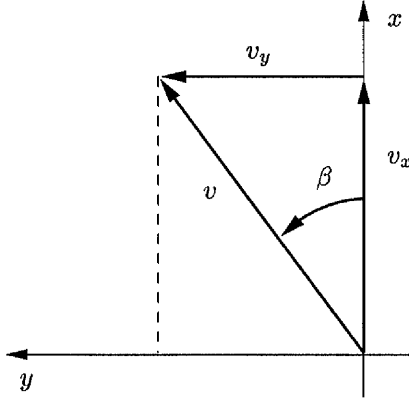


Figure A.8: Definition of the side slip angle

Inserted in Eq.(A.36), we get

$$m \begin{pmatrix} \dot{v} \cos \beta - v \dot{\beta} \sin \beta - v \dot{\Psi} \sin \beta \\ \dot{v} \sin \beta + v \dot{\beta} \cos \beta + v \dot{\Psi} \cos \beta \end{pmatrix} = \sum_{i=1}^4 \mathbf{D}(\delta_i) \begin{pmatrix} F_{xi} \\ F_{yi} \end{pmatrix} \quad (\text{A.41})$$

$$m \begin{pmatrix} \cos \beta & -v \sin \beta \\ \sin \beta & v \cos \beta \end{pmatrix} \begin{pmatrix} \dot{v} \\ \dot{\beta} \end{pmatrix} + mv \dot{\Psi} \begin{pmatrix} -\sin \beta \\ \cos \beta \end{pmatrix} = \sum_{i=1}^4 \mathbf{D}(\delta_i) \begin{pmatrix} F_{xi} \\ F_{yi} \end{pmatrix}$$

We introduce the following abbreviations

$$\mathbf{R}(v, \beta) = \begin{pmatrix} \cos \beta & -v \sin \beta \\ \sin \beta & v \cos \beta \end{pmatrix} \quad (\text{A.42})$$

with

$$\det(\mathbf{R}) = v \quad (\text{A.43})$$

$$\mathbf{R}^{-1}(v, \beta) = \frac{1}{v} \begin{pmatrix} v \cos \beta & v \sin \beta \\ -\sin \beta & \cos \beta \end{pmatrix} \quad (\text{A.44})$$

This results in

$$\begin{pmatrix} \dot{v} \\ \dot{\beta} \end{pmatrix} + \dot{\Psi} \begin{pmatrix} v \cos \beta & v \sin \beta \\ -\sin \beta & \cos \beta \end{pmatrix} \begin{pmatrix} -\sin \beta \\ \cos \beta \end{pmatrix} = \frac{\mathbf{R}^{-1}(v, \beta)}{m} \sum_{i=1}^4 \mathbf{D}(\delta_i) \begin{pmatrix} F_{xi} \\ F_{yi} \end{pmatrix}$$

$$\begin{pmatrix} \dot{v} \\ \dot{\beta} \end{pmatrix} + \begin{pmatrix} 0 \\ \dot{\Psi} \end{pmatrix} = \frac{\mathbf{R}^{-1}(v, \beta)}{m} \sum_{i=1}^4 \mathbf{D}(\delta_i) \begin{pmatrix} F_{xi} \\ F_{yi} \end{pmatrix} \quad (\text{A.45})$$

A.5 Balance of Torques

The balance of torques is given by

$$J\ddot{\Psi} = M \quad (\text{A.46})$$

where the torques are given by Eq.(A.28)

$$J\ddot{\Psi} = \sum_{i=1}^4 \mathbf{g}_i^T(h_i, \theta_i) \mathbf{D}(\delta_i) \cdot \begin{pmatrix} F_{xi} \\ F_{yi} \end{pmatrix} \quad (\text{A.47})$$

A.6 Determination of the Tyre Slip Angle

Figure A.9 shows the definition of the tyre fixed coordinate system. The total velocity of the tyre over ground is indicated by v_R . A positive tyre slip angle α_R increases the lateral force F_y in y_R -direction.

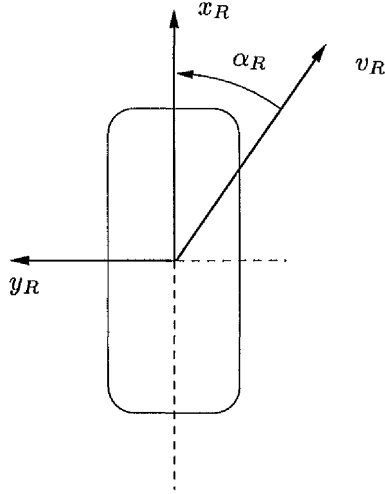


Figure A.9: Definition of the tyre slip angle

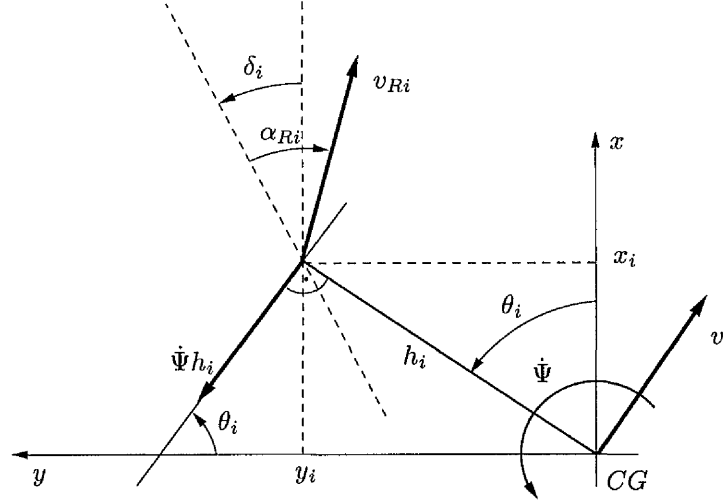


Figure A.10: Compound of the total tyre velocity

The total tyre velocity over ground v_{Ri} is the sum of the velocity v of the centre of gravity and the component of the yaw motion orthogonal to the axis h_i .

$$v_{Rxi} = v_x - \dot{\Psi} h_i \sin \theta_i \quad (\text{A.48})$$

$$v_{Ryi} = v_y + \dot{\Psi} h_i \cos \theta_i \quad (\text{A.49})$$

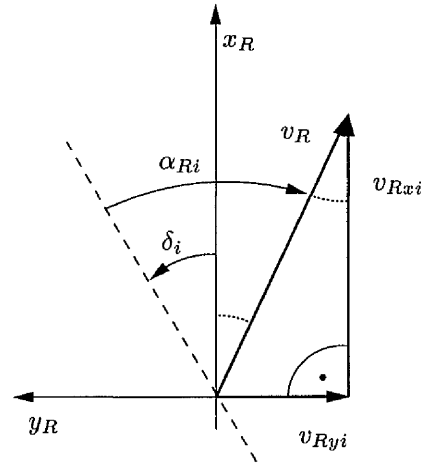


Figure A.11: Tyre side slip angle in local coordinates

From figure A.11 we get

$$\tan(\alpha_{Ri} - \delta_i) = -\frac{v_{Ryi}}{v_{Rxi}} \quad (\text{A.50})$$

and with Eq.(A.48) and Eq.(A.49)

$$\tan(\alpha_{Ri} - \delta_i) = \frac{-v_y - \dot{\Psi}h_i \cos \theta_i}{v_x - \dot{\Psi}h_i \sin \theta_i} \quad (\text{A.51})$$

Solving this for α_{Ri} yields

$$\alpha_{Ri} = \delta_i + \arctan \left(\frac{-v_y - \dot{\Psi}h_i \cos \theta_i}{v_x - \dot{\Psi}h_i \sin \theta_i} \right) \quad (\text{A.52})$$

and expressed with total velocity v and side slip angle β of the vehicle

$$\alpha_{Ri} = \delta_i + \arctan \left(\frac{-v \sin \beta - \dot{\Psi}h_i \cos \theta_i}{v \cos \beta - \dot{\Psi}h_i \sin \theta_i} \right) \quad (\text{A.53})$$

A.7 Wheel Dynamics

The wheel dynamics is described by:

$$J_{wheel}\dot{\omega}_i = -T_{bi}\text{sgn}(\omega_i) - R_{dyn}F_{x_i} + T_{d_i} \quad (\text{A.54})$$

where T_{bi} is the brake torque, R_{dyn} is the dynamic wheel radius and T_{d_i} is the engine torque.

A.8 Vertical forces

A full model of the car would include the pitch and roll dynamics of the body and the suspension system. The simplified model used here takes only into account the *stationary* distribution of the load on the tyres. The stationary distribution of the load on the tyres (vertical force) F_z for each wheel is calculated from lateral and longitudinal acceleration using the equation:

$$F_{z_i} = \frac{m}{2} \left[\frac{g \cdot l_{i\pm 2} + a_x \cdot h_{SP} \cdot (-1)^{\text{int}(\frac{i+1}{2})}}{l_v + l_h} + a_y \cdot h_{SP} \cdot k_{q_i} \right], \quad (\text{A.55})$$

where $i = 1 \dots 4$ is the wheel number, $l_1 = l_2 = l_v$, $l_3 = l_4 = l_h$, $b_1 = b_2 = b_v$ and $b_3 = b_4 = b_h$ are the distances between the wheels and CG, h_{SP} , is the height of CG. The factors $k_{qv} = k_{q1} = -k_{q2}$, $k_{qh} = k_{q3} = -k_{q4}$ are for the stationary distribution of the pitch moment between front and rear. When using Eq. A.55 for simulation the values a_x and a_y of acceleration will have to be delayed in order to avoid an algebraic loop.

A.9 Linear four-wheel cornering car model

The nonlinear four-wheel model is linearised for the steady state cornering. The set-point is $\beta = 0$, $v = v_0$, $\dot{\Psi} = \dot{\Psi}_0$ and $\delta_i = \delta_{i0}$. The forces F_{x_i} are assumed as to be zero.

$$\dot{x} = Ax + Bu \tag{A.56}$$

where

$$x = \begin{pmatrix} v \\ \beta \\ \dot{\Psi} \end{pmatrix} \quad A = \begin{pmatrix} a_{11} & a_{12} & a_{13} \\ a_{21} & a_{22} & a_{23} \\ a_{31} & a_{32} & a_{33} \end{pmatrix}$$

$$u = \begin{pmatrix} \delta_1 \\ \delta_2 \\ \delta_3 \\ \delta_4 \end{pmatrix} \quad B = \begin{pmatrix} b_{11} & b_{12} & b_{13} & b_{14} \\ b_{21} & b_{22} & b_{23} & b_{24} \\ b_{31} & b_{32} & b_{33} & b_{34} \end{pmatrix} \tag{A.57}$$

$$\begin{aligned}
 a_{11} &= \frac{1}{m} \sum_{i=1}^4 \left(-\sin(\delta_{i_0}) \frac{\partial F_{y_i}}{\partial v} \Big|_{SP} \right) \\
 a_{12} &= \frac{1}{m} \sum_{i=1}^4 \left(\cos(\delta_{i_0}) F_{y_i} + \sin(\delta_{i_0}) \frac{\partial F_{y_i}}{\partial \beta} \Big|_{SP} \right) \\
 a_{13} &= \frac{1}{m} \sum_{i=1}^4 \left(-\sin(\delta_{i_0}) \frac{\partial F_{y_i}}{\partial \Psi} \Big|_{SP} \right) \\
 a_{21} &= \frac{1}{mv_0} \sum_{i=1}^4 \left(\cos(\delta_{i_0}) \left(\frac{\partial F_{y_i}}{\partial v} \Big|_{SP} - \frac{1}{v_0} F_{y_i} \right) \right) \\
 a_{22} &= \frac{1}{mv_0} \sum_{i=1}^4 \left(\sin(\delta_{i_0}) F_{y_i} + \cos(\delta_{i_0}) \frac{\partial F_{y_i}}{\partial \beta} \Big|_{SP} \right) \\
 a_{23} &= \frac{1}{mv_0} \sum_{i=1}^4 \left(\cos(\delta_{i_0}) \frac{\partial F_{y_i}}{\partial \Psi} \Big|_{SP} \right) \\
 a_{31} &= \frac{1}{J} \sum_{i=1}^4 \left(-h_i \sin(\Theta_i) \quad h_i \cos(\Theta_i) \right) \begin{pmatrix} -\sin(\delta_{i_0}) \frac{\partial F_{y_i}}{\partial v} \Big|_{SP} \\ \cos(\delta_{i_0}) \frac{\partial F_{y_i}}{\partial v} \Big|_{SP} \end{pmatrix} \\
 a_{32} &= \frac{1}{J} \sum_{i=1}^4 \left(-h_i \sin(\Theta_i) \quad h_i \cos(\Theta_i) \right) \begin{pmatrix} -\sin(\delta_{i_0}) \frac{\partial F_{y_i}}{\partial \beta} \Big|_{SP} \\ \cos(\delta_{i_0}) \frac{\partial F_{y_i}}{\partial \beta} \Big|_{SP} \end{pmatrix} \\
 a_{33} &= \frac{1}{J} \sum_{i=1}^4 \left(-h_i \sin(\Theta_i) \quad h_i \cos(\Theta_i) \right) \begin{pmatrix} -\sin(\delta_{i_0}) \frac{\partial F_{y_i}}{\partial \Psi} \Big|_{SP} \\ \cos(\delta_{i_0}) \frac{\partial F_{y_i}}{\partial \Psi} \Big|_{SP} \end{pmatrix} \quad (A.58)
 \end{aligned}$$

$$\begin{aligned}
 b_{1i} &= \frac{1}{m} \left(-\sin(\delta_{i_0}) \frac{\partial F_{y_i}}{\partial \delta_i} \Big|_{SP} - F_{y_i} \cos(\delta_i) \right) \\
 b_{2i} &= \frac{1}{m} \left(\cos(\delta_{i_0}) \frac{\partial F_{y_i}}{\partial \delta_i} \Big|_{SP} - \frac{1}{v} F_{y_i} \sin(\delta_i) \right) \quad (A.59) \\
 b_{3i} &= \frac{1}{J} \left(-h_i \sin(\Theta_i) \quad h_i \cos(\Theta_i) \right) \begin{pmatrix} -F_{y_i} \cos(\delta_{i_0}) - \sin(\delta_{i_0}) \frac{\partial F_{y_i}}{\partial \delta_i} \Big|_{SP} \\ -F_{y_i} \sin(\delta_{i_0}) + \cos(\delta_{i_0}) \frac{\partial F_{y_i}}{\partial \delta_i} \Big|_{SP} \end{pmatrix}
 \end{aligned}$$

The Forces F_{y_i} and their derivatives at $\beta = 0$ are:

$$\begin{aligned}
F_{y_i} &= F_{z_i} c_R \sin \alpha_i \\
&= F_{z_i} c_r \sin(\delta_i + \arctan(\frac{-v \sin(\beta) - \dot{\Psi} h_i \cos(\Theta_i)}{v \cos(\beta) - \dot{\Psi} h_i \sin(\Theta_i)})) \\
&= F_{z_i} c_R \left(\sin \delta_i \cos \left(\arctan \left(\frac{-v \sin \beta - \dot{\Psi} h_i \cos \Theta_i}{v \cos \beta - \dot{\Psi} h_i \sin \Theta_i} \right) \right) \right. \\
&\quad \left. \dots + \cos \delta_i \sin \left(\arctan \left(\frac{-v \sin \beta - \dot{\Psi} h_i \cos \Theta_i}{v \cos \beta - \dot{\Psi} h_i \sin \Theta_i} \right) \right) \right) \tag{A.60}
\end{aligned}$$

$$\begin{aligned}
\frac{\partial F_{y_i}}{\partial v} &= F_{z_i} c_r \cos(\delta_i - \arctan(\frac{\dot{\Psi} h_i \cos(\Theta_i)}{v - \dot{\Psi} h_i \sin(\Theta_i)})) \dot{\Psi} h_i \cos(\Theta_i) \dots \\
&\quad \dots \left(v - \dot{\Psi} h_i \sin(\Theta_i) \right)^{-2} \left(1 + \frac{\dot{\Psi}^2 h_i^2 (\cos(\Theta_i))^2}{(v - \dot{\Psi} h_i \sin(\Theta_i))^2} \right)^{-1} \tag{A.61}
\end{aligned}$$

$$\begin{aligned}
\frac{\partial F_{y_i}}{\partial \beta} &= -F_{z_i} c_r \cos(\delta_i - \arctan(\frac{\dot{\Psi} h_i \cos(\Theta_i)}{v - \dot{\Psi} h_i \sin(\Theta_i)})) v \dots \\
&\quad \dots \left(v - \dot{\Psi} h_i \sin(\Theta_i) \right)^{-1} \left(1 + \frac{\dot{\Psi}^2 h_i^2 (\cos(\Theta_i))^2}{(v - \dot{\Psi} h_i \sin(\Theta_i))^2} \right)^{-1} \tag{A.62}
\end{aligned}$$

$$\begin{aligned}
\frac{\partial F_{y_i}}{\partial \dot{\Psi}} &= F_{z_i} c_r \cos(\delta_i - \arctan(\frac{\dot{\Psi} h_i \cos(\Theta_i)}{v - \dot{\Psi} h_i \sin(\Theta_i)})) \dots \\
&\quad \dots \left(\frac{h_i \cos(\Theta_i)}{v - \dot{\Psi} h_i \sin(\Theta_i)} - \frac{\dot{\Psi} h_i^2 \cos(\Theta_i) \sin(\Theta_i)}{(v - \dot{\Psi} h_i \sin(\Theta_i))^2} \right) \dots \\
&\quad \dots \left(1 + \frac{\dot{\Psi}^2 h_i^2 (\cos(\Theta_i))^2}{(v - \dot{\Psi} h_i \sin(\Theta_i))^2} \right)^{-1} \tag{A.63}
\end{aligned}$$

$$\frac{\partial F_{y_i}}{\partial \delta_i} = F_{z_i} c_r \cos(\delta_i - \arctan(\frac{\dot{\Psi} h_i \cos(\Theta_i)}{v - \dot{\Psi} h_i \sin(\Theta_i)})) \tag{A.64}$$

The steering angles at the setpoint are calculated from the steady-state cornering of the "bicycle"-model. The equations of the steady-state steering angles $\delta_{f_0}(\dot{\Psi}_0)$ and $\delta_{r_0}(\dot{\Psi}_0)$ are as follows:

$$\begin{aligned}
 \delta_{f_0}(\dot{\Psi}_0) &= \frac{1}{2} \left(\arcsin \left[\frac{2mv_0\dot{\Psi}_0}{F_{z_f}c_r \left(\frac{l_f}{l_r} + 1 \right)} - \dots \right. \right. \\
 &\quad \left. \left. \dots + \sin \left(\arctan \left(\frac{\dot{\Psi}_0 l_f}{v_0} \right) \right) \right] + \arctan \left(\frac{\dot{\Psi}_0 l_f}{v_0} \right) \right) \\
 \delta_{r_0}(\dot{\Psi}_0) &= \frac{1}{2} \left(\arcsin \left[\frac{2mv_0\dot{\Psi}_0}{F_{z_r}c_r \left(\frac{l_r}{l_f} + 1 \right)} - \dots \right. \right. \\
 &\quad \left. \left. \dots - \sin \left(\arctan \left(\frac{\dot{\Psi}_0 l_r}{v_0} \right) \right) \right] - \arctan \left(\frac{\dot{\Psi}_0 l_r}{v_0} \right) \right)
 \end{aligned} \tag{A.65}$$

A.10 The "bicycle" model

The classical single-track model [108, 10] is obtained by lumping the two front wheels into one wheel in the centerline of the vehicle, the same is done with the rear wheels. The variables denotes the following quantities: δ_f , δ_r are the front and rear steering angles, l_f , l_r are the distances between the center of gravity and the front (rear) wheel base and F_{y_f} , F_{y_r} are the side forces at the front (rear) wheel. The forces and moments are:

$$\begin{aligned}
 F_{y_i} &= F_{z_i} c_R \sin \alpha_i \\
 &= F_{z_i} c_R \left(\sin \left(\delta_i + \arctan \left(\frac{-v \sin \beta - \dot{\Psi} h_i \cos \Theta_i}{v \cos \beta - \dot{\Psi} h_i \sin \Theta_i} \right) \right) \right)
 \end{aligned} \tag{A.66}$$

$$\begin{bmatrix} f_x \\ f_y \\ m_z \end{bmatrix} = \begin{bmatrix} -\sin \delta_f & \sin \delta_r \\ \cos \delta_f & \cos \delta_r \\ l_f \cos \delta_f & -l_r \cos \delta_r \end{bmatrix} \begin{bmatrix} F_{y_f} \\ F_{y_r} \end{bmatrix} \tag{A.67}$$

The dynamic equations are:

$$\begin{bmatrix} mv(\dot{\beta} + r) \\ m\dot{v} \\ J\dot{\psi} \end{bmatrix} = \begin{bmatrix} -\sin \beta & \cos \beta & 0 \\ \cos \beta & \sin \beta & 0 \\ 0 & 0 & 1 \end{bmatrix} \begin{bmatrix} f_x \\ f_y \\ m_z \end{bmatrix} \quad (\text{A.68})$$

B Definitions

Definition B.0.1 (Lie derivative[?]) *The derivative of a scalar state dependent function ¹ $\rho(x)$ along a vector field $f(x(t))$ is called Lie derivative and is defined as*

$$L_f \rho(x) = \frac{\partial \rho(x)}{\partial x} f(x(t)).$$

The Lie derivative is again a scalar function, and therefore recursively applicable.

$$L_f^k \rho(x) = L_f(L_f^{k-1} \rho(x)) \quad \text{mit} \quad L_f^0 \rho(x) = \rho(x).$$

Definition B.0.2 (class- \mathcal{K} function[66]) *A continuous function $\alpha : \mathbb{R}^+ \rightarrow \mathbb{R}^+$ is said to belong class- \mathcal{K} if it is strictly increasing and $\alpha(0) = 0$.*

Definition B.0.3 (class- \mathcal{KL} function[66]) *A continuous function $\beta : \mathbb{R}^+ \times \mathbb{R}^+ \rightarrow \mathbb{R}^+$ is said to belong class- \mathcal{KL} if, for each fixed s , the mapping $\beta(r, s)$ belongs to class- \mathcal{K} with respect to r and, for each fixed r , the mapping $\beta(r, s)$ is decreasing with respect to s and $\beta(r, s) \rightarrow 0$ as $s \rightarrow \text{inf}$.*

Definition B.0.4 (Supremum[24]) *The supremum $\sup \mathbb{S}$ of a (nonempty) subset \mathbb{S} of the extended reals $\overline{\mathbb{R}} = \mathbb{R} \cup \{\pm\infty\}$ is the smallest value $y \in \overline{\mathbb{R}}$ such that for all $x \in \mathbb{S}$ we have $x \leq y$.*

Definition B.0.5 (Infimum[24]) *The infimum $\inf \mathbb{S}$ of a (nonempty) subset \mathbb{S} of the extended reals $\overline{\mathbb{R}} = \mathbb{R} \cup \{\pm\infty\}$ is the largest value $y \in \overline{\mathbb{R}}$ such that for all $x \in \mathbb{S}$ we have $x \geq y$.*

¹

$$\frac{\partial \rho(x)}{\partial x} = \left(\frac{\partial \rho(x)}{\partial x_1}, \frac{\partial \rho(x)}{\partial x_2}, \dots, \frac{\partial \rho(x)}{\partial x_n} \right)$$

Definition B.0.6 (Argmin) *The argmin-operator*

$$\text{argmin} : \mathbb{R}^N \longrightarrow \mathcal{I} \tag{B.1}$$

chooses the index $k = \text{argmin}_{i \in \mathcal{I} = \{1, \dots, N\}}(\mathbf{q})$ of the smallest component of the cost vector $\mathbf{q} = (Q_1, \dots, Q_N)^T$.

Definition B.0.7 (Phase margin ϕ_r [48]) *The intersection of the Nyquist diagram of the open loop system transfer function $L(j\omega)$ with the unit circle around the point $(0, 0)$ that is nearest to the the point $(-1, 0)$ is called phase margin and has the angular separation of*

$$\phi_r = \text{arc}\{L(j\omega_c)\} + \pi \tag{B.2}$$

whereby the the respective frequency ω_c is called cut off frequency of the unit circle.

Definition B.0.8 (Gain margin A_r [48]) *The intersection of the Nyquist plot of the open loop system transfer function $L(j\omega)$ and the negative real axis that is nearest the point $(-1, 0)$ is called reciprocal gain margin, that means*

$$A_r = \frac{1}{L(j\omega_r)} \tag{B.3}$$

where ω_r is the gain crossover frequency.

Definition B.0.9 (Dissipativity[110]) *Assume that associated with the system H (cf. Fig. B.0.9) is a function $w : \mathbb{R}^m \times \mathbb{R}^m \longrightarrow \mathbb{R}$ called the supply rate, which is locally integrable for every $u \in U$, that is, it satisfies $\int_{t_0}^{t_1} \|w(u(t), x(t))\| dt < \infty$ for all $t_0 < t_1$. Let X be a connected subset of \mathbb{R}^n containing the origin. We say that the system H is dissipative in X with the supply rate $w(u, x)$ if there exists a function $S(x)$, $S(0) = 0$, such that for all $x \in X$, $S(x) \geq 0$ and*

$$S(x(T)) - S(x(0)) \leq \int_0^T w(u(t), x(t)) dt \tag{B.4}$$

for all $u \in U$ and all $T \geq 0$ such that $x(t) \in X$ for all $t \in [0, T]$. The function $S(x)$ is then called storage function.

Definition B.0.10 (Sector margin[110]) *The nonlinear feedback system (H, k) (cf. Fig. B.0.9) is said to have a sector margin (α, β) if the perturbed closed-loop system (H, k, Δ) is globally asymptotically stable for any Δ which is of the form $\text{diag}\varphi_1(\cdot), \dots, \varphi_m(\cdot)$ where $\varphi_i(\cdot)$'s are locally Lipschitz static nonlinearities which belong to the sector (α, β) .*

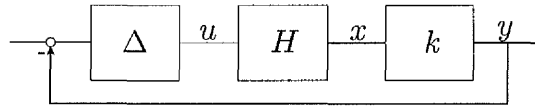


Figure B.1: Nonlinear feedback loop with the control law $k(x)$ and input uncertainty Δ [110]

Definition B.0.11 (Disk margin[110]) *The nonlinear feedback system (H, k) (cf. Fig. B.0.9) is said to have a disk margin $D(\alpha)$ if the perturbed closed-loop system (H, k, Δ) is globally asymptotically stable for any Δ which is globally asymptotically stable and input feedforward passive(ν)², $\nu > \alpha$, with a radially unbounded storage function.*

²A system H is said to be input feedforward passive if it is dissipative with respect to the supply rate $w(u, x) = u^T x - \nu u^T u$ for some $\nu \in \mathbb{R}$.